UNIVERSIDADE DO ALGARVE
FACULDADE DE CIÊNCIAS E TECNOLOGIA

An Integrated thermochronology, organic maturation and provenance study in the South Portuguese Zone and Algarve Basin (South Portugal)

BRUNO MIGUEL GREGÓRIO RODRIGUES

Dissertação para a obtenção do grau de Doutor no ramo Geociências,
especialidade de Geologia

Tese orientada por:

Doutor Paulo Fernandes
(Faculdade de Ciências e Tecnologia,Universidade do Algarve)

Doutor David Chew
(Department of Geology, Trinity College Dublin, Irlanda)

Doutor Raul Jorge
(Faculdade de Ciências, Departamento de Geologia, Universidade de Lisboa)

2014

Título: An Integrated thermochronology, organic maturation and provenance study in the South Portuguese Zone and Algarve Basin (South Portugal)

Declaro ser o autor deste trabalho, que é original e inédito. Autores e trabalhos consultados estão devidamente citados no texto e constam da listagem de referências incluída.

(Bruno Rodrigues)

Aos meus avós, Maria José, Maria da Conceição, Vitorino e Fernando. Tudo na vida só se consegue com bases fortes e duradouras.

***O que mais há na terra é paisagem*.**
(*Here, it's mostly countryside, land.)*

José Saramago in
Levantado do Chão (Raised from the Ground).

AGRADECIMENTOS

Em primeiro lugar gostaria de agradecer sinceramente ao meus orientadores, o Doutor Paulo Fernandes, o Doutor David Chew e o Doutor Raul Jorge.

Ao Doutor Paulo Fernandes pela sua amizade, dedicação, confiança e disponibilidade para transferência constante de conhecimentos sobre maturação orgânica a geologia regional. Todo este trabalho de doutoramento não teria existido sem o seu planeamento e concepção do plano de trabalhos inicial. Todos os momentos passados em conjunto foram extremamente enriquecedores. Desde já o meu grande obrigado e espero que ter estado à altura das expectativas criadas, desejando muito mais trabalho conjunto no futuro.

Ao Doutor David Chew o muito obrigado pela aceitação em ser meu orientador, pela sua permanente disponibilidade, paciência, atenção e troca de conhecimentos. O seu pragmatismo carregado de confiança permitiram ultrapassar as situações mais adversas quando tudo parecia perdido. Sem o seu auxilio e clareza, o planeamento inicial não teria sido tão eficaz.

Ao Doutor Raul Jorge pela amizade e disponibilidade tanto para o trabalho de campo e laboratorial como para longos debates e esclarecimento sobre as dúvidas que iam surgindo. Um muito obrigado por tudo.

Durante todo o período dos trabalhos de doutoramento, muitas foram as pessoas que me ajudaram de várias maneiras e às quais gostaria de deixar uma palavra sincera de agradecimento, nomeadamente:

Um especial agradecimento à Doutora Zélia Pereira e ao Doutor Narciso Ferreira do LNEG de São Mamede de Infesta pela utilização dos seus laboratório e pela hospitalidade e carinho durante as estadias no Porto. Mais a sul, no LNEG de Beja, ao Doutor João Matos pela preciosa informação sobre os afloramentos e disponibilidade para localizar e facilitar as amostras num labirinto de sondagens.

Durante as longas estadias em Dublin, o acolhimento, preocupação e interesse demonstradas pelo Doutor Geoof Clayton foram de grande conforto. Nos laboratórios, o "terror" e ajuda prestada pelo Frank foram de estrema importância. Para ambos, muito obrigado.

Ao Doutor Fin Stuart e à Doutora Luigia pela disponibilidade em me receberem no SUERC, em Glasgow, e apresentarem-me aos "deuses" do Hélio, abrindo-me assim uma porta para um mundo misterioso. Pela paciência, compreensão a extrema atenção prestada, apesar do caos laboratorial provocado, um muito obrigado

Durante este percurso existiram muitos momentos bons, e outros menos bons, nos quais tive sempre a companhia de muitos colegas e amigos que me apoiaram. Felizmente foram muitos, e, cada um à sua maneira, tiveram um papel importante neste trabalho. Sem a vossa ajuda teria sido muito mais difícil. Muito obrigado a todos!

Obrigado a toda a minha família pelo o apoio incondicional desde sempre. Em particular à minha mãe pelas longas e árduas horas a processar uma quantidade enorme de amostras para que eu conseguisse ter tudo feito dentro do período estabelecido.

Por último, este trabalho não teria sido possível sem o apoio financeiro da Fundação para a Ciência e Tecnologia, através da bolsa de doutoramento com a referência SFRH/BD/62213/2009 e do Centro de Investigação Marinha e Ambiental (CIMA) da Universidade do Algarve.

INDEX

RESUMO……8
ABSTRACT……..……..……12
I-INTRODUCTION..... 13
1.1 OBJECTIVES..... 14
1.2 METHODOLOGY 14
1.3 THESIS STRUCTURE..... 15
1.4 SCIENTIFIC PUBLICATIONS..... 15
1.4.1 Publications in peer review journals..... 16
1.4.2 Publications in congress..... 16
II–GEOLOGICAL SETTING AND SAMPLING 18
2.1 GEOLOGICAL SETTING..... 18
2.1.1 Ossa Morena Zone..... 18
2.1.2 South Portuguese Zone..... 20
2.1.3 Permian Viar Basin..... 24
2.1.4 Algarve Basin..... 25
2.1.5 Monchique Alkaline Complex..... 26
2.2 PREVIOUS WORK IN THE STUDIED AREA..... 27
2.2.1 Maturation studies..... 27
2.2.2 Low-temperature thermochronology studies..... 29
2.2.3 Previous provenance studies on the Baixo Altentejo Flysch Group..... 30
2.3.2 Provenance studies on Upper Triassic Silves Sandstones in Algarve Basin 31
2.3 SAMPLING..... 31
2.3.1 Organic Maturation Sampling..... 32
2.3.2 Sampling for low-temperature thermochronology, geochronology and provenance studies 34
2.3.3 Borehole Samples 37
III–FUNDAMENTALS OF APPLIED TECHNIQUES 38
3.1 VITRINITE REFLECTANCE..... 38
3.3 LOW-TEMPERATURE THERMOCHRONOLOGY: APATITE (U-Th)/He 42
3.4 U-Pb GEOCHRONOLOGY..... 43
IV–VITRINITE REFLECTANCE ANALYSES 45
4.1 SAMPLING..... 45
4.2 SAMPLE PROCESSING 45
4.3 VITRINITE REFLECTANCE RESULTS AND MODELATION..... 48
4.3.1 Borehole results 48
4.3.2 Results from Outcrop Samples 49
4.4 SUMMARY..... 54
V–APATITE FISSION TRACK ANALYSES 56
5.1 SAMPLES..... 56
5.2 HEAVY MINERAL SEPARATION AND APATITE CONCENTRATION..... 56
5.3 SAMPLE PREPARATION FOR APATITE FISSION TRACK ANALYSES 56
5.4 APATITE FISSION TRACK MEASUREMENTS..... 58
5.5 APATITE U AND - ICPMS ANALYTICAL TECHNIQUE 59
5.6 APATITE FISSION TRACK RESULTS..... 61
5.6.2 FT results from the Baixo Alentejo Flysch Group samples..... 64
5.6.2.1 Mértola Fm. samples..... 64
5.7 SUMMARY..... 71
VI–APATITE (U-Th)/He AGE ANALYSES 72

6.1 SAMPLE PREPARATION AND ANALYTICAL PROCEDURES 72
6.2 APATITE (U-Th)/He AGES RESULTS 73
5.3 DISCUSSION AND SUMMARY 73
VII–U-Pb ZIRCON AND APATITE GEOCHRONOLOGY 75
7.1 SAMPLE SELECTION AND PREPARATION 75
7.2 ZIRCON ICPMS ANALYTICAL TECHNIQUE 75
7.3 APATITE ICPMS ANALYTICAL TECHNIQUE 76
7.4 ZIRCON U-PB GEOCHRONOLOGY RESULTS 78
7.4.1 South Portuguese Zone 78
7.4.1.1 Mértola Formation 78
7.4.1.2 Mira Formation 79
7.4.1.3 Brejeira Formation 79
7.5 APATITE U-Pb GEOCHRONOLOGY RESULTS 81
7.5.2 South Portuguese Zone 82
7.5.2.1 Mértola Formation 82
7.5.2.2 Mira Formation 82
7.5.2.3 Brejeira Formation 82
7.5.3 Algarve Basin 82
7.5.4 Monchique Alkaline Complex 83
7.6 DISCUSSION AND INTERPRETATION OF RESULTS FROM THE OSSA-MORENA SAMPLES 84
7.7 SOUTH PORTUGUESE ZONE DISCUSSION AND INTERPRETATION OF RESULTS 85
7.8 DISCUSSION AND INTERPRETATION OF THE UPPER TRIASSIC SANDSTONES OF THE ALGARVE BASIN 91
7.9 SUMMARY 92
VIII–FORWARD AND INVERSE MODELING OF LOW-TEMPERATURE THERMOCHRONOMETER DATA 94
8.1 FORWARD AND INVERSE MODELING PRINCIPLES 94
8.2 FORWARD AND INVERSE MODELING RESULTS 95
8.2.1 Ossa Morena Zone 95
8.2.1.1 Sample PIAS 1 95
8.2.1.2 Sample LP1 97
8.2.2 South Portuguese Zone - Mértola Formation (Sample CST4) 98
8.2.3 Monchique Alkaline Complex (MM1) 100
8.3 SUMMARY 102
IX–APATITE REE AS PROVENANCE INDICATOR 103
9.1 REE IN APATITE 103
9.2 APATITE REE RESULTS 104
9.2.1 Ossa Morena (PIAS1, LP1) 106
9.2.2 South Portuguese Zone 107
9.2.2.1 Mértola Formation (FM1, CST1-4, OL1, CT1-13) 107
9.2.2.2 Mira Formation (AO1, SC1) 108
9.2.2.3 Brejeira Formation (AR1) 109
9.2.3 Algarve Basin (CM1, QR1, TL1) 109
9.2.4 Monchique Alkaline Complex (MM1, MMP1) 110
9.3 SUMMARY 111
X–CONCLUSIONS 112
10.1 THERMAL HISTORY 112
10.2 GEOCHRONOLOGY AND MINERAL PROVENANCE 114

10.3 IMPLICATION IN ECONOMICAL GEOLOGY 115
10.4 SUGESTIONS FOR FUTURE WORKS 116
REFERENCES 117

RESUMO

Com objetivo de reconstruir a história térmica da Zona Sul Portuguesa e da Bacia do Algarve foi realizado um estudo sistemático com auxílio de três metodologias complementares: medição da reflectância da vitrinite, datações de traços de fissão e de datações (U-Th)/He de apatites. A vitrinite é um grupo de maceral que deriva das paredes celulares ou dos tecidos lenhosos de plantas, e que é bastante abundante em rochas sedimentares, em particular em margas e xistos argilosos. A reflectância da vitrinite é sensível à temperatura num processo irreversível, ou seja, indica a temperatura máxima a que uma rocha sedimentar esteve sujeita durante a diagénese, sendo um excelente indicador da maturação das rochas fonte de hidrocarbonetos. Para esse efeito, foram recolhidas sessenta e cinco amostras de rochas de afloramentos do Grupo do Flysch do Baixo Alentejo, da Bacia do Algarve e da Bacia de Viar. Foram ainda recolhidas dez amostras em dois furos de prospecção mineira que interceptaram a Formação de Mértola do Grupo do Flysch do Baixo Alentejo. As litologias selecionadas foram xistos argilosos, margas e argilitos. Os traços de fissão são defeitos criados na estrutura cristalina dos cristais devido ao decaimento por fissão espontânea do ^{238}U. Os traços de fissão ficam preservados no cristal quando a temperatura ambiente das rochas permanece abaixo da temperatura de *annealing* ("*reset*"), que no caso da apatite se situa entre os 60 e os 120ºC, dependendo entre outros, do conteúdo em Cl. Medindo os traços de fissão e determinando o conteúdo dos diferentes isótopos de U, é possível determinar o período em que o cristal, e consequentemente toda a rocha, terá permanecido sob temperaturas inferiores à de *annealing*. Já as datações pelo método (U-Th)/He consistem nas medições dos isótopos ^{4}He, U e Th presente em cada cristal. À semelhança dos traços de fissão, estas idades vão sendo progressivamente "apagadas" com o aquecimento, ocorrendo o *reset* total aproximadamente aos 75ºC nos minerais de apatite.

No sentido de inferir sobre a proveniência das formações do Grupo do Flysch do Baixo Alentejo e do Triásico da Bacia Algarvia, foram obtidos dados U-Pb e de elementos traços (REE) de zircões e apatites através de ablasão a laser no departamento de Geologia do Trinity College Dublin, Irlanda.

Para os estudos de termocronologia de baixa temperatura, geocronologia e proveniência sedimentar, foram recolhidos um total de cinquenta e cinco amostras de rochas de afloramentos da Ossa Morena, Zona Sul Portuguesa e da Bacia Algarvia. Outras doze

amostras foram recolhidas de dois furos de prospecção mineira localizados na Zona Sul Portuguesa.

No que se refere à história térmica, as paleotemperaturas calculadas a partir da reflectância da vitrinite para as amostras do Grupo do Flysch do Baixo Alentejo, situam-se entre os 236 e os 326ºC. A paleotemperatura mais elevada (414ºC) desta unidade foi registada no contacto com Complexo Alcalino intrusivo de Monchique. As idades de traços de fissão indicaram que o teor em Cl das apatites mostrou ter uma forte influência sobre as idades obtidas. Todas as amostras do Grupo do Flysch do Baixo Alentejo sofreram o "reset" após a deposição, apresentando idades Cretácicas (111-59,9 Ma) e uma única idade do Jurássico superior (amostra OL1-157,9 Ma). As idades dos traços de fissão das amostras recolhidas em litologias da Zona Ossa Morena e da Zona Sul Portuguesa indicam que exumação deve ter ocorrido como um bloco contíguo nestas duas zonas tectonoestratigráficas. Através da modelação térmica foi possível constatar que as amostras da Zona Ossa Morena (Pias1 e PL1) apresentam um arrefecimento lento a moderado até aos 240 Ma, seguindo-se um arrefecimento rápido durante o Triásico até aproximadamente à temperatura de retenção parcial da apatite aos 200 Ma. Uma última fase de arrefecimento gradual iniciou-se no granito Pias aos 65 Ma até que fosse atingida uma temperatura superficial. A taxa de exumação estimada para o granito de Pias é de 30 m/Ma desde os 65 Ma até ao presente. Na amostra do granito de El Pedroso, a última fase de arrefecimento iniciou-se às 35 Ma. Desde então até o presente foi inferida uma taxa de exumação de 65m/Ma.

A modelação inversa efetuada na amostra (????) da Formação de Mértola do Grupo do Flysch do Baixo Alentejo da Zona Sul Portuguesa, apresenta um episódio de aquecimento após a subsidência que se encontra relacionado com a ultima fase da tectónica Varisca. Depois de ter sido atingida a temperatura máxima de 300°C aos 320 Ma, a amostra arrefeceu até uma temperatura de 150 °C aos 260 Ma. Dos 260 Ma até aos 20 Ma, a amostra permaneceu na zona de retenção parcial da apatite. Esse longo período a uma temperatura constante pode estar relacionado a uma possível re-subsidência associada à deposição de sedimentos mesozóicos da Bacia do Algarve, pois a amostra localiza-se próximo do contacto entre estas duas unidades geológicas. Dos 20 Ma até à atualidade pode ser inferida uma taxa de exumação de 75m/Ma

Na Bacia do Algarve os valores poder refletor da vitrinite medidos para as unidades do Triásico situam-se entre os 1-1,1%Rr, correspondendo a paleotemperaturas entre os 148 e 158ºC. No caso das litologias do Cretácico inferior (0,6%Rr), na parte ocidental da Bacia do

Algarve, as paleotemperaturas máximas não foram suficientes para fazer o *reset* do sistema de traços de fissão da apatite. No entanto, as amostras recolhidas na Praia da Luz, perto do contato com a intrusão básica da Ponta das Ferrarias, indicam que o efeito térmico desta intrusão é intenso mas restrito a uma distância máxima de cerca de 2 km do contato com o corpo magmático intrusivo. A modelação térmica realizada para as margas do Cretácico Inferior em contacto e para diferente distâncias da intrusão, sugere uma temperatura máxima de 275ºC alcançada pelas amostras mais perto do contacto intrusivo e que estas arrefeceram para uma temperatura ca. 100ºC em apenas 10 000 anos.

As idades de traços de fissão da apatite obtidas nas amostras de arenitos do Triásico Superior da Bacia Algarvia, são mais antigas do que a idade de deposição, o que significa que as amostras não sofreram o *reset* total. Assim, a anomalia térmica criado pela intrusão Complexo Alcalino de Monchique foi muito circunscrita a uma zona perto do contato não afetando significativamente os processos térmicos de maturação regional da Bacia do Algarve. No entanto, os efeitos térmicos de pequenas intrusões relacionadas com o Complexo Alcalino de Monchique na Bacia do Algarve não poderão ser totalmente negligenciados.

Através da modelação térmica do Complexo Alcalino de Monchique foi possível verificar que este arrefeceu rapidamente desde temperaturas magmáticas (> 600ºC) para cerca de 70°C, temperatura das rochas encaixantes no momento da intrusão, num curto espaço de tempo (3 Ma). Se considerarmos um gradiente geotérmico normal, o Complexo Alcalino de Monchique deverá ter-se instalado a cerca de 2 km de profundidade. Desde os 69 aos 5 Ma o CAM permaneceu a uma temperatura constante próximo da temperatura de retenção parcial da apatite. Dos 5 Ma até à atualidade as amostras arrefeceram desde os 50ºC até à temperatura superficial, podendo ser inferida uma taxa de exumação de 0,3km/Ma dos 5 Ma até ao presente.

A geocronologia de zircões e apatites detríticas, bem como o conteúdo em elementos Terras Raras das apatites, permitiram inferir sobre a sua origem sedimentar. Verificou-se que os espectros de idades U-Pb de zircões detríticos e também as idades ^{207}Pb corrigidas do Grupo do Flysch do Baixo Alentejo apresentaram diferenças significativas entre as formações de Mértola/Mira e da Formação Brejeira. Mais concretamente, os espectros de idades U-Pb dos zircões detritícos das formações de Mértola e Mira indicam ambas uma proveniência extrabasinal (Zona Ossa-Morena) e intrabasinal (Zona Sul Portuguesa). A abundância de zircões detríticos nos intervalos 500-750 Ma e 900-1100 Ma na Formação Brejeira, sugerem uma área fonte com origem nos terrenos da Avalónia-Meguma, com uma menor reciclagem

do Domino Sul Português (Formação Tercenas). Já os arenitos do Triásico da Bacia Algarvia têm origem em múltiplas fontes, onde zircões detríticos com idades U-Pb pérmicas estão mais presentes na parte oriental da bacia, o que pode refletir uma contribuição local de bacias Pérmico-Triásicas existentes em Espanha, e.g. a Bacia de Viar.

Como complemento foram ainda datados dois granitos da Zona da Ossa Morena (granito de Pias e El Pedroso) que forneceram idades corrigidas de ^{207}Pb em apatite de 334,9±4,3 Ma para o granito de Pias-Pedrogão e de 340,5±7.6Ma para o granito de El Pedroso, caindo os dois granitos no intervalo de idades dos corpos plutónicos do Carbonífero da Ossa-Morena Zona definidos por Salman (2004).

As informações sobre a história térmica resultante deste estudo podem ter um impacto sobre o potencial económico para exploração de gás convencional e não convencional na Zona Sul Portuguesa. Os valores do poder refletor da vitrinite medidos nas amostras da Zona Sul Portuguesa correspondem a uma temperatura máxima entre os 236 e 326ºC. Estas temperaturas foram atingidas após a subsidência e durante a deformação tectónica. A deformação foi seguida de uma fase de arrefecimento relacionada com uma fase de exumação até aos 200 Ma. Os hidrocarbonetos gerados após a deposição devem ter sido libertados durante esse período. Dos 200 Ma até aos 20 Ma a temperatura permaneceu constante entre os 100 e os 60°C, no entanto as rochas já se encontravam sobrematuras em relação as fases de geração de hidrocarbonetos. A exumação pronunciada que se fez sentir no sul do território Português desde o Cretácico Superior pode ter destruído qualquer sistema petrolífero existente. No entanto, a história deposicional e térmica na parte da Bacia Algarvia localizada no offshore poderá ter sido diferente, pelo que estudos mais estudos e mais detalhados serão necessários para se compreender o potencial total da Bacia Algarvia.

Palavras-chave: Zona Sul Portuguesa, Bacia Algarvia, Traços de fissão da apatite, poder refletor da vitrinite, datações (U-Th)/He, zircões detríticos, proveniência sedimentar.

ABSTRACT

Organic maturation levels (vitrinite reflection) were combined with low-temperature thermochronometers (apatite fission track analysis and (U-Th)/He in apatite) to construct temperature-time paths for the Upper Palaeozoic rocks of the South Portuguese Zone and the Mesozoic rocks of the Algarve Basin. Detrital zircon ages were also studied in order to constrain the sedimentary source regions and basin fill history of the Baixo Alentejo Flysch Group from South Portuguese Zone and the Upper Triassic sandstones from the Algarve Basin. The maximum temperature attained in the South Portuguese Zone was 326 ºC and occurred at 320 Ma. All the samples from the South Portuguese Zone have been totally reset after deposition and yield apatite fission track ages ranging from the Cretaceous (111 to 59.9 Ma) to the Upper Jurassic (157.9 Ma). The fission track ages from the Upper Triassic sandstone did not reset after de deposition, however, the intrusion of the Monchique Alkaline Complex (MAC) and related swarm of dikes had local influence upon organic maturation.

Inverse modelling on apatite samples from the MAC indicate that it cooled very fast from initial magmatic temperatures to around 70ºC. The rock sample studied stayed at a constant temperature close to the top of the apatite partial annealing zone from 68.7 Ma to 5 Ma. Since 5 Ma until the present the MAC underwent an exhumation of ca. 300 m/Ma.

The U-Pb detrital zircon and apatite ages from the Mértola and Mira formations suggest sedimentary provenance areas from a detrital intrabasinal source (South Portuguese Zone) and from areas associated with the magmatic arc related rocks located at the southern border of the Ossa Morena Zone. The U-Pb detrital zircon ages obtained for the Brejeira Formation suggest a source area related to the Avalonian/Meguma terranes and also from recycled clastic sediments associated to the South Portuguese Domain. The ages from the Algarve Basin Upper Triassic sandstones suggest that they are derived from multiple sources terranes with Permian zircons ages more abundant in the samples located in the eastern part of the basin.

Key-Words: South Portuguese Zone, Algarve Basin, Apatite Fission tracks, vitrinite reflectance, (U-Th)/He datations, detrital zircons, sedimentary provenance.

I - INTRODUCTION

Low-temperature thermochronology is widely used to determine the cooling histories of crustal rocks and to constrain the timing and rates of exhumation processes. Information on the maximum temperature reached by a sedimentary rock can be obtained from vitrinite reflectance that is the most reliable indicator of thermal maturation in sedimentary rocks, as the chemical reactions which control the increase of reflectance in vitrinite are irreversible. Therefore, vitrinite reflectance can be considered as a non-retrogressive palaeogeothermometer for diagenetic and low-grade metamorphic conditions. Despite the large amount of research that has been undertaken on the South Portuguese Zone and the Algarve Basin, the thermal history is not well constrained. The timing and duration of burial and cooling events is still unknown or misunderstood. Combining low-temperature thermochronometers and vitinite reflectance will allow the identification and characterisation of the major episodes of heating and cooling which have affected the Variscan basement of the South Portuguese Zone, in particular the Baixo Alentejo Flysch Group, and the Meso-Cenozoic sedimentary sequences of the Algarve Basin.

The sedimentary provenance of the Baixo Alentejo Flysch Group from South Portuguese Zone and from the basal unit of the Algarve Basin, namely the Upper Triassic Silves Sandstones, remains shrouded in controversy. The detrital record of sedimentary basins that occur adjacent to tectonic terranes with distinct tectono-thermal histories can be used to discriminate their original source area(s). For instance, the U–Pb ages of individual detrital zircon and apatite grains are commonly used in sedimentary provenance analysis providing a reliable guide to the ages of basement source and can be integrated with other techniques such as petrographic studies and geochemical data. In this way, several samples were dated by the U-Pb detrital zircon and apatite method in the Baixo Alentejo Flysch Group and in the Algarve Basin to better constrain its sedimentary sources.

This research had a duration of 48 months and was supported by the Foundation of Science and Technology (FCT) through a PhD Grant (reference number SFRH/BD/62213/2009).

1.1 OBJECTIVES

The propose objectives of this research project are:

- Assess the maximum palaeotemperatures attained by the Baixo Alentejo Flysch Group of South Portuguese Zone and Algarve Basin using vitrinite reflectance (VR);
- Establish the timing and duration of cooling after peak metamorphism by using multiple low-temperature thermochronological techniques;
- Infer the magnitude and timing of crustal exhumation based on vitrinite reflectance and low temperature thermochronometry;
- Integrate these data (vitrinite reflectance and low temperature thermochronometry) to reconstruct the burial and exhumations histories of Baixo Alentejo Flysch Group of South Portuguese Zone and Algarve Basin;
- Use these results to assess the potential of offshore petroleum systems in terms of the timing of source organic maturation and tectonic history of potential reservoirs;
- Investigate the influence of apatite mineral composition on fission track and (U-Th)/He data and to integrate these techniques with VR data;
-Investigate the REE apatite composition as a provenance host rock indicator;
-Investigate the provenance of the Baixo Alentejo Flysch Group and the Upper Triassic Silves Sandstones from the Algarve Basin based on their U-Pb detrital zircon and apatite age spectra.

1.2 METHODOLOGY

A detailed description of the analytical methods employed in this study will be described in each respective chapter. As it was impossible to prepare and analyse all the samples in the same research institution, it was necessary accomplish the tasks in different locations. The sample preparation for organic maturation analyses was fully processed in the laboratory facilities of University of the Algarve (UAlg). The heavy mineral separation was undertaken at the University of the Algarve (UAlg), at the Departamento de Geologia da Faculdade de Ciências of Lisbon University (DG/FCUL) and at the Department of Geology, Trinity College Dublin. All the fission track and U-Pb measurements were undertaken at the Department of Geology, Trinity College Dublin. The (U-Th)/He analyses were performed in the laboratories of the Scottish Universities Environmental Research Centre (SUERC), in Glasgow.

1.3 THESIS STRUCTURE

This thesis is structured in the following way:

Chapter I presents an introduction to the thesis including its objectives and its structure.

In chapter II the regional geological setting of the study region is presented along with a summary of previous research. In this chapter the sampling strategy is also presented.

The main techniques used in this research (vitrinite reflectance, thermochronology (apatite fission track and (U-Th)/He) and geochronology (detrital zircon and apatite U-Pb) are described in chapter III.

In chapter IV the methodology used for maturation studies and the results of vitrinite reflectance measurements are presented and discussed.

The apatite fission track methodology and respectively results are presented and discussed in chapter V. The following chapter (chapter VI) will be dedicated to the apatite (U-Th)/He dating and its interpretation (taking into account the results obtained in chapter V).

In chapter VII the detrital zircon and apatite U-Pb ages are presented. The detrital zircon and apatite ages will be used as provenance indicators and discussed in the context of the geodynamic evolution of the South Portuguese Zone and the development of the Algarve Basin.

Based on the results obtained in the previous chapters some of the data were modelled using forward and inverse modelling approaches. The results of the modelling are described and discussed in chapter VIII. When possible, this study combines apatite fission track analysis and apatite (U-Th)/He dating to construct temperature-time paths for the South Portuguese Zone and the Algarve Basin.

In chapter IX is presented the apatite REE compositions and its use as provenance indicator is discussed.

Chapter X is dedicated to the conclusions of this research project.

1.4 SCIENTIFIC PUBLICATIONS

During this PhD, the results were published in peer review journals and in congress abstracts. A short publications list is provided below.

1.4.1 Publications in peer review journals (annex I)

- **Rodrigues**, B., Chew, D., Jorge, R.C.G.S., Fernandes, P, Oliveira, J.T. Veiga-Pires, C. (submitted). Detrital zircon geochronology of the Carboniferous Baixo Alentejo Flysch Group (South Portugal) - constraints on the provenance and geodynamic evolution of the South Portuguese Zone;

- Fernandes, P., **Rodrigues, B.,** Matos, V., Borges, M., Clayton, G. (*2012*) Organic maturation of the Algarve Basin (southern Portugal) and its bearing on thermal history and hydrocarbon exploration. Marine and Petroleum Geology. doi: 10.1016/j.marpetgeo.2013.06.015;

- Jorge, R., Fernandes, P., **Rodrigues, B.**, Pereira, Z., Oliveira, J (2013) Geochemistry and provenance of the Carboniferous Baixo Alentejo Flysh Group, South Portuguese Zone. Sedimentary Geology 284-285, 133-148 pp. doi:10.1016/j.sedgeo.2012.12.005;

- Fernandes, P. , Musgrave, J., Clayton, G., Pereira, Z., Oliveira, J. , Goodhue, R. , **Rodrigues, B.** (2012) New evidence concerning the thermal history of Devonian and Carboniferous rocks in the South Portuguese Zone. Journal of the Geological Society, 647-654 pp. doi:10.1144/jsg2011-156;

- **Rodrigues, B.**, Dias, P., Jorge, R.C.G.S., Fernandes, P. (2011) Geochemical Signatures in Detrital Tourmalines as Indicators for Sediment Provenance: The Baixo Alentejo Flysch Group, South Portuguese Zone . Mineralogical Magazine, Vol. 75 (3), 2011 p. 1740.

1.4.2 Publications in congress (abstracts and oral communications)

- **Rodrigues, B.**, Fernandes, P., Chew, D., Jorge, R.C.G.S., Fernandes, P. (2013) História térmica do Grupo do Flysch do Baixo Alentejo. 9ª Conferência Anual do GGET/SGP (Grupo de Geologia Estrutural e Tectónica da Sociedade Geológica de Portugal, Estremoz, pp.97-10;

- **Rodrigues, B.**, Fernandes, P., Chew, D., Jorge, R.C.G.S., Fernandes, P., Veiga-Pires, C., Oliveira, J.T. (2013) Geocronologia de zircões detríticos do Grupo do Flysch do Baixo Alentejo – contributos para a proveniência e geodinâmica da Zona Sul Portuguesa**.** 9ª Conferência Anual do GGET/SGP (Grupo de Geologia Estrutural e Tectónica da Sociedade Geológica de Portugal, Estremoz, pp.101-103;

- **Rodrigues, B.**, Fernandes, P., Chew, D., Jorge, R. (2012) Termocronologia de Baixa Temperatura do Sul de Portugal. 46º Congresso Brasileiro de Geologia e 1º Congresso de Geologia dos Países de Língua Portuguesa, Santos - SP, Brasil, Anais do congresso ref. PAP010709;

- Fernandes, P., Matos, V., **Rodrigues, B.**, Borges, M., Clayton, G. (2012) Maturação orgânica da Bacia Mesozoica Algarvia (SUl de Portugal) - Implicações para a exploração de hidrocarbonetos. 46º Congresso Brasileiro de Geologia e 1º Congresso de Geologia dos Países de Língua Portuguesa, Santos - SP, Brasil, Anais do congresso ref. PAP009773;

- **Rodrigues, B**., Fernandes, P., Matos, V., Borges, M., & Clayton, G. (2012) The thermal history of the Mesozoic Algarve Basin (South Portugal) and its implication for hydrocarbon exploration. Third Central & North Atlantic Conjugate Margins Conference Trinity College Dublin, 22-24 August 2012, Abstracts volume, pp. 83-84.

II – GEOLOGICAL SETTING AND SAMPLING

The geological setting of the studied area, sampling strategy and sample descriptions are presented in this chapter.

2.1 GEOLOGICAL SETTING

The study area covers a large geographical region from the western and southern Atlantic coast (Fig. 2.1), as far east as Seville parallel and as far north as Beja. The following section briefly describes the geological evolution of the sampling localities.

Figure 2.1 Geographic location of the studied area. The inlet boxes show the location of the geologic maps in figures 2.2 (A), 2.3 (B) and 2.4 (C).

2.1.1 Ossa Morena Zone

The Ossa Morena Zone (OMZ) is one of the major tectonostratigraphic units of the Iberian Variscan Belt. It is composed of folded, thrusted and metamorphosed rocks of Precambrian and Palaeozoic age and abundant intrusive bodies emplaced before and during the Variscan orogenic cycle (Antunes, 2006).

In the Portuguese part of the Ossa Morena Zone several sectors with distinct stratigraphy and structure have been identified and these have been subdivided into different tectonostratigraphic units, also termed "sectors" or "domains" (Carvalho *et al.*, 1971; Delgado

et al., 1977; Apalategui *et al.*, 1990; Oliveira *et al.*, 1991). They are from north to south: Blastomylonitic Belt Sector; Alter do Chão-Elvas Sector; Estremoz-Barrancos Sector; Montemor-Ficalho Sector; Évora Massif; Beja Igneous Complex and the Beja Acebuches Ophiolite complex. The Blastomylonitic Belt Sector in the north and the Beja Acebuches Ophiolite complex at the south of the Ossa Morena Zone are considered to be two orogenic sutures and thus the limits of the Ossa Morena Zone are defined based on the presence of basic igneous rocks with oceanic affinities (Azor, 2004; Pérez-Estaún *et al.*, 2004). The Ossa Morena Zone is not the main subject of this study and a reader is advised to consult the referenced authors for more detailed information.

Regarding the evolution of the OMZ, it commenced with the erosion of the Cadomian chain in late Proterozoic times, when a large Lower Cambrian carbonate platform built up over a large area (Oliveira *et al.*, 1991). Extensional tectonism during the Marianian (Lower Cambrian) generated tholeitic basic volcanics and several sedimentary depocenters, which were rapidly filled up with sediments during a Middle Cambrian marine regression. During the Middle Cambrian, a renewed pulse of extensional tectonism led to the development of sedimentary basins that filled up with terrigenous sediments, alkaline basalts and minor peralkaline volcanics. Tectonic blocks generated during this extensional phase were rotated and uplifted leading to the karstification of the Lower Cambrian carbonates (Oliveira *et al.*, 1991). The Ordovician sedimentary rocks are usually terrigenous and fine grained with interbedded alkaline basalts and rest unconformably on the Middle Cambrian sediments, indicating an upper Cambrian depositional hiatus (Oliveira *et al.*, 1991). At the top of the Ordovician sediments occurs an extensive shallow water sandstone unit, which is associated with a polygenic conglomerate. In early Devonian times sedimentation was dominated by shallow-water terrigenous and carbonate sediments. During the Middle Devonian, uplift of the OMZ took place as a consequence of subduction to the south. The Late Devonian and Early Carboniferous were marked by oblique collision between the OMZ and the South Portuguese Zone, characterized by obduction in the SE and subduction in the NW (Oliveira *et al.*, 1991).

Magmatic activity related to the Variscan orogenic cycle is represented by volcanic and plutonic rocks with ages clustered in the age interval 345-280 Ma (e.g. Pinto, 1987; Sánchez-Carretero *et al.*, 1990; Dunning *et al.*, 2002; Salman, 2004). According to their relationships with respect to the main Variscan tectonic events, the Variscan granitoids are generally subdivided into two groups: syn-tectonic and late/post-tectonic (Antunes, 2006).

2.1.2 South Portuguese Zone

The northern boundary of the South Portuguese Zone with the Ossa Morena Zone is defined by the Beja Acebuches Ophiolite which is interpreted as a remnant of the Rheic Ocean that separated the Euramerican South Portuguese Zone from the Ossa Morena Zone (Oliveira 1990; Quesada *et al.,* 1994; Oliveira & Quesada, 1998; Braid *et al.,* 2011; Oliveira *et al.,* 2013a).

The South Portuguese Zone is divided into four domains (Oliveira, 1990; Ribeiro *et al.,* 1990), which are from NE to SW, the Pulo do Lobo Antiform, the Pyrite Belt, the Baixo Altentejo Flysch Group and the Southwest Portugal Domain (Fig. 2.2).

The Pulo do Lobo Antiform has been interpreted as representing an exhumed suture zone or accretionary prism that records the final stages of the closure of the Rheic Ocean and the terminal collision between Gondwana and Laurussia (e.g. Eden, 1991; Onézime *et al.* 2003; Oliveira *et al*., 2013b). The Pulo do Lobo Formation crops out in the core of the Pulo do Lobo Antiform and consists of highly deformed phyllites and quartzites with intercalations of amphibolites of mid-ocean ridge basalt (MORB) affinity in the lower parts of the sequence (Munhá, 1983). U-Pb detrital zircon data from the quartzites suggest a maximum depositional age of 438 Ma (Silurian) for this formation (Braid *et al.,* 2011). Flysch-type successions crop out on the northern and southern flanks of the Pulo do Lobo Antiform. These rocks are dated by palynomorphs as Frasnian to late Famennian in age (Pereira *et al.,* 2006, 2008).

The Iberian Pyrite Belt succession consists of phyllites and quartzites of the Phyllite Quartzite Group overlain by volcanic and sedimentary rocks of the Volcano-Sedimentary Complex (Oliveira, 1990). Palynomorphs in the uppermost part of the Phyllite Quartzite Group indicate a Late Devonian (Strunian) age (Pereira *et al.,* 2008). The Iberian Pyrite Belt volcanism resulted from a local phase of extensional tectonism and is bi-modal in composition with the felsic component dominant (Munhá, 1983, 1990; Mitjavila *et al.*, 1997). The Iberian Pyrite Belt rocks are dated as Late Devonian to late Viséan (382.7-330 Ma) based on palynomorphs and rare conodont assemblages (Boogaard, 1963, 1967; Oliveira *et al.,* 2004; Pereira *et al.,* 2007, 2008). Zircons extracted from felsic volcanic rocks yield U-Pb ages ranging from 349 to 385 Ma (Nesbit *et al*., 1999; Barrie *et al*., 2002; Dunning *et al*., 2002; Rosa *et al.*, 2009; Oliveira *et al.,* 2013a).

The Baixo Altentejo Flysch Group represents the development of a foreland basin that formed as a result of an oblique collision between the South Portuguese Zone and the Ossa Morena Zone, with associated tectonic stacking that propagated from the NE to SW (Oliveira *et al.,* 1979; Oliveira, 1990; Silva *et al.,* 1990; Pereira, 1997, 1999). The Baixo Alentejo Flysch Group comprises three formations that are, from oldest to youngest, the Mértola, Mira and Brejeira formations (Fig. 2.2). These units are dated as late Viséan (345-326 Ma), Serpukhovian to early Bashkirian (326-315 Ma), and late Bashkirian to late Moscovian (315-307 Ma) respectively (Oliveira *et al.,* 1979; Korn, 1997; Pereira, 1999; Pereira *et al.,* 2006, 2008). The Mértola Formation comprises beds of greywacke of variable thickness interbedded with shales, siltstones, conglomerates and rare mudflows, with the greywacke beds exhibiting sedimentary structures typical of turbidites (Oliveira & Wagner Genthis, 1983). The average modal composition of greywackes from the Mértola Formation is $Qt_{46.2}F_{26.9}L_{26.19}$, where Qt is the modal abundance of quartz, F is the modal abundance of feldspar and L is the sum of all lithic fragments (Jorge *et al.,* 2013). The Mira Formation is comprised of greywackes interbedded with shales and rare conglomerates (Oliveira *et al.,* 1979). The average modal composition of the greywackes from the Mira Formation is $Qt_{61.7}F_{7.6}L_{30.7}$ (Jorge *et al.,* 2013). The overlying Brejeira Formation is divided into two distinct belts that were recognized during regional geological mapping (Oliveira *et al.,* 1979; Oliveira & Wagner Genthis, 1983). The basal beds consist of quartzites and quartz-wackes interbedded with shales while the younger belt consists of immature greywackes interbedded with shales. The average modal composition of greywackes from the Brejeira Formation is $Qt_{83.1}F_{6.7}L_{10.1}$. Abundant quartz grains are rounded to sub-rounded and well sorted (Jorge *et al.,* 2013). The clastic lithologies in this formation contain abundant clasts of sedimentary rocks and metamorphic quartz but are poor in volcanic fragments (Oliveira & Wagner Genthis, 1983; Jorge *et al.,* 2013). The Mira and Brejeira formations are interpreted as the result of progressive progradation of turbiditic sedimentation towards the SW (Oliveira & Wagner Genthis, 1983; Oliveira, 1990).

The Southwest Portugal Domain succession comprises Late Devonian quartzites and shales of the Tercenas Formation followed by a mud-dominated carbonate platform sequence of the Carrapateira Group which ranges in age from the Tournaisian to the late Bashkirian (358.9-315.2 Ma) (Pereira, 1999). A recent U-Pb detrital zircon study from the Tercenas Formation quartzites confirms a maximum depositional age of Late Devonian (367±6.4 Ma) for this formation (Pereira *et al.,* 2012).

Late Palaeozoic palaeotectonic reconstructions suggest that the South Portuguese Zone was part of the Avalonia Plate (e.g., Martinez-Catalán *et al.,* 1997; Oliveira & Quesada, 1998; la Rosa *et al.,* 2002; Von Raumer *et al.,* 2003; Ribeiro *et al*., 2007; Jorge, 2009; Jorge *et al.,* 2013). The collision of this plate with the margin of the Ossa Morena Zone (an outboard part of Gondwanan Iberia) in early Visean times led to the cessation of volcanism in the Iberian Pyrite Belt and a phase of tectonic inversion, resulting in a pulse of rapid uplift on the southwest border of the Ossa Morena Zone and the development of a SW-prograding trough on the Avalonian margin (Oliveira & Quesada, 1998; Jorge *et al.,* 2013).

The angular unconformity between the South Portuguese Zone and the Algarve basin marks the southern boundary of South Portuguese Zone.

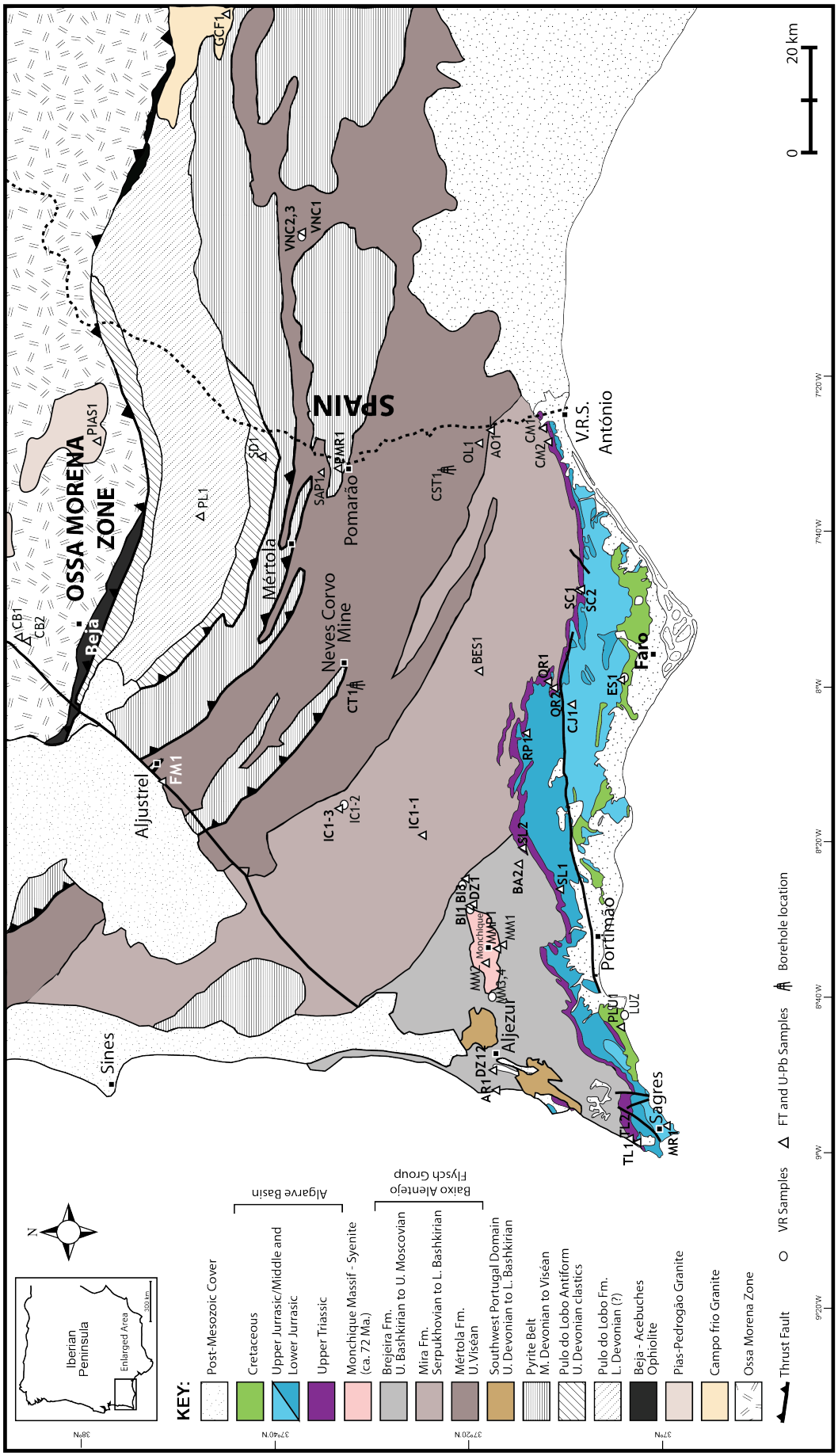

Figure 2.2 Simplified geologic map of the Monchique Alkaline Complex (adapted from Valadares, 2004) with sample locations marked. It corresponds to the inset A in figure 2.1.

2.1.3 Permian Viar Basin

The Viar Basin is an elongate basin that strikes NW-SE and crops in the Sierra Norte of the Seville province (fig. 2.1B and fig. 2.3). Is an intra-orogenic half-graben located between the South Portuguese Zone and the Ossa Morena Zone (Sierra *et al*, 2009). The Permian Viar Basin is a result of various extensional–compressive tectonic episodes that occurred along the the South Portuguese Zone-Ossa Morena Zone boundary during the final stages of the Variscan Orogeny (Simancas, 1983; García-Navarro & Sierra, 1998). This is the southernmost occurrence of Permian strata in Iberian (Wagner & Mayoral, 2007). The Viar Basin consists of conglomerates, sandstones and lutites with minor intercalated limestone, mafic and felsic volcanic rocks (Sierra *et al.*, 2000). Sedimentation started with fluvial conglomerates and sandstones with a sedimentary provenance mainly from the Ossa Morena Zone (Wagner & Mayoral, 2007; Sierra *et al*, 1999) The sedimentations had stopped due to volcanic activity that fill up the paleotopography (Wagner & Mayoral, 2007; Sierra *et al*, 1999). However, the location of the volcanic vent is difficult to ascertain, probably as a result of later compressive deformation (Sierra *et al*, 1999).

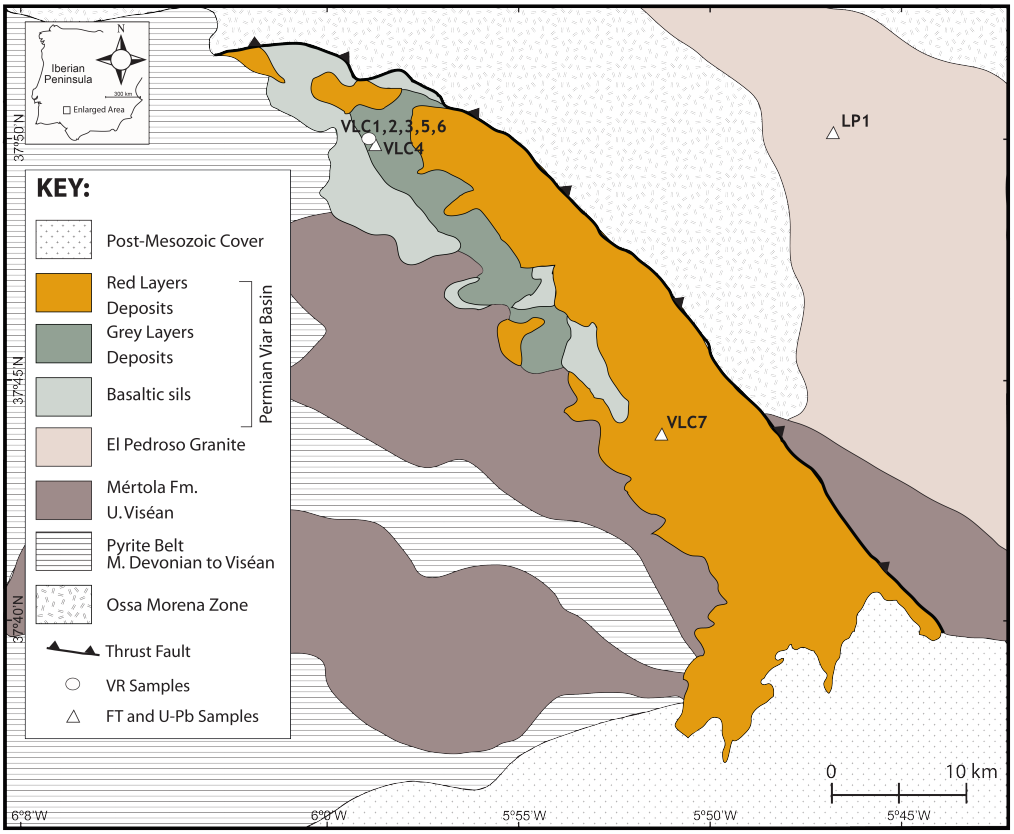

Figure 2.3 Simplified geologic of Permian Viar Basin with the sample location (adapted from Sierra, 2009). It corresponds to the inlet B in figure 2.1.

2.1.4 Algarve Basin

The Algarve Basin is the southernmost geological province of mainland Portugal and unconformably overlies the South Portuguese Zone. The basin strikes E-W and crops out onshore from Cap São Vicente to the Portuguese-Spanish border (Fig. 2.1 and 2.2). More than 3 km of mostly marine sediments accumulated during Mesozoic-Cenozoic times (Mannuepella, 1992). The Mesozoic strata accumulated on a passive margin that formed during successive extensional phases from the Late Triassic to the Middle Cretaceous related to the opening of the North Atlantic Ocean (Mannupella *et al.,* 1988).

Sedimentation in the Algarve Basin was initiated in Late Triassic times with the deposition of continental red beds and evaporites, which unconformably overlie folded and faulted Carboniferous strata (Palain, 1976). The red bed succession consists of sandstones and conglomerates at the base (Silves sandstones), overlain by variated mudstones interbedded with siltstones and dolomites. On top of these strata, to the south of the E-W trending Algibre Fault, there are thick evaporitic deposits, whereas north of this major structure, the evaporites are virtually absent. These strata are overlain by volcanic rocks associated with the Central Atlantic Magmatic Province (CAMP) (Martins *et al.*, 2008; Verati *et al.*, 2007). The Lower Jurassic Algarve CAMP magmatism was dated by the $^{40}Ar/^{39}Ar$ method at 198.1±1.6 to 198.4 ± 2.8 Ma (Verati *et al.,* 2007). It consists of subaerial lava flows, peperites and pyroclastic deposits, and contemporaneous resedimented volcanic material (Martins *et al.*, 2008). Some sedimentary layers are interbedded with effusive and explosive volcanic products which are indicative of coeval volcanism and sedimentation (Martins *et al.*, 2008). The CAMP mark the end of the first phase of rifting in the Algarve Basin. After this important magmatic episode, marine carbonate sedimentation became well-established across the Algarve Basin between the Sinemurian to Tithonian (199-145 Ma). During this interval, lateral facies changes in the limestone facies across the basin allow its division into the Western (Sagres), the Budens-Lagoa, and the Eastern (Faro) sub-basins (Mannupella *et al.*, 1988). These small sub-basins are separated by major north-south trending faults, which were probably active during deposition. Three main sedimentary cycles separated by regional unconformities related either to global sea level variations or to regional tectonic events (Mouterde, 1971; Mannupella *et al.*, 1988; Terrinha *et al.*, 2002) are recognized in the Jurassic marine carbonates of the Algarve Basin. There is evidence of extensional tectonism associated with four rifting phases which are in turn associated with four mega-sedimentary cycles: three in the Jurassic (Lower, Medium and Upper) and one in the Lower Cretaceous (Mannupela *et al.*, 1988). The main

carbonate lithologies found in the Algarve Basin are shallow water limestones, sometimes with coral and sponge bioherms, pelagic limestones marls, bioherms and dolomites (*e.g.* Manuppella *et al.*, 1988; Oliveira, 1992).

The Lower Cretaceous sedimentary interval is represented by a mixed carbonate and siliciclastic succession (Rey, 2006) which attains its maximum thickness (*ca.* 1500 m) in the central Algarve. The basal units consists of marls and dolomites that rest conformably on Upper Jurassic limestones. These are followed by marls, dolomites, sandstones and mudstones that were deposited in nearshore and continental settings. During the Aptian to Albian interval (125-101 Ma), depositional conditions become more uniform across the basin, resulting in the accumulation of variated muds of possible lagoonal origin (the Aptian Luz Marls).

Miocene strata were deposited unconformably over the Mesozoic sequences in sedimentary basins controlled by Alpine tectonics. The main phase of inversion of the Mesozoic strata occurred during Late Cretaceous and Cenozoic times (Kullberg *et al*., 1992, Terrinha, 1998), synchronous with igneous activity associated with the Monchique Alkaline Complex. Although the main batholith of the Monchique Alkaline Complex intrudes only greywackes and shales of the Brejeira formation, minor intrusions related to the Monchique Syenite dyke swarm intrude the Algarve Basin succession, especially in the Western Sub-Basin (Manuppela *et al.*, 1998) as in the case of the Ponta das Ferrarias Intrusion near Lagos (Henriques, 1954). Plio-Quaternary clastic deposits unconformably overlie the Palaeozoic, Mesozoic and Miocene strata, and exhibit sedimentary facies consistent with eustatic sea-level changes related to Late Cenozoic climatic fluctuations (Moura, 1998).

2.1.5 Monchique Alkaline Complex

The Monchique Alkaline Complex (MAC) is located in South Portugal and was intruded into the shales and greywackes of the Brejeira Formation (Fig. 2.1C and 2.4). The MAC shows a sub-elliptical shape of nearly 80 km^2 and defines two main hills: Foia (902 m) in the western part and Picota (773 m) in the eastern part. The host rocks are truncated by the intrusive complex, except in the western and eastern extremes where the regional structure of the host rock is sub-parallel to the contact with the MAC (Valadares, 2004).

The MAC is composed by multiple intrusions of nepheline syenite, intermediate and

ultrabasic rocks and several brecciated formations (Valadares, 2004). The MAC has been dated by several methods giving a Late Cretaceous age of *ca.* 72 Ma: (K-Ar 72±2 Ma-MacIntyre & Berger, 1982; Rb-Sr 72±1.5 Ma-Bernard-Griffiths *et al.*, 1997, 72±2 Ma-Rock, 1978; Amphibole 72.7±2.7 Ma-Miranda *et al.*, 2009; Whole rock 71.5±3.6 Ma-Miranda *et al.*, 2009). It is part of the Iberian Alkaline Igneous Province that includes other intrusions of the same age such as Sines and Sintra (Rock, 1982; MacIntyre & Berger, 1982). The intrusion has created a halo of contact metamorphism of a uniform thickness of 200 m, except in the northwest sector where it is up to 1 km wide (Valadares, 2004).

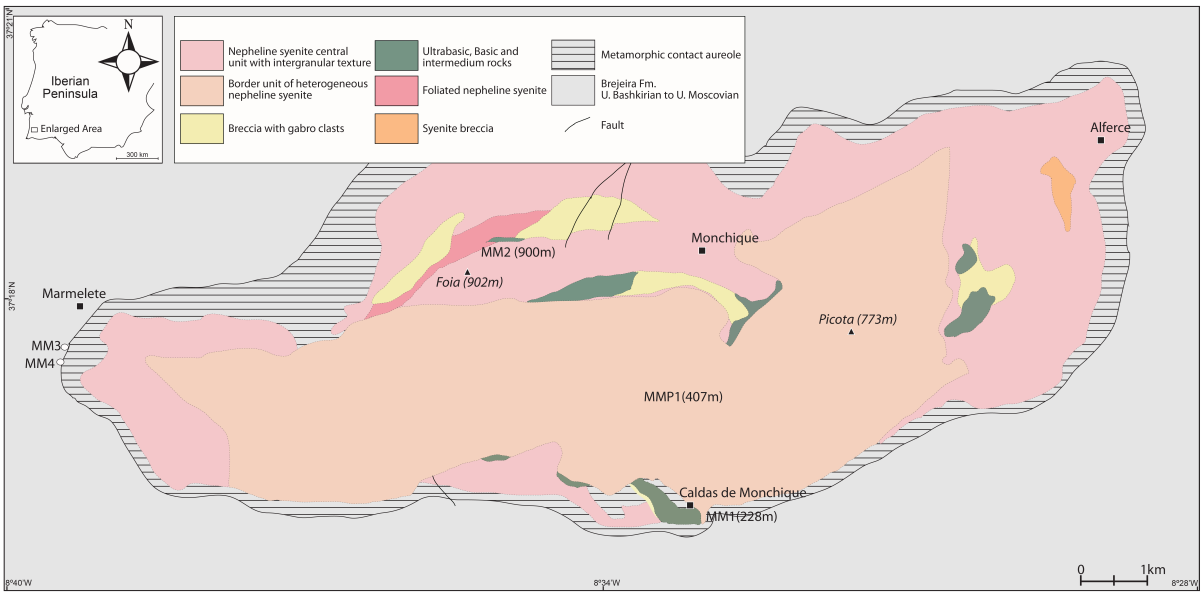

Fig. 2.4 Simplified geologic map of the Monchique Alkaline Complex with the sample locations marked (adapted from Valadares, 2004). It corresponds to inset C in figure 2.1.

2.2 PREVIOUS WORK IN THE STUDIED AREA

2.2.1 Maturation studies

Several maturation works have been published on the studied area, mainly on organic maturation but also with some studies on clay crystallinity. A comprehensive study of the thermal history of the Baixo Altentejo Flysch Group was published by McCormack *et al.* (2007), determining a mean vitrinite reflectance (VR) of 4.28% Rr for this domain and suggesting that the timing of maturation was post-Variscan deformation, within the late Carboniferous–late Triassic interval due the relatively low VR values os Triassic samples (1.1 % Rr).

In the Tercenas Formation and in the Viséan Murração Formation from Southwest Portugal Domain, a few samples indicate maturation levels of *ca.* 3.2% *Rr* (McCormack, 1998;

McCormack *et al.* 2007). In the Carrapateira Group, also from the Southwest Portugal Domain, the maturation levels range from 2.5-4% Rr (Moço *et al.,* 1998). These values for the Southwest Portugal Domain are lower than the mean maturation value of *c.* 4.83% *Rr* for the younger Brejeira Formation of the Baixo Altentejo Flysch Group (Fernandes *et al.*, 2012).

In the Pyrite Belt in the São Domingos mine area, the VR values range from 4.6 to 5.2% *Rr,* indicating a meta-anthracite coal rank (Pereira *et al.* 2006).

Diagenetic and metamorphic conditions within the South Portuguese Zone have also been studied by means of clay mineral crystallinity (Munhá, 1983, 1990; McCormack, 1998; Abad *et al.,* 2001). These studies show a decrease in crystallinity from epizone conditions in the NE to the late diagenetic zone in the SW. Vitrinite reflectance of the organic matter from the flysch successions of the Pulo do Lobo Antiform indicates that meta- anthracite coal rank was attained post-late Devonian (Pereira *et al.,* 2006).

Fernandes *et al.* (2012) revised the maturation values in the Baixo Altentejo Flysch Group in order to better constraint the timing of maturation. There was no observal increase in VR in the studied borehole, which did not allow a meaningful regional palaeogeothermal gradient calculation to be made for the Baixo Altentejo Flysch Group. The Baixo Altentejo Flysch Group in general does not display any great variability in VR, with *Rr* ranging from 3.80 to 5.55% and there is not clear any correlation between the *Rr* means in the three formations investigated. The mean peak palaeotemperatures for the Mértola, Mira and Brejeira formations are 311, 302 and 310 °C respectively. Fernandes *et al.* (2012) suggested that the attainment of peak temperatures during late Pennsylvanian times was as a consequence of simple pre-tectonic burial in a high geothermal gradient context and that during the Variscan deformation the temperatures remained high but did not exceed the maximum attained prior to deformation. The advective heating by hot fluids expelled during Variscan folding and thrusting produced relatively uniform high temperatures in the upper crust and may overprinted any existing vertical VR gradient. The evidence for high temperatures having been maintained for some time after deformation is provided by the similarity of vitrinite reflectance in Carboniferous rocks at the surface. The anomalously low maturity of platform-facies rocks in the Aljezur–Bordeira antiforms may be a consequence of this area having been a 'sink' for descending, relatively cool fluids Fernandes *et al.* (2012).

More recently Fernandes *et al.* (2013) published a comprehensive study of the thermal history

of Algarve Basin. It was observed in the entire Algarve Basin that maturation levels increase with the increasing age of the strata, indicating that burial was the main process controlling maturation. The values of vitrinite reflectance range from 0.52-0.7% Rr in the Lower Cretaceous to 1-1.1% Rr in the Upper Triassic Hettangian. The Miocene rocks that unconformably overlie the Mesozoic strata are immature, showing values of 0.42 and 0.47% Rr. The palaeogeothermal maximum gradients in the onshore Algarve Basin range from 52 º C/km in Sagres-Lagos to 24.7 ºC/km in Faro area. The author suggests that peak temperatures of all the stratigraphic units were attained in latest Cretaceous time. Regarding the VR values, the estimated thicknesses of cover removed is ca. 800 m in the Sagres-Lagos area and *ca*. 4 000 m in the Faro area suggest either continuous sedimentation in the Algarve Basin through much of the Late Cretaceous or a substantial section eroded at the base of the Miocene unconformity.

2.2.2 Low-temperature thermochronology studies

Stapel (1999) undertook an apatite fission track study along a profile across the Algarve and Sierra Morena (Spain) in order to analyse if the different geophysical characteristics of the West and Central Iberian Regions are also expressed in its cooling history. His study covers the South Portuguese, Ossa Morena and Central Iberian Zones. The fission track ages establish a clear difference between the South Portuguese Zone and the Central Iberian Zone. The South Portuguese Zone shows fission track ages and track lengths of 111.6±9.83 Ma and 13.81±1.04μm and 113.3±9.77 Ma. The Ossa Morena Zone shows a dispersion of apatite fission track ages (55.98±3.94 Ma, 69.94±6.52 Ma and 113.7±17.1 Ma) with a Cenozoic component not present in the South Portuguese Zone. The confined track lengths have the same order of magnitude that in the South Portuguese zone, with values of 13.43±1.17 μm and 13.63±1.14 μm in the samples with a Cenozoic age. The forward modeling results indicate that the fission track age records an actual cooling event, namely a rapid cooling around 120 Ma and an recent cooling episode related to an uplift phase from 40 Ma until present.

Valadares (2004) report apatite fission track ages from the Monchique Alkaline Complex of 72.5±2.8 Ma, with confined fission tracks lengths of 13.68±0.22 μm. This value is coincident with the emplacement of Monchique at *ca.* 72 Ma (Rock, 1978; Miranda *et al*, 2009). The authors suggest several phenomena that could yield a fission track age which is identical to

the emplacement age: (1) the intrusion occurred in low depth crust levels; (2) heat dissipation through convection processes; (3) convection of fluids that removed the thermal anomaly associated with intrusion; (4) a compressive stage between the Cenomanian and Paleogene that rapidly uplifted the Monchique Alkaline Complex through the apatite partial annealing zone.

2.2.3 Previous provenance studies on the Baixo Altentejo Flysch Group

Early provenance studies of the Baixo Alentejo Flysch Group from South Portuguse Zone mostly employed palaeocurrent and petrographic analysis (Boogaard, 1967; Schermerhorn, 1971; Oliveira & Wagner Genthis, 1983; Moreno, 1988, 1993; Moreno & Sáez, 1989). Palaeocurrent analyses from the Mértola Formation exhibit a complex pattern with predominant flow directions from the north (Oliveira & Wagner Genthis, 1983). The sparse palaeocurrent data from the Mira Formation indicate that the predominant flow directions were towards the northwest (Oliveira & Wagner Genthis, 1983). The Brejeira Formation exhibits flow directions mainly to the southeast and east with some paleocurrent measurements indicating flow towards the southwest and north (Oliveira & Wagner Genthis, 1983).

Early petrographic analyses of the Mértola Formation suggested that most of the lithic clasts were derived from the Phyllite Quartzite Group and Volcano-Sedimentary Complex (Boogaard, 1967), with also a small contribution from the southwest border of the Ossa Morena Zone (Oliveira & Wagner Genthis, 1983). Moreno (1988, 1993) and Moreno and Sáez (1989) infer that two coeval turbidite systems fed the Mértola Formation derived from two different sources (the Ossa Morena Zone and the Pyrite Belt). However, reworked Cambrian to Early Devonian palynomorphs commonly occur in the Brejeira Formation (Pereira, 1999) and indicate a source area for this stratigraphic unit from outside the South Portuguese Zone, as no rocks older than the Mid-Devonian crop out within the South Portuguese Zone.

Jorge *et al.* (2013) undertook a comprehensive major- and trace-element geochemistry study on all three formations of the Baixo Alentejo Flysch Group. This study concluded that the source area for the sedimentary rocks of the Mértola and Mira formations was derived mainly from the SW border of the Ossa Morena Zone (Fig. 1). The provenance of the youngest Brejeira Formation was suggested to be either from an internal orogenic source alone or with

a contribution from an external source, possibly Avalonia. Although the second scenario was favoured by Jorge *et al.* (2013), this question remains open.

U-Pb detrital zircon analyses that have been undertaken on the Mértola Formation rocks suggest that the Iberian Pyrite Belt and the internal zones of the Ossa Morena Zone were the main sources (Jorge, 2009; Pereira *et al.*, 2012). However, there are presently no U-Pb detrital zircon data from the other formations of the Baixo Alentejo Flysch Group and the provenance and evolution of the group as a whole remains uncertain. In recent years several U-Pb zircon dating studies have been undertaken on the Ossa Morena Zone (*e.g.* Cordani *et al.,* 2006), the Volcano-Sedimentary Complex of the Iberian Pyrite Belt (*e.g.* Rosa *et al.*, 2009) and the different domains of the South Portuguese Zone (Jorge, 2009; Braid *et al.*, 2011; Pereira *et al.*, 2012). In this work we present U-Pb detrital zircon data from the Mértola, Mira and Brejeira formations of the Baixo Alentejo Flysch Group. The aim of this study is to compare the U-Pb detrital zircon data with the different models proposed for the provenance of the Baixo Alentejo Flysch Group in order to further constrain the tectonic setting of this Carboniferous basin in the context of the evolution of the SW Iberian Variscides.

2.3.2 Provenance studies on Upper Triassic Silves Sandstones in Algarve Basin

In the Algarve Basin, the siliciclastic sediments of the Upper Triassic termed the Silves Sandstones (Rocha, 1976), are comprised of sandstones and conglomerates with oblique stratification and lenticular structures (Palain, 1976). These sediments were deposited in a fluvial sedimentary environment and were associated with numerous alluvial fans deposited on Variscan basement (Palain, 1976). Palaeocurrents indicate a sedimentary provenance mainly from the NE to SW and is assumed that the Variscan basement was the main sedimentary source for the Silves Sandstones (Palain, 1976). The lack of isotopic ages from the Upper Triassic makes its provenance an open question.

2.3 SAMPLING

Sampling was carried out in three campaigns during the first year of work. The sampling campaigns were designed to complement the existing and published thermochronology, organic maturation and provenance data.

2.3.1 Organic Maturation Sampling

A total of forty-two samples were collected from outcrops (fig. 2.2, 2.3) in the Baixo Alentejo Flysch Group, in the Algarve Basin and in the Permian Viar Basin to constrain the maximum temperatures attained and to allow a better understanding of the thermal history (including the planned fission tracks results) and also to increase the geographic spread of the existing organic maturity database. A total of ten samples from two mineral exploration boreholes (CST1 and CT1) located in the Mértola Formation from South Portuguese Zone were also sampled (see point 2.3.3). The lithologies sampled were shales, mudstones and clays. Where possible, the samples were collected at localities where low-thermochronology samples were taken (see 2.3.2). In the Baixo Alentejo Flysch Group, two samples were taken from the Mértola Formation, three from the Mira Formation and five from the Brejeira Formation (table 1, fig. 2.2). In the Permian Viar Basin, five samples were collected (table 2.1, fig. 2.4). In the Algarve Basin four samples were collected in Lower cretaceous Sobral formation in Faro sub-basin. Other twenty-three outcrop samples were collected from the Lower Cretaceous Luz Marls and Mudstones located near the *ca.* 150 m thick basic intrusion at Ponta das Ferrarias at the eastern end of the Praia da Luz (Lagos) in the eastern Algarve sub-basin (table 2.1, fig. 2.2). The samples were collected in the same layer, at different distances from the intrusion as shown in figure 2.5.

Ponta das Ferrarias	
Sample	**Distance (m)**
L1	0.1
L2	0.3
L3	0.5
L4	0.8
L5	1
L6	1.3
L7	1.5
L8	2
L9	3
L10	4
L11	7
L12	9
L13	11
L14	13
L15	20
L16	25
L17	30
L18	40
L19	75
L20	100
L21	150
L22	200
L23	2000

Figure 2.5 Illustration of the sampled layer and the proximity to the intrusion. Dashed lines correspond to local faults.

Table 2.1 List of samples collected for maturation studies. The Samples from Praia da Luz are indicated in fig. 2.5. 1-Pereira, 1999; 2-Oliveira *et al.*, 1979; 3-Korn, 1997; 4- Pereira *et al.,*2006*;5*- Rey, 2006; 6-Sierra *et al*, 2009.

Outcrop Samples					
Sample	**Lithology**	**Formation**	**Stratigraphy**	**Latitute**	**Longitude**
RIT1	Shale	Mértola Fm.	Visean[1,2,3,4]	37º43'07.75"N	6º34'46.93"W
RIT2	Shale	Mértola Fm.	Visean[1,2,3,4]	37º43'07.75"N	6º34'46.93"W
VNC2	Shale	Mira Fm.	Serpukhovian-early Bashkirian[1,2,3,4]	37º37'22.65"N	7º01'23.39"W
VNC3	Shale	Mira Fm.	Serpukhovian-early Bashkirian[1,2,3,4]	37º37'22.65"N	7º01'23.39"W
IC1-2	Shale	Mira Fm.	Serpukhovian-early Bashkirian[1,2,3,4]	37º25'25.9"N	8º19'14.3"W
BA1	Shale	Brejeira Fm.	Bashkirian-late Moscovian[1,2,3,4]	37º15'34.17"N	8º22'53.24"W
BI2	Shale	Brejeira Fm.	Bashkirian-late Moscovian[1,2,3,4]	37º20'23.4"N	8º28'13.29"W
AR2	Shale	Brejeira Fm.	Bashkirian-late Moscovian[1,2,3,4]	37º17'43.31"N	8º52'21.03"W
MM3	Shale	Brejeira Fm.	Bashkirian-late Moscovian[1,2,3,4]	37º18'2.2"N	8º39'40.19"W
MM4	Shale	Brejeira Fm.	Bashkirian-late Moscovian[1,2,3,4]	37º18'6.72"N	8º39'35.75"W
MB2	Shale	Brejeira Fm.	Bashkirian-late Moscovian[1,2,3,4]	37º21'5.73"N	8º24'53.13"W
JVN1	Shale	Esteval Fm.	Barremian[5]	37º21'16.3"N	7º49'12.7"W
JVN2	Shale	Esteval Fm.	Barremian[5]	37º21'16.3"N	7º49'12.7"W
JVN4	Shale	Esteval Fm.	Barremian[5]	37º28'32.3"N	7º46'39.8"W
VLC1	Shale	Viar Basin	Lower Permian[6]	37º49'43.8"N	5º58'19.56"W
VLC2	Shale	Viar Basin	Lower Permian[6]	37º49'43.8"N	5º58'19.56"W
VLC3	Shale	Viar Basin	Lower Permian[6]	37º49'43.8"N	5º58'19.56"W
VLC5	Shale	Viar Basin	Lower Permian[6]	37º49'43.8"N	5º58'19.56"W
VLC6	Shale	Viar Basin	Lower Permian[6]	37º49'43.8"N	5º58'19.56"W
Borehole CST1					
Sample	**Lithology**	**Formation**	**Stratigraphy**	**Latitute**	**Longitude**
CST1(13.87)	shale	Mértola Fm.	Visean[1,2,3,4]	37º22'52.07"N	7º32'4.69"W
CST1(56.6)	shale	Mértola Fm.	Visean[1,2,3,4]	37º22'52.07"N	7º32'4.69"W
CST1(88.8)	shale	Mértola Fm.	Visean[1,2,3,4]	37º22'52.07"N	7º32'4.69"W
CST1(146.35)	shale	Mértola Fm.	Visean[1,2,3,4]	37º22'52.07"N	7º32'4.69"W
CST1(211.8)	shale	Mértola Fm.	Visean[1,2,3,4]	37º22'52.07"N	7º32'4.69"W
CST1(281)	shale	Mértola Fm.	Visean[1,2,3,4]	37º22'52.07"N	7º32'4.69"W
CST1(354.9)	shale	Mértola Fm.	Visean[1,2,3,4]	37º22'52.07"N	7º32'4.69"W
CST1(401)	shale	Mértola Fm.	Visean[1,2,3,4]	37º22'52.07"N	7º32'4.69"W
CST1(483.5)	shale	Mértola Fm.	Visean[1,2,3,4]	37º22'52.07"N	7º32'4.69"W
CST1(524.5)	shale	Mértola Fm.	Visean[1,2,3,4]	37º22'52.07"N	7º32'4.69"W
CST1(582.5)	shale	Mértola Fm.	Visean[1,2,3,4]	37º22'52.07"N	7º32'4.69"W
CST1(646.9)	shale	Mértola Fm.	Visean[1,2,3,4]	37º22'52.07"N	7º32'4.69"W
CST1(677)	shale	Volc-sed complex	Visean[1,2,3,4]	37º22'52.07"N	7º32'4.69"W
CST1(717.8)	shale	Volc-sed complex	Visean[1,2,3,4]	37º22'52.07"N	7º32'4.69"W
Borehole CT1					
Sample	**Lithology**	**Formation**	**Stratigraphy**	**Latitute**	**Longitude**
CT1-10.2	shale	Mértola Fm.	Visean[1,2,3,4]	37º32'20.34"N	7º59'51.79"W
CT1-62.8	shale	Mértola Fm.	Visean[1,2,3,5]	37º32'20.34"N	7º59'51.79"W
CT1-108.1	shale	Mértola Fm.	Visean[1,2,3,6]	37º32'20.34"N	7º59'51.79"W
CT1-141.6	shale	Mértola Fm.	Visean[1,2,3,7]	37º32'20.34"N	7º59'51.79"W
CT1-212.1	shale	Mértola Fm.	Visean[1,2,3,8]	37º32'20.34"N	7º59'51.79"W
CT1-265.9	shale	Mértola Fm.	Visean[1,2,3,9]	37º32'20.34"N	7º59'51.79"W
CT1-314.7	shale	Mértola Fm.	Visean[1,2,3,10]	37º32'20.34"N	7º59'51.79"W
CT1-359.4	shale	Mértola Fm.	Visean[1,2,3,11]	37º32'20.34"N	7º59'51.79"W
CT1-421.2	shale	Mértola Fm.	Visean[1,2,3,12]	37º32'20.34"N	7º59'51.79"W
CT1-475.7	shale	Mértola Fm.	Visean[1,2,3,13]	37º32'20.34"N	7º59'51.79"W
CT1-526.6	shale	Mértola Fm.	Visean[1,2,3,14]	37º32'20.34"N	7º59'51.79"W
CT1-585.5	shale	Mértola Fm.	Visean[1,2,3,15]	37º32'20.34"N	7º59'51.79"W
CT1-677	shale	Mértola Fm.	Visean[1,2,3,16]	37º32'20.34"N	7º59'51.79"W

2.3.2 Sampling for low-temperature thermochronology, geochronology and provenance studies

A total of fifty-five outcrop samples were collected for low-temperature thermochronology, geochronology and sedimentary provenance studies. The lithologies sampled were greywackes, quartz-greywackes, sandstones, quartzites, dolerites, granites and syenites (table 2.2). The samples were collected mainly for low-temperature thermochronology studies and, when possible and the mineral content were adequate, were also used for U-Pb geochronology and sedimentary provenance studies. A total of twelve samples from two mineral exploration boreholes (CST1 and CT1) located in the South Portuguese Zone were also sampled (see point 2.3.3).

The samples were collected in order to make a "transect" that covered the Ossa Morena Zone through the South Portuguese Zone, crossing the Monchique Alkaline Complex and into the Algarve Basin. The "transect" is not a straight line but often consists of several samples collected from the oldest to youngest formations in a given region as shown in figure 2.2. Although the Ossa Morena Zone is not one of the objectives of this study, in order to control the relative movements between the Ossa Morena Zona and the South Portuguese Zone, two samples from Late Variscan granites (PIAS1 and LP1) and two samples from the Beja Igneous domain (CB1 and CB2) were sampled (fig. 2.2 and 2.3 and table 2.2). In the Permian Viar basin two samples were collected, one from coarse tuffs (VLC4) and another from a red sandstones (VLC7). In the Monchique Alkaline Complex three samples were collected at different altitudes and from distinct units. One sample was collected from the highest point (MM2) in a central unit of nepheline syanite with intergranular texture. The other two samples were collected from the border unit of nepheline syanite in the contact with the country rock (MM1) and in a quarry (MMP1) (Table 2.2, fig. 2.4).

In an attempt to constrain the thermal history of the Baixo Alentejo Flysch Group prior to the deposition of Algarve basin sediments and also to constrain the thermal history of the base units of the Algarve Basin, several samples were collected along the angular unconformity between these two units. The samples were collected along the unconformity from west to east. Five samples (TL1, SL2, QR2, SC2 and CM2) are from the Upper Triassic Silves sandstones of the Algarve Basin. The other five samples are from greywackes from the Brejeira formation (TL1, BA2), the Mira Formation (QR1, SC1, CM1) and the Baixo Alentejo Flysch Group (table 2.2 and fig 2.2 and 2.6).

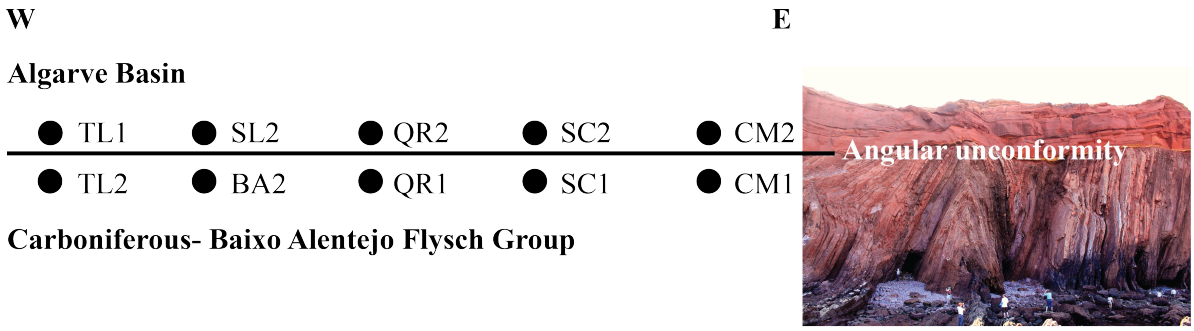

Figure 2.6 Illustration of the sampling along the angular unconformity between the South Portuguese Zone and the Algarve Basin. The sample locations are represented in fig. 2.2.

Other samples from the Lower Jurassic to Lower Cretaceous in the Algarve Basin were collect from different locations (fig. 2.2 and table 2.1) in order to cover different ages in the the basin stratigraphy. Samples SL1 and RP1 were dolerites of the Central Atlantic Magmatic Province. Samples MR1, PLU1, CJ1 and ES1 are clastic rocks (ranging from Bajocian to Barremian in age) that are associated with phases of tectonic inversion in the basin.

Table 2.2 List of samples collected for low-temperature thermochronology, geochronology and sedimentary provenance studies. 1-Pin et *al.*, 1999; 2-Dallmeyer *et al.*, 1993; 3-Pereira, 1999; 4-Oliveira *et al.*, 1979; 5-Korn, 1997; 6-Pereira *et al.,* 2006*;7*-Dunning *et al.*, 2002; 8-Palain, 1976; 9-Verati *et al.*, 2007; 10,11-Rey, 2006; 12-Manupela *et al.*, 1988; 13-MacIntyre & Berger, 1982; 14-Bernard-Griffiths *et al.*, 1997; 15-Storetvedt *et al.*, 1987; 16-Miranda *et al., 2009*; 17-Sierra *et al.*, 2009.

Sample	Lithology	Age (Ma)		Elev. a.s.l. (m)	Latitude	Longitude
Ossa Morena Zone						
LP1	Granite	Visean[+]	340±7.6	374	37º49'51.39"N	5º46'22.84"W
PIAS1	Granite	Visean[+]	334.9±4.3	366	37º59'48.39"N	7º28'1.64"W
CB1	Diorite	Tournaisian-Visean[1,2]	350-340	163	38°7'9.3"N	7°50'52.12"W
CB2	Diorite	Tournaisian-Visean[1,2]	350-341	184	38°6'39.52"N	7°51'17.82"W
South Portuguese Zone - Pulo do Lobo Formation						
PL1	Greywacke	Frasnian-late Famennian[3]	385-359	58	37°48'16.34"N	7°37'59.54"W
South Portuguese Zone - Mértola Formation						
FM1	Greywacke	Late Visean[3,4,5,6]	345-328	138	37º52'37.29"N	8º11'23.62'W
FM3	Intrusion	Unknown	-	134	37º52'37.29"N	8º11'23.62"W
PMR1	Greywacke	Late Visean[3,4,5,6]	345-328	150	37º34'3.8"N	7º31'45.4"W
SAP1	Dolerite	Unknown	-	106	37º35'50.5"N	7º31'51.8"W
VNC1	Greywacke	Serpukhovian	328-318	80	37º 37' 22.65"N	7º01'23.39"W
OL1	Greywacke	Visean[3,4,5,6]	345-328	95	37º19'28.86"N	7º28'53.45"W
SD1	Intrusion	Unknown	-	200	37º41'49.8"N	7º30'20.9"W
CT1-13	Greywacke	Visean[3,4,5,6]	345-328	104	37º32'20.34"N	7º59'51.79"W
CT1-110	Greywacke	Visean[3,4,5,6]	345-328	-123	37º32'20.34"N	7º59'51.79"W
CT1-202	Greywacke	Visean[3,4,5,6]	345-328	-215	37º32'20.34"N	7º59'51.79"W
CT1-312	Greywacke	Visean[3,4,5,6]	345-328	-325	37º32'20.34"N	7º59'51.79"W
CT1-484	Greywacke	Visean[3,4,5,6]	345-328	-497	37º32'20.34"N	7º59'51.79"W
CT1-607	Greywacke	Visean[3,4,5,6]	345-328	-620	37º32'20.34"N	7º59'51.79"W
CST1-4	Greywacke	Visean[3,4,5,6]	345-328	227	37º22'52.07"N	7º32'4.69"W
CST1-86	Greywacke	Visean[3,4,5,6]	345-328	-90	37º22'52.07"N	7º32'4.69"W
CST1-268	Greywacke	Visean[3,4,5,6]	345-328	-272	37º22'52.07"N	7º32'4.69"W
CST1-413	Greywacke	Visean[3,4,5,6]	345-328	-417	37º22'52.07"N	7º32'4.69"W
CST1-600	Greywacke	Visean[3,4,5,6]	345-328	-604	37º22'52.07"N	7º32'4.69"W
CST1-815	Greywacke	Visean[3,4,5,6]	345-328	-819	37º22'52.07"N	7º32'4.69"W
GCF1	Granite	Visean[3,4,5,6]	354.9±4.5	471	37º45'54.26"N	6º36'2.94"W
South Portuguese Zone - Mira Formation						
AO1	Greywacke	Serpukhovian-early Bashkirian[3,4,5,6]	315-307	25	37º18'30.8"N	7º26'57.49"W
SC1	Greywacke	Serpukhovian-early Bashkirian[3,4,5,6]	315-307	161	37º9'18.05"N	7º47'45.63"W
CM1	Greywacke	Serpukhovian-early Bashkirian[3,4,5,6]	315-308	23	37º12'57.76"N	7º26'50.09"W
QR2	Greywacke	Serpukhovian-early Bashkirian[3,4,5,6]	315-307	150	37º11'54.18"N	8º0'20.31"W
IC1-1	Greywacke	Serpukhovian-early Bashkirian[3,4,5,6]	315-307	230	37º25'25.9"N	8º19'14.3"W
IC1-3	Greywacke	Serpukhovian-early Bashkirian[3,4,5,6]	315-307	180	37º34'12.1"N	8º15'42.07"W
BES1	Greywacke	Serpukhovian-early Bashkirian[3,4,5,6]	315-307	514	37º19'43.03"N	7º58'1.82"W
South Portuguese Zone - Brejeira Formation						
BI1	Intrusion	Unknown	-	333	37º20'22.84"N	8º28'12.41"W
BI3	Intrusion	Unknown	-	290	37º20'42.17"N	8º28'27.29"W
AR1	Greywacke	Bashkirian-late Moscovian[3,4,5,6]	307-311	2	37º17'43.31"N	8º52'21.03"W
TL2	Greywacke	Bashkirian-late Moscovian[3,4,5,6]	307-311	84	37º3'30.54"N	8º58'24.81"W
BA2	Greywacke	Bashkirian-late Moscovian[3,4,5,6]	307-311	80	37º15'34.17"N	8º22'53.24"W
MB1	Greywacke	Bashkirian-late Moscovian[3,4,5,6]	307-311	232	37º21'5.77"N	8º24'53.05"W
DZ1	Greywacke	Bashkirian-late Moscovian[3,4,5,6]	307-311	197	37º21'12''N	8º24'57.8''W
DZ2	Greywacke	Bashkirian-late Moscovian[3,4,5,6]	307-311	25	37º19'29.5''N	8º48'20.8''W
Algarve Basin						
CM2	Sandstone	Upper Triassic [8]	±200	25	37º12'22.01"N	7º28'28.65"W
QR1	Sandstone	Upper Triassic [8]	±200	176	37º12'36.51"N	7º59'28.54"W
TL1	Sandstone	Upper Triassic [8]	±200	71	37º3'7.62"N	8º58'45.23"W
SC2	Sandstone	Upper Triassic [8]	±200	151	37º9'13.83"N	7º47'45.04"W
SL2	Sandstone	Upper Triassic [8]	±200	120	37º15'10.84"N	8º20'54.43"W
SL1	Dolerite	Hettangian[9]	198	34	37º11'30.09"N	8º26'11.93"W
RP1	Dolerite	Hettangian[9]	198	306	37º14'46.53"N	8º6'6.98"W
MR1	Sandy limestone	Bajocian[10]	171-167	5	37º0'17.64"N	8º56'29.47"W
PLU1	Sandstone	Aptian[11]	125-112	4	37º5'4.61"N	8º43'47.53"W
CJ1	Conglomerate	Oxfordian-Kimmeridgian[12]	161-150	247	37º10'7.71"N	8º2'21.41"W
ES1	Sandstone	Barremian[11]	130-125	53	37º4'58.4"N	7º59'14.22"W
Cretaceous-Monchique						
MMP1	Syenite	Campanian [13,14,15,16]	72±2	407	37º17'53.49"N	8º34'00.69"W
MM1	Syenite	Campanian [13,14,15,16]	72±2	228	37º17'6.13"N	8º33'16.24"W
MM2	Syenite	Campanian [13,14,15,16]	72±3	900	37º18'58.99"N	8º35'39.84"W
Permian Viar Basin						
VLC4	Coarse Tuffs	Lower Permian[17]	299-270	210	37º 49' 49.48"N	5º 58' 23.29"W
VLC7	Sandstone	Lower Permian[17]	299-270	74	37º 43' 39.28"N	5º 51' 05.71"W

2.3.3 Borehole Samples

Two mineral exploration boreholes were sampled (CST1 and CT1, see fig. 2.2 for location). The borehole CST1 (Corte de São Tomé) (fig. 2.6) was drilled by Billiton Portuguesa-Desenvolvimento Lda. in 1984 and it reached a depth of 890 m. The upper 717 m consists of interbedded shales and greywackes of the Mértola Formation of the Baixo Alentejo Flysch Group. Below 717 m the succession comprises shales and fine to coarse volcaniclastic rocks of the Volcano-Sedimentary Complex of the Iberian Pyrite Belt. The borehole CT1 (Cotovio) (fig. 2.6) was drilled by AGC-Minas de Portugal, Lda in 2008 and it reached a depth of 1888 m. The upper 692 m consists of interbedded shales and greywackes of the Mértola Formation of the Baixo Alentejo Flysch Group. Below 692 m the succession comprises shales and fine to coarse volcaniclastic rocks of the Volcano-Sedimentary Complex of the Iberian Pyrite Belt. Below 1176 m the degree of chloritization increases and jasper and chert horizons are common. The Mértola Formation was extensively sampled with shale samples taken in spaced regular intervals for vitrinite reflectance studies and greywackes for low-temperature thermochronology studies (fig. 2.6 and table 2.1 and 2.2). Only two shale samples and one greywacke were collected in the borehole CST1 in the Volcano-Sedimentary Complex.

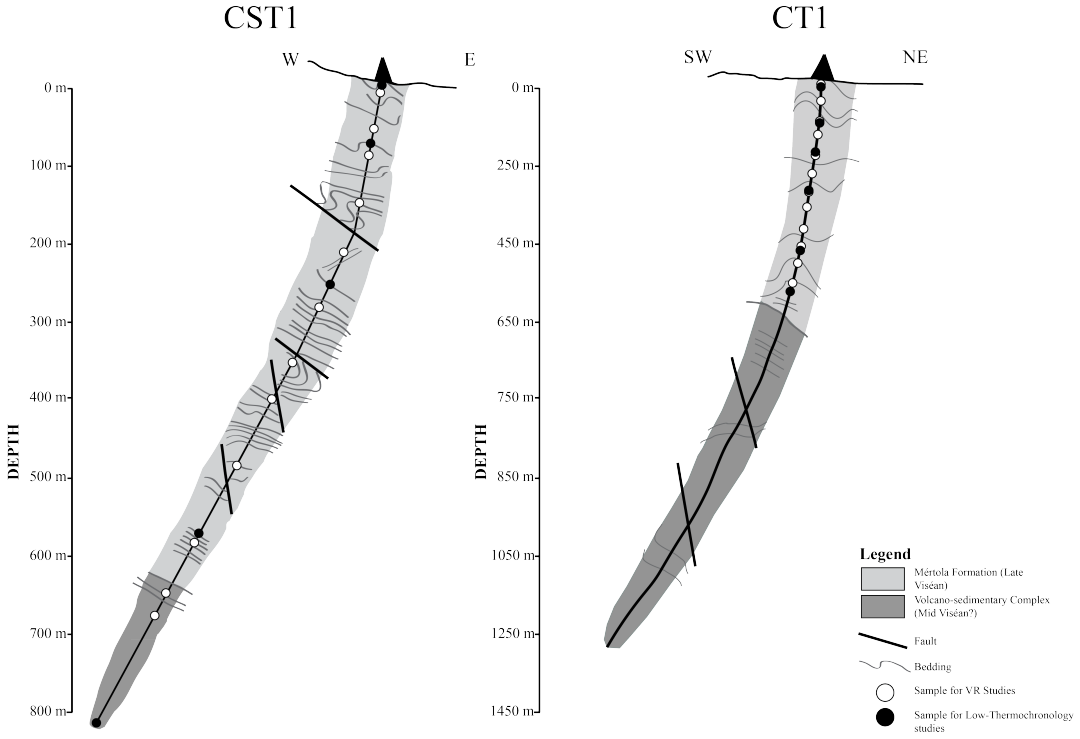

Figure 2.6 Geology and sample location from the boreholes CST1 and CT1. The location of the boreholes are represented in figure 2.2.

III–FUNDAMENTALS OF APPLIED TECHNIQUES

The aim of this chapter is to introduce some of the analytical techniques used in the following chapters. It is beyond the scope of this chapter to give a detailed and in-depth description of the principles behind each methodology used. However, the key references for each method are given in the follow sections. The instrumental procedures are described in the chapters corresponding to each method.

3.1 VITRINITE REFLECTANCE

The term vitrinite was first proposed as a maceral group by Stopes (1935). In incident light microscopy the organic matter components, macerals, are identified on the basis of their optical properties. They are very common in coals and are also found in sedimentary rocks as dispersed organic matter. Macerals are microscopic organic entities derived from terrestrial, lacustrine and marine plant remains and are modified by deposition processes, early diagenesis and subsequent thermal evolution (Suárez-Ruiz *et al.*, 2012). There are three maceral groups: huminite/vitrinite, liptinite and inertinite. In this chapter only vitrinite will be discussed. Vitrinite can be defined chemically as an organic compound formed by polyaromatic nuclei, heteroatomic ketone and carboxyl groups which are surrounded by peripheral aliphatic chains. The exact proprieties of vitrinite depend on their origin, namely if it is derived from lignin or cellulose, or a combination of both. The amount of biodegradation that occurs during the early stages of organic diagenesis is also important (Fermont, 1988). The initial chemical composition of the botanical vitrinite percursors and the amount of initial biodegradation are important and influence the vitrinite reflectance. The reflectance increase observed in vitrinite is intrinsically related to the chemical changes that occur in its structure during coalification. The chemical structure of vitrinite can be represented by several "clusters" of condensed aromatic rings linked with chains and stacked on top of one another. With increasing maturity, these "clusters" fuse together into larger, condensed aromatic ring structures. Eventually, they form sheets of condensed rings that assume an orderly structure. Both the increases in the size of these sheets and their preferred orientation cause greater reflectivity (Stachs *et al.*, 1982). Other chemical changes that occur during coalification include the increase in the carbon content of vitrinite and a progressive decrease in the oxygen

and hydrogen content. The chemical reactions as vitrinite undergoes increasing maturation are also responsible for the anisotropy observed at higher ranks.

Temperature is considered to be the principal factor that controls the increase of vitrinite reflectance, although other factors do have some effects, like stress, time and pressure (Murchinson *et al.*, 1985). Chemical reactions which affect vitrinite particles during organic maturation are irreversible and their reaction rates rise exponentially with a linear rise in temperature. Consequently, the increase in the magnitude of vitrinite reflectance also increases exponentially with a linear rise in temperature.

Cook (1991) compiled some of the main distinguishing features of vitrinite from other maceral groups. One of these features is primarily based on its morphology. In sections perpendicular to bedding, most vitrinite occurs as elongate lenses. In sections parallel to bedding the vitrinite particles are commonly more equidimensional and are less likely to show rounded outlines. Other distinguishing proprieties are the reflectance and the autofluorescence. At low and medium ranks, vitrinite has a reflectance higher than that of liptinite macerals and lower than that of inertinite macerals. In the middle and upper ranks the liptinite reflectance converges on that of vitrinite. Within the anthracite range, the maximum reflectance of vitrinite converges on that of the macerals of the inertinite group, but the minimum reflectance of vitrinite remains less than that of inertinite macerals. Bireflectance of vitrinite is low at low ranks but becomes distinct in the middle and upper part of the bitumous coal rank range. Within the semi-anthracite, anthracite and meta-anthracide rank range, bireflectance become high to extreme and is an important feature for vitrinites in this rank range. Over the whole range of coal rank in any given sample, vitrinite typically shows a much lower dispersion of maximum reflectance about the mean that the other maceral groups, which is another property that shows the importance of its use. Over the rank range from 1 to about 1.8 % the reflectance dispersion, which is generally low for vitrinite, becomes an important property in distinguishing vitrinite. When the vitrinite reflectance becomes greater than about 2.0 %, its distinctive bireflectance becomes a major feature to aid in the distinction of vitrinite from inertinite, except in the case of some thermally altered rocks. The relief is another distinctive feature of vitrinite macerals. At low and medium ranks the vitrinite exhibits negative polishing relief compared with other macerals. Over the rank range from 1 % to about 1.8 % the polishing relief of vitrinite increases and vitrinite has a tendency to fracture in compactation structures.

In summary, there are several characteristics of vitrinite that make it an excellent palaeotemperature indicator:

- Vitrinite reflectance may be considered a non-retrogressive palaeogeothermometer for low-grade metamorphic conditions (Stach *et al.*, 1982);
- Vitrinite is distributed in a wide range of sedimentary facies and may be obtained from a wide range of lithologies (Dow & O'Connor, 1982);
- Measurement of vitrinite reflectance is precise and standardised by the international guidelines of the ICCP (2001);
- The vitrinite reflectance technique is relatively cheap, easy and quick to measure and the results are reproducible;
- The reflectance of vitrinite increases more uniformly through the entire coal rank range than any other maceral group (Stach *et al.*, 1982);
- Reflectance is an objective parameter and is measured on a numerical scale and not estimated like spore color;
- Small quantities of rock (less than 50 g) generally have sufficient vitrinite grains and small vitrinite particles (more than 2 μm) can be measured;
- At high ranks (above 2,5 % Rm), vitrinite reflectance is essentially the only quantitative microscopic parameter that can be used to determine levels of organic maturation.

3.2 LOW-TEMPERATURE THERMOCHRONOLOGY: APATITE FISSION TRACK

Uranium is a radioactive element that decays by α and β emission but a small proportion of ^{238}U also decays by spontaneous fission. The Fission-track (FT) method is based on the accumulation of narrow damage trails (fission-tracks) in uranium-rich mineral grains, which form as a result of spontaneous nuclear fission decay of ^{238}U in nature (Fleischer & Hart, 1972). Nuclear fission is a process during which a heavy, unstable nucleus splits into a pair of fragments of similar size with the release of a few neutrons and energy that results from the kinetic energy of the fission fragments (Tagami & O'Sullivan, 2005). The fission fragments with massive positive charges are propelled from reaction site in opposite direction creating a damage trail (FT) along the trajectories of the two fragments (Tagami & O'Sullivan, 2005). The cross section of the track has a nearly circular shape of 6-10 nm diameter in apatite mineral grains (Paul *et al.*, 1993). For its entire range, the track is a cylinder over a certain

length and tapers down in diameter near its end (Dunlap *et al.*, 1997) in one or both terminals of a fission track (Carlson *et al.*, 1990). Fission tracks are originally 10–20 μm long and their initial length depends on the density of the crystal lattice (~16 μm in apatite). Owing to their narrow width, fission tracks in their natural state ('latent' tracks) are visible only using transmission electron microscopy (Paul & Fitzgerald, 1992). However they can be 'revealed' to become visible under an optical microscope with ≥1000 x magnification, by polishing and chemically etching the surface of the crystal.

Since each spontaneous fission event creates one fission track, the track density is a function of the rate of fission decay, the concentration of ^{238}U and the fission-track age of the sample (Braun *et al.*, 2006). If a host rock is subjected to elevated temperatures, fission tracks that have been formed up to that point in time are shortened progressively and eventually erased by the thermal recovery of damage (Fleischer & Hart, 1972). This occurs by a diffusive process called annealing, during which atoms and electrons move through the crystal lattice towards the ionized track. As for all diffusive processes, fission-track annealing takes place at strongly temperature-dependent rates. As a result of annealing, the etchable length of a track, which is initially similar for all tracks in a given mineral structure, will be progressively shortened (Green *et al.*, 1986; Carlson *et al.*, 1990). Because the mean length of the tracks in a sample determines the probability that they intersect an internal surface, the track density (and thus the apparent fission-track age) is also reduced during annealing (Green, 1988). The temperature of total annealing for fluorapatite is 120±10 ºC. Above these temperatures, annealing takes place at a faster rate than track production, so the effective apatite fission-track age remains perpetually zero. The annealing rate also depend on the crystallographic orientation of the tracks, with tracks orthogonal to the C-axis of the mineral annealing more rapidly than those parallel to the C-axis (Green *et al.*, 1986; Donelick *et al.*, 1999). The mean width of fission-track etched pits has been proposed as a proxy measure for the varying annealing kinetics arising from compositional and structural variation (Ketcham *et al.*, 1999; Barbarand *et al.*, 2003). Because of the chemical and crystallographic dependence of annealing rates, the track-length distributions (measured as the standard deviation) become wider and single-grain ages become more dispersed with increasing annealing. The effects of annealing can be quantified by measuring the lengths of horizontal confined tracks (Gleadow *et al.*, 1986), i.e. tracks parallel to the polished face of the grain that do not cut the surface but have been etched because they intersect cracks or other tracks allowing access to the etchant.

Confined track lengths can provide unique thermal history information. The distribution of

confined lengths of freshly produced induced tracks is characterized by a narrow, symmetrical distribution with a mean length of around 16.3 μm and a standard deviation of the distribution of approximately 0.9 μm. In volcanic and related rocks which have cooled very rapidly, and never been reheated above about 50 ºC, the distribution is also narrow and symmetric, but with a shorter mean length of 14.5 to 15 μm, and a standard deviation of the distribution of approximately 1.0 μm. In granitic basement terranes, which are thought never to have been significantly disturbed thermally since their original post-emplacement cooling, the distribution becomes negatively skewed, with a mean around 12 or 13 μm and a standard deviation between 1.2 and 2 μm. This distribution is thought to characterize slow continuous cooling from temperatures from 120ºC to ambient surface temperatures. More complex thermal histories produce correspondingly complex distributions of confined tracks. The continuous production of tracks through time, coupled with the fact that the length of each track shrinks to a value characteristic of the maximum temperature it has experienced, gives a final length distribution which directly reflects the nature of the variation of temperature with time. Most distinctive of the numerous possible forms of the final distribution are the bimodal distributions, which give clear evidence of a two-stage history, including high and low temperature phases.

Over the past three decades, fission-track thermochronology has become established as a widely used technique for constraining the low-temperature thermal histories of rocks. Excellent reviews of the technique have been provided by Hurford (1983), Brown *et al.* (1994), Gallagher *et al.* (1998), Gleadow & Brown (2000) and Ravenhurst & Donelick (1992), while in-depth discussions of the theory can be found in Fleischer & Hart (1972) and Wagner and Van den Haute (1992).

3.3 LOW-TEMPERATURE THERMOCHRONOLOGY: APATITE (U-Th)/He

The production of ^{4}He (α particles) from uranium (U) and thorium (Th) series decay in rocks and minerals was the first geochronological dating method to be proposed early in the twentieth century (Rutherford, 1907; Soddy, 1911,1914). However, at that time geoscientists were pursuing only 'absolute' or formation ages of rocks, notably in a quest to constrain the age of the Earth (Holmes, 1913). Since He diffuses easily out of the mineral lattice (a phenomenon that was not very well understood at the time), ages determined using U, Th and He measurements were consistently much younger than those calculated using the U–Pb

couple. Interest in the technique has been revived since Zeitler *et al.* (1987), who proposed that the diffusive loss of He could be quantified and that He ages could be used to constrain cooling through very low temperatures. Subsequent diffusion experiments (Wolf *et al.*, 1996; Farley, 2000) have demonstrated that the apatite (U–Th)/He thermochronometer is sensitive to temperatures as low as 40 ºC, with effective closure occurring around 70 ºC, depending on the cooling rate and mineral grain size. Results of several (U–Th)/He studies in boreholes (Warnock *et al.*, 1997; House *et al.*, 1999) have supported this temperature range in natural settings, within the uncertainty of the thermal histories experienced by the borehole samples. The position of the He partial-retention zone has been compared with the partial-annealing zone of fission tracks in apatite and it was found that their relative positions were consistent with the laboratory-derived estimates (Warnock *et al.*, 1997; House *et al.*, 1997; Stockli *et al*., 2000) The low closure temperatures of the (U–Th)/He system, especially in apatite, make it particularly sensitive to near-surface cooling and thermal perturbations (Farley, 2000)

Because of the high diffusivity of He through most minerals and the relative rarity of He in the environment, initial or excess He is usually not a concern. However, two factors are known to bias strongly the measured He ages: α-ejection and (U–Th)-rich inclusions. The first is related to the fact that the α particles produced by nuclear decay have a kinetic energy that allows them to travel up to 20 μm through the crystal lattice (Farley, 2000), and potentially to be ejected from the mineral. This effect is corrected for by using numerical models of α-ejection for simplified grain geometries and homogeneous U distributions (Farley *et al.*, 1996). The second potential problem is related to the fact that many apatite grains contain minor inclusions of actinide-rich minerals such as zircon and monazite that contribute to the ^{4}He abundance in the sample but, because they are not fully dissolved by the standard chemical dissolution methods used on apatite, do not contribute to the U and Th measurements. Samples that contain such inclusions will therefore present 'parentless' He and yield excessively old ages. Minimizing this problem requires very careful sample selection by screening every grain to be dated, for even the smallest inclusions under a high-magnification optical microscope.

3.4 U-Pb GEOCHRONOLOGY

Uranium has three naturally occurring radioactive isotopes, ^{238}U, ^{235}U and ^{234}U. Each of these isotopes is the parent of a chain of radioactive daughter products that ends in stable isotopes of Pb. None of the parent isotopes decay directly to Pb, but instead follows a sequence of

alpha and beta decays, that create a series of intermediate daughter isotopes, and always ultimately result in a stable isotope of Pb (Bateman, 1910). Unlike other chronometers, the U-Pb system exploits two independent decay schemes, ^{235}U to ^{207}Pb and ^{238}U to ^{206}Pb, where both the ^{238}U and ^{235}U decay constants are relatively precise and accurately known (Jaffey *et al.*, 1971). The half-lives of ^{238}U (ca. 4.5 Ga) and ^{235}U (ca. 0.7 Ga) are all much longer than those for their respective daughters. This means that we can assume the production rate of the daughter product is equal to the decay rate of the parent. Therefore, the decay of U isotopes can be treated as though as it occurred directly to the respective Pb isotopes (Faure & Mensing, 2005). The advantage of two independent chronometers in the same mineral is that it is possible to detect small amounts of open system behaviour such as Pb loss or inheritance from an older component. The different half lives of ^{238}U and ^{235}U means that by the Neoproterozoic much smaller amounts of ^{235}U (relative to^{238}U) remain due to the higher decay rate, therefore smaller amounts ^{207}Pb are produced per increment relative to ^{206}Pb. Although all three dates can be calculated from most published analyses, the relative precisions are related to the analytical technique employed. When dating minerals, it is assumed that the system has been closed during its history, which in this case is the assumption of no Pb or U loss/gain. U is a mobile element in oxidizing environments, and can be lost during weathering. Also, radiation damage of the crystals in which the U and Pb are contained can facilitate Pb loss (Holmes, 1954). The effects of Pb loss on the calculated age can be minimised if we assume that the Pb lost has the same isotopic composition as the Pb that is remaining. If this is correct, we can calculate an age based on the $^{207}Pb/^{206}Pb$ ratio, which will be insensitive to Pb loss. Several publications which describe the U-Pb geochronology system in more detail include Hanchar & Hoskin, 2003 and Corfu, 2012.

IV – VITRINITE REFLECTANCE ANALYSES

4.1 SAMPLING

A total of 48 samples were collected (fig. 2.2, 2.3) to complete a large organic maturity dataset for the Baixo Alentejo Flysch Group in the South Portuguese Zone and in the Algarve Basin. The samples were collected from outcrops and from two mineral exploration boreholes (CST1 and CT1) that intersect the Mértola Formation of the Baixo Alentejo Flysch Group and the volcano-sedimentary complex of the South Portuguese Zone (fig. 2.2, 2.6). All samples were mudstones and shales. The sampling strategy and the detailed description of the samples were described in chapter II. The results will constrain the maximum temperatures attained and allow a better understanding of the thermal history including the apatite fission track results. A batch of samples previously collected and studied in the context of projects "Hydrocarbon source-rock potential of the Algarve Basin" (PTDC/CTE-GEX/72694/2006) and "An Integrated Research on Provenance Indicators of the Baixo Alentejo Flysch Group: Geological Histories 'Concealed' in Sediments-PROVENANCE" (POCI/CTE-GEX/60278/2004) were also used for compilation and comparison of the results. The published results (Fernandes *et al.*, 2012; Fernandes *et al.*, 2013) of these two research projects are presented in annex I.

4.2 SAMPLE PROCESSING

The sample preparation for organic maturation analyses was undertaken in the laboratory facilities of University of the Algarve (UAlg). The method of sample preparation for vitrinite reflection studies was adapted from Fernandes (2000) and consists of two steps (fig. 4.1). The first part comprised the isolation and concentration of the organic residues (kerogen) from the rock samples using cold acids, whilst the second part consisted of mounting and polishing the organic residues.

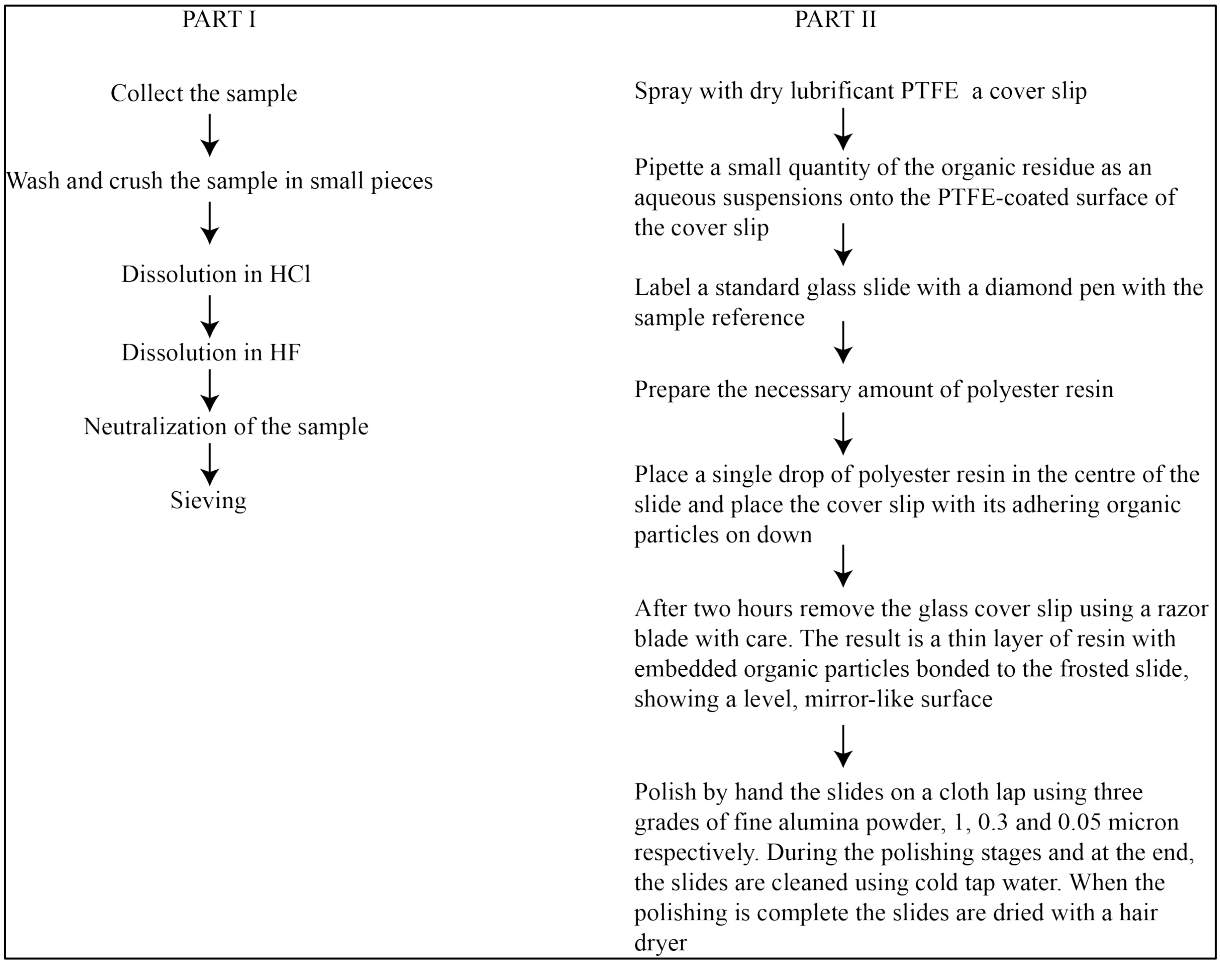

Figure 4.1 Sample preparation for vitrinite reflection studies, adapted from Fernandes (2000).

Firstly, the samples were washed and crushed into small pieces (gravel sized fragments). Approximately 150 g of the crushed rock was put inside a teflon beaker with Hydrochloric acid (HCl) until all the carbonates were dissolved. Afterwards, the HCl was washed by successive decants and Hydrofluoric acid (HF) was added to the beaker and maintained until all the minerals (including silicates) were dissolved. During this stage the sample was stirred twice a day to ensure that the whole sample reacted with the acid. When all the mineral content had been dissolved, the used HF was removed by successive decants using distilled water in order to neutralize the organic residuum. When neutralized, the concentrated organic matter was wet sieved using a 15 microns mesh sieve cloth. The organic concentrate was then collected with a pipette and stored in small beakers.

The organic matter concentrate was mounted in thin sections using the techniques adapted from Hillier & Marshall (1988). The procedures were as follows:

1- Spray a cover slip on one side with dry lubrificant PTFE (polytetrafluoroethylene) and let it dry for a few minutes;
2- Pipette a small quantity of the organic residue as an aqueous suspension onto the PTFE-coated surface of the cover slip, allowing a wide dispersion on the cover slip, and wait two days until it is completely dry;
3- Label a standard glass slide with a diamond pen with the sample reference;
4- Prepare the necessary amount of polyester resin and mix 1 % of liquid hardener. Gently stir to avoid the formation of air bubbles in the resin;
5- Place a single drop of polyester resin in the centre of the slide and place the cover slip with its adhering organic particles on top;
6- After two hours carefully remove the glass cover slip using a razor blade. The result is a thin layer of resin with embedded organic particles bonded to the frosted slide, showing a level, mirror-like surface;
7- Polish by hand the slides on a cloth lap using three grades of fine alumina powder, 1, 0.3 and 0.05 micron respectively. During the polishing stages and at the end, the slides are cleaned using cold tap water. When the polishing is complete the slides are dried with a hair dryer.

The vitrinite measurements were made using an Olympus BX51 reflected light microscope, equipped with an Olympus/SIS CView 3 high-resolution digital colour camera. The vitrinite reflectance (VR) measurements were made using the image processing modules supplied with Matlab® in the Mirone suite (Luis, 2007). This graphical tool calibrates a scale of 256 grey levels with standards of know reflectivity. The standards used in this study have a reflectivity of 0.428, 0.595, 1.715, 3.15 and 5.37, for incident light with a wavelength of 546 nm and immersed in a oil with a refraction index of 1.518 at 20 ºC (room temperature). The greyscale images of the vitrinite particles are imported to this routine and the reflectance values are measured. Whenever possible, a total of 100 vitrinite particles were measured. When the lack of vitrinite particles did not allow this number of analyses to be acheived, a minimum of 30 VR measurements was accepted as statically valid (Mackowsky, 1982; McCormack, 1998, Fernandes *et al.,* 2013).

Mean random vitrinite reflectance (%Rr) was the vitrinite reflectance (VR) parameter chosen for maturation because the mounting technique that was used provides non-oriented vitrinite particles, and also because %Rr is the most widely used organic maturation parameter in the

oil industry and is readily correlated with other maturity parameters (Fernandes *et al.*, 2013). The VR values measured are projected in histograms (annex II) using the "DataGraph®" software that also calculates the mean and standard deviation. The arithmetic mean was considered to be the true vitrinite reflectance value for the sample. The palaeotemperatures of the samples were calculated using an empirical equation described by Barker (1988) that correlates VR values with peak temperatures attained by the samples during burial:

$$T(ºC)=104\ln(R_o+148) \quad (1)$$

where T is the maximum palaeotemperature attained by the rock and R_o the VR value measured.

4.3 VITRINITE REFLECTANCE RESULTS AND MODELATION

4.3.1 Borehole results (CST1 and CT1)

The two boreholes located in the South Portuguese Zone intersect the Mértola Formation of the Baixo Alentejo Flysch Group and the Volcano-Sedimentary Complex of the Iberian Pyrite Belt (see chapter II for more details). Eleven samples from CST1 and eight from CT1 provide measurable vitrinite particles. The results are show in the table 4.1.

Table 4.1 Vitrinite reflectance results for the boreholes CST1 and CT1. The palaeotemperatures valueswere calculated using the equation by Barker (1988). Rr(%) - vitrinite reflectance values in percentage, SD-standard deviation, n-number of vitrinite particles measured.

Borehole CST1								
Sample	**Depth (m)**	**Rr(%)**	**SD**	**n**	**Lithology**	**Formation**	**Stratigraphy**	**Palaeotemperature (ºC)**
CST1(1)	13.8	4.33	0.26	76	shale	Mértola Fm.	late Viséan	300.4
CST1(2)	56.6	4.49	0.26	88	shale	Mértola Fm.	late Viséan	304.1
CST1(3)	88.8	4.61	0.33	73	shale	Mértola Fm.	late Viséan	306.9
CST1(5)	211.8	4.57	0.27	53	shale	Mértola Fm.	late Viséan	306,0
CST1(6)	281.8	4.13	0.29	96	shale	Mértola Fm.	late Viséan	295.5
CST1(7)	354.9	4.61	0.26	60	shale	Mértola Fm.	late Viséan	306.9
CST1(8)	401	4.58	0.28	52	shale	Mértola Fm.	late Viséan	306.3
CST1(9)	483.5	4.94	0.35	79	shale	Mértola Fm.	late Viséan	314.1
CST1(11)	582.5	3.78	0.38	41	shale	Mértola Fm.	late Viséan	286.2
CST1(12)	646.9	4.56	0.27	39	shale	Volc-sed complex	mid Viséan	305.8
CST1(13)	677	5.34	0.41	79	shale	Volc-sed complex	mid Viséan	322.2
Borehole CT1								
Sample	**Depth (m)**	**Rr(%)**	**SD**	**n**	**Lithology**	**Formation**	**Stratigraphy**	**Palaeotemperature (ºC)**
CT1(2)	62.8	4.37	0.27	40	shale	Mértola Fm.	late Viséan	301.4
CT1(3)	108.1	4.01	0.37	69	shale	Mértola Fm.	late Viséan	292.4
CT1(4)	141.6	4.55	0.28	87	shale	Mértola Fm.	late Viséan	305.6
CT1(7)	314.7	5.3	0.4	63	shale	Mértola Fm.	late Viséan	321.4
CT1(8)	359.4	4.58	0.31	87	shale	Mértola Fm.	late Viséan	306.3
CT1(10)	475.7	4.48	0.36	58	shale	Mértola Fm.	late Viséan	303.9
CT1(11)	526.6	4.16	0.29	51	shale	Mértola Fm.	late Viséan	296.3
CT1(12)	584.5	3.94	0.29	76	shale	Mértola Fm.	late Viséan	290.6

In borehole CST1, the vitrinite reflectance (VR) ranges from 3.78 to 5.74 %. VR values do not show any increase with the depth through the 677 m of the section. Peak

paleotemperatures calculated using the empirical Barker equation give a range of maximum temperatures between 295 and 322 ºC. In borehole CT1 the same trend evident in borehole CST1 is observed. The VR values range between 3.94 and 5.3 %. VR values do not show any increase with the depth through the 584 m of section. The peak temperatures give a range of maximum temperatures between 290 and 321 ºC. The lack of downhole increase in VR in both boreholes hampers the calculation of palaeogeothermal gradients for the boreholes. These results are in agreement with the values for the Baixo Alentejo Flysch Group presented by Fernandes *et. al* (2012), Fernandes (2000) and McCormack (1999). The palaeotemperatures determined clearly show that these lithologies had passed through the temperature windows that reset the low-thermochronometers applied in this study.

4.3.2 Results from Outcrop Samples

In order to compare the VR results with the low-thermochronology studies, ten outcrop samples were collected, where possible, from the same outcrops where the samples for thermochronology were collected. (fig. 2.2).

In the Baixo Alentejo Flysch Group the vitrinite reflectance values range between 2.34 and 5.57, with a highest value (12.94 %) measured from shales of the Brejeira Formation, located near the intrusive contact of the Monchique Alkaline Complex (MAC) (fig. 2.4). The VR values measured from the outcrops correspond to paleotemperatures between 236 and 326 ºC, whereas near the MAC the paleotemperatures reach a maximum of 414 ºC.
The samples from the Cretaceous strata have a value of 0.69 %Rr, corresponding to a maximum palaeotemperature of 109 ºC.

Table 4.2 Vitrinite reflectance results from outcrops. The values of palaeotemperature given were calculated using the equation by Barker (1988). Rr(%) – vitrinite reflectance values in percentage, SD-standard deviation, n-number of vitrinite particles measured.

Outcrops Samples									
Sample	**Rr(%)**	**SD**	**n**	**Lithology**	**Formation**	**Stratigraphy**	**Palaeotemperature (ºC)**	**Latitute**	**Longitude**
RIT2	2.34	0.32	88	Shale	Mértola Fm.	mid Viséan	236.4	37º43'07.75"N	6º34'46.93"W
VNC2	3.66	0.32	86	Shale	Mira Fm.	Serpukhovian	282.9	37º37'22.65"N	7º01'23.39"W
VNC3	3.46	0.37	81	Shale	Mira Fm.	Serpukhovian	277.1	37º37'22.65"N	7º01'23.39"W
IC1-2	5.57	0.49	91	Shale	Mira Fm.	mid Viséan	326.6	37º25'25.9"N	8º19'14.3"W
BA1	3.86	0.41	30	Shale	Brejeira Fm.	Serpukhovian	288.5	37º15'34.17"N	8º22'53.24"W
AR2	4.22	0.29	80	Shale	Brejeira Fm.	Moscovian	297.7	37º17'43.31"N	8º52'21.03"W
MM3	12.94	1.68	30	Shale	Brejeira Fm.	Moscovian	414.3	37º23'13.8"N	7º43'40.9"W
JVN1	0.69	0.03	43	Shale	Esteval Fm.	Cretaceous	109.4	37º21'16.3"N	7º49'12.7"W
JVN2	0.69	0.03	43	Shale	Esteval Fm.	Cretaceous	109.4	37º21'16.3"N	7º49'12.7"W
JVN4	0.69	0.08	25	Shale	Esteval Fm.	Cretaceous	109.4	37º28'32.3"N	7º46'39.8"W

Besides the set of samples collected from the outcrops, a batch of twenty-three samples were collected from the Lower Cretaceous Luz Mudstones located near the *ca.* 150 m basic intrusion at Ponta das Ferrarias near Lagos (fig. 2.5). These samples were collected in order to assess the effect of the intrusion on the regional vitrinite reflectance values.

Assuming that the heat flux associated to the igneous intrusion has a symmetrical behaviour either side of the intrusion, samples were collected from the same layer located on the western side of the intrusion and from a distance of *ca.* 2 km as shown on figure 4.1. The results are presented in figure 4.2 and table 3.3. At the contact with the intrusion the VR reaches a maximum value of 1.68 %. The values decrease to 1.1 % at 30 cm from the contact. After this point the VR have some small variations but the main trend is a gradual decrease with the increase in distance from the intrusion, until approximately 2 km the background VR value of 0.66 % described by Fernandes *et al.* (2012) for this area is reached. A possible explanation for the variations in VR values near the contact with the intrusion could be related to the dissipation of heat by the percolation of water along faults and along the contact due to the differences in permeability between the igneous rocks and the mudstones. Raymond & Murchison (1988) state that the degree of sediment compaction, the volume of pore water and the initial maturation level of the organic matter at the time of magmatic intrusion influence the variations in VR more significantly than does the magma temperature.

Table 4.3 Vitrinite reflectance results for the Praia da Luz Marls. The values of palaeotemperatures given were calculated using Barker (1988). Rr(%)-vitrinite reflectance values, SD-standard deviation, n-number of vitrinite particles measured.

Ponta das Ferrarias					
Sample	Distance (m)	Rr(%)	SD	n	Palaeotemperature (°C)
L1	0.1	1.68	0.07	37	202
L2	0.3	1.1	0.08	33	158
L3	0.5	1.12	0.04	2	160
L4	0.8	1.32	0.13	55	177
L5	1	1.42	0.2	75	184
L6	1.3	1.42	0.17	47	184
L7	1.5	1.24	0.16	60	170
L8	2	1.31	0.26	51	176
L9	3	1.32	0.19	51	177
L10	4	1.41	0.18	86	184
L11	7	1.22	0.11	54	169
L12	9	1.31	0.14	66	176
L13	11	1.2	0.08	55	167
L14	13	1.29	0.14	65	174
L15	20	1.25	0.15	77	171
L16	25	1.25	0.15	64	171
L17	30	1.17	0.1	34	164
L18	40	1.04	0.09	40	152
L19	75	1.09	0.11	58	157
L20	100	1.21	0.1	20	168
L21	150	1.08	0.13	20	156
L22	200	0.99	0.06	51	147
L23	2000	0.66	0.15	52	105

Figure 4.1 Illustration of the sampled layer and the proximity to the intrusion. Dashes lines correspond to local faults.

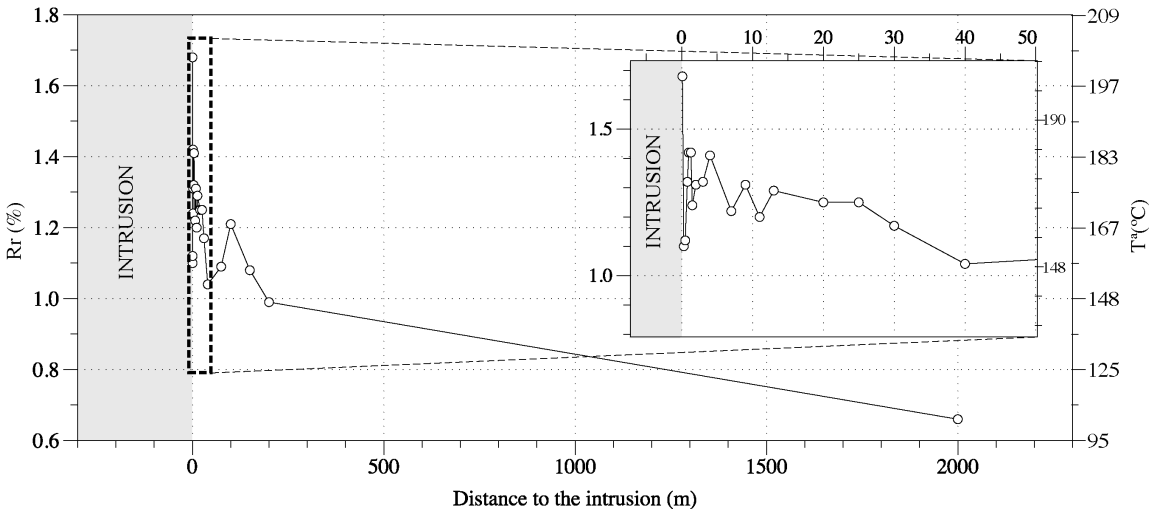

Figure 4.2 Vitrinite reflectance results from the Praia da Luz Marls.

The thermal response of the Praia da Luz Marls to the igneous intrusion was modelled using a simple Matlab® script (Ehlers & Farley, 2003). The model use the assumption that the heat loss from magmatic bodies primarily occurs through conduction (Spear, 1993) and due to the finite shape of the magmatic bodies, the thermal evolution of a magmatic body and its surrounding area can be quantified in 1D assuming: (1) the emplacement of magmatic bodies occur rapidly compared to the post-emplacement thermal equilibration of the surrounding country rock; (2) the geometry of the magmatic bodies are small (less than 10km); (3) the latent heat of fusion from the conversion of melt to crytsallized rock is neglected to quantify

the first-order consequence of magmatism (Ehlers & Farley, 2003). It is also assumed that the intrusion is planar with a width L. A coordinate system with the origin in the centre of the intrusion is employed. The initial conditions used by the model are at time t = 0 the temperature T equals the intrusion T_i within and at the edges of the intrusion [-(L/2)<z<(L/2)] and the temperature T_b equals the background country rock temperature at distances [(L/2)<z<-(L/2)]. With these conditions the equation used in the model is given by Carslaw & Jaeger (1959):

$$T(z,t) = Tb + \frac{Ti-Tb}{2}\left[\text{erf}\left(\frac{L/2-z}{2\sqrt{\alpha t}}\right) + erf\left(\frac{L/2+z}{2\sqrt{\alpha t}}\right)\right] \quad (2)$$

where *erf* is the error function and *z* is measured as the distance from the center of intrusion. The model allows for the introduction of boundary conditions such as the intrusion width, intrusion temperature, country rock temperatures and thermal diffusivity.

The intrusion at Ponta das Ferrarias is described as hypabyssal and resulted from multiple crystallization phases (Henriques, 1954). In the model the intrusion was assumed to be shallow and into country rocks with a background temperature of ca. 100 ºC (Fernandes *et al.*, 2013). Due to multiple intrusion phases an initial temperature of 500 ºC was assumed. A thermal diffusivity of 32 km^2Ma^{-1} was also assumed for modelling proposes. Figure 4.3A and 4.3B show the results of the thermal evolution model of the Ponta das Ferrarias intrusion as well as the thermal evolution of the country rocks. The results of the modelling show that between 20 and 1000 years after the emplacement of the intrusion, the temperature in the centre of the intrusion decreased from ca. 500 ºC to ca. 200 ºC. Whereas, in the wall of the intrusion (75 m from the centre) the temperature decrease from ca. 275 ºC to 190 ºC. During the same period the country rock temperatures at a distance < 2 km increase from a temperature of 100 ºC to near 275 ºC at the contact with the intrusion and decrease back towards to the background temperature at 2 km distance. The temperature at the contact remains elevated (30 ºC) above the background temperature after 10 000 years. After 0.1 Ma the temperature at the contact is only 10 ºC above the background temperature and at 1 Ma the temperature had equilibrated with the background temperature. In the country rocks at a distance of 1 km from the intrusion, the temperature increased in the first 10 000 years to a value ca. 14 ºC above the background temperature. After 0.1 Ma the temperature remains 9 ºC

higher that the background temperature and had completely equilibrated 1 Ma after emplacement.

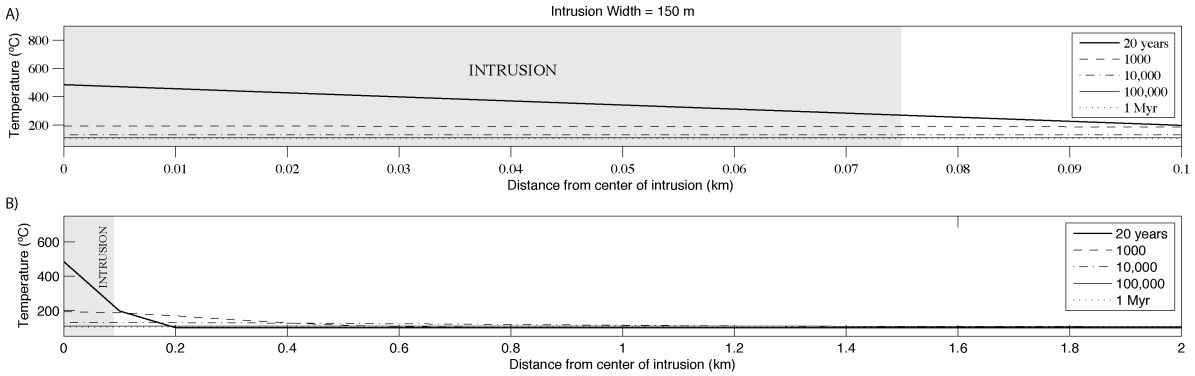

Figure 4.3 Thermal evolution model of the Ponta das Ferrarias intrusion as well as the thermal evolution of the country rocks.

If we compare the measured palaeotemperature data with the modeled temperature results (fig. 4.4) it is clear that the response of vitrinite was not instantaneous with the increase of temperature associated with the emplacement of the igneous rocks. The VR measurements fall between the modelling VR curves corresponding to results between 1000 and 10 000 years after the intrution, indicating a short heating event.

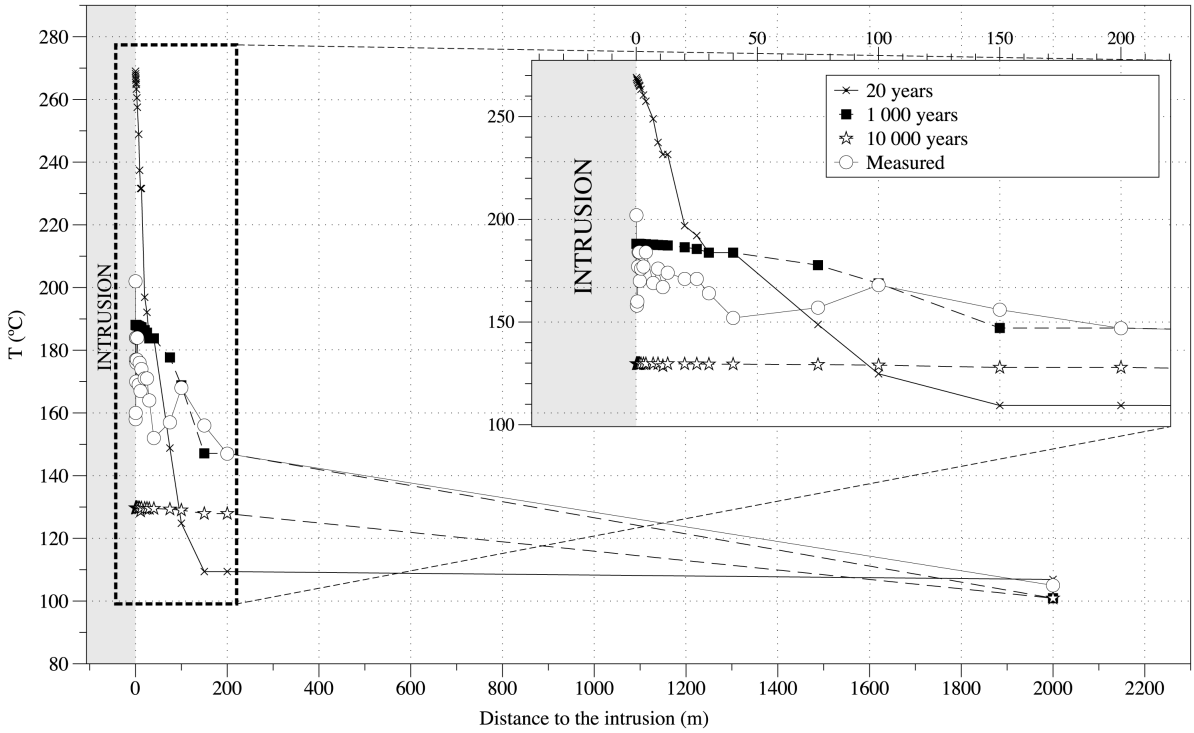

Fig. 4.4 Measured Palaeotemperature data (from VR) compared with the modeled temperature results.

Fernandes *et al*. (2013) suggested that the high palaeogeothermal gradient of *ca.* 52 ºC km^{-1} calculated for the Sagres-Lagos region in the western part of the Algarve Basin, could be attributed to the conductive heating related to Late Cretaceous igneous activity. For the parameters used in the modelling, equilibrium between the intrusion and the country rocks was attained 0.1 My after the intrusion. These results show that the VR values for the country rocks were attained before the intrusion as stated by Fernandes *et al.* (2013) and the thermal effect of the intrusion is restricted to an area near the contact. Nevertheless, it is not conclusive if the Cretaceous intrusions may have affected the geothermal gradient in the Western part of the Algarve Basin on a more regional scale.

4.4 SUMMARY

Fernandes *et al.* (2012) suggested that the maximum burial temperatures in the Baixo Alentejo Flysch Group from the South Portuguese Zone were between 276–325 °C and they were achieved prior to Variscan deformation but remained high during and after deformation. The same authors suggests that an advective heat transfer regime in the South Portuguese Zone which produced relatively uniform high temperatures in the upper crust, overprinting any existing vertical VR gradient. The VR data presented in the two boreholes studied is consistent with the data and conclusions of Fernandes *et al.* (2012). The samples collected from the boreholes CST1 and CT1 do not show any VR increase with the depth. The calculated palaeotemperatures for the outcrop samples are between 236 and 326 ºC and agree well with the VR data presented by Fernandes *et al.* (2012) for the Baixo Alentejo Flysch Group. The highest VR value was measured near the Monchique Alkaline Complex (MAC) corresponding to a palaeotemperature of 414 ºC, indicating high temperatures related with the emplacement of the MAC. The metamorphic aureole caused by the intrusion of the MAC is estimated to be between 0.2 and 1 km wide (Rock, 1978; González-Clavijo & Valadares, 2003). The thermal impact from small intrusions related to the Monchique Alkaline Complex in the Algarve Basin could not be totally neglected, nevertheless in the Baixo Alentejo Flysch Group the lithologies jad already attained a temperature following deposition and the VR values are not the results of small intrusions.

The VR results show that the temperatures attained in the South Portuguese Zone and in particular the Baixo Alentejo Flysch Group were high and significantly above the "resetting" temperatures for the apatite fission track system and also for the apatite (U-Th)/He system. Therefore, it is possible to use both these thermochronological systems to constrain the recent

thermal history of the Baixo Alentejo Flysch Group.

In the Algarve Basin the VR values measured for the Upper Triassic-Hettangian units is 1-1.1 % (Fernandes *et al.*, 2013; McCormack *et al.*, 2007) and correspond to palaeotemperatures between 148 and 158 ºC. This range of temperatures is higher than the "resetting" temperature for both the apatite fission track and the apatite (U-Th)/He systems.

The samples collected at Praia da Luz, near the contact with the basic intrusion at Ponta das Ferrarias, show that the thermal effect of intrusion is restricted to a maximum length of ca. 2 km from the intrusive contact. So, in the case of the Lower Cretaceous lithologies in the western part of the Algarve Basin, the maximum burial paleotemperatures attained were not enough to reset the apatite fission track system. Only near igneous intrusions did the temperatures rise enough to reset to the apatite fission track system. In these situations it might be possible to use the apatite fission track system to date the age of the intrusion as opposed to the country rock thermal history. However, the thermal modelling presented here for the Lower Cretaceous Luz Mudstones intruded by the basic rocks at Ponta das Ferrarias, suggests that near the intrusive contact maximum temperatures of 275 ºC were attained but reduced to 100 ºC after only 10 000 years.

V–APATITE FISSION TRACK ANALYSES

In this chapter the analytical methodology for apatite fission track analyses are described and the results obtained are presented and discussed.

5.1 SAMPLES

A total of sixty-seven samples were collected for low-temperature thermochronology, geochronology and sedimentary provenance studies. The sampling strategy and sample descriptions were provided in chapter II. The lithologies sampled were greywackes, quartz-greywackes, sandstones, quartzites, granites and syenites.

5.2 HEAVY MINERAL SEPARATION AND APATITE CONCENTRATION

The heavy mineral separation was made using standard separation and concentration procedures (jaw crushing, Wilfley table, heavy liquids and magnetic separation) at the Faculdade de Ciências e Tecnologia of University of the Algarve (FCT/UAlg), at the Departamento de Geologia da Faculdade de Ciências of Lisbon University (DG/FCUL) and at the Department of Geology, Trinity College Dublin. The 63-200 μm size fraction was selected for the studies since it yielded the highest proportion of heavy minerals.

5.3 SAMPLE PREPARATION FOR APATITE FISSION TRACK ANALYSES

After the mineral separation and apatite concentration, it is necessary to prepare apatite grain mounts before the apatite fission track (FT) analyses were performed. The procedure for mounting the apatite for counting is described in Donelick *et al.* (2005) and Ketchman (2011) and are summarized in figure 5.1. The first step is the preparation of mineral mounts with no or, at least, minimal surface relief. This is made by the preparation of an epoxy resin (e.g. Struers® epofix). Next, a few drops of resin were placed onto a slide and the apatite grains were put over the resin. The mixture of resins and apatite grains were then stirred around with the help of a wooden toothpick to ensure that they sink onto the glass surface of the slide and were also randomly spread out, so that they would form a single layer of grains on the slide. The mounts were then placed in a dry oven at a temperature of 30 ºC, for 12 hours to ensure that the resin was completely hardened. The mounts are then ready for the grinding stage,

which is intended to grind down the surface of the mount, expose the apatite grains and make a flat surface. This was achieved by grinding the mounts on a rotating wet sand paper (2400 micro-mesh grade) during as many steps as necessary until the grains were exposed. Between each step, the mount was checked under a microscope in reflected light to see if all the grains were exposed. The next step was polishing the mount using an automated polishing machine with different diamond slurry compounds (6 μm, 3 μm, 1 μm and 0,25 μm) on cloth mats. Once again, between each step the mount was checked under a microscope to verify the quality of the polishing and to see if the mount could pass to the next stage of polishing. This procedure was continued until the surface of the apatite grain mount was perfectly polished.

Once the mount surfaces were free of scratches and imperfections, the exposed apatite grains in each mount were etched by immersing them in dilute HNO_3, to reveal spontaneous fission tracks that intersected the polished apatite grain surface. The protocol employed was 5.5 N HNO_3 for 20 s at 21 ºC. Once removed from the etchant, the mounts were immersed and stirred for a few seconds in a beaker with distilled water and then immersed and stirred again in a second beaker also with distilled water. Then, the mounts were removed from the distilled water and dried with a paper towel.

When the number of mounts for an individual sample was in large number, a selection was sent to a nuclear reactor to be irradiated with ^{238}Cf. After the irradiation the etching procedures for the mounts are the same as for a regular mount.

In order to know the exact microscope coordinates of the analysed grains in each mount, it was necessary to fix a set of precise marks in each mount. These reference marks make it possible to use the mounts in different stage systems like a LA-ICP-MS, or later reinsert them on the FT stage and recall the stored locations from an apatite grain mount file. The reference marks were scanning electron microscope target grids that were glued to the mount surface. The target grids are 3mm diameter copper discs with an interior grid and a small letter at the centre. Three different grid patterns with the letters A, L and Q were used. The grids were mounted in order to form a triangle on the edge of the grain mount.

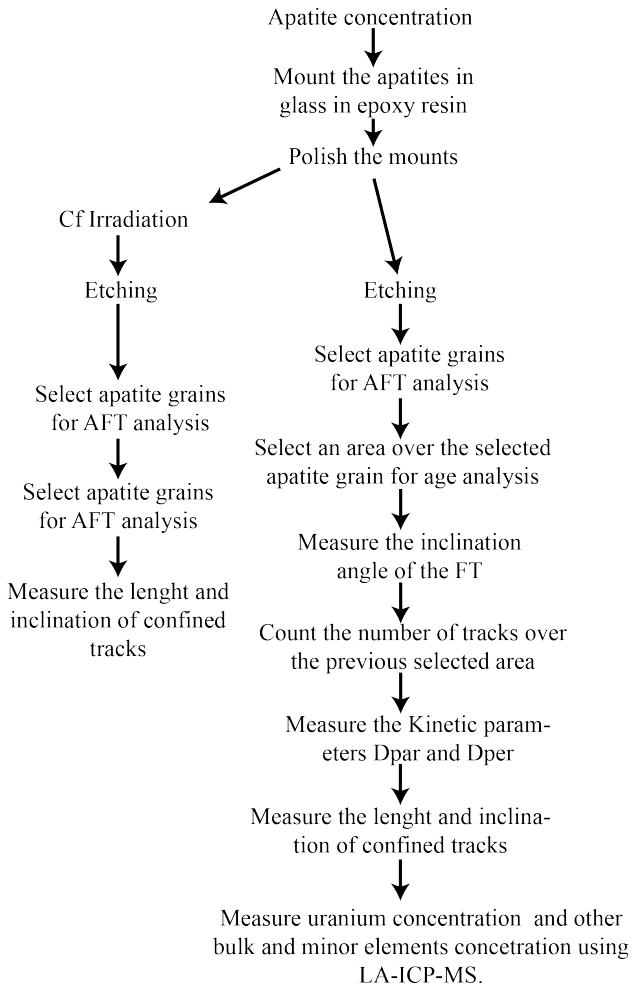

Figure 5.1 Procedures used from the apatite concentration in heavy mineral separation up to FT counting and track length measurements.

5.4 APATITE FISSION TRACK MEASUREMENTS

The apatites were observed under a Carl Zeiss AxioImager Z1 microscope coupled to an Autoscan stage system. An Olympus/SIS CViewIII high-resolution digital colour camera was used to capture the images into the Autoscan® Fission Track Studio software. The software controls both the stage and the camera, and also has measuring tools that can be used for counting the number of tracks and for measuring track lengths, tracks orientations and other track dimensions (dpar, dper, c-axis, etc).

The first step in the determination of the FT ages consisted in the selection of the grains that are parallel to the crystallographic c-axis. This was done using a cross-polarised filter under transmitted light as grains parallel to the c-axis are brightest under cross-polarised light. After the selection of the grains, it was necessary to delimit an area for track counting, which could not be smaller than the size of the laser beam (30 μm). With all the grains selected and the areas delimited, it was then possible to start counting the spontaneous tracks, the length of

confined tracks, and some kinetic parameters such as Dpar and Dper. The procedures used to measure these parameters using the Fission Track Studio package software are described in Ketcham (2011).

5.5 APATITE U AND LA-ICPMS ANALYTICAL TECHNIQUE

Apatite uranium concentrations were measured using a Photon Machines Analyte Excite 193 nm ArF Excimer laser ablation system coupled to a Thermo Scientific iCAP Qc ICPMS in Trinity College Dublin. The analytical protocol employed is described in detail in Chew & Donelick (2012), and integrates uranium concentration measurements for apatite fission track dating with REE and trace element analyses along with the isotopes required for required for U-Th-Pb geochronology. The time interval for the baseline correction was 15 s and the analysis was 45 s. The laser spot size was set at 30 μm with a repetition rate of 4 Hz and a fluence of 3.1 mJ/cm^2 to yield spot depths typically 10 μm deep. A HelEx 2-volume sample cell was used with a He carrier gas flow of 800 mL/min. Ar and N_2 as an additional di-atomic gas to enhance sensitivity (flow rate of 6 mL / min) were admixed downstream. Typically 28 isotopes were measured in each apatite sample. Of these isotopes, ^{43}Ca was used as the internal standard to correct for drift in instrument sensitivity and variations in ablation volume during sessions. Common trace elements in apatite (e.g. Cl, Mn, Sr and Y) and the REE were determined along with the seven isotopes (^{200}Hg, ^{204,206,207,208}Pb, ^{232}Th and ^{238}U) commonly required for U-Th-Pb geochronology. Data reduction for both trace element concentration measurements and U-Th-Pb geochronology was undertaken using the freeware Iolite package of Paton *et al.* (2011). The Iolite approach involves processing an entire analytical session (typically > 5 h) of data, which is not only more efficient but also greatly improves the consistency and reliability of data reduction.

Trace element concentration measurements were undertaken using the "Trace Elements" data reduction scheme in Iolite. Cl concentration measurements followed the analytical protocol of Chew *et al.* (2014a). The ^{35}Cl background-corrected signals for each apatite analysis were normalized to the internal standard (^{43}Ca) and then sample-standard bracketing was employed using apatites of known Cl concentration (Bamble chlorapatite and Durango fluorapatite).

Uranium concentration in unknown apatites followed the analytical protocol of Donelick *et al.* (2005). In contrast to the ICPMS absolute calibration approach of Hasebe *et al.* (2003), which employs the ^{238}U fission-decay constant, a fission track registration factor and a calibration factor for etching and observation, Donelick *et al.* (2005) used a modified zeta

calibration approach (*cf.* Hurford & Green, 1983) for ICPMS apatite U concentration measurements. The method assumes that the apatite ^{43}Ca signal intensity during a given LA-ICP-MS session acts as a proxy for the volume of apatite ablated, and hence the apatite $^{238}U/^{43}Ca$ ratio yields relative U concentration measurements. In this study an extensive primary LA-ICPMS session was undertaken on crystals of Durango apatite that were previously counted for fission tracks to yield a primary LA-ICPMS zeta factor. These same crystals of Durango apatite were then analysed in subsequent LA-IPCMS (along with apatite unknowns for fission-track dating) to yield a session-specific calibration factor on the primary zeta value. Inter-session drift in both the primary and subsequent LA-ICPMS sessions was corrected for by monitoring the $^{238}U/^{43}Ca$ ratio of NIST612 standard glass. The main difficulty in apatite fission-track dating by LA-ICPMS is ensuring that the uranium distribution with the portion of sample that generates fission tracks on the polished apatite surface is quantified spatially, both horizontally (i.e. along the surface of the grain mount) and vertically. The spontaneous track density in the samples analysed in this study was high enough to detect possible U zonation, while depth-related variations in U concentration were accounted for here by incorporating a function within the Iolite "Trace elements" data reduction scheme that weights appropriately the $^{238}U/^{43}Ca$ ratio with depth. As LA–ICPMS is a destructive technique high quality 3-D images of all the counted grains were archived for potential reinvestigation in the future.

Apatite U-Th-Pb geochronology was undertaken using a modified version of VizualAge data reduction scheme (Petrus & Kamber, 2012) for Iolite. This data reduction scheme (VizualAge_UcomPbine) can correct for variable amounts of common Pb in any U–Pb accessory mineral standard as long as the standard is concordant in the U/Pb (and Th/Pb) systems after common Pb correction (Chew *et al.*, 2014b). A ca. 1 cm sized crystal of Madagascar apatite (Thomson *et al.*, 2012) which has yielded a weighted average ID-TIMS concordia age of 473.5 ± 0.7 Ma (Cochrane *et al.*, 2014) was used as the primary apatite reference material in this study. McClure Mountain syenite apatite ($^{207}Pb/^{235}U$ TIMS age of 523.51 ± 1.47 Ma; Schoene & Bowring, 2007) and Durango apatite (31.44 ± 0.18 Ma, McDowell *et al.*, 2005) were employed as secondary standards. Common Pb correction employed weighted mean average ^{207}Pb-corrected ages. An iterative approach based on terrestrial Pb evolution models (Stacey & Kramers, 1975) was used to calculate the initial Pb isotopic composition for detrital apatite samples as described in Chew *et al.* (2011).

5.6 APATITE FISSION TRACK RESULTS

Only twelve samples (LP1, PIAS1, FM1, CST1-4, CT1-13, OL1, AO1, SC1, AR1, CM2, QR1, TL1, MMP1, MM1) from a total of sixty-seven collected samples yielded good or acceptable quantities of apatite for fission track measurements. This was due to the lack of apatites in clastic lithologies and the small apatite grain size in some igneous lithologies. The fission track ages from these twelve samples are shown in table 5.1.

Sample	Lithology	Age (Ma)		Elev. amsl (m)	No. Of grains	Ns	Σpiξ2i	1σΣpiξ2i	χ2	P(χ2)	Cl (wt%)	1σ Cl wt%	FT Age (Ma)	1σ (Ma)	dpar	dper	Track lenghts n	mean (µm)	s.d. (µm)
Ossa Morena Zone																			
LP1	Granite	Viséan[+]	340±7,6	374	13	987	6.17E-05	1.08E-06	12.83	0.38	0.53	0.09	**148.0**	6.1	1.38	0.30	263	9.91	1.87
PIAS1	Granite	Viséan[+]	334,9±4,3	366	21	2581	2.22E-04	3.26E-06	14.07	0.83	0.02	0.02	**108.2**	3.4	1.33	0.28	39	11.59	1.65
South Portuguese Zone - Mértola Formation																			
FM1 (Cl(wt%)<0,35)	Greywacke	Viséan[1,2,3,4]	345-326	138	10	423	4.96E-05	1.28E-06	77.99	0.00	0.12	0.10	**79.4**	4.6	1.18	0.39	-	-	-
FM1 (Cl(wt%)>0,35)	Greywacke	Viséan[1,2,3,4]	345-326	138	8	586	2.54E-05	1.09E-06	133.27	0.00	0.50	0.10	**212.6**	13.3	1.18	0.25	-	-	-
CST1-4	Greywacke	Viséan[1,2,3,4]	345-326	227	20	1003	1.12E-04	7.73E-03	10.27	0.95	0.27	0.07	**90.8**	3.8	1.31	0.31	40	11.04	1.99
CT1-13	Greywacke	Viséan[1,2,3,4]	345-326	104	4	173	1.45E-05	4.96E-07	17.88	0.00	0.28	0.18	**111.0**	9.5	-	-	-	-	-
OL1	Greywacke	Viséan[1,2,3,4]	345-326	95	8	334	1.89E-05	7.03E-07	2.67	0.91	0.64	0.28	**157.9**	10.3	1.59	0.34	7	9.97	2.61
South Portuguese Zone - Mira Formation																			
AO1	Greywacke	Serpukhovian-early Bashkirian[1,2,3,4]	315-307	25	19	1190	1.10E-04	1.40742E-06	18.90	0.40	0.28	0.10	**100.1**	3.7	1.58	0.33	9	10.52	2.53
SC1	Greywacke	Serpukhovian-early Bashkirian[1,2,3,4]	315-307	161	6	334	4.29E-05	1.01E-06	8.69	0.12	0.32	0.16	**72.5**	4.6	1.35	0.29	7	12.44	0.90
South Portuguese Zone - Brejeira Formation																			
AR1	Greywacke	Bashkirian-late Moscovian[1,2,3,4]	307-311	2	8	120	1.88E-05	4.38E-07	3.85	0.80	0.09	0.05	**59.9**	5.7	1.16	0.24	5	13.18	2.33
Algarve Basin - Upper Triassic																			
CM2	Sandstone	Upper Triassic [5]	±200	25	8	382	1.67E-05	3.78337E-07	13.58	0.06	0.32	0.39	**210.8**	12.5	1.30	0.36	-	-	-
QR1	Sandstone	Upper Triassic [5]	±200	176	6	283	1.29E-05	2.48E-07	10.59	0.06	0.26	0.30	**225.7**	14.9	1.30	0.33	-	-	-
TL1	Sandstone	Upper Triassic [5]	±200	71	18	1453	5.97E-05	7.87E-07	10.90	0.86	0.11	0.14	**223.9**	7.9	1.30	0.29	54	10.10	1.53
Cretaceous Monchique Complex																			
MMP1	Syenite	Campanian [6,7,8,9]	72±2	407	5	151	2.04E-05	6.11E-07	1.03	0.91	0.03	0.02	**69.1**	6.1	1.26	0.22	-	-	-
MM1	Syenite	Campanian [6,7,8,9]	72±2	228	5	121	2.92E-05	6.92E-07	0.25	0.99	0.02	0.01	**46.1**	4.4	1.25	0.28	84	12.70	0.80

Table 5.1 Apatite Fission Track results.

5.6.1 FT results: Ossa Morena Zone (fig. 5.2)

The LP1 granite yielded a FT age of 148±6.1 Ma. The mean track length is 9.91 μm with a standard deviation of 1.87 μm. The high number of confined tracks is due to the Cf irradiation that this sample was subjected to. The track lengths are relatively short and their distribution indicates that this sample has stayed for a long period of time in the partial annealing zone and has a recent cooling history. The average Dpar is 1.38 μm and Dper 0.30 μm.

The PIAS1 granite yielded a FT age of 108.2±3.4 Ma. The mean track length is 11.59 μm with a standard deviation of 1.65 μm. The confined track distribution show an almost bimodal pattern that could be related to a complex history with more than one stage within the apatite partial annealing zone. The average Dpar is 1.33 μm and Dper 0.28 μm.

For these two samples there is no clear relationship between the following parameters: FT ages and the Cl content, FT ages and Dpar and between Dpar and the Cl content. However, despite the samples being situated at a similar elevation and in the same geological unit, these two granites may have experienced different thermal stories. Recent tectonism or the difference in granite (the content of Cl in apatites from sample LP1 (0.52 wt%) is higher than in sample Pias 1 (0.02 wt%) may explain the older FT age) could be a likely explanation for the difference in FT ages between the two samples. Despite the difference in FT ages of the two samples, they are consistent with the FT ages obtained by Stapel (1999) for the Variscan Zone.

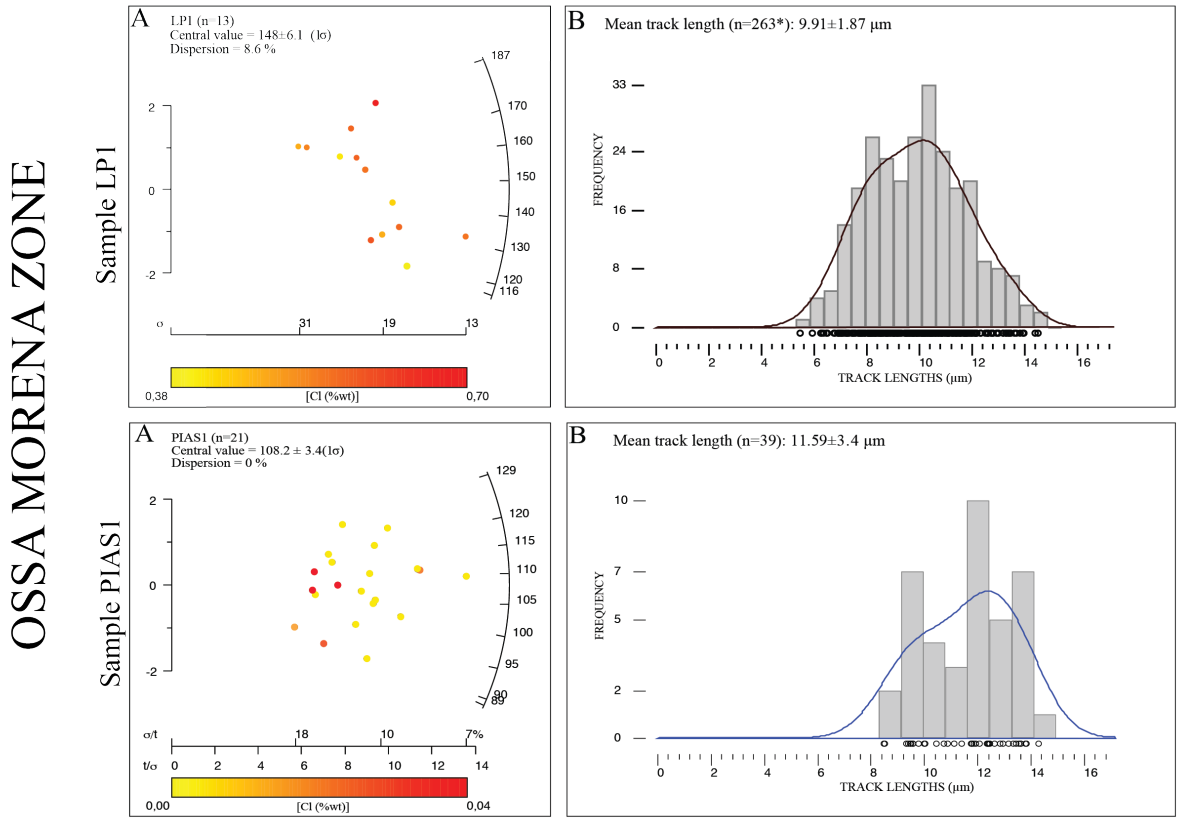

Figure 5.2 AFT results from Ossa Morena Zone. Sample LP1 was subjected to ^{238}Cf irradiation.

5.6.2 FT results from the Baixo Alentejo Flysch Group samples

It was possible to determine FT ages from seven samples of the Baixo Alentejo Flysch Group from the South Portuguese Zone. However only one sample (CST1-4) from the Mértola Formation yielded enough confined tracks to allow modelling of the data.

5.6.2.1 Mértola Fm. samples (fig. 5.3)

The FM1 greywacke has two populations of FT ages. These two populations were defined based on the Cl content. The first population, with a Cl content lower than 0.35 wt% yielded an FT age of 79.4±4.6 Ma with a Dpar of 1.18 µm and a Dper of 0.39 µm. The second population with a Cl content higher than 0.35 yielded a FT age of 212.6±13.3 Ma with a Dpar of 1.18 µm and a Dper of 0.25 µm. No confined tracks were observed in this sample. The oldest FT age is younger than the depositional age, meaning that the FT ages were at least partially reset after deposition. The two populations of FT ages could indicate that the sample was not totally annealed – possibly only the low Cl apatites were totally reset.

The CST4-1 greywacke yielded an FT of 90.8±3.8 Ma. The mean track length is 11.04μm with a standard deviation of 1.99μm. The average Dpar is 1.31 μm and Dper 0.31 μm. There was not any observed relationship between FT ages and Cl content, FT age and Dpar, and Cl content and Dpar. The track lengths are relatively short and its broad distribution indicating that the sample resided for a long period of time in the partial annealing zone.

In sample CT1-13 only 4 grains were analysed, yielding an age of 111±9.5 Ma. No confined tracks were observed in this sample and no relationship was observed between between FT ages and Cl content, FT age and Dpar, and Cl content and Dpar

The OL1 greywacke yielded an age of 157.9±10.3 Ma. The mean track length is 9.97 μm with a standard deviation of 2.61μm. The number of confined tracks is very low and their distributions do not allow for any firm interpretations. There was no observed relationship between FT ages and Cl content, FT age and Dpar, and Cl content and Dpar.

The samples from the Mértola Formation were collected in different geographic locations and stratigraphic levels (chapter II). The FT ages show that all apatites were reset after deposition. The older FT age in sample FM1 (216 Ma) is from apatites with high Cl (>0.35 wt%) content. The higher Cl content in these grains means that they could resist to the annealing and preserved an older thermal history. The others samples gave Cretaceous ages, meaning that after the Triassic the Mértola Formation lithologies were buried again reaching temperatures above 120 ºC.

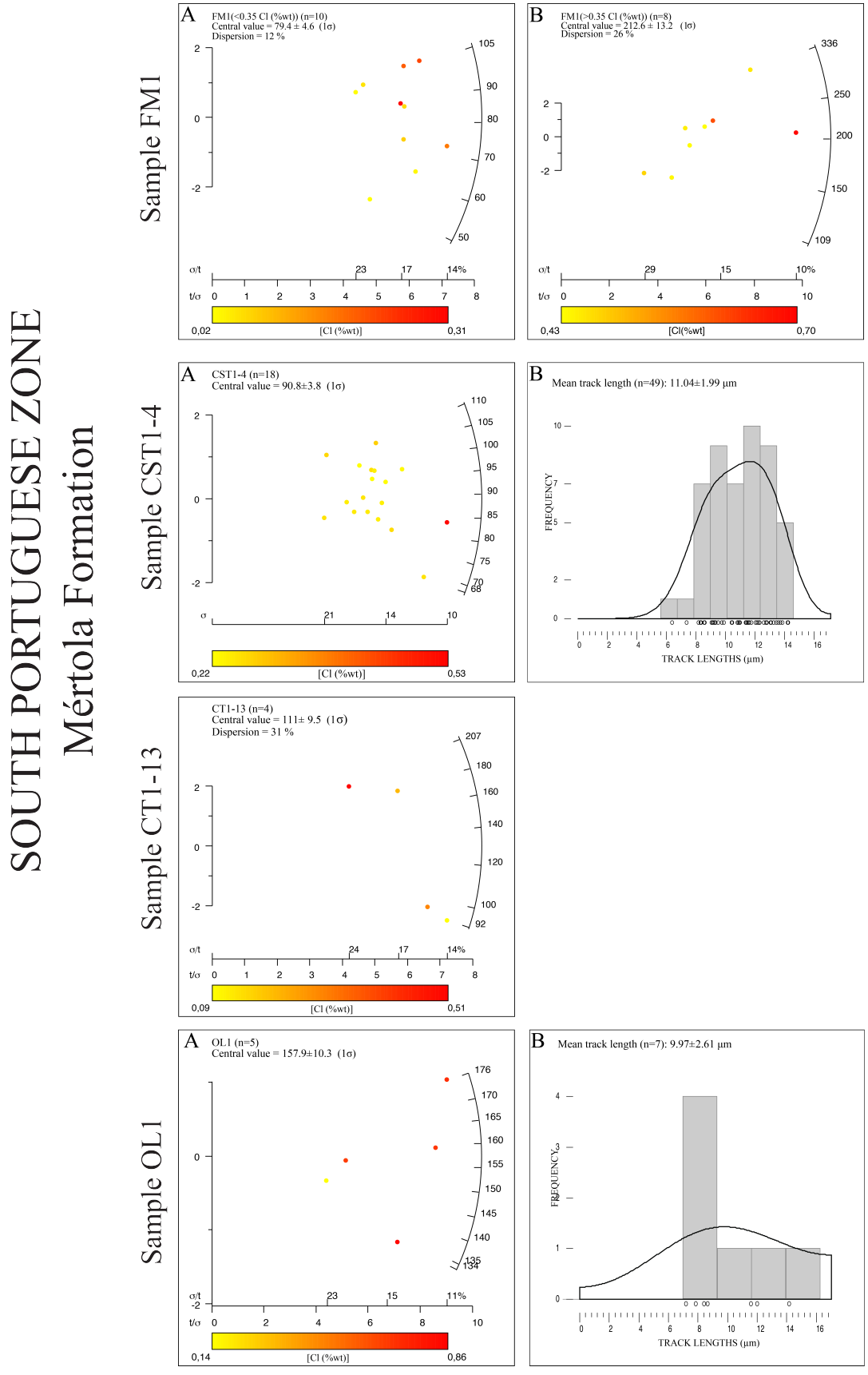

Figure 5.3 FT results from Mértola Formation from the Baixo Alentejo Flych Group of South Portuguese Zone.

5.6.2.2 Mira Fm. Samples (fig. 5.4)

The AO1 greywacke yielded an FT age of 100.1±3.7 Ma. The mean track length is 10.52 µm with a standard deviation of 2.57 µm. The average Dpar is 1.58 µm and Dper 0.33 µm.

The SC1 greywacke yielded an FT age of 72.5±4.6 Ma. The mean track length is 12.44 µm with a standard deviation of 0.9 µm. The average Dpar is 1.35 µm and Dper 0.29 µm. The track length distribution shows a pattern that could be related to a long period residing in the partial annealing zone.

In these two samples there was no observed relationship between FT ages and Cl content, FT age and Dpar, and Cl content and Dpar. Both samples yield Cretaceous FT ages.

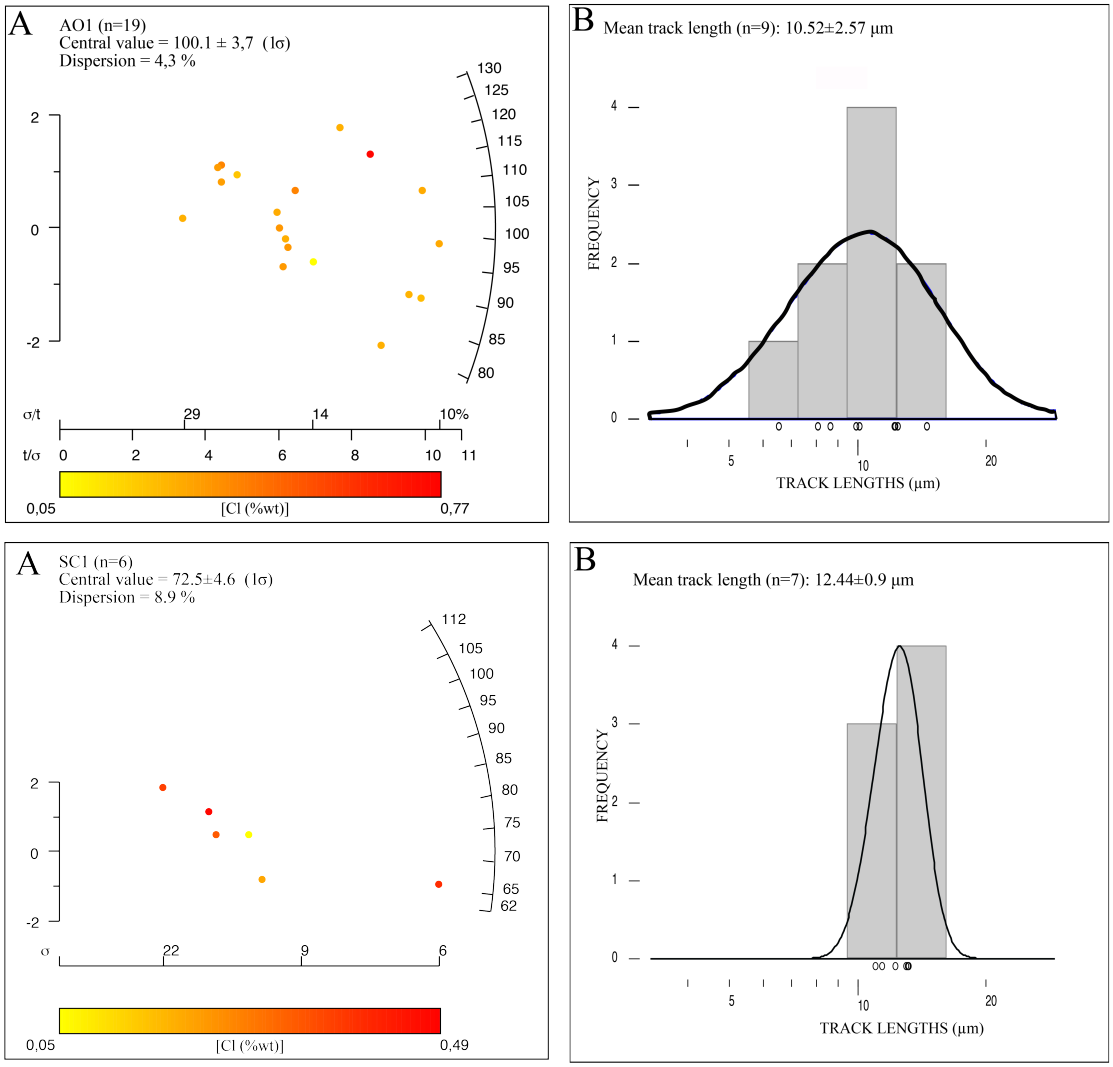

Figure 5.4 AFT results from the Mira Formation of the Baixo Alentejo Flych Group of the South Portuguese Zone.

5.6.2.3 Brejeira Formation samples (fig. 5.5)

The AR1 greywacke yielded an FT |age of 59.9±5.7 Ma. Only 5 grains show measurable confined tracks and therefore no firm interpretations can be drawn from the track length data. However, the mean track length is 13.18 µm with a standard deviation of 2.33 µm. The average Dpar is 1.16 µm and Dper 0.24 µm. There was no observed relationship between FT ages and Cl content, FT age and Dpar, and Cl content and Dpar. The FT age of 59.9 Ma indicates a Palaeogene age that was also identified in the Ossa Morena Zone north of Seville (Stapel, 1999).

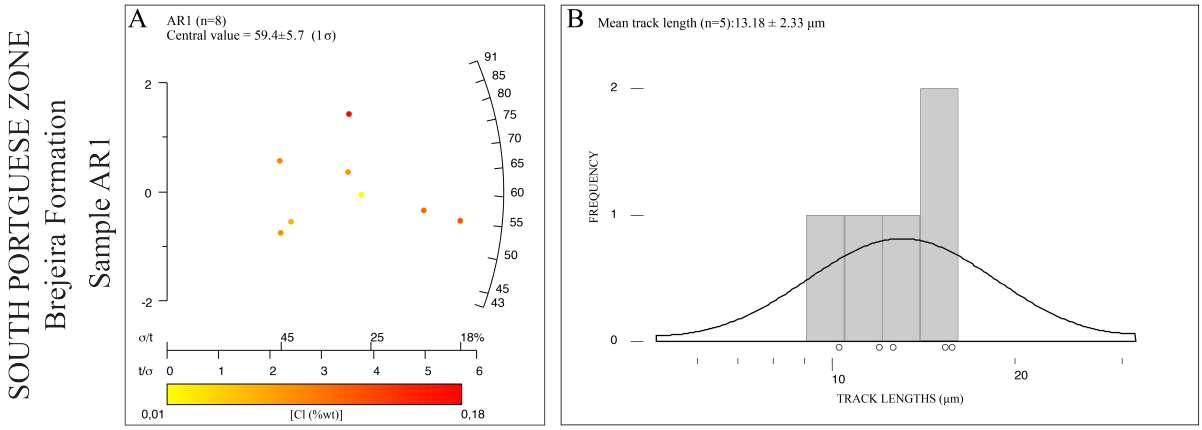

Figure 5.5 FT results from the Brejeira Formation from the Baixo Alentejo Flych Group of the South Portuguese Zone.

5.6.3 FT results from the Algarve Basin samples (fig. 5.6)

Several samples from the Algarve Basin were collected but only the samples from the Silves Upper Triassic sandstones yielded enough apatites for FT studies, and from them only three samples yielded enough apatite to determine FT ages.

The CM2 sandstone sample yielded an FT age of 210.8±12.5 Ma. The average Dpar is 1.30µm and Dper 0.36 µm. The QR1 sandstone yielded an FT age of 225.7±14.9 Ma. The average Dpar is 1.30 µm and Dper 0.33 µm. The TL1 sandstone yielded an FT age of 223.9±7.9 Ma. The mean track length is 10.1 µm with a standard deviation of 1.53 µm. The high number of confined tracks is due to the Cf irradiation that this sample was subjected to. The track lengths are relatively short and its distribution indicates that the sample may have resided for a long period of time in the partial annealing zone and underwent a recent phase of exhumation. The average Dpar is 1.30 µm and Dper 0.29 µm.

In these three samples there was no observed relationship between FT ages and Cl content, FT age and Dpar, and Cl content and Dpar.

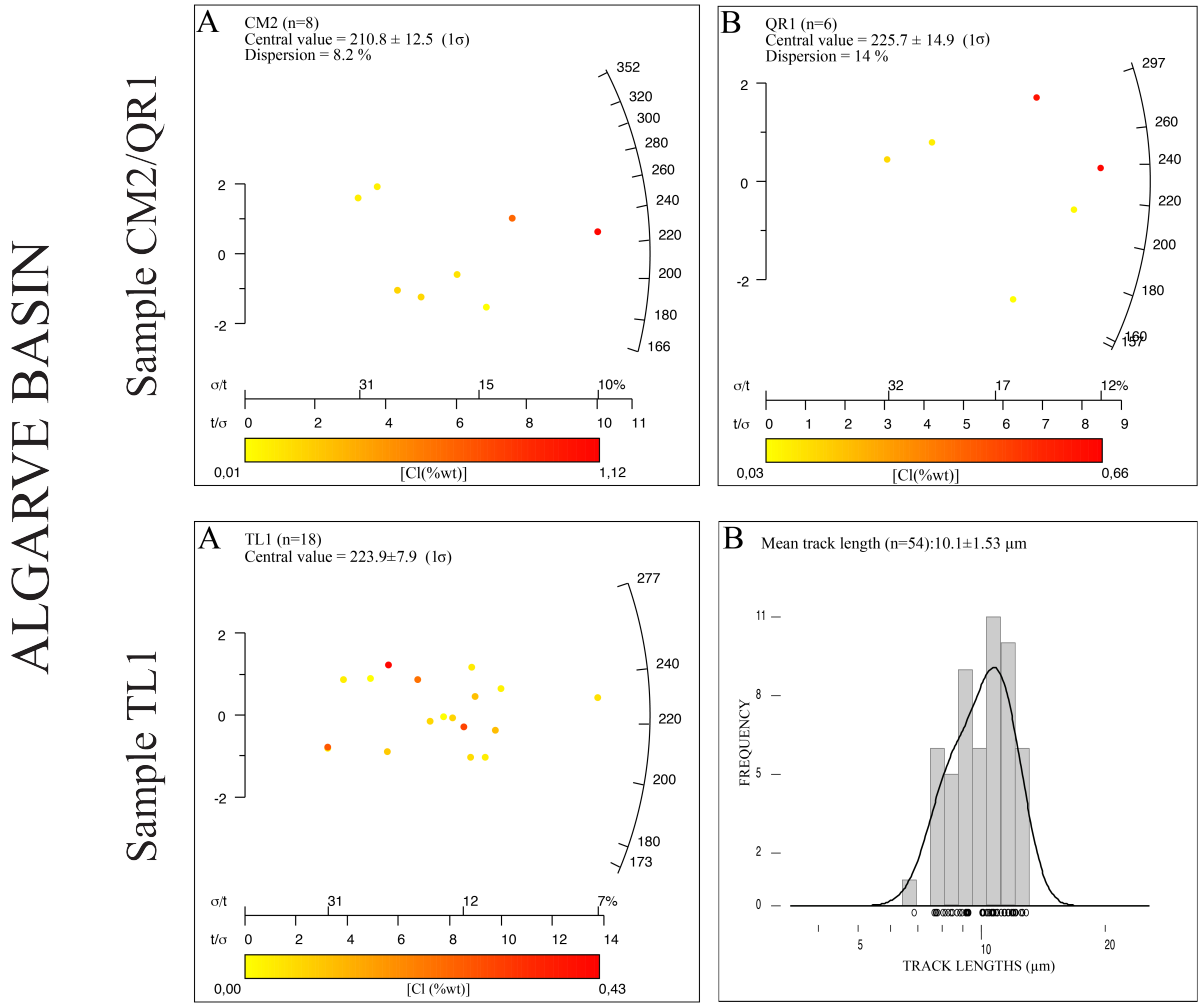

Fig. 5.6 FT results from the Algarve Basin.

The apatite FT ages for the Upper Triassic samples are all older than the depositional age (±200 Ma). These ages mean that the samples did not reset pre-depositional fission tracks. However, the length of confined tracks in sample TL1 is relatively short, indicating that the sample was buried to temperatures higher than 60 ºC. Although, a high number of confined tracks was measured, due to the complex thermal story of these detrital apatites it was not viable to model sample TL1.

5.6.4 FT results Cretaceous Alkaline Monchique complex (fig. 5.7)

The MM1 syenite yielded an FT age of 46.1±4.4 Ma. The mean track length is 12.7 µm with a standard deviation of 0.8 µm. The average Dpar is 1.25 µm and Dper 0.28 µm.

The MMP1 syenite yielded an FT age of 69.1±6.1 Ma. The average Dpar is 1.26 µm and Dper 0.22 µm. In these two samples there was no observed relationship between FT ages and Cl content, FT age and Dpar, and Cl content and Dpar.

The apatites of the Monchique Alkaline Complex (MAC) yielded FT ages that are younger than 72 Ma, the emplacement age of the MAC (Rock, 1978; MacIntyre & Berger, 1982; Bernard-Griffiths *et al.*, 1997; Valadares, 2004; Miranda *et al.*, 2009). The apatite FT age of the sample MMP1, at 407 m, is 23 Ma older than the sample MM1 at 228 m. This indicates that the uplift occurred immediately post-intrusion or contemporaneous to the intrusion. The narrow shape of the distribution of confined tracks lengths reveal a rapid cooling history. In chapter VI the forward modelling of sample MM1 will be discussed in detail.

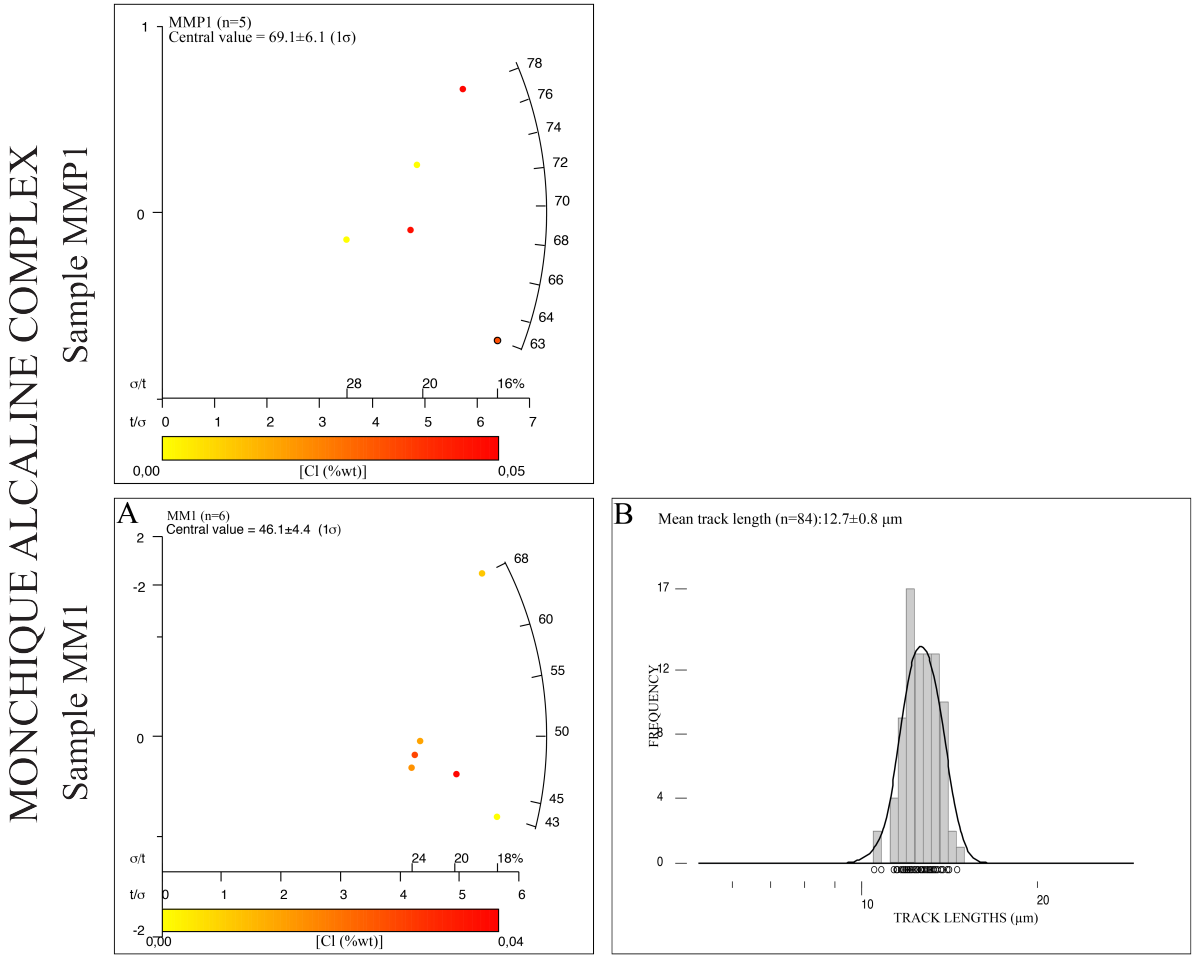

Figure 5.7 AFT results from the Monchique Alkaline Complex.

5.7 SUMMARY

Despite the large number of samples collected, only 18% (12) yielded an adequate concentration of apatite for FT tracks studies. This was due to several factors: (1) in the detrital samples the apatite content is extremely low probably due to the lack of apatite in the source rocks. In the Upper Triassic sandstone samples from the Algarve Basin, the apatite content change even within the same horizon; (2) In some igneous intrusive rocks collected apatites was not observed in thin section or after heavy mineral separation; (3) For some granite and syenite samples it is not always possible to undertake apatite fission track analyses because the size of the crystals can be very small.

Concerning the apatite fission tracks results, some remarks should be highlighted:

- There is a notable similarity between the FT ages in the Ossa Morena Zone and the South Portuguese Zone indicating that uplift must have occurred as a block in these two Variscan Zones;
- The samples from the Ossa Morena zone are at the same elevation but are far apart from each other. The different ages could be related to the Cl content of apatites (average Cl content of 0.52 wt% in sample LP1 and 0.02 wt% in sample Pias1) or due to different local tectonic settings;
-All the Baixo Alentojo Flysch Group samples have been totally reset after deposition and yield FT ages ranging from the Cretaceous (111 to 59.9 Ma) to the Upper Jurassic (Sample OL1-157.9 Ma);
- In the FM1 greywacke sample the Cl content has a strong influence on the FT ages;
- The FT ages from the Upper Triassic sandstone samples from the Algarve Basin indicate that all ages are older than the depositional age, meaning that the samples were not buried to temperatures exceeding 100 ºC;
- The syenite samples from Monchique Alkaline Complex yield different FT ages that could be related to different elevations (and different exhumation histories);
- The Monchique samples have FT ages similar to the country rock FT ages (the Baixo Alentejo Flysch Group samples), which could suggest that the Monchique Alkaline Complex was intruded into rocks that had an ambient temperature of *ca.* 90 ºC. If we consider a palaeogeothermal gradient of 30 ºC/km, the emplacement depth should be near 3 km.

VI–APATITE (U-Th)/He AGE ANALYSES

In this chapter the analytical methodology for (U-Th)/He apatite dating and the results obtained will be presented and discussed.

6.1 SAMPLE PREPARATION AND ANALYTICAL PROCEDURES

The (U-Th)/He analyses were performed on single crystals of apatite using the laboratory facilities at the Scottish Universities Environmental Research Centre (SUERC). Apatite crystals without fractures or inclusions and with a euhedral habit were selected. The samples from detrital lithologies contained few apatite grains and when present they were usually rounded or fractured. Therefore, it was only possible to analyse apatites from a single detrital sample (TL1) from Upper Triassic Silves sandstones of the Algarve Basin and from four igneous rock samples, two from the Ossa Morena Zone (PIAS1, PL1) and two from the Monchique Alkaline Complex (MM1 and MMP1). All these samples were already described and in chapters II and IV.

Apatite grains smaller than ~50 μm were avoided for (U-Th)/He dating, because such grains are subject to significant alpha recoil loss and therefore requiring large corrections which cause significant errors in the calculated ages (Farley, 2000). The selected grains were then individually photographed, measured and packed into 1 mm long high purity Pt-foil tubes. The tubes were placed in individual 2 mm holes in a copper sample pan. Helium was extracted from the minerals by heating the foil packets to 600 °C during 1-10 min with an 808 nm diode laser. The extracted gases were purified in an all-metal clean-up line, on a pair of liquid N-cooled charcoal traps. ^{4}He concentrations were measured using an electron multiplier in a Hiden HAL4 quadrupole mass spectrometer by peak-height comparison to a calibrated standard ^{4}He. After the Helium extraction, each grain was unpacked, recovered and the U and Th were extracted by hot acid dissolution using HCl and HF, following the procedures of SUERC. The digested crystals were spiked with known amounts of tracer-isotopes (^{230}Th-^{235}U) and the solutions were then analyzed on a Plasmaquad PQ2.5 inductively coupled plasma mass spectrometer. Durango apatite was used as the age reference (Young *et al.,* 1969; McDowell & Keizer, 1977; Farley, 2000). The ages were calculated using a spreadsheet developed internally at SUERC.

6.2 APATITE (U-Th)/He AGES RESULTS

Five Durango apatite fragments were analysed as reference material giving an average age of 30.45±0.64 Ma. This age is in agreement with the assumed (U-Th)/He age for the Durango apatite of 31.9±0.5 Ma (Young *et al.,* 1969; McDowell & Keizer, 1977; Farley, 2000).
From the Ossa Morena Zone the LP1 granite sample gave a mean (U-Th)/He age of 60.5±1.2 Ma and the PIAS1 granite gave a mean (U-Th)/He age of 108±4.85 Ma. The TL1 sandstone from the Algarve Basin gave a (U-Th)/He age 142.9±2.5 Ma. In the Alkaline Monchique Complex two samples were analysed. The MMP1 and MM1 syenites gave mean (U-Th)/He ages of 32.0±1.65 Ma and 38.5±0.8 Ma, respectively.

Table 6.1 (U-Th)/He age results.

Sample	Age	Elev. Absl (m)	^{4}He	^{238}U	^{232}Th	Bulk age	corrected age
Reference Sample							
Durango			2.30E-8	0.95	22.43	30.3 ± 0.5	**30.3 ± 0.5**
			3.36E-8	1.61	36.89	26.8 ± 0.4	**26.8 ± 0.4**
			1.72E-9	0.063	1.39	36.6 ± 1.2	**36.6 ± 1.2**
			1.94E-9	0.098	2.26	25.5 ± 0.5	**25.5 ± 0.5**
			3.95E-9	0.499	2.28	33.0 ± 0.6	**33.0 ± 0.6**
Ossa Morena Zone							
LP1	Visean	374	2.51E-10	0.039	0.08	39.1 ± 0.8	**47.1 ± 0.9**
			1.64E-9	0.198	0.36	48.6 ± 0.9	**78.3 ± 1.5**
			8.5E-10	0.124	0.28	38.1 ± 0.8	**56.1 ± 1.2**
PIAS1	Visean	366	2.18E-10	0.026	0.03	61.8 ± 2.4	**110.4 ± 2.4**
			2.93E-10	0.039	0.02	61.9 ± 4.2	**106.7 ± 7.3**
Algarve Basin							
TL1	Upper Triassic	71	1.98E-9	0.117	0.1	118.5 ± 2.1	**162.3 ± 2.9**
			3.37E-9	0.093	0.56	124.8 ± 2.1	**158.0 ± 2.6**
			3.29E-10	0.022	0.07	83.3 ± 1.9	**108.2 ± 2.4**
Cretaceous-Monchique							
MMP1	Campanian	407	2.66E-9	0.121	3.31	24.4 ± 0.5	**24.4 ± 0.5**
			1.16E-9	0.055	1.07	31.5 ± 0.7	**31.5 ± 0.7**
			1.59E-9	0.062	1.42	33.3 ± 0.7	**33.3 ± 0.7**
			3.16E-9	0.020	0.22	38.8 ± 4.7	**38.8 ± 4.7**
MM1	Campanian	228	1.73E-9	0.296	1.46	22.4 ± 0.4	**38.2 ± 0.8**
			1.36E-9	0.071	1.72	23.7 ± 0.6	**33.8 ± 0.9**
			3.09E-9	0.094	2.93	32.6 ± 0.5	**43.5 ± 0.7**

5.3 DISCUSSION AND SUMMARY

The apatite (U–Th)/He thermochronometer records the cooling of rocks through the 35–80 °C temperature interval and can be used to determine the timing and rate of exhumation of the uppermost 1–3 km of the Earth's crust (Farley, 2000; Farley, 2002; Brady, 2002). However,

apatite (U–Th)/He apparent ages will generally reflect residence for extended periods of time at temperatures where helium is neither quantitatively retained nor lost by diffusion (Wolf *et al.*, 1998). The analysis of a single age apatite mineral grain is not totally conclusive of a thermal history, but incorporating both apatite FT and (U-Th)/He ages into forward modelling, a more restricted range of thermal history solutions can be extracted. This methodology will be addressed in chapter VIII.

In the Ossa Morena Zone the LP1 granite sample yields a He age of 60.5±1.2 Ma, and the apatite FT age for the same sample is 148±6.1 Ma. This difference in age indicates that the sample stayed a long period of time in a temperature near the partial annealing/retention zone and it had a recent cooling history, based on the fission track lengths data described in chapter V. The PIAS1 granite also from the Ossa Morena Zone, has a (U-Th)/He age of 108±4.85 Ma, similar to the apatite FT age (108±3.4 Ma), that can be related with He implantation.

In the Algarve Basin the TL1 sandstone has a mean (U-Th)/He age of 142.9±2.5 Ma and the apatite FT age for this sample indicates that it has been reset after the deposition. This conclusion does not agree with burial thermal histories curves modelled by Fernandes *et al.* (2013) for the Sagres-Lagos area that indicate that the maximum temperature may have been attained during the late Cretaceous. However, the burial thermal history was constrained for the Lagos area whereas the number of samples studied was superior to the Sagres area. In fact, the stratigraphic and paleontological data (Rocha, 1976) indicate that Sagres area constituted a topographic high that separated the west Portuguese margin from the southern Portuguese margin in the Jurassic. Both Mesozoic and Cenozoic sedimentary sequences are much thinner in this area than in any other part of the basin (Terrinha, 1998). So, the sample TL1 may belong to a block that could constitute a structural high throughout the Mesozoic times. With this assumption and considering the maximum palaeogeothermal gradients calculated for this area of 52 ºC/km (Fernandes *et al.*, 2013), burial under a 1.5 km thick succession would be enough to reset the (U-Th)/He ages.

In the Monchique Alkaline Complex the MM1 syenite yields a mean (U-Th)/He age of 38.5±0.8 Ma with is similar to sample MMP1 (mean (U-Th)/He age of 32.0±1.65 Ma).

VII–U-Pb ZIRCON AND APATITE GEOCHRONOLOGY

In this chapter the analytical methodology for U-Pb detrital zircon and apatite dating will be presented and discussed.

7.1 SAMPLE SELECTION AND PREPARATION

Four greywackes samples from the Baixo Alentejo Flysch Group (fig. 2.1) were selected for detrital zircon dating. The selected samples were: sample FM1 collected at the base of the Mértola Formation, *ca.* 100 m above the contact with the Volcano-Sedimentary Complex; sample AO1 collected at the base of the Mira Formation; and two samples from the Brejeira Formation, DZ1 and DZ12, collected from two different stratigraphic levels. Sample DZ1 was collected from quartz-wacke beds positioned at the lower part of the Brejeira Formation while sample DZ12 was collected from greywacke beds in the upper part of this formation. Zircons grains were separated and concentrated as described in chapter V. Zircons were mounted in 2.5 cm epoxy mounts and polished to approximately half thickness prior to analysis.

The apatites analysed for U-Pb dating were from the same samples that was selected for fission track analyses. The analysed samples were described in chapter II and V, and correspond to: samples PIAS1 and LP1 from the Ossa-Morena Zone; samples FM1, CST1-4, CT1-13 and OL1 from the Mértola Formation; sample AO1 from Mira Formation; sample AR1 from the Brejeira Formation; samples TL1, QR1, SC1 and CM2 from Upper Triassic Silves Sandstones from the of the Algarve Basin; and samples MM1 and MMP1 from the Monchique Alkaline Complex. The apatites were already mounted for FT analyses and only the grains selected for FT measurements were analysed.

7.2 ZIRCON ICPMS ANALYTICAL TECHNIQUE

Zircon U-Pb data was collected from the Baixo Alentejo Flysch Group samples using a Photon Machines Analyte Exite 193 nm ArF Excimer laser-ablation system coupled to a Thermo Scientific iCAP Qc at the Department of Geology Trinity College Dublin. Nine isotopes (^{88}Sr, ^{91}Zr, ^{200}Hg, $^{204,206,207,208}Pb$, ^{232}Th and ^{238}U) were acquired for each of the four zircon samples using a 30 μm laser spot, a 4 Hz laser repetition rate and a fluence of 3.31 J/cm^2. The analytical procedure utilized repeated blocks of four zircon standards followed by 20 unknown samples. The four zircon standard analyses comprised two analyses of the

primary standard 91500 zircon ($^{206}Pb/^{238}U$ TIMS age of 1065.4±0.6 Ma; Wiedenbeck *et al*., 1995), followed by one analysis each of Plešovice zircon (weighted mean $^{206}Pb/^{238}U$ TIMS age of 337.13 ± 0.37 Ma; Sláma *et al.,* 2008) and Temora 2 zircon ($^{206}Pb/^{238}U$ TIMS age of 416.8 ± 1.3 Ma; Black *et al.,* 2004).

The raw isotope data were reduced using the "Vizual Age" data reduction scheme (Petrus & Kamber, 2012) of the freeware IOLITE package of Paton *et al*. (2011). User-defined time intervals are established for the baseline correction procedure to calculate session-wide baseline-corrected values for each isotope. The time-resolved fractionation response of individual standard analyses is then characterised using a user-specified down-hole correction model (such as an exponential curve, a linear fit or a smoothed cubic spline). The data reduction scheme then fits this appropriate session-wide "model" U-Th-Pb fractionation curve to the time-resolved standard data and the unknowns. Sample-standard bracketing is applied after the correction of down-hole fractionation to account for long-term drift in isotopic or elemental ratios by normalizing all ratios to those of the U-Pb reference standards. During the course of analysis, the Plešovice and Temora 2 secondary zircon standards yielded LA-ICPMS U-Pb ages of 337.7 ± 1.0 Ma and 417.7 ± 1.4 Ma respectively.

7.3 APATITE ICPMS ANALYTICAL TECHNIQUE

Apatite uranium concentrations were measured using a Photon Machines Analyte Excite 193 nm ArF Excimer laser ablation system coupled to a Thermo Scientific iCAP Qc ICPMS in Trinity College Dublin. The analytical protocol employed is described in detail in Chew & Donelick (2012), and integrates uranium concentration measurements for apatite fission track dating with REE and trace element analyses along with the isotopes required for required for U-Th-Pb geochronology. The time interval for the baseline correction was 15 s and the analysis was 45 s. The laser spot size was set at 30 μm with a repetition rate of 4Hz and a fluence of 3.1 mJ/cm^2 to yield spot depths typically 10 μm deep. A HelEx 2-volume sample cell was used with a He carrier gas flow of 800 mL/min. Ar and N_2 as an additional di-atomic gas to enhance sensitivity (flow rate of 6 mL / min) were admixed downstream. Typically 28 isotopes were measured in each apatite sample. Of these isotopes, ^{43}Ca was used as the internal standard to correct for drift in instrument sensitivity and variations in ablation volume during sessions. Common trace elements in apatite (e.g. Cl, Mn, Sr and Y) and the REE were determined along with the seven isotopes (^{200}Hg, $^{204,206,207,208}Pb$, ^{232}Th and ^{238}U) commonly required for U-Th-Pb geochronology. Data reduction for both trace element concentration

measurements and U-Th-Pb geochronology was undertaken using the freeware Iolite package of Paton *et al.* (2011). The Iolite approach involves processing an entire analytical session (typically > 5 h) of data, which is not only more efficient but also greatly improves the consistency and reliability of data reduction.

Trace element concentration measurements were undertaken using the "Trace Elements" data reduction scheme in Iolite. Cl concentration measurements followed the analytical protocol of Chew *et al.* (2014a). The ^{35}Cl background-corrected signals for each apatite analysis were normalized to the internal standard (^{43}Ca) and then sample-standard bracketing was employed using apatites of known Cl concentration (Bamble chlorapatite and Durango fluorapatite).

Uranium concentration in unknown apatites followed the analytical protocol of Donelick *et al.* (2005). In contrast to the ICPMS absolute calibration approach of Hasebe *et al.* (2003), which employs the ^{238}U fission-decay constant, a fission track registration factor and a calibration factor for etching and observation, Donelick *et al.* (2005) used a modified zeta calibration approach (*cf.* Hurford & Green, 1983) for ICPMS apatite U concentration measurements. The method assumes that the apatite ^{43}Ca signal intensity during a given LA-ICP-MS session acts as a proxy for the volume of apatite ablated, and hence the apatite $^{238}U/^{43}Ca$ ratio yields relative U concentration measurements. In this study an extensive primary LA-ICPMS session was undertaken on crystals of Durango apatite that were previously counted for fission tracks to yield a primary LA-ICPMS zeta factor. These same crystals of Durango apatite were then analysed in subsequent LA-IPCMS (along with apatite unknowns for fission-track dating) to yield a session-specific calibration factor on the primary zeta value. Inter-session drift in both the primary and subsequent LA-ICPMS sessions was corrected for by monitoring the $^{238}U/^{43}Ca$ ratio of NIST612 standard glass. The main difficulty in apatite fission-track dating by LA-ICPMS is ensuring that the uranium distribution with the portion of sample that generates fission tracks on the polished apatite surface is quantified spatially, both horizontally (i.e. along the surface of the grain mount) and vertically. The spontaneous track density in the samples analysed in this study was high enough to detect possible U zonation, while depth-related variations in U concentration were accounted for here by incorporating a function within the Iolite "Trace elements" data reduction scheme that weights appropriately the $^{238}U/^{43}Ca$ ratio with depth. As LA–ICPMS is a destructive technique high quality 3-D images of all the counted grains were archived for potential reinvestigation in the future.

Apatite U-Th-Pb geochronology was undertaken using a modified version of VizualAge data reduction scheme (Petrus & Kamber, 2012) for Iolite. This data reduction scheme (VizualAge_UcomPbine) can correct for variable amounts of common Pb in any U–Pb accessory mineral standard as long as the standard is concordant in the U/Pb (and Th/Pb) systems after common Pb correction (Chew *et al.*, 2014b). A ca. 1 cm sized crystal of Madagascar apatite (Thomson *et al.*, 2012) which has yielded a weighted average ID-TIMS concordia age of 473.5 ± 0.7 Ma (Cochrane *et al.*, 2014) was used as the primary apatite reference material in this study. McClure Mountain syenite apatite ($^{207}Pb/^{235}U$ TIMS age of 523.51 ± 1.47 Ma; Schoene & Bowring, 2007) and Durango apatite (31.44 ± 0.18 Ma, McDowell *et al.*, 2005) were employed as secondary standards. Common Pb correction employed weighted mean average ^{207}Pb-corrected ages. An iterative approach based on terrestrial Pb evolution models (Stacey & Kramers, 1975) was used to calculate the initial Pb isotopic composition for detrital apatite samples as described in Chew *et al.* (2011).

7.4 ZIRCON U-PB GEOCHRONOLOGY RESULTS

Results are presented as Concordia diagrams and as probability density plots (fig. 7.1 and 7.3). Only data that are less than 20% discordant and with an analytical precision (2σ) better than 10% are shown on figures 7.1 and 7.2. $^{206}Pb/^{238}U$ ages were used for all ages quoted in the text and for all grains on the probability density plots. The U–Pb LA-ICPMS data are shown in the annex III. All Concordia diagrams and probability density plots were drawn using Isoplot v3.0 (Ludwig, 2003).

7.4.1 South Portuguese Zone

7.4.1.1 Mértola Formation (FM1)

A total of 50 zircon grains were analysed in sample FM-1 (the Mértola Formation with a depositional age of 345-326Ma). Sample FM1 is dominated by U-Pb zircon ages within the 326-388 Ma age range (corresponding to 34 grains) and a peak at 336 Ma. A sub-population of U-Pb zircon ages occurs within the 440-619 Ma interval (corresponding to 11 grains), with two peaks at 498 and at 582 Ma, Five U-Pb zircons analyses were encountered in the interval 637-2193 Ma (the U-Pb age age of the oldest zircon).

7.4.1.2 Mira Formation (AO1)

A total of 40 zircon grains were analysed in sample AO1 from the Mira Formation (depositional age of 326-315 Ma). A cluster of U-Pb zircon ages occurs within the interval 316-369 Ma, with a peak at 323 Ma, and comprises more than 50% of the data (21 grains). A sub-population occurs within the 400-612 Ma age range, with a peak at 482 Ma, corresponding to 12 grains. Lastly, seven zircon grains occur within the interval 1267-2428 Ma.

7.4.1.3 Brejeira Formation (DZ1, DZ12)

Samples DZ1 and DZ12 were collected from the Brejeira Formation (depositional age of 315-307 Ma). A total of 79 grains in sample DZ1 and 65 in sample DZ12 were analysed. The youngest grain in sample DZ1 yielded an age of 367 Ma. Two well-defined sub-populations are evident in sample DZ1. One occurs within the interval 367-447 Ma, with a peak at 420 Ma, and is represented by 13 grains. The second population, corresponding to 40 grains, shows a large spectrum of ages within the interval 519-675Ma, with a peak at 608 Ma. Twenty-six zircons grains yielded ages in the interval 720-2150 Ma.

The youngest grain in sample DZ12 yielded an age of 350 Ma. Two small sub-populations lie within the intervals 350-371 Ma (4 grains) and 415-421 Ma (3 grains), with peaks at 366 and 415 Ma, respectively. A prominent sub-population between 498-687 Ma (34 grains) exhibits two peaks at 623 Ma and 530 Ma respectively. The remaining 24 zircons yielded ages between 720 and 2649 Ma. Only two Archean zircon grains (2649 and 2708 Ma) were identified.

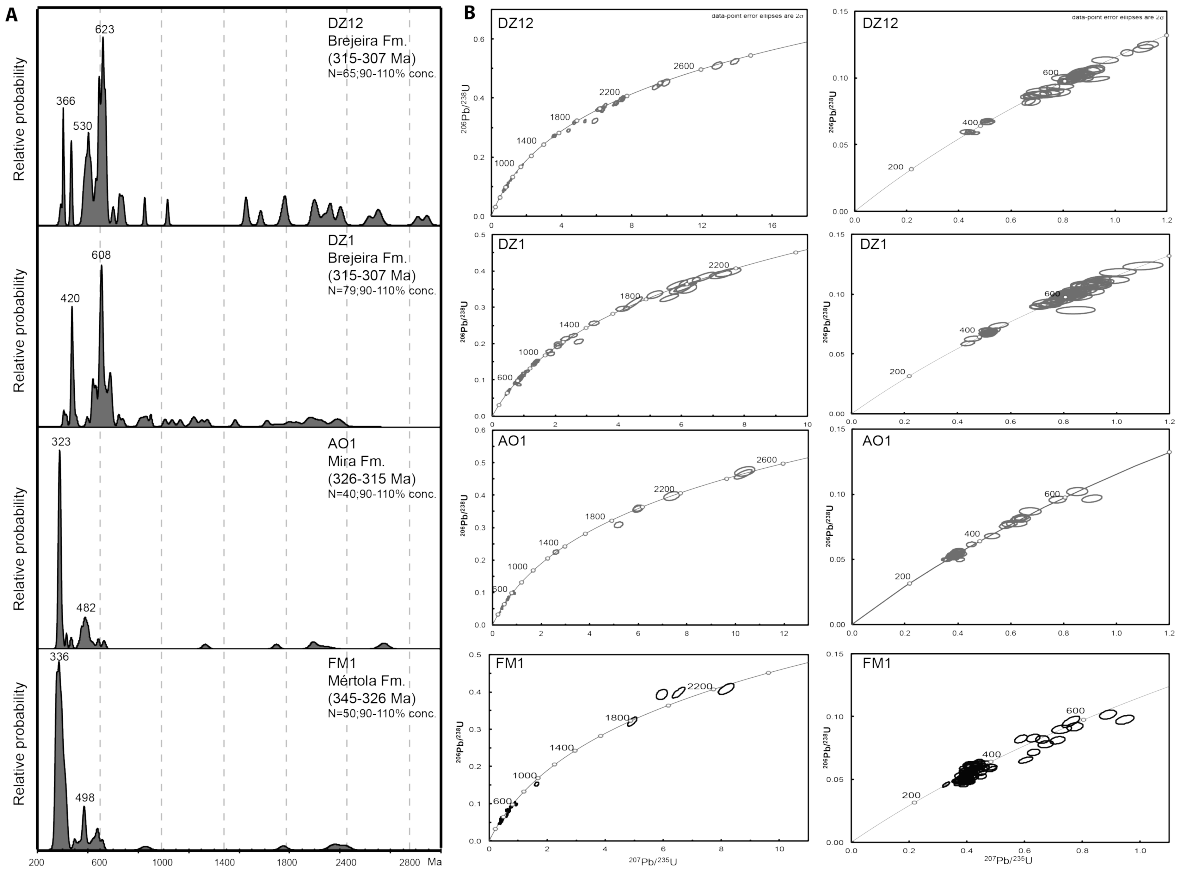

Figure 7.1 In the left column the U–Pb LA-ICP-MS zircon age probability density plots are presented. All ages are $^{206}Pb/^{238}U$ ages. Data which were more than 20 % discordant or with an analytical precision worse than 10 % (2σ) are excluded. Numbers on the probability density peaks are the ages of the peak maxima (in Ma). In two columns in the right, the concordia plots of U-Pb analytical data are presented. Ellipses represent 2σ uncertainties. Data that are more than 20 % discordant or with analytical precision worse than 10 % (2σ) are not shown. Plots and concordia diagrams were drawn using Isoplot v3.0 (Ludwig, 2003).

Samples CM2 and TL1 were collected from the Upper Triassic "Silves Sanstone" Formation from the Algarve Basin (depositional age of 200 Ma). A total of 88 zircon grains in sample CM2 and 61 grains in sample TL1 were analysed. The youngest grain in sample CM2 yielded an age of 204 Ma. Three well-defined sub-populations are observed in sample CM2. The first occurs within the age interval of 204-633 Ma, with peaks at 269 Ma, 435 Ma and 577 Ma, and is represented by a total of 54 grains. The second population occurs in the age interval 745-1064 Ma, with a peak at 918 Ma and is represented by 13 grains. The last population shows a large spectrum of ages within the age interval 1412-2479 Ma, corresponding to 20 grains. The oldest grain yielded an age of 3096 Ma.

The sample TL1 have a small population defined in the age interval of 308-322 Ma (corresponding to 34 grains), with a peak at 312 Ma. The sample is dominated by U-Pb zircon ages within a 403-760 Ma age range (corresponding to 46 grains), with a peak at 557 Ma. Another two sub-population of U-Pb zircon ages occurs within the 925-1221 Ma and 1904-

3110 Ma intervals (corresponding to 5 grains in each interval). The oldest zircon yielded a U-Pb age of 3110 Ma.

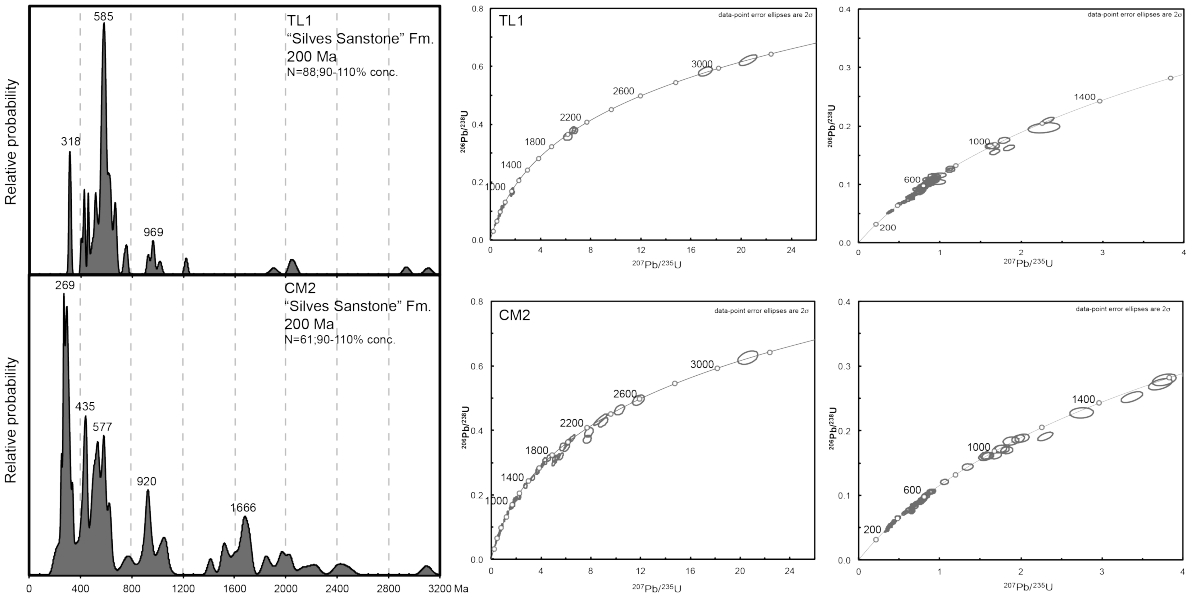

Figure 7.2 In the left column the U–Pb LA-ICP-MS zircon age probability density plots are presented. All ages are $^{206}Pb/^{238}U$ ages. Data which were more than 20 % discordant or with an analytical precision worse than 10% (2σ) are excluded. Numbers on the probability density peaks are the ages of the peak maxima (in Ma). In two columns in the right, the concordia plots of U-Pb analytical data are presented. Ellipses represent 2σ uncertainties. Data that are more than 20% discordant or with analytical precision worse than 10% (2σ) are not shown. Plots and concordia diagrams were drawn using Isoplot v3.0 (Ludwig, 2003).

7.5 APATITE U-Pb GEOCHRONOLOGY RESULTS

The results of apatite geochronology are presented as weighted average ^{207}Pb-corrected ages diagrams (fig. 7.3). The U–Pb LA-ICP-MS data are shown in annex IV. The weighted average diagrams were drawn using Isoplot v3.0 (Ludwig, 2003).

Unlike the mineral zircon, apatite is unstable in acidic groundwaters and weathering profiles, having a limited mechanical stability in sedimentary transport systems (Morton & Hallsworth, 1999). It is, therefore, likely to represent only first cycle detritus, and would yield complementary information to detrital zircon provenance studies (Chew *et al.*, 2011).

7.5.1 Ossa-Morena Zone (PIAS1, LP1)

The apatites from samples PIAS1 and LP1 from the Ossa-Morena Zone were dated.
In the sample PIAS1, 24 apatite grains were analysed giving a mean ^{207}Pb-corrected age for the granite of 334.9±4.3 Ma., whereas the sample LP1 gave a mean ^{207}Pb-corrected age of 340.5±7.6 Ma from 19 analysed apatite grains.

7.5.2 South Portuguese Zone

7.5.2.1 Mértola Formation (FM1, OL1, CST4-1, CT1-13)

In the Mértola Formation the dated samples yield ^{207}Pb-corrected ages that span between 329-357 Ma. Nineteen grains of sample FM1 were analysed, giving a mean age of 334±14 Ma. In sample OL1 eight grains were measured, giving a mean age of 346±26 Ma. In sample CST4-1 20 grains were analysed giving a mean age of 329±12 Ma and finally, seven apatites from sample CT1-13 were analysed gave a mean age of 357±23 Ma.

7.5.2.2 Mira Formation (AO1)

Only one sample from the Mira Formation was analysed. In sample AO1, eleven apatite grains were analysed and gave a mean ^{207}Pb-corrected age of 330±11 Ma (ranging from 254-388 Ma).

7.5.2.3 Brejeira Formation (AR1)

In sample AR1 from Brejeira Formation 12 apatites were analysed, giving a mean ^{207}Pb-corrected age of 517±94 Ma (ranging from 301-388 Ma).

7.5.3 Algarve Basin (CM2, SC1, QR1, TL1)

Four samples from the Upper Triassic Silves Sandstones in the Algarve Basin were analysed. In the sample CM2, six grains were analysed giving a mean ^{207}Pb-corrected age of 371±82 Ma. Eight apatite grains from sample SC1 were analysed giving a mean ^{207}Pb-corrected age of 315±18 Ma. In the sample QR1 six grains were analysed yielding a range of ^{207}Pb-corrected ages from 214 to 518 Ma. In Sample TL1 twenty-six grains were analysed, yielding ^{207}Pb-corrected ages ranging from 277 to 910 Ma.

7.5.4 Monchique Alkaline Complex (MM1, MMP1)

Two samples from the Monchique Alkaline Complex (MAC) were analysed. Sample MM1 gave a mean ^{207}Pb-corrected age of 70.9±4.6 Ma from the six analysed apatite grains. In sample MMP1 eighteen apatites were analysed giving an age of 89±18 Ma. Both these ages are within the accepted age interval for the emplacement of the MAC of 72±2 Ma (Rock, 1978; MacIntyre & Berger, 1982; Bernard-Griffiths *et al*., 1997; Miranda *et al.*, 2009).

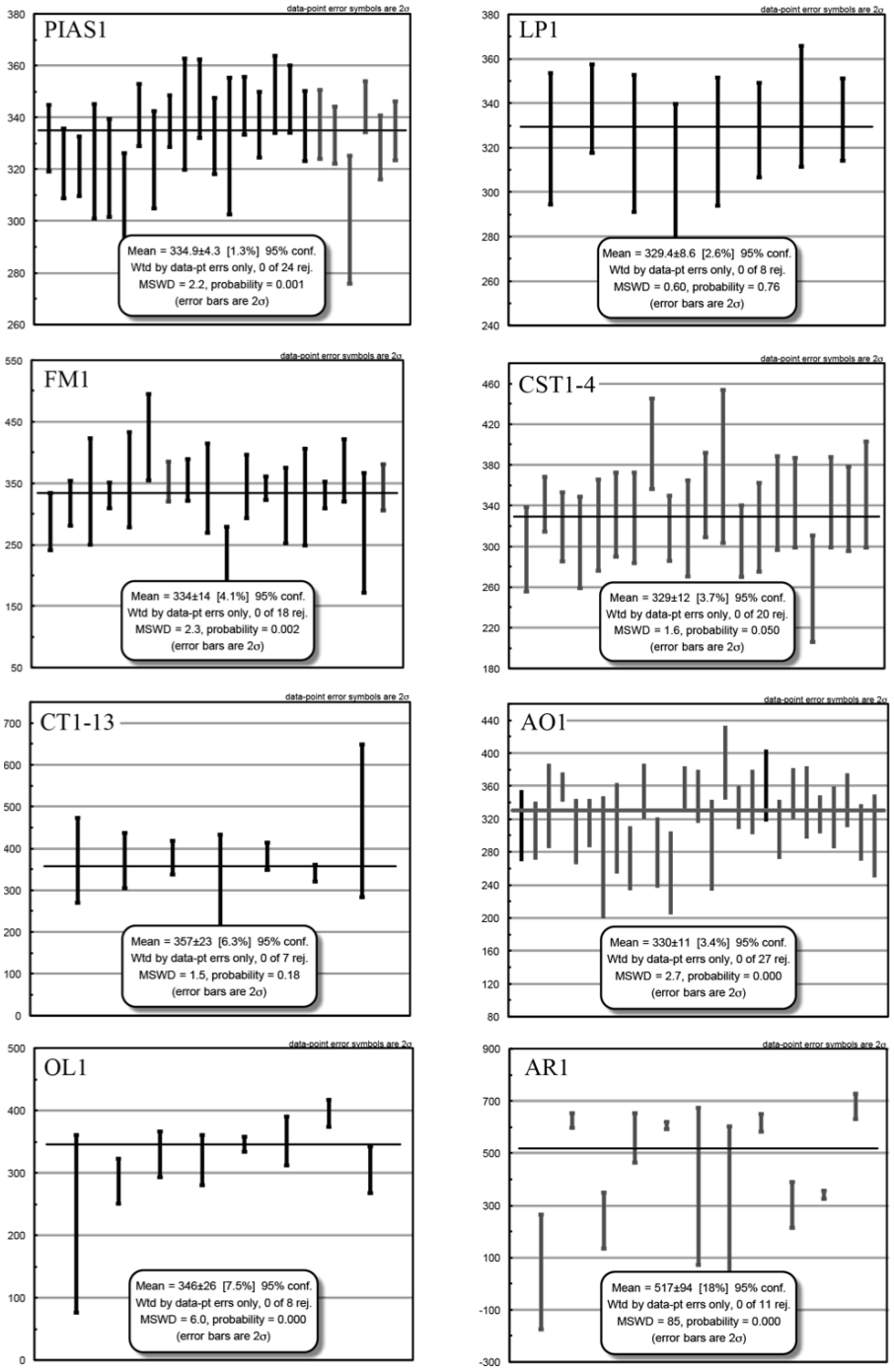

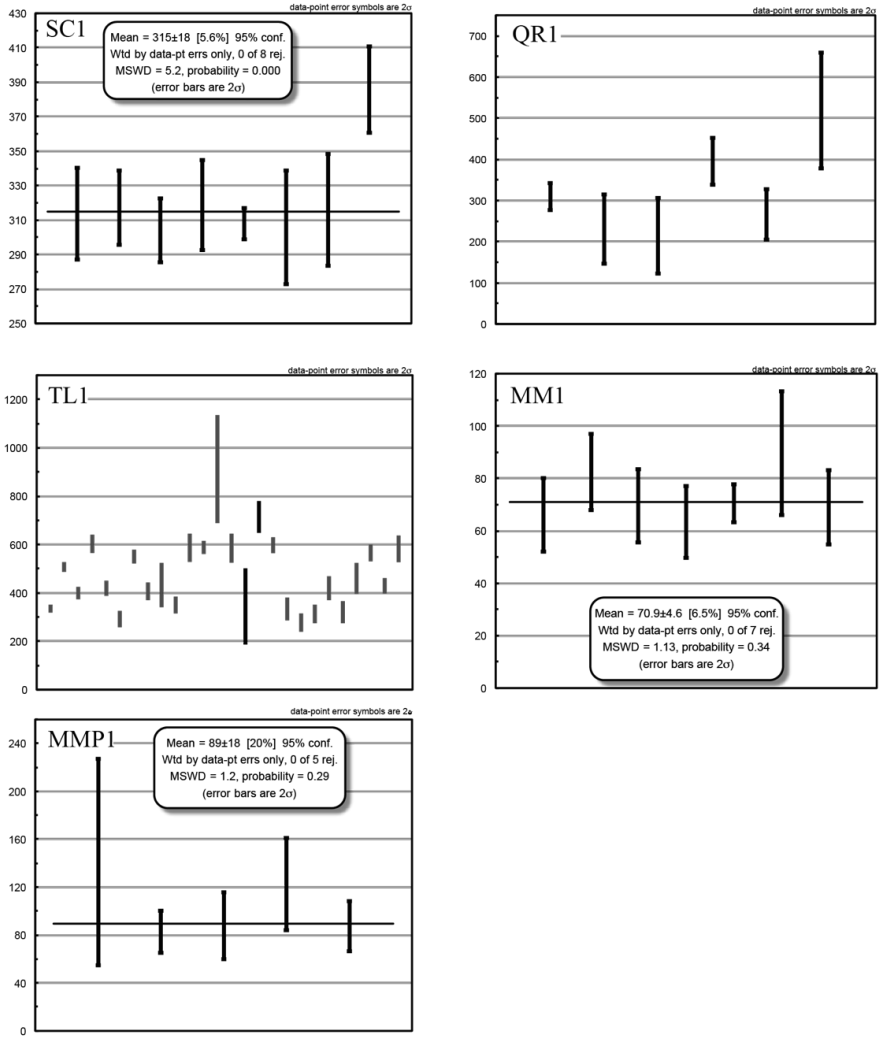

Figure 7.3 Weighted average ^{207}Pb-corrected ages for the apatite samples dated in this study.

7.6 DISCUSSION AND INTERPRETATION OF RESULTS FROM THE OSSA-MORENA SAMPLES

In the Ossa Morena Zone magmatic activity related to the Variscan orogenic cycle is represented by volcanic and plutonic rocks with ages clustered in the age interval 345-280 Ma (e.g. Pinto, 1987; Sánchez-Carretero *et al.*, 1990; Dunning *et al.*, 2002; Salman, 2004). However older granitic bodies from the interval 532-505 Ma are also represented (Salman, 2004). It is beyond the scope of this work to characterize the granites of the Ossa Morena Zone. Nevertheless, it is important to know the age of the granites bodies for thermochronological modelling (Chapter VIII-Forward and Inverse Modeling of Low-temperature thermocronometer data). These new ages also could be useful in future regional

geology studies.

The Pias-Pedrogão granite was dated in the Pedrogão area by Rb-Sr in micas (Mendes, 1967, 1968) and by K-Ar in muscovites (Carvalho *et al.*, 1971), yielding ages of 301, 305 and 308±4 Ma, respectively. The sample PIAS1 was collected near the village of Pias giving an apatite ^{207}Pb-corrected mean age of 334.9±4.3 Ma. This age is 30 Ma older that the previous geochronology data (Mendes, 1967,1968; Carvalho *et al.*, 1971). Different closure temperatures for the different geochronologic systems employed can explain this difference. Another explanation could be that the Pias and Pedrogão are two independent granite bodies with different ages. The obtained age of 334.9±4.3 Ma for the Pias granite is within the range 348-332 Ma defined by Salman (2004) for the Carboniferous plutonic bodies in the Ossa-Morena Zone.

The granite of El Pedroso is considered post or synorogenic with respect to Variscan deformation (IGME, 1975), but unlike the Pias granite its age is unknown. The apatites from sample LP1 gave a ^{207}Pb-corrected mean age of 340.5±7.6 Ma, therefore, the El Pedroso granitic body also falls within the age range of the Carboniferous plutonic bodies the Ossa-Morena Zone defined by Salman (2004).

7.7 SOUTH PORTUGUESE ZONE DISCUSSION AND INTERPRETATION OF RESULTS

The South Portuguese Zone is viewed as a key unit within the context of the evolution of the Variscan Orogeny in Iberia (Oliveira, 1990). The deposition of the Mértola Formation has been interpreted as resulting from the oblique collision between the South Portuguese Zone and the SW border of the Ossa-Morena Zone. This compressive tectonic regime began in the Late Visean and caused enhanced uplift and subsequent erosion of the Ossa Morena Zone and the palaeoseafloor of the South Portuguese Zone by thrust stacking (Oliveira *et al.*, 2006; Pereira *et al.,* 2006; Jesus *et al.,* 2007; Rosas *et al.,* 2008). During the Visean an average exhumation rate of ca. 2.6 km/Ma for the central areas of the Ossa Morena Zone was estimated using ^{40}Ar–^{39}Ar geochronology (Pereira *et al.,* 2012a).

In the Mértola Formation samples, 68 % of the zircons (sample FM1) and all the apatites (samples FM1, OL1, CST4-1 and CT1-13) are encountered within the interval 326-388 Ma (fig. 7.1). There are several possible sources in the South Portuguese Zone and Ossa-Morena Zone for detritus of this age. These include (1) volcanism in the Iberian Pyrite Belt (IPB) that

is constrained to the Famennian (375 Ma) and Tournaisian (345 Ma) (Rosa *et al.,* 2009; Barrie *et al.,* 2002); (2) the Campo Frio Batholith in the South Portuguese Zone which has yielded crystallization ages of between 360-349 Ma (De la Rosa *et al*., 2002; Rosas *et al.,* 2008); (3) syn-collisional magmatism and metamorphism on the southwest border of the Ossa-Morena Zone which is constrained to between 355-320 Ma (Santos *et al.,* 1987; Azor *et al.,* 2008, Jesus *et al.,* 2007). Additionally, a volcanic contribution from the Visean Toca da Moura and Cabrela volcano-sedimentary complexes of the Ossa-Morena Zone is also possible (Pereira *et al*., 2006). If we consider the rapid exhumation rates inferred for the Ossa Morena Zone during the Visean (Pereira *et al.,* 2012a), it is possible that these igneous rocks were exhumed and eroded very quickly after their emplacement. The Mértola Formation contains abundant clasts of both felsic and mafic volcanic rocks (Oliveira & Wagner Genthis, 1983; Jorge *et al.,* 2013) that suggest a provenance from the Pyrite Belt (Schermerhorn, 1971; Moreno & Sáez, 1989; Moreno, 1993). 22 % of the U-Pb zircon ages are encountered within the interval 410-630 Ma. This is consistent with a source in the Iberian Pyrite Belt and the Ossa Morena Zone where Early Palaeozoic detrital zircon is common (Barrie *et al.,* 2002; Braid *et al.,* 2011; Pereira *et al.,* 2012; Jorge, 2009). 10% of U-Pb zircon analyses are encountered within an interval of 637-2193 Ma. This age population is common in the detrital zircons of the Phyllite Quartzite Group rocks (Jorge, 2009).

The detrital zircon age spectrum of the Mira Formation sample (AO1) and the detrital apatite data are very similar to that of the Mértola Formation (fig. 7.1) The detrital zircon population in the 316-369 Ma interval exhibits a peak at 323 Ma and corresponds to 53 % of all the ages determined. The abundance of U-Pb zircon ages close to the depositional age of this formation (323-315 Ma) indicates the increasing importance of an extra-basinal source due to the absence of zircons of this age in the South Portuguese Zone. The mean ^{207}Pb-corrected age of detrital apatites (330±11 Ma) corroborates this. The probable source(s) for this zircon and apatite population is the Variscan intrusives and their associated volcanic rocks on the southwest border of the Ossa-Morena Zone (Santos *et al*., 1987; Azor *et al.,* 2008; Jesus *et al.,* 2007). A second sub-population within a 400-612 Ma age range, with a peak at 482 Ma, corresponds to 30 % of the U-Pb zircon ages. The source for zircons within this age interval is probably the same as that described above for the Mértola Formation (i.e. the Iberian Pyrite Belt and the Ossa Morena Zone).

In summary, the detrital zircon age spectra and the detrital apatite ages of the siliciclastic

sedimentary rocks of the Mértola and Mira formations imply they have a strong extra-basinal contribution component (the Ossa-Morena Zone) as well as a minor intra-basinal contribution (the South Portuguese Zone). The detrital apatite ages show the contribution of an extra-basinal component. There is also a close similarity in the petrographic and geochemical signatures of the sedimentary rocks of the Mértola and Mira formations as both have source area(s) dominated by a granitoid composition with a minor contribution from mafic rocks (Jorge *et al.,* 2013).

The detrital zircon spectra and detrital apatite ages of the Brejeira Formation are different from those of the Mértola and Mira formations (fig. 7.1). In the Brejeira Formation zircons younger than 350 Ma are absent in contrast with the detrital zircon age spectra of the Mértola and Mira formations. Zircons ages within the interval 367-467 Ma correspond to 16 % (sample DZ1) and 11 % (DZ12) of all dated grains, with a peak at 420 Ma in sample DZ1 and two peaks at 366 and 415 Ma in sample DZ12. Both samples contain abundant detrital zircons in the interval 470-800 Ma (53% in the sample DZ1 and 45% in the sample DZ12) with the main peaks at 680 Ma and 623 Ma, respectively. The detrital apatites from sample AR1 show a mean ^{207}Pb-corrected age of 517±94 Ma that falls in the previous interval (470-800 Ma). Ages in the interval 470-800 Ma is generally correlated with tectono-magmatic events that affected the Cadomian-Avalonian Belt in Neoproterozoic-Lower Palaeozoic times. Zircons of this age are also present in the Phylite Quartzite Group (Jorge, 2009; Braid *et al.,* 2011) and in the Tercenas Formation in the South Portuguese Domain (fig. 2.2; Pereira *et al.,* 2012b). Zircons within the 900 – 1100 Ma interval are also present in the Brejeira Formation. Zircons of this age are common within the Avalonia-Meguma terranes (Nance *et al.,* 1991; Barr *et al.,* 2003; Collins & Buchan, 2004; Murphy *et al.,* 2004a,b; Fyffe *et al.,* 2009; Murphy *et al.,* 2010). Notably, detrital zircons in the 900 – 1100 Ma age range are absent in both the Mértola and Mira Formations.

The data suggest that until late Serpukhovian times (315 Ma, top Mira Formation), the Ossa-Morena Zone and South Portuguese Zone contributed, in different proportions, to a foreland basin represented by the Mértola and Mira formations (fig. 7.4, fig 7.5). If we assume that the model of prograding flysch sedimentation accompanying tectonic imbrication is correct, it would be reasonable to assume that both formations shared the same source region and underwent a considerable amount of sedimentary reworking. Our data indicate that this is valid for the Mértola and Mira formations but not for the Brejeira Formation. Therefore, we

suggest that a physical barrier had existed since mid Visean times separating the Mira and Brejeira formations. We also suggest that this physical barrier could be related to the forebulge that was formed in response to the tectonic stacking in the north and the sediment load of the Mértola and Mira formations in the adjacent foreland basin (Fig 7.4, 7.5). During the deposition of the Mértola Formation, that coincided with the initial phase of foreland basin development, the position of the forebulge coincided with the shallow marine facies of the Carrapateira Group in the South Portuguese Domain as suggested by Oliveira & Quesada (1998).

From the late Bashkirian onwards tectonic loading and the progressive filling up of the foreland basin with a thick sedimentary pile (now represented by the Mértola and Mira formations), may have caused uplift of the forebulge separating the foreland basin from the backbulge depocentre. The continued development of the tectonic load in the north combined with subsidence in the foreland basin may have caused the migration of the forebulge towards the depocentre of the foreland basin (e.g. Allen & Allen, 2006). The maximum sea level lowstand during Early Bashkirian times (Ross & Murphy, 1988; Haq & Shutter 2008) may also have contributed to an efficient separation of the two depocentres and to possible erosion and reworking of the sedimentary rocks. In this proposed model for the evolution of the Baixo Alentejo Flysch Group, the Brejeira Formation was deposited in the backbulge depozone. The detrital zircon data in this study suggest the main source area for the Brejeira Formation was the Avalonia-Meguma terrane on the SW border of the foreland basin. The quartzites of the lower Brejeira Formation could be related to reworking of the sediments associated with the forebulge barrier when sea level started to rise during the mid to Late Bashkirian (Ross & Murphy, 1988; Haq & Shutter, 2008; Pereira *et al.,* 2007).

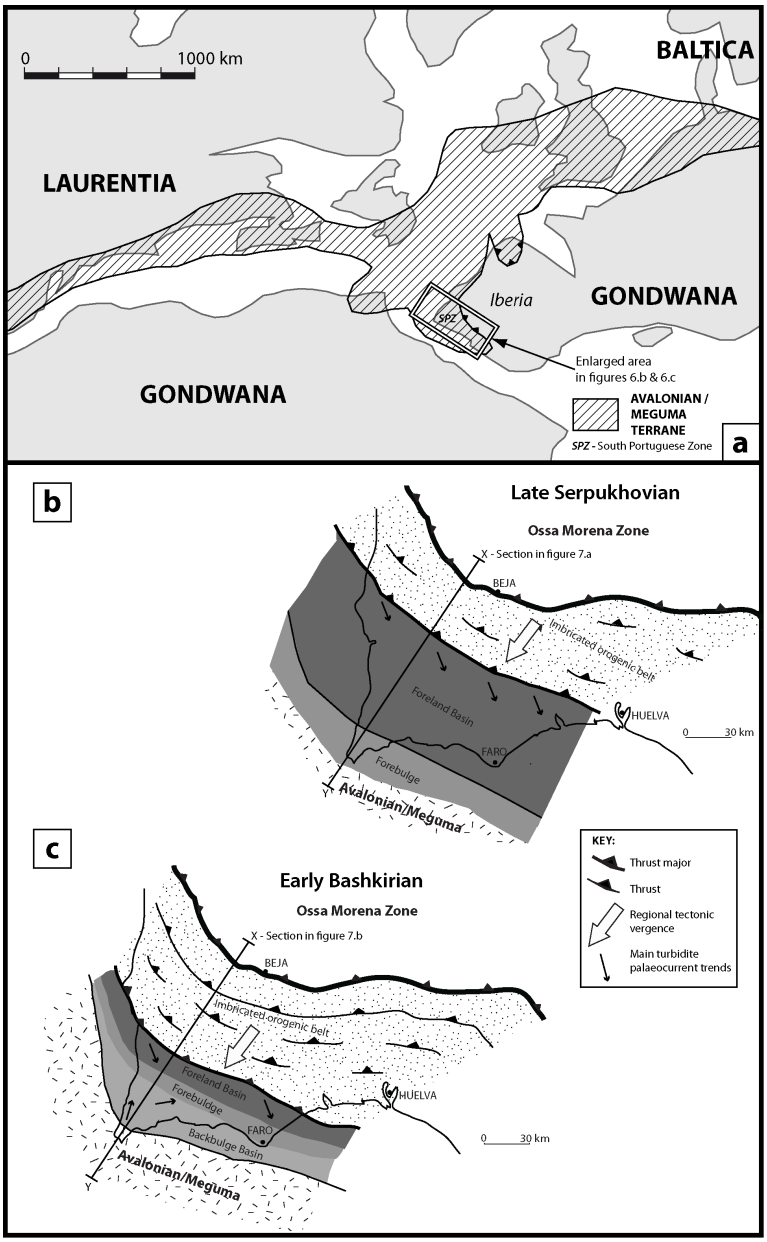

Figure 7.4 Schematic palaeogeographic reconstruction during Pennsylvanian times showing the position of the SPZ in relation to adjacent terranes (adapted from Simancas *et al.,* 2004). Geodynamic evolution of the SPZ during the deposition of the Baixo Alentejo Flysch Group in (b) the Late Serpukhovian and (c) the Early Bashkirian (adapted from Oliveira *et al.,* 2013b). Line X-Y corresponds to the cross sections illustrated in figure 7.5.

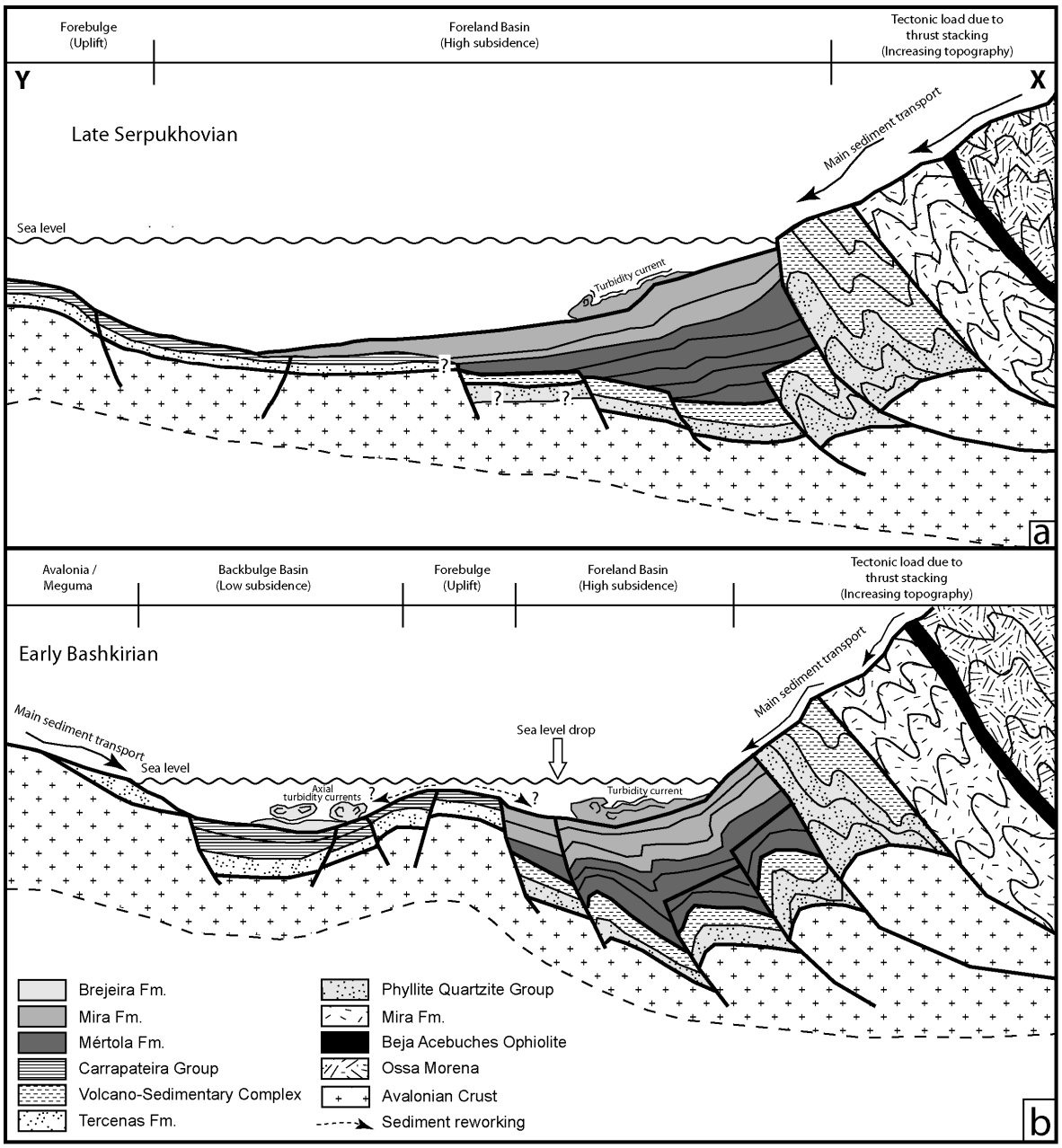

Figure 7.5 Schematic cross-section illustrating the tectonic and basin fill evolution of the Baixo Alentejo Flysch Group. a) Late Serpukhovian. Prograding flysch sedimentation (Mértola and Mira formations) accompanying tectonic imbrication in the north. There is an increase in the tectonic load due to thrust stacking and a consequent increase in foreland basin subsidence and forebulge uplift. b) Early Bashkirian. There is continuous uplift of the forebulge due to the increase in the tectonic load in the foreland basin and the formation of a physical barrier coinciding with the forebulge, which may have been accentuated by a eustatic sea level fall. The Brejeira Formation was deposited in the backbulge basin, which progrades axially southwards and onlaps onto the platform-facies rocks of the Southwest Portugal Domain. Thrusting continued in the north and started to involve the Mértola and Mira formations.

7.8 DISCUSSION AND INTERPRETATION OF THE UPPER TRIASSIC SANDSTONES OF THE ALGARVE BASIN

The Upper Triassic is a period of transition associated with the beginning of the break-up of the Pangean supercontinent and the development of the Mesozoic basins, in a globally warm and dry climate (Ziegler, 1990; Frakes *et al.,* 1992; Dercourt *et al.,* 1993; Boucot & Gray, 2001). In the Algarve Basin, the siliciclastic sediments of the Upper Triassic, termed the "Silves Sandstones" (Rocha, 1976), are comprised of sandstones and conglomerates organized into positive sequences, with oblique stratification and lenticular structures (Palain, 1976). These sediments were likely deposited in a fluvial sedimentary environment associated with numerous alluvial fans in a semi-desert region, above the Variscan basement (Palain, 1976). Palaeocurrents indicate a sedimentary provenance mainly from NE to SW and S and is assumed that the Variscan basement was the main sedimentary source for the Silves Sandstones (Palain, 1976). The sedimentary provenance analysis of the Upper Triassic in the Algarve Basin is extremely complex. The deposition in a fluvial sedimentary environment, where several alluvial fans may overlap in the alluvial plain at the base of a mountain range that was being eroded, makes it difficult to constrain the sedimentary provenance. In this scenario, the drainage network started eroding lithologies that were overlapped and juxtaposed during the Variscan orogeny and contributed in different proportions to the Upper Triassic basins, yielding different detrital zircon and apatite ages that are difficult to correlate to a specific area/formation.

The samples from the Upper Triassic Silves Sandstones in the Algarve Basin were collected at the same stratigraphic level above the Carboniferous-Mesozoic angular unconformity (chapter II). The detrital zircon spectra from sample CM2 shows a population in the interval 204-633 Ma, with peaks at 269, 435 and 577 Ma. It is possible to define a Permian population (15% of the total, corresponding to 13 grains) (fig. 7.2). In Portugal there are uncertainties about the deposition of Permian sediments due to absence of rocks from that age, but it is very well constrained in the Viar Basin (fig. 2.4) located in southern Spain (Sierra *et al.*, 2009 and references therein). Sample TL1 has a small zircon population in the age interval 308-322 Ma (corresponding to 34 grains), with a peak at 312 Ma and the Permian age are absent. The palaeocurrents are distinct from the two sample locations. For the locality where sample CM2 was located, the main palaeocurrents directions are from the NE, while for sample TL1 they are from W and SW (Palain, 1976). Although the palaeocurrents only recorded the very last piece of paleoflow, it is possible to assume that a strong contribution from the Permian Viar

Basin for the east part of the Algarve Basin. However, detrital apatites of Permian age were found in all samples meaning a possible extension of this episodic fluvial contribution. Regarding the apatite detrital ages, the CM2 and SC1 showing mean ^{207}Pb-corrected ages of 371±82 Ma and 315±18 Ma, respectively. These ages are also present in detrital apatites from samples QR1 and TL1. There are several possible sources in the South Portuguese Zone and Ossa-Morena Zone for zircons and apatites of this age (308-370 Ma) and they were discussed in section 7.7. During the deposition of the Silves Sandstones, the BAFG could have been eroded and contributed to the sediments of the Algarve Basin. So, it is possible to assume a contribution from the "Variscan mountain chain" with small contributions from local areas like the Permian Viar Basin.

Sample CM2 shows a continuous detrital zircon age spectra from all temporal periods, with peaks at 577, 920 and 1666 Ma. Sample TL1 yields a more restricted age interval with peaks at 585 and 969 Ma. A BAFG provenance could be inferred for these samples since the most probable source for the Upper Triassic sediments were the BAFG and other rock units of the SPZ.

The detrital apatite and zircon U-Pb data show possible multiple sources. A local component is possible for the ubiquitous Permian and Carboniferous ages. However, the abundance of Precambrian ages could be related to either the South Portuguese and Ossa Morena Zones lithologies or the Avalonia-Meguma terranes (Nance *et al.,* 1991; Barr *et al.,* 2003; Collins & Buchan, 2004; Murphy *et al.,* 2004a,b; Fyffe *et al.,* 2009; Murphy *et al.,* 2010) and could contribute to the Algarve Basin. In conclusion, a combination of sources is envisaged for the Triassic sediments. A detailed study of the provenance of the Triassic in Portugal study is necessary to understand better the different sedimentary sources.

7.9 SUMMARY

Regarding the detrital and igneous apatite and zircon U-Pb results, some conclusions can be drawn:

- The two granites samples from the Ossa Morena zone yield an apatite mean ^{207}Pb-corrected age of 334.9±4.3 Ma for Pias-Pedrogão Granite and 340.5±7.6 Ma for El Pedroso granitic body;
- The two samples from the Monchique Alkaline complex (MAC) gave an apatite mean ^{207}Pb-corrected age of 70.9±4.6 (MM1) and 89±18 Ma (MMP1). Both these ages are within the

accepted interval accepted for the emplacement of the MAC age of 72±2 Ma (Rock, 1978; MacIntyre and Berger, 1982; Bernard-Griffiths *et al.*, 1997; Miranda *et al.*, 2009);

- U-Pb detrital zircon spectra and ^{207}Pb-corrected apatite ages from the Baixo Alentejo Flysch Group show significant differences between the Mértola/Mira formations and the Brejeira Formation. The main peaks in the detrital zircon spectra of the Mértola and Mira formations are at c. 330 Ma in contrast to the Brejeira Formation where the main peaks are at c. 615 Ma. The same difference is reflected in the detrital apatite ages where in the Mértola they range between 329-357 Ma and in the Mira they range between 254-388 Ma. This is in contrast to the Brejeira Formation (ranging from 301-388 Ma). Moreover, U-Pb detrital zircon ages of 900–1100 Ma are encountered in the Brejeira Formation but are absent in the Mértola and Mira formations. spectra difference between the Mértola/Mira and Brejeira formations is also supported by independent geochemical and petrographic studies (Jorge *at al.* 2013). The U-Pb detrital zircon age spectra of the Mértola and Mira formations indicate a provenance from both extrabasinal (Ossa-Morena Zone) and intrabasinal (South Portuguese Zone) sources. The abundance of detrital zircon in the 500-750 Ma and 900-1100 Ma age range intervals in the Brejeira Formation suggests a source region in the Avalon-Meguma terranes with minor recycling from the South Portuguese Domain (Tercenas Formation). The different provenance areas for the units of the Baixo Alentejo Flysch Group are attributed to the presence of a physical barrier (forebulge) that formed during the development of the foreland basin. This barrier was active since mid Visean times and separated the sub-basins where the Mértola/Mira and Brejeira Formation sediments accumulated;

- In the Upper Triassic siliciclastic "Silves Sandstones" is derived from multiple sources. Permian ages that are more pronounced in the samples located in the eastern part of the basin and could reflect a local contribution of the Viar Basin or similar basins in Spain. A detailed study of the provenance of the Upper Triassic in Portugal is necessary to understand better its sedimentary sources.

VIII–FORWARD AND INVERSE MODELING OF LOW-TEMPERATURE THERMOCHRONOMETER DATA

In this chapter the low-temperature thermochronology modelling will be described and is based on the data presented in previous chapters.

8.1 FORWARD AND INVERSE MODELING PRINCIPLES

Fission tracks in minerals (e.g. apatite, zircon) forms continuously over time at a rate that depends solely upon the initial concentration of uranium present in the minerals. Earlier-formed fission tracks tend to be shorter than later-formed tracks, as they will have had more time to anneal, and may have experienced higher temperatures. The distribution of fission-tracks observed in a mineral represents a sampling off all tracks formed and annealed during its residence below the total annealing temperature. In essence, they preserve an integrated thermal history, making this thermochronometer a uniquely powerful tool for thermal history reconstruction (Ketcham, 2005). A detail report of the fission track behaviour with respect to different time-temperature histories was described in Chapter III.

Whenever possible, the samples with acceptable quality and quantity of data were used to model its thermal history using the HeFTy software v.1.7.0 (Ketcham & Donelick, 2000). HeFTy is a computer program for forward and inverse modelling of low-temperature thermochronometric systems, including apatite fission-track, (U-Th)/He ages, and vitrinite reflectance (Ehlers & Farley, 2003). Forward modeling is the process of predicting what thermochronometer measurements one would expect for a sample that has undergone a particular temperature history (Ketcham, 2011). By superimposing measured data, a comparison between the predicted results and measured values is possible. The inverse modeling is the process by (1) which a large number of forward models are generated by HeFTy, (2) the predicted thermochronometer results are compared to the measured values for each forward model, and (3) the good and acceptable forward models are used to provide quantitative constraints on time-temperature histories that are permitted by the measured data (Ketcham, 2011).

The input values are the age of the sample, the apatite fission-track measurements, the confined track lengths, is some cases the (U-Th)/He ages and finally the vitrinite reflectance values. Before starting the inverse modelling it is necessary to draw a forward model, that is a prediction of a temperature history based on previously obtained information, such as the

period when peak temperatures were attained, uplift episodes, etc. Furthermore, this information could also be used to constrain the paths over determined time-temperature intervals. In this study, data has been modelled using the Ketcham *et al.* (1999) annealing model. For each run in an inverse model some constraints were added to improve the quality of the modelled thermal paths in comparison with the measured values. For comparing the results obtained, the software use two statistics to gauge how well the data and the model results match. They are the Kolmogorov-Smirnov test (or K-S Test) and Kuiper's Statistic. More details on how the software uses these statistic tests are described in detail in Ketcham & Donelick (2000) and Ketcham (2005). Ketcham (2011) consider for each of those statistics that a "good" result corresponds to a value of 0.50 or higher, which is the expected value if the time-temperature path and kinetic model are in fact the correct ones. An "acceptable" result corresponds to a value of 0.05 or higher. These values indicate that the model has not failed the null hypothesis test that forms the basis of these statistics. A model is considered "good" if two conditions are met. First, the mean of goodness of fitness (GOF) test value must be at least 0.5. Second, the minimum GOF value must be greater than 1/(N+1), where N is the number of GOF tests that were run. A model is considered "acceptable" if all statistics for all populations are above 0.05. The "Age GOF" is the goodness-of-fit between the age data and age predicted by the model. The results of thermal histories modelled are show with different code colours. Each good path is displayed as a yellow line, and each acceptable path is displayed as a green line. A region encompassing all acceptable paths is coloured in green.

8.2 FORWARD AND INVERSE MODELING RESULTS

8.2.1 Ossa Morena Zone (PIAS 1, LP1)

8.2.1.1 Sample PIAS 1

The Pias granite (sample PIAS1) is located within the Ossa Morena Zone. The mean apatite U-Pb age of the granite is 334.9±4.3 Ma and it yields a fission track age of 108.2±3.4 Ma. The fission tracks lengths yield a mean value of 13.32±1.8 μm. The apatite (U-Th)/He mean age is 108±4.85 Ma, which is very similar to the FT age most probably to He implantation in the apatite giving and older age that was expected, so it was not used in the modelling.

To design the forward model (the blue line in fig. 8.1) a moderate cooling rate of (5.7 ºC/Ma) from the age of granite emplacement at 340 Ma until a temperature of 100 ºC in the Upper Triassic at 200 Ma was used. Although the sample would have been expected to cool quickly

from magmatic emplacement temperatures, subsequent Variscan orogenesis (325 °C (Fernandes *et al.*, 2012)) likely resulted in high ambient temperatures and a slow cooling rate. A temperature of 100ºC was adopted considering a normal geothermal gradient (30 ºC/Ma) for the sample at 3 km depth, which is estimated from the distance to the Carboniferous-Mesozoic unconformity, situated 90 km to south. For the inverse modelling no particular constraints were added, only the crystallization age and the actual temperature (dashed red line). The green lines represent the good-fit paths and the black line represents the best-fit model.

The inverse model results show that the values obtained for the fission track ages of 112 Ma (G.O.F.= 0.21) and confined fission track lengths of 13.69±1.44 µm (G.O.F.= 0.2) agree with the measured data. The model results show a slow cooling history since intrusion (334.9 Ma) until near 240 Ma, from a temperature of 500 ºC to 400 ºC. After the 235 Ma until 200 Ma the sample cooled from a temperature of 400 ºC to 100 ºC at a rate of 8.5 ºC/Ma. From 200 Ma until 65 Ma the sample cooled at a rate of 5.2 ºC/Ma until it reached 75 ºC. From 65 Ma until the present the sample cooled at a rate of c. 1 ºC/Ma to near surface temperatures.

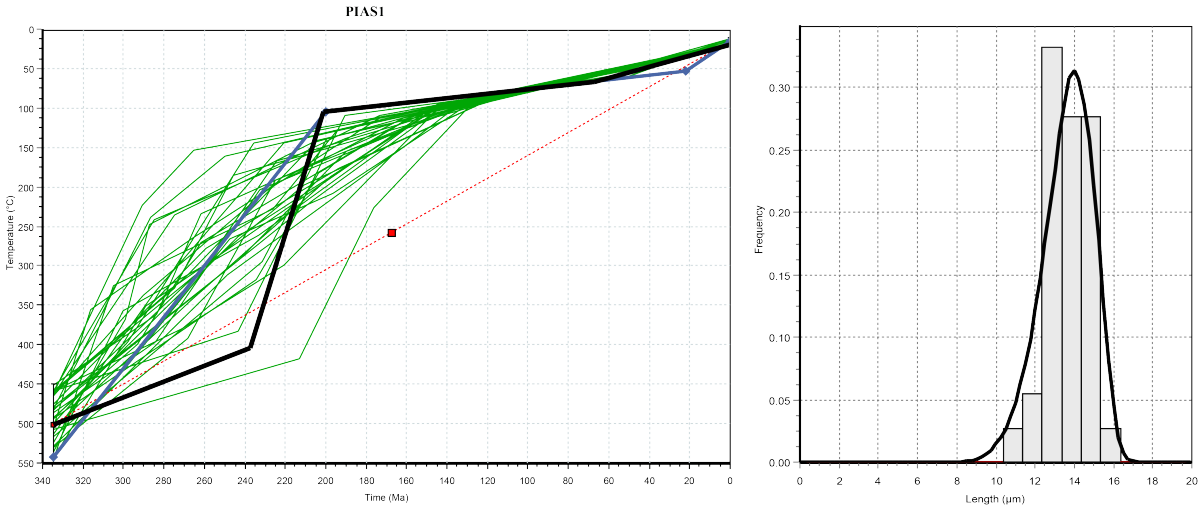

Figure 8.1 Completed inversion model for the sample PIAS1. The left plot show the paths for the model that best fits all AFT data. The right plot show the measured fission track lengths (vertical bars) and the modeled fission track lengths (black curve).

Table 8.1 Modeled and measured results for sample PIAS1.

	Modeled	Measured	G.O.F.	Oldest FT
Fission track ages	112 Ma	108.3±3.4 Ma	0.21	163 Ma
Track length	13.69±1.44µm	13.32±1.08µm	0.2	

8.2.1.2 Sample LP1

The El Pedroso (sample LP1) granite was emplaced within the Ossa Morena Zone. The mean apatite U-Pb age of the granite is 340.5±7.6 Ma and it yields a fission track age of 148.3±6 Ma. The fission tracks lengths yield a mean length of 12.51±1.3 μm. The mean apatite (U-Th)/He age is 60.5±1.2 Ma.

To design the forward model (blue line in fig. 8.2) a slow to moderate cooling path from 340 Ma until a temperature near 75 ºC in the Triassic at 200 Ma was considered based on the same considerations used for the Pias granite model. In the LP1 sample it was necessary to consider a temperature of 75 ºC at 200 Ma instead of 100º C in order to better adjust the model to the observed data. After a period at temperatures of 60-70 ºC, a fast cooling event from 15 Ma to near surface temperatures was invoked.

For the inverse modelling no particular constraints were. The green lines represent the good-fit paths and the black line represents the best-fitting model. The inverse model results show that the values obtained for the fission track ages of 141 Ma (G.O.F.=0.22), for the confined fission track lengths of 12.92±1.27 μm (G.O.F.=0.11) and for the He ages of 25.4 Ma (G.O.F.=0.07) agree with the measured data (table 8.2).

The model results show a slow cooling history since the intrusion (340.5 Ma) until ca. 250 Ma, from a temperature of 500 ºC to 370 ºC. After 250 Ma until the 210 Ma the sample cools from a temperature of 370 ºC to 80 ºC at a rate of 7 ºC/Ma. The oldest fission track in the model simulation has an age of 220 Ma. Since the 210 Ma until 35 Ma the granite cools very slowly at a rate of 0.05 ºC/Ma until reaching 70 ºC. From 35 Ma until the present day the sample cools ata a rate of c. 3.5 ºC/Ma to near surface temperatures. The model did not fit the He age with the measured He age, however it passed in the test with a G.O.F of 0.07.

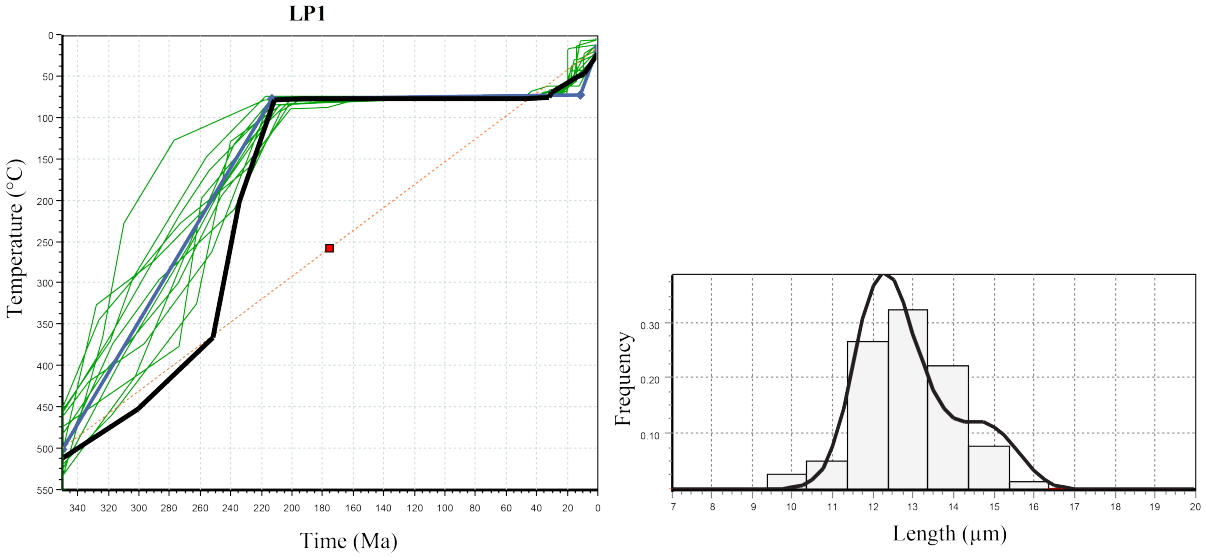

Figure 8.2 Completed inversion model for the sample LP1. The left plot show the paths for the model that best fits all AFT data and He ages. The right plot show the fission track lengths measured (vertical bars) and the fission track lengths modeled (black curve).

Table 8.2 Modeled and measured results for sample LP1.

	Modeled	Measured	G.O.F.	Oldest FT
Fission track ages	141 Ma	148.3±6 Ma	0.22	220 Ma
Track length	12.92±1.27µm	12.51±1.13µm	0.11	
He age	25.4 Ma	45.8±11.4 Ma	0.07	

8.2.2 South Portuguese Zone - Mértola Formation (Sample CST1-4)

Sample CST4 belongs to the Mértola Formation from the South Portuguese Zone, with a depositional age of between 344-326 Ma. Apatites from this sample show a fission-track age of 90.8±3.8 Ma with a mean confined track length of 11.04±1.99 µm. The vitrinite reflectance for the shale in contact with this sample is 4.2±0.4 %R_r, which is equivalent to a maximum temperature between 290 and 310 ºC.

To design the forward model the following conditions were considered: rapid burial followed by maximum heating after deposition due to an advective fluid flow system (Fernandes *et al.,* 2012). With these peak temperatures all the FT ages should be reset. Considering the position of the Carboniferous-Mesozoic unconformity that outcrops ca. 20 km south of the location of this sample, this sample was near the surface, most probably during the Permian (due to the absence of Permian rocks). At 200 Ma (Upper Triassic) a temperature of 100 ºC was adopted based on an inferred sample depth of 2.5 km depth (based on the geometry of the Carboniferous-Mesozoic unconformity surface) using a typical gradient (30 ºC/km). Regarding the inverse modelling, for each run a constraint was added to improve the quality

of the modelled thermal paths in comparison with the observed data. In the first running, no constraints were added and no paths were obtained (fig. 8.3).

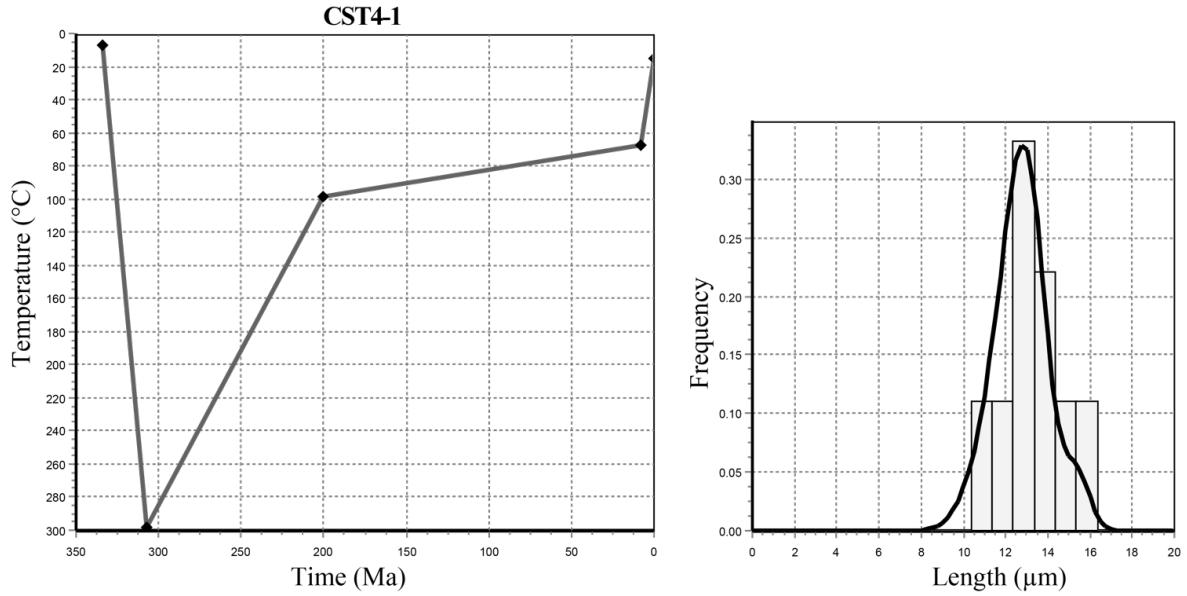

Figure 8.3 Results from the first run of inversion model for the sample CST1-4. The left plot shows the paths for the model that best fits all AFT data. The right plot shows the fission track lengths measured (vertical bars) and the fission track lengths modeled (black curve).

For the second run (fig. 8.4) a constraint box between 300-325 Ma and 270-325 ºC was added to constrain the maximum temperature reached by the sample. Several different paths that can explain the thermal history of the sample were obtained.

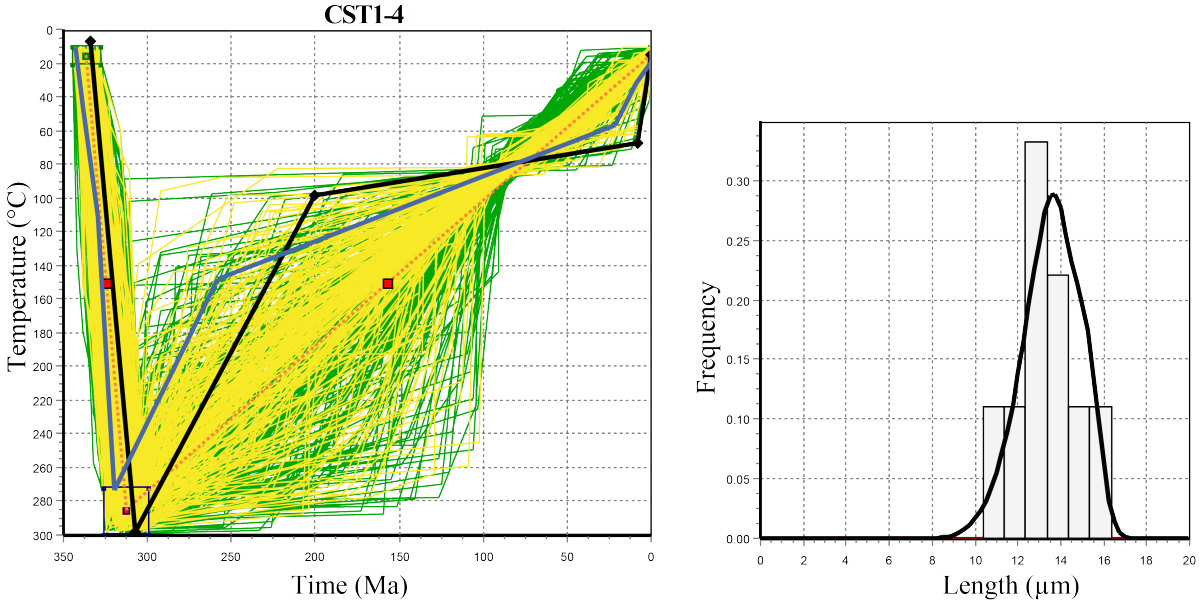

Figure 8.4 Completed inversion model for the sample CST1-4. The left plot shows the paths for the model that best fits all AFT data. The right plot shows the fission track lengths measured (vertical bars) and the fission track lengths modeled (black curve).

Table 8.3 Modeled and measured results for sample CST1-4.

	Modeled	Measured	G.O.F.	Oldest FT
Fission track ages	90.8 Ma	90.8±3.8 Ma	0.99	135 Ma
Track length	13.28±1.51μm	11.04±1.99μm	0.9	

The values obtained from the inverse model for the fission track ages of 90.8 Ma (G.O.F.=0.99) and for the confined track lengths of 13.28±1.51 μm (G.O.F.=0.9) agree with the measured data (table 8.3). The model result shows a heating episode relating to burial and the last phase of Variscan tectonics. After the maximum temperature was reached at 320 Ma, the sample cooled at a rate of 2 ºC/Ma until to 150 ºC at 260 Ma. The sample then resided for a long period in the partial retention zone until 20 Ma, which allows for the reduction of the fission track lengths and the large dispersion in their distribution (standard deviation of 1.99 μm). The oldest fission track in the model simulation has an age of 135 Ma. During this period the cooling rate was very low at c. 0.4 ºC/Ma. This could be attributed to the deposition of Mesozoic sediments. From 20 Ma until the present day, the cooling rate was c. 2 ºC/Ma.

8.2.3 Monchique Alkaline Complex (MM1)

The MM1 syenite belongs to the Monchique Alkaline Complex (MAC). The apatite U-Pb age of this sample is 70.9±4.6 Ma and it yields a fission track age of 49.6±4.3 Ma. The fission tracks lengths yield a mean length of 12.7±0.8 μm. The apatite (U-Th)/He mean age is 38.5±0.8 Ma.

Considering the fission track ages from the Baixo Alentejo Flysch Group from the South Portuguese Zone (ranging from 157 to 59.9 Ma), this demonstrates that the Baixo Alentejo Flysch Group formations were already at a temperature below 100 ºC before or during the Monchique Alkaline Complex intrusion. This implies that the host rock was "cold" and located ca. 2 km depth if a normal palaeogeothermal gradient of 30 ºC/km was considered. So, the forward model has been designed to reflect a thermal history of a sample that underwent rapid cooling after intrusion, followed by a long period in the partial retention zone that may reduce considerably the fission track lengths, and a recent and rapid cooling event that may have started at 5 Ma.

For the inverse model no constraints were added to the model in the first run and no results were obtained. In a second run a constraint was added in order to contrain the host rock temperature (between 60 and 100 °C) at the time of intrusion (72 Ma) (fig. 8.5).

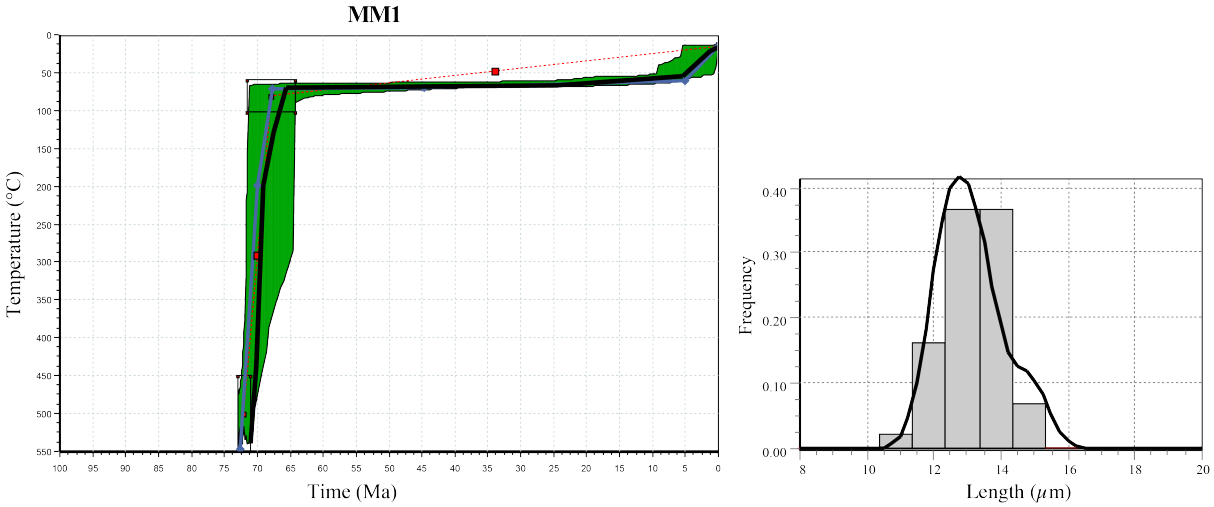

Figure 8.5 Completed inversion model for the sample MM1. The left plot shows the envelope paths for the model that best fits all AFT data. The right plot shows the fission track lengths measured (vertical bars) and the fission track lengths modeled (black curve).

Table 8.4 Modeled and measured results for sample MM1.

	Modeled	Measured	G.O.F.	Oldest FT
Fission track ages	53.9 Ma	49.6±4.3 Ma	0.31	68.7 Ma
Track length	12.99±1μm	12.7±0.8μm	0.3	

The results attained from the inverse model provided very interesting data on the thermal evolution of the MAC. The values produced by the inverse model for the fission track ages of 53.9 Ma (G.O.F.=0.31) and for the confined track lengths of 12.99±1 μm (G.O.F.=0.31), are similar to those measured (table 8.4). After the intrusion, the sample cooled in a period of 6 Ma from magmatic temperatures to ca. 100 ºC. This rapid decrease in temperature was due, most probably, to the host rock temperature during the intrusion, which had an ambient temperature of ca. 100 ºC. At, approximately, 66 Ma the sample was at a temperature of 70 ºC. The oldest fission track obtained by the model is 68.7 Ma. The sample stayed at near constant temperatures the top of the partial retention zone (ca. 60 ºC) from 68.7 Ma to 5 Ma, allowing for the observed reduction in the fission track lengths. From 5 Ma to present day times, the sample cooled from a temperature of 50 ºC to near-surface temperatures. If we consider a normal geothermal gradient of 30 °C/Ma, from 5 Ma to the present day, the MAC was exhumed at 0.3 km/Ma.

8.3 SUMMARY

Considering the results attained by the forward and inversion modelling, the samples from the Ossa-Morena Zone (Pias1 and CST4-1) exhibit a similar thermal history. Both samples exhibits low to moderate cooling rate until 240 Ma and subsequent fast cooling throughout the Triassic until 200 Ma to a temperature within the apatite PAZ, which allows for the observed reduction in the confined fission track lengths. The last phase of cooling to near surface temperatures started in the Pias Granite at 65 Ma. If we assume a paleogeothermal gradient of 30 °C/km, an estimated exhumation rate of 30 m/Ma can be considered for the Pias granite from 65 Ma to the present day. In the El Pedroso granite sample, the last phase of cooling started at 35 Ma. Assuming a paleogeothermal gradient of 30 °C/km an exhumation rate of 65 m/Ma from 35 Ma until the present day is inferred.

The greywacke sample CST1-4 was the only sample modelled from the Baixo Alentejo Flysch Group from the South Portuguese Zone. It shows a heating episode after burial that is related to the last phase of Variscan tectonics. After the maximum temperature of 300 ºC was attained at 320 Ma, the sample cooled to a temperature of 150 ºC at 260 Ma. From 260 Ma until 20 Ma, the sample stayed in the apatite PAZ, which allowed for the observed reduction in the fission track lengths and the large dispersion in the track length distribution. This could be related to possible reburial associated with deposition of the Mesozoic sediments of the Algarve Basin. From 20 Ma until the present day, and considering a typical paleogeothermal gradient of 30 ºC/Ma, an exhumation rate of *ca.* 75 m/Ma can be inferred for this sample.

The syenite sample MM1 from the Monchique Alkaline Complex, cooled very fast from initial magmatic temperatures to around 70 ºC. This rapid cooling event was most probably associated with thermal relaxation from magmatic temperatures to ambient host rock temperatures, of 70 ºC. It is most likely that the intrusion of the MAC was at very shallow depths in the crust (*ca.* 2 km depth). The sample stayed at a constant temperature near to the top of the partial annealing zone from 68.7 Ma to 5 Ma, allowing for the observed reduction in the fission track lengths. From 5 Ma to the present times, the sample cooled from a temperature of 50 ºC to near surface temperatures. If we consider a typical geothermal gradient of 30 °C/Ma, the MAC underwent an exhumation of 0.3 km/Ma from 5 Ma to the present day.

IX – APATITE REE AS PROVENANCE INDICATOR

9.1 REE IN APATITE

Apatite is a widespread accessory mineral and its abundance is directly related to the phosphorus content of the rock and inversely with increasing silica content (Bergstøl, 1972; Laznicka, 1993; Frietsch & Perdahl, 1995). The crystallisation of phosphate phases is an important process in natural systems as the residence of important trace elements such as U, Th, Sr, and REE is at least partly controlled through melt/phosphate mineral equilibrium (Toplis & Dingwell, 1996). Apatite may concentrate a high proportion of whole-rock REE, Sr, U and Th (Ayers & Watson, 1993; Roeder *et al.*, 1987). As a result, apatite is a potentially sensitive recorder of the trace-element chemistry of the rock system at the time of its crystallization. (Sha & Chappell, 1999; Belousova, 2000; Belousova *et al.*, 2001). So, the compositional REE variations can yield specific information regarding the parent rock type allowing the effective recognition of the host rock (fig. 9.1) (Belousova *et al.,* 2002). Within individual rock types, the trace-element patterns of apatite are sensitive to the degree of fractionation and oxidation state of the host magma, which are important parameters in determining mineral potential (Belousova *et al.*, 2002). However, apatites from some rock types show a wide range of trace-element composition even within single samples, and apatites from granitoids and pegmatites show particularly large standard deviations. This reflects the compositional variation found across large crystals from pegmatites, and between individual grains within single samples. Both features may be explained by evolution in the parental melt composition during fractionation, or by late crystallization of apatite from isolated pockets of residual melts that are slightly different in composition and trapped in the interstices between early-crystallizing major minerals (Belousova *et al.,* 2002). Another discriminating factor is the presence (or absence) of an Eu anomaly. In general, the amplitude of Eu anomalies in apatites increases towards more fractionated rocks and probably is controlled by the crystallisation of feldspars, which preferentially concentrate Eu^{2+} from the melt (Budzinski & Tischendorf, 1989).

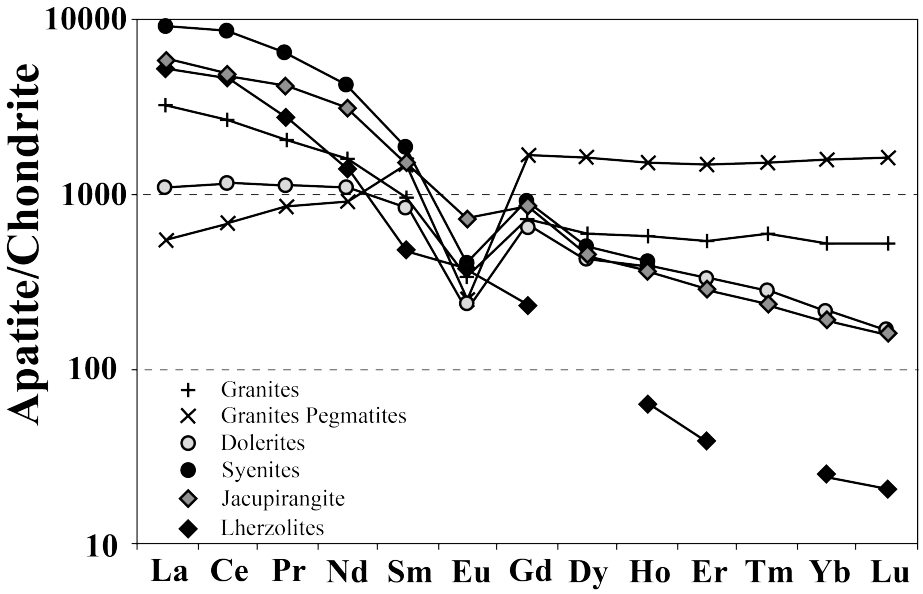

Figure 9.1 Chondrite-normalised averaged trace-element abundances of apatites from different rock types (adapted from Belousova *et al.,* 2002)

One of the advantages of using the laser ablation technique in fission track studies is the possibility to measure minor and trace elements along with the REE. Although this was not the primary goal of this thesis, an attempt was made to infer the provenance of the apatites analysed for fission track analysis based on their REE content. The methodology applied to extract the REE data was the same as described in chapter VII. All the results from the analyses are normalised relative to a Ca stoichiometric concentration in apatite of 393600 ppm. The chondrite normalization was undertaken using the values given by McDonough & Sun (1995).

9.2 APATITE REE RESULTS

In the follow sections the results (fig. 9.2 and annex V) were described and grouped similar to the previous chapters.

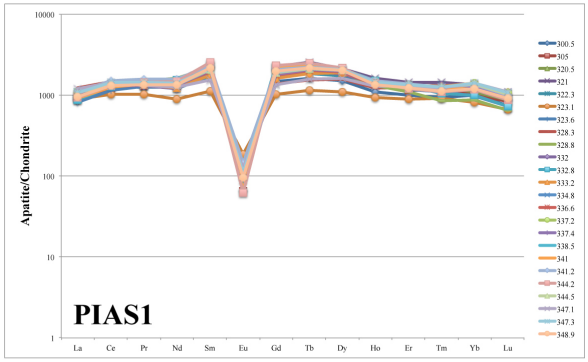
Apatite/Chondrite
PIAS1
La Ce Pr Nd Sm Eu Gd Tb Dy Ho Er Tm Yb Lu

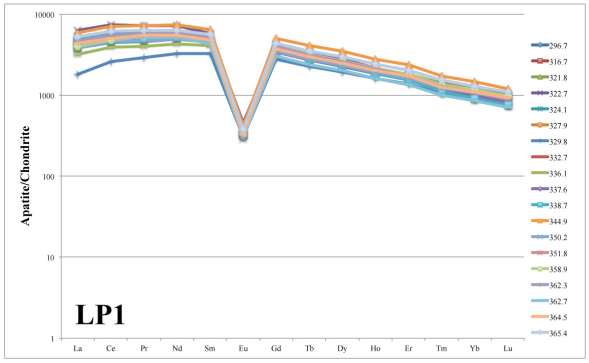
Apatite/Chondrite
LP1
La Ce Pr Nd Sm Eu Gd Tb Dy Ho Er Tm Yb Lu

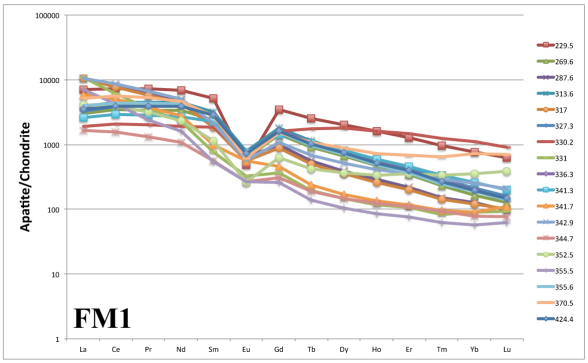
Apatite/Chondrite
FM1
La Ce Pr Nd Sm Eu Gd Tb Dy Ho Er Tm Yb Lu

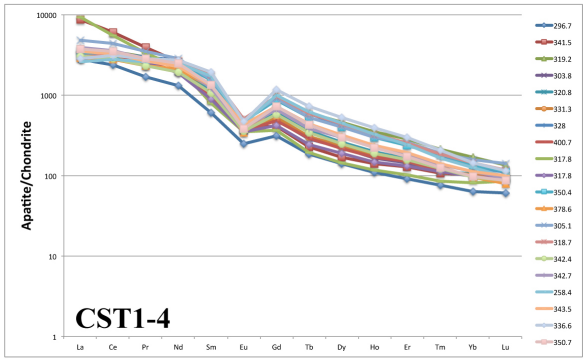
Apatite/Chondrite
CST1-4
La Ce Pr Nd Sm Eu Gd Tb Dy Ho Er Tm Yb Lu

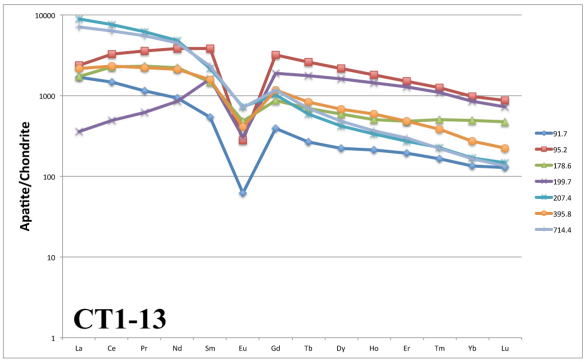
Apatite/Chondrite
CT1-13
La Ce Pr Nd Sm Eu Gd Tb Dy Ho Er Tm Yb Lu

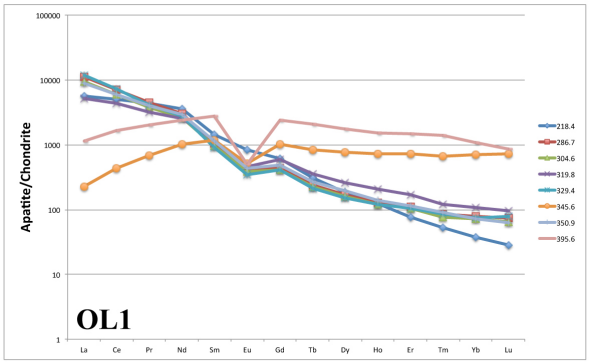
Apatite/Chondrite
OL1
La Ce Pr Nd Sm Eu Gd Tb Dy Ho Er Tm Yb Lu

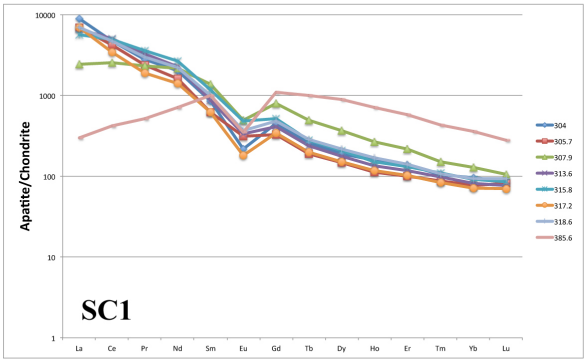
Apatite/Chondrite
SC1
La Ce Pr Nd Sm Eu Gd Tb Dy Ho Er Tm Yb Lu

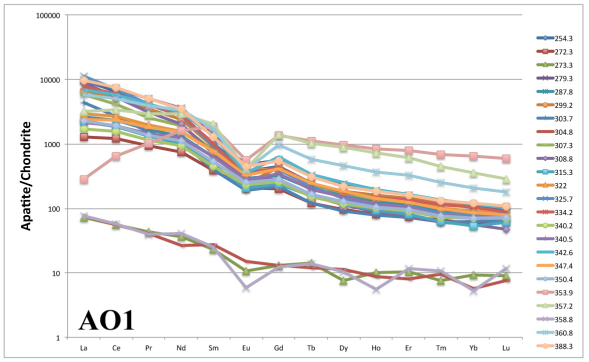
Apatite/Chondrite
AO1
La Ce Pr Nd Sm Eu Gd Tb Dy Ho Er Tm Yb Lu

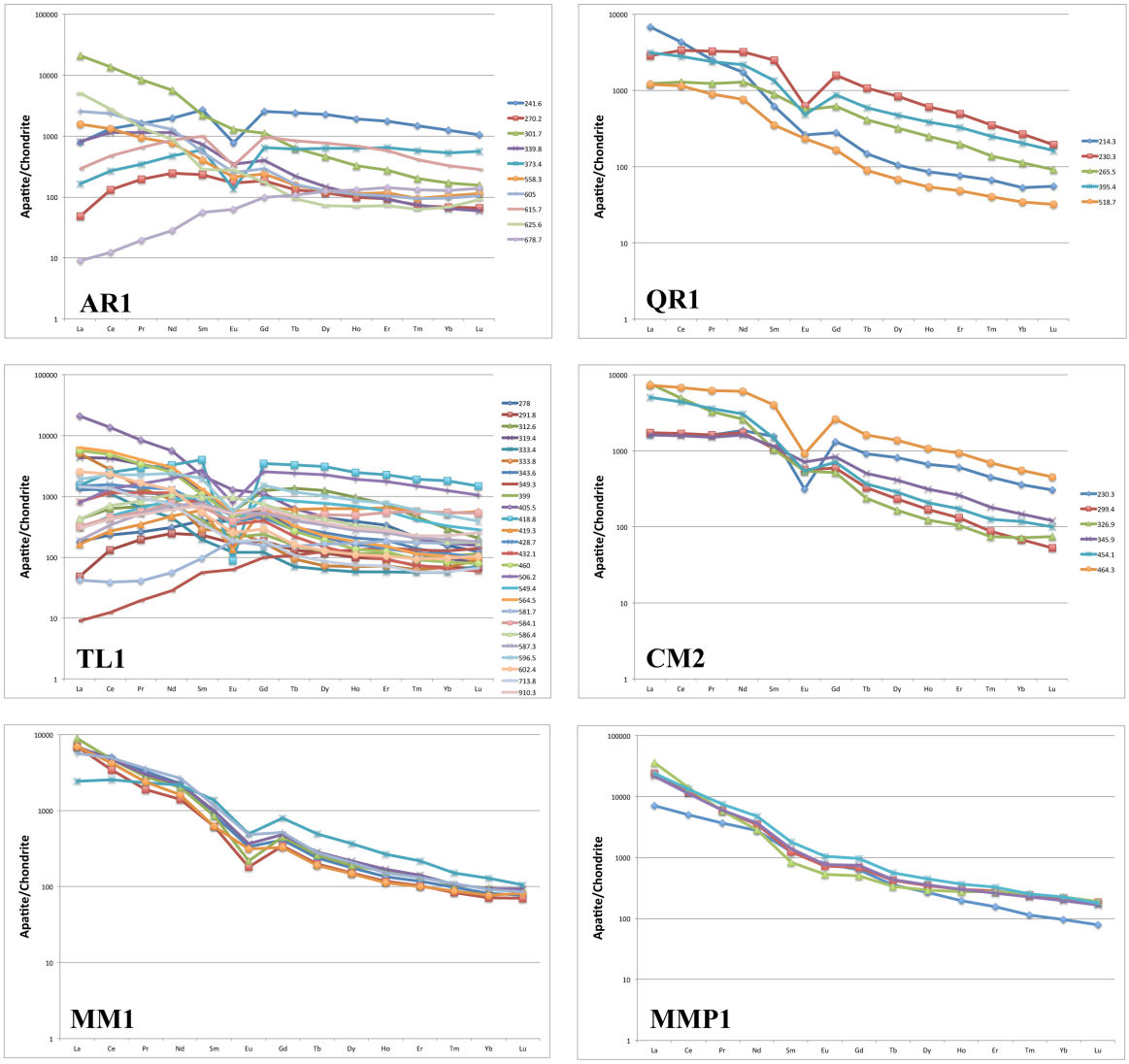

Figure 9.2 Chondrite-normalised trace-element abundances of apatites from the different samples. Data from Annex V. Chondrite values from McDonough & Sun (1995).

9.2.1 Ossa Morena (PIAS1, LP1)

All apatites from the granite samples PIAS1 and LP1 from Ossa Morena Zone show trace-element patterns characteristic of felsic rocks with a pronounced Eu anomaly. In sample LP1 the apatites are mildly HREE depleted whereas in the sample PIAS1 the REE profile is essentially flat (fig. 9.2). In the discriminant plot (fig. 9.3) all the apatites from sample LP1 fall within the "granitoid" field. The apatites from sample PIAS1 fall within the "granite pegmatite" and "granitoid" fields. Some apatites from sample PIAS1 fall outside the defined fields defined by Belousova *et al.,* 2002.

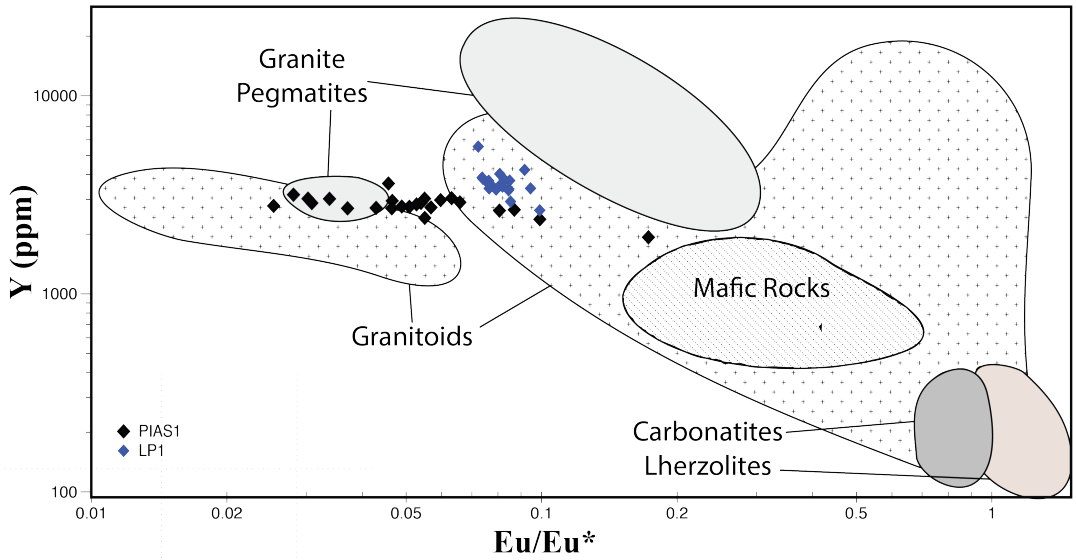

Figure 9.3 Projection of the Y vs Eu/Eu* values from Ossa Morena samples on a discriminant plot of different rock types. Fields adapted from Belousova *et al.,* 2002.

9.2.2 South Portuguese Zone

9.2.2.1 Mértola Formation (FM1, CST1-4, OL1, CT1-13)

The apatites from greywacke sample FM1 show a flat to mildly depleted LREE pattern with a moderate negative Eu anomaly (fig. 9.2). The HREE are mildly to moderately depleted. On the discriminant plot (fig. 9.4), apatite from sample FM1 is associated with mafic lithologies. The apatites from greywacke sample CST4 are HREE depleted with a well defined negative Eu anomaly (fig. 9.2). On the discriminant plot (fig. 9.4) this sample is associated, with mafic and ultramafic lithologies. The apatites from sample CT1-13 show two types of patterns, one typical of felsic rocks and the other of mafic rocks (fig. 9.2). The apatites in sample OL1 also show two patterns, but in this case typical of mafic and ultramafic rocks (fig. 9.2). On the discriminant plot (fig. 9.4) the majority of apatites fall within the "mafic" and "ultramafic" fields and in the lower part of the "granitoid" field (lower Si content). However, there are also some apatites from the three samples, that fall within the "granitoid" and "granite pegmatite" fields.

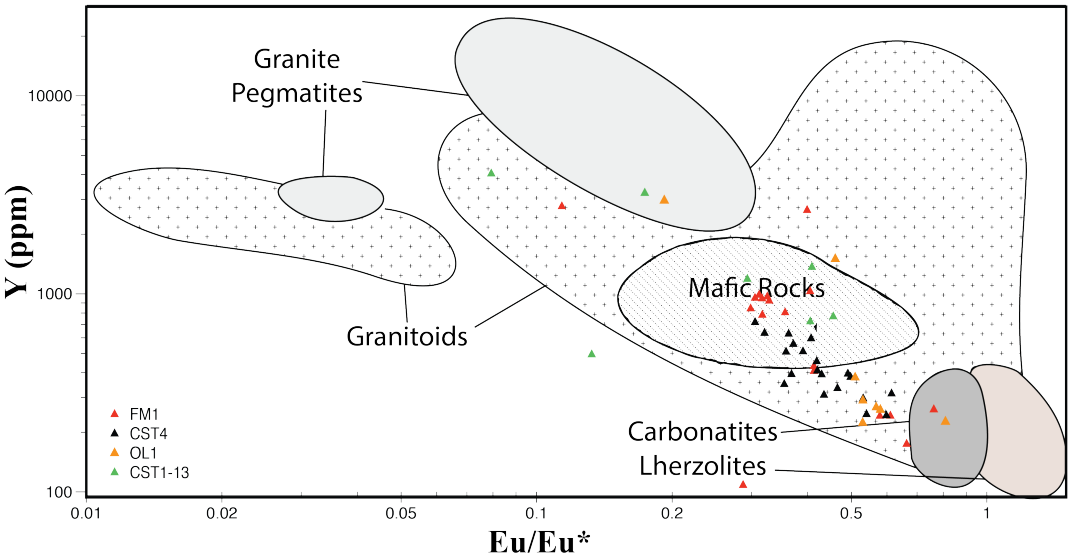

Figure 9.4 Projection of the Y vs Eu/Eu* values from the Mértola Formation samples on a discriminant plot of different rock types. Fields adapted from Belousova *et al.,* 2002.

9.2.2.2 Mira Formation (AO1, SC1)

The apatites from sample AO1 show are HREE depleted with a small negative Eu anomaly (fig. 9.2). This pattern is characteristic of mafic lithologies. Only one apatite grain exhibits a pattern typical of felsic rocks. Three apatites yield extremely low REE contents. Sample SC1 is HREE depleted with a small negative Eu anomaly (fig. 9.2). On the discriminant plot (fig. 9.5) the samples fall in the "mafic" and "ultramafic" fields and in lower part of the "granitoid" field (lower Si content).

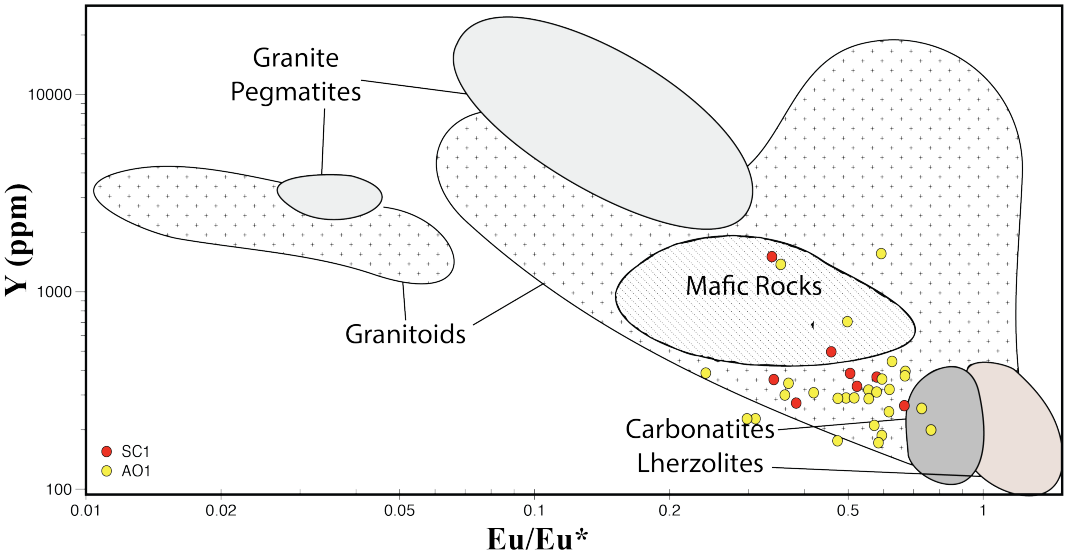

Figure 9.5 Projection of the Y vs Eu/Eu* values from Mira formation samples in discriminant plot of different rock types. Fields adapted from Belousova *et al.,* 2002.

9.2.2.3 Brejeira Formation (AR1)

The apatites from sample AR1 show differing REE patterns typical of felsic, mafic and intermediate magmatic lithologies (fig. 9.2). This is clearly observed on the discriminant plot (fig. 9.6) where the dispersion of the data is significant. The samples fall in the "mafic", "ultramafic" and "granitoid" fields, though, the number of apatite grains analyzed were not large enough to draw more definitive interpretations on the apatite provenance.

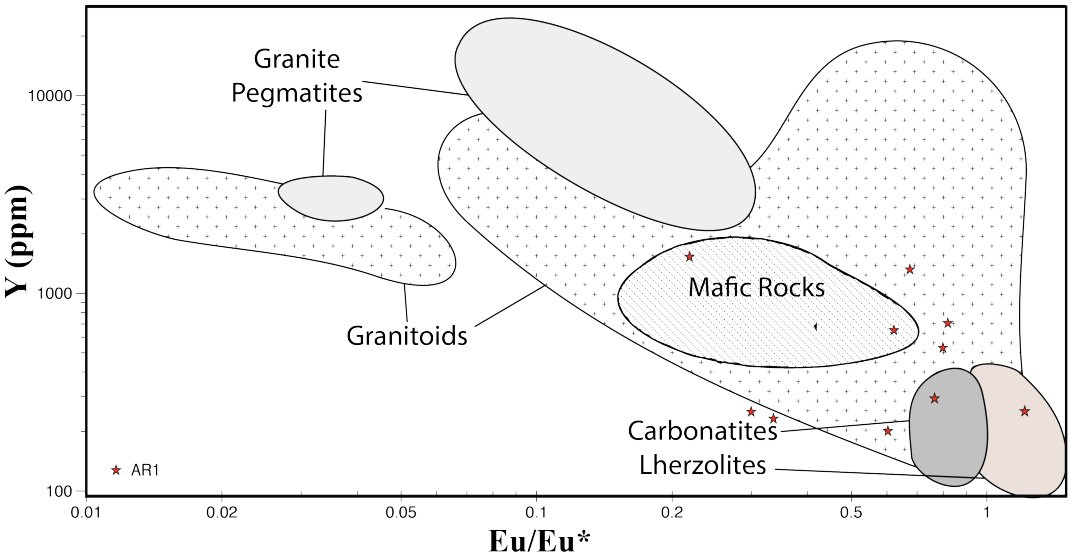

Figure 9.6 Projection of the Y vs Eu/Eu* values from Brejeira formation samples on a discriminant plot of different rock types. Fields adapted from Belousova *et al.,* 2002.

9.2.3 Algarve Basin (CM1, QR1, TL1)

The apatites from sample CM2 and from sample QR1 show trace-element patterns characteristic of mafic and intermediate lithologies (fig. 9.2). Sample TL1 yields apatites with a large variation in REE patterns but the dominant patterns are typical of felsic and intermediate lithologies (fig. 9.2). The dispersion in the discriminant plot (fig. 9.7) is very high and the samples fall in nearly all the fields described.

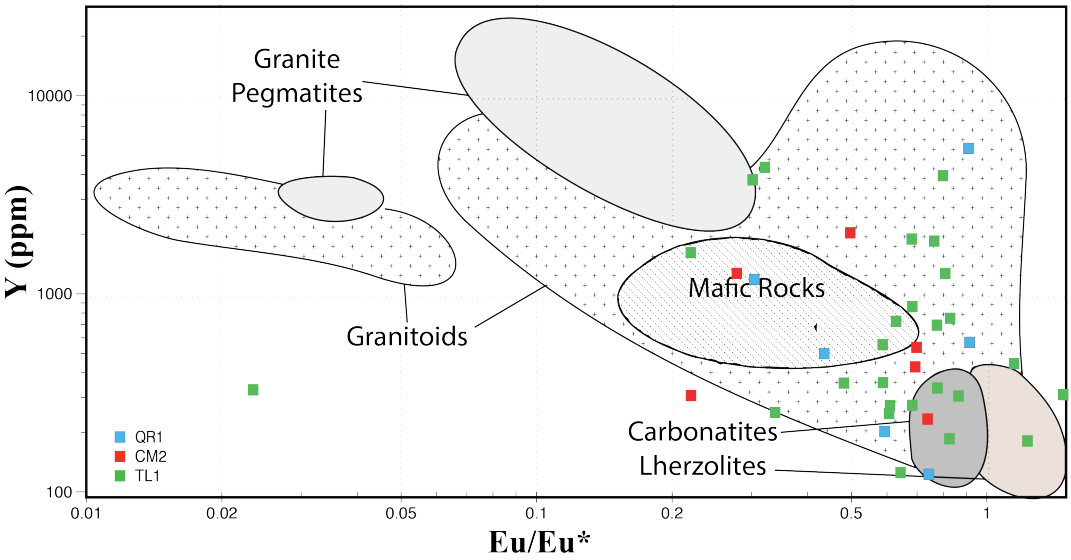

Figure 9.7 Projection of the Y vs Eu/Eu* values from Triassic samples from Algarve basin samples on a discriminant plot of different rock types. Fields adapted from Belousova *et al.,* 2002.

9.2.4 Monchique Alkaline Complex (MM1, MMP1)

The apatites from sample MM1 are strongly HREE depleted with a small negative Eu anomaly and the REE pattern is typical of intermediate igneous rocks such as syenites (fig. 9.2). The apatites in sample MMP1 show the same pattern but with only a very minor Eu anomaly (fig. 9.2). Extreme LREE enrichment depletion relative to the HREE is characteristic of apatites from mantle derived peridotites and carbonatites (Belousova *et. al*, 2002), i.e rocks with a low Si content like the syanites.

In the discriminant plot (fig. 9.8) the samples fall in the field of granites and one apatite falls in the carbonatite field. This high sample dispersion is an example of how simple changes in the magma fractionation can affect the apatite REE content.

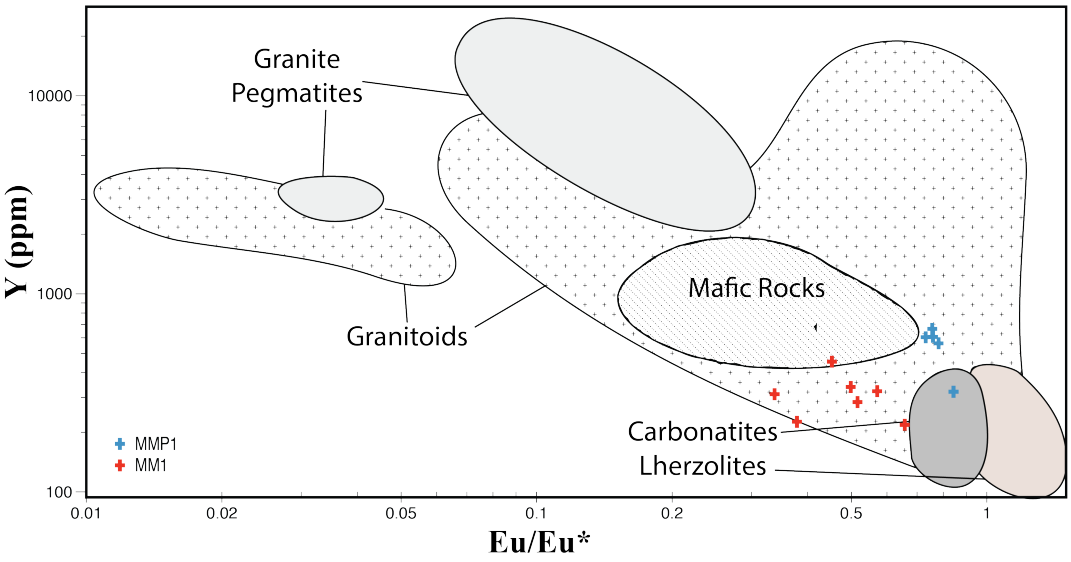

Figure 9.8 Projection of the Y vs Eu/Eu* values from Monchique Alkaline Complex samples on a discriminant plot of different rock types. Fields adapted from Belousova *et al.,* 2002.

9.3 SUMMARY

The analyses of apatite rare-elements patterns may be use to infer the chemical composition of the source rock of apatites. In the present work only a few trace elements were analyzed in addition to the REE and it was not possible to to calculate other discriminant ratios (Sr versus Y and Mn, (Ce/Yb)cn versus the sum of REE, and Y against Eu/Eu*) that can be more useful to reveal the nature of the source rocks. Only the Y vs Eu/Eu* discriminatiion plot was possible to use. In general, the analyses of the REE patterns and the Eu anomalies are more useful than the discriminant plots. The dispersion of values in the granitic rocks is an example of how it is dangerous to use only one discriminant plot to ascertain the parent igneous rock type. The REE patterns and the discriminant plot show some differences between the Mértola and Mira formations and the Brejeira Formation. The mafic contribution is more pronounced in the Mértola and Mira formations than in the Brejeira Formation. This difference was already detected in geochronologic (chapter VII), geochemistry and petrologic studies (Jorge *et al.*, 2013). The samples from Algarve Basin (CM1, QR1, TL1) show a great dispersion of possible source rocks types.

X – CONCLUSIONS

The work undertaken in this PhD research was focused on the investigation of the thermal history of the South Portuguese Zone and the Algarve Basin. The original study area was expanded to include the southern limit of the Ossa Morena Zone. Another field of investigation was the sedimentary provenance of the Baixo Alentejo Flysch Group of South Portuguese Zone and the Algarve Basin. Several techniques (vitrinite reflectance, thermochronology (apatite fission track and (U-Th)/He) and geochronology (detrital zircon and apatite U-Pb) were applied to achieve the objectives proposed in chapter I. The main results of this thesis can be synthetized in the following sections.

10.1 THERMAL HISTORY

The vitrinite reflectance and calculated palaeotemperatures for the outcrop samples in the Baixo Alentejo Flysch Group are between 236 and 326 ºC and agree with the vitrinite reflectance (VR) data presented by Fernandes *et al.* (2012). This range of temperatures are clearly above the temperature of partial annealing zone (PAZ) of the apatite fission track system and also of the He partial retention zone of (HePRZ) of the (U-Th)/He system and thus these thermochronological data record the exhumation history of the Baixo Alentejo Flysch Group.

- The samples collected from boreholes CST1 and CT1 in the Mértola Formation from the South Portuguese Zone do not show any increase in VR with depth. The results agree with the model proposed by Fernandes *et al.* (2012) that suggests there was an advective heat transfer regime in the South Portuguese Zone which produced relatively uniform high temperatures in the upper crust, overprinting any existing vertical VR gradient;

- The highest VR value in Baixo Alentejo Flysh Group was measured in the Brejeira Formation, near the Monchique Alkaline Complex (MAC) corresponding to a palaeotemperature of 414 ºC, indicating high temperatures related with the emplacement of the MAC. The metamorphic aureole caused by the intrusion of the MAC is estimated to be between 0.2 and 1 km wide (Rock, 1978; González-Clavijo & Valadares, 2003). The thermal aureoles from small intrusions related to the Monchique Alkaline Complex in the Baixo

Alentejo Flysch Group can be neglected because the lithologies already attained elevated temperatures during their previous (Variscan) thermal history;

- The Cl content in apatites have a strong influence on the FT ages obtained;

-All the Baixo Alentejo Flysch Group samples were totally reset after deposition and yield Cretaceous AFT ages (111 to 59.9 Ma) with one Upper Jurassic age (Sample OL1-157.9 Ma);

- The AFT ages in the Ossa Morena Zone and South Portuguese Zone indicate that exhumation must have occurred as a contiguous block in these two Variscan Zones;

- The samples from the Ossa Morena Zone (Pias1 and PL1) exhibit low to moderate cooling until 240 Ma, followed by a fast cooling throughout the Triassic until *ca.* 200 Ma to a temperature within the apatite partial annealing zone. The last phase of cooling to near surface temperatures started in the Pias granite at 65 Ma. If we assume a paleogeothermal gradient of 30 °C/km, an estimated exhumation rate of 30 m/Ma can be considered for the Pias granite from 65 Ma to the present day. In the El Pedroso granite sample, the last phase of cooling started at 35 Ma. Since then until the present an exhumation rate of 65 m/Ma was inferred;

- The greywacke sample CST1-4 from the Baixo Alentejo Flysch Group from the South Portuguese Zone shows a heating episode after burial related to the last phase of Variscan tectonism. After the maximum temperature of 300 ºC was attained at 320 Ma, the sample cooled to a temperature of 150 ºC at 260 Ma. From 260 Ma until 20 Ma, the sample stayed in the apatite partial annealing zone (PAZ). This long period within this narrow temperature window could be related to a possible reburial associated with deposition of the Mesozoic sediments of the Algarve Basin. From 20 Ma until the present day an exhumation rate of 75 m/Ma can be inferred for this sample;

- In the Algarve Basin the VR values measured for the Upper Triassic-Hettangian units is 1-1.1 % (Fernandes *et al.*, 2013; McCormack *et al.*, 2007) and correspond to palaeotemperatures between 148 and 158 ºC. This range of temperatures means that the apatite fission track and the apatite (U-Th)/He systems record the exhumation history of the Algarve Basin;

- In the case of the Lower Cretaceous lithologies (VR=0.6%) in the western part of the Algarve Basin, the maximum burial paleotemperatures attained were not enough to reset the apatite fission track system;

- The samples collected at Praia da Luz, near the contact with the basic intrusion at Ponta das Ferrarias, show that the thermal effect of this intrusion is restricted to a maximum distance of ca. 2 km from the intrusive contact. In these situations it might be possible to use the apatite fission track system within the intrusion aureole to date the age of the intrusion. The thermal modelling for the Lower Cretaceous Luz Mudstones intruded by the basic rocks at Ponta das Ferrarias, suggests that near the contact maximum temperatures of 275 ºC were attained and which cooled to 100 ºC after only 10 000 years;

- The AFT ages from the Upper Triassic sandstone samples from the Algarve Basin indicate that all ages are older than the depositional age, meaning that the samples did not pass through the apatite partial annealing zone. So, the thermal anomaly created by the MAC intrusion did not affect the Algarve Basin lithologies. However, the thermal effect from small intrusions related to the Monchique Alkaline Complex in the Algarve Basin could not be totally neglected;

- The syenite sample MM1 from the Monchique Alkaline Complex, cooled very fast from initial magmatic temperatures to around 70 ºC. This rapid cooling event was most probably associated with thermal relaxation from magmatic temperatures to ambient host rock temperatures (70 ºC). It is most likely that the intrusion of the MAC was at very shallow depths in the crust (*ca.* 2 km depth). The sample stayed at a constant temperature close to the top of the partial annealing zone from 69 Ma to 5 Ma. From 5 Ma to the present times, the sample cooled from a temperature of 50 ºC to near surface temperatures. If we consider a typical geothermal gradient, the MAC underwent an exhumation rate of 0.3 km/Ma from 5 Ma to the present day.

10.2 GEOCHRONOLOGY AND MINERAL PROVENANCE

Regarding the detrital/igneous apatite and zircon U-Pb results and also the REE apatite contents, some conclusions can be drawn:

- The two granites samples from the Ossa Morena Zone (Pias and El Pedroso) yielded an apatite mean ^{207}Pb-corrected age of 334.9±4.3 Ma for Pias-Pedrogão Granite and 340.5±7.6 Ma for El Pedroso granitic body. The calculated age of the Pias-Pedrogão granite is 30 Ma older that the previous geochronologic data (Rb-Sr in micas (Mendes, 1967; Mendes, 1968) and K-Ar in muscovites (Carvalho *et al.*, 1971). Different closure temperatures for the different geochronologic systems employed can explain this difference. Both granites analysed (Pias and El Pedroso) fall within the age range of the Carboniferous plutonic bodies in the Ossa-Morena Zone defined by Salman (2004);

- U-Pb detrital zircon spectra and also the ^{207}Pb-corrected apatite ages from the Baixo Alentejo Flysch Group show significant differences between the Mértola/Mira formations and the Brejeira Formation. This difference was also detected in the apatite REE analyses (chapter VIII) and in the geochemistry and petrologic studies (Jorge *et al.*, 2013);

-The U-Pb detrital zircon age spectra of the Mértola and Mira formations indicate a provenance from both extrabasinal (Ossa-Morena Zone) and intrabasinal (South Portuguese Zone) sources. The abundance of detrital zircon in the 500-750 Ma and 900-1100 Ma age intervals in the Brejeira Formation suggests a source region in the Avalon-Meguma terranes with minor recycling from the South Portuguese Domain (Tercenas Formation);

- The different provenance areas for the units of the Baixo Alentejo Flysch Group are attributed to the presence of a physical barrier (forebulge) that formed during the development of the foreland basin. This barrier was active since mid Visean times and separated the sub-basins where the Mértola/Mira and Brejeira Formation sediments accumulated;

- The sandstones from the Upper Triassic were derived from multiple sources. Permian ages are more pronounced in the samples located in the eastern part of the basin and could reflect a local contribution from the Permian Spanish basins.

10.3 IMPLICATION IN ECONOMICAL GEOLOGY

The thermal history information derived in this study may have an impact on the economical potential for conventional gas exploration in South Portuguese zone. The vitrinite reflectance values in the South Portuguese Zone corresponds to a maximum temperature between 236

and 326 ºC. These post-deposition temperatures were achieved not only from the burial, but also from tectonic deformation. Deformation was followed by a cooling phase related to a phase of exhumation until 200 Ma which is consistent with the presence of a Carboniferous-Triassic unconformity in the geological record. Oil and gas generated after the deposition may have been lost during this phase. From 200 Ma until the 20 Ma the temperature remains constant between 100 and 60 ºC within the apatite partial annealing zone (and the oil window), however the rocks shows at these stage were already overmature. The pronounced exhumation since the Late Cretaceous may have destroyed any petroleum system. Nevertheless the history in the offshore basins could be different and more detailed studies on offshore are required.

The sedimentary input to the offshore basins since the Late Cretaceous, as result of the uplift and subsequent exhumation, must have created reservoirs for the Algarve Basin petroleum system and more studies will be necessary to ascertain this.

10.4 SUGESTIONS FOR FUTURE WORKS

Although many samples were collected during this project, it was not possible to obtain fission track data from all of these samples due to the problems reported in chapter V. A complementary study in Southwest Portugal Domain and in the Brejeira Formation will be necessary to explain if the SW Portuguese region has a different thermal history compared to the rest of South Portugal as suggested by Fernandes *et al.* (2012).

The thermal history of the Algarve Basin is well constrained onshore but not in the offshore. Maturation and low-temperature thermochronology studies should be undertaken on the new oil exploration boreholes that will be drilled in this basin in the near future and the results compared with the onshore thermal history.

It is also important that a detailed study be carried out on the provenance of the Upper Triassic sandstones in Portugal to understand better its sedimentary sources as this too remains uncertain.

REFERENCES

Abad, I., Mata, M.P., Nieto, F., Velilla, N., 2001. The phyllosilicates in diagenetic rocks of the South Portuguese Zone, Southwestern Portugal. Canadian Mineralogist, 39, 1571–1589.

Allen, P. & Allen, J., 2005. Basin Analysis: Principles and Applications, 2nd ed., Blackwell Publishing, 549 pp.

Antunes, A., 2006. Rochas Granitóides da Zona de Ossa Morena: Magmatismo, Geodinâmica e reconstituição geohistórica. Unpublished MSc thesis, Universidade de Aveiro, 181 pp.

Apalategui, O., Eguiluz, L., Quesada, C., 1990. Ossa Morena Zone, Structure. In: R.D. Dallmeyer and E. Martínez-García (Eds.): Pre-Mesozoic Geology of Iberia, Springer-Verlag, 2, pp. 80-219.

Ayers, J. & Watson, E., 1993. Apatite/fluid partitioning of rare earth elements and strontium: experimental results at 1.0 GPa and 1000 jC and application to models of fluid– rock interaction. Chemical Geology 110, pp. 299-314.

Azor, A. (coord.), 2004. Zona de Ossa-Morena. In Vera Torres, J. A. Geología de España. Sociedad Geológica de España e Instituto Geológico y Minero de España. pp. 165–198.

Azor, A., Rubatto, D., Simancas, J.F., González Lodeiro, F., Martínez Poyatos, D., Martín Parra, L.M., Matas, J., 2008. Rheic Ocean ophiolitic remnants in southern Iberia questioned by SHRIMP U–Pb zircon ages on the Beja–Acebuches amphibolites. Tectonics 27, TC5006.

Barbarand, J., Carter, A., Wood, I., Hurfor, A., 2003. Compositional and structural control of fission track annealing in apatite. Chemical Geology 198, pp. 107-137.

Barker, C., 1988. Geothermics of petroleum systems: implications of the stabilization of kerogen thermal maturation after a geologically brief heating duration at peak temperature, In: Magoon, L.B. (Eds.), Petroleum systems of the United States: U.S. Geological Survey Bulletin, 1870, pp. 26–29.

Barr, S.M., Davis, D.W., Kamo, S., White, C.E., 2003. Significance of U–Pb detrital zircon ages in quartzite from peri-Gondwanan terranes, New Brunswick and Nova Scotia, Canada. Precambrian Research 126, pp. 123–145.

Barrie, C., Amelin, Y., Pascual, E., 2002. U-Pb Geochronology of VMS mineralization in the Iberian Pyrite Belt. Mineralium Deposita, 37, pp. 684–703.

Bateman, H., 1910. Solution of a system diferential equations occurring in the theory of radioactive transformations. Proceedings of the Cambridge Philosophical Society.15, pp. 423-427.

Belousova, E.A., 2000. Trace elements in zircon and apatite: application to petrogenesis and mineral exploration. PhD thesis. Macquarie University, Australia.

Belousova, E.A., Walters, S., Griffin, W.L., O'Reilly, S.Y., 2001. Trace element signatures of apatites from granitoids of Mount Isa Inlier, north-west Queensland, Australia. Australian Journal of Earth Sciences. 48, pp. 603-619.

Belousova, E.A., Griffin, W.L., O'Reilly, S.Y., Fisher, N.I., 2002. Apatite as an indicator mineral for mineral exploration: Trace-element compositions and their relationship to host rock type. Journal of Geochemical Exploration 76 (1), pp. 45–69.

Bergstøl, S., 1972. The jacupirangite at Kodal, Vestford, Norway. A potential magnetite, ilmenite and apatite ore. Min. Depos. 7, pp. 233-246.

Bernard-Giffiths, J., Gruau, J., Cornen, J., Azambre, B., Macé, J., 1997. Continental Lithospheric Contribution to Alkaline Magmatism: Isotopic (Nd, Sr, Pb) and Geochemical (REE) Evidence from Serra de Monchique and Mount Ormonde Complexes. Journal of Petrology, 38, nº 1, pp. 115-132.

Black, L., Kamo, S., Allen, C., Davis, D., Aleinikoff, J., Valley, J., Mundil, R., Campbell, I., Korsch, R., Williams, I., Foudoulis, C., 2004. Improved $^{206}Pb/^{218}U$ microprobe geochronology by the monitoring of a trace-element-related matrix effect; SHRIMP, ID-TIMS, ELA-ICP-MS and oxygen isotope documentation for a series of zircon standards. Chemical Geology 205, pp. 115–140.

Boogaard, M., 1963. Conodonts of upper Devonian and Lower Carboniferous age from Southern Portugal. Geologie en Mijnbouw, 42, pp. 248–259.

Boogaard, M., 1967. Geology of Pomarão region (Southern Portugal). PhD thesis, University of Amsterdam.

Boucot, A. & Gray, J., 2001. A critique of Phanerozoic climatic models involving changes in the CO2 content of the atmosphere. Earth-Science Reviews 56, pp. 1-159.

Brady, R.J., 2002. Very high slip rates on continental extensional faults: new evidence from (U–Th)/He thermochronometry of the Buckskin Mountains, Arizona. Earth Planet. Sci. Lett. 197, pp. 95–104.

Braid, J., Murphy, J., Quesada, C., Mortensen, J., 2011. Tectonic escape of a crustal fragment during the closure of the Rheic Ocean: U–Pb detrital zircon data from the Late Palaeozoic Pulo do Lobo and South Portuguese zones, southern Iberia. Journal of the Geological Society, London, 168, pp. 383–392.

Braun, J., van der Beek, P. A., Batt, G., 2006. Quantitative Thermochronology: Numerical Methods for the Interpretation of Thermochronological Data. Cambridge Univ. Press, 272 p.

Brown, R.W., Summerfield, M., Gleadow, A., 1994. Apatite fission track analysis: its potential for the estimation of denudation rates and implications for models of long-term landscape development. In M. J. Kirby (ed.), Process Models and Theoretical Geomorphology, New York, John Wiley and Sons Ltd, pp. 23–53.

Budzinski, H., Tischendorf, G., 1989. Distribution of REE among minerals in the Hercynian postkinematic granites of Westerzgebirge-Vogland, GDR. Z. Geol. Wiss. 17 (11), pp. 1019-1031.

Carlson, H. & Jaeger, C., 1959. Conduction of Heat in Solids. Clarendon, Oxford, 3th edition.

Carlson, W.D., Donelick, R.A., Ketcham, C., 1999. Variability of apatite fission track annealing kinetics I: Experimental results. American Mineralogist, v. 84, pp. 1213-1223.

Carvalho, D., Goínhas, J., Oliveira, V., Ribeiro, A., 1971. Observações sobre a geologia do sul de Portugal e consequências metalogenéticas. Estudos Notas e Trabalhos do SFM 20/1-2, pp. 153-199.

Chew, D.M., Sylvester. P.J., Tubrett, M.N., 2011. U-Pb and Th-Pb dating of apatite by LA-ICPMS. Chemical Geology, 280, pp. 200-216.

Chew, D.M. & Donelick, R.A., 2012 Combined apatite fission track and U-Pb dating by LA-ICPMS and its application in apatite provenance analysis. In: Quantitative Mineralogy and Microanalysis of Sediments and Sedimentary Rocks (Ed. Sylvester, P.) Mineralogical Association of Canada Short Course 42, pp. 219-247.

Chew, D.M., Donelick, R.A., Donelick, M.B., Kamber, B.S., Stock, M., 2014a. Apatite chlorine concentration measurements by LA-ICP-MS. Geostandards and Geoanalytical Research, 38, pp. 23-35.

Chew, D.M., Petrus, J., Kamber, B., 2014b. U-Pb LA-ICPMS dating using accessory mineral standards with variable common Pb. Chemical Geology, 363C, pp. 185-199.

Cochrane, R., Spikings, R.A., Chew, D.M., Wotzlaw, J.F., Chiaradia, M., Tyrrell, S., Schaltegger, U., 2014. High temperature (>350°C) thermochronology and mechanisms of Pb loss in apatite. Geochimica et Cosmochimica Acta, 127, pp. 39-56.

Collins, A.S. & Buchan, C., 2004. Provenance and Age Constraints of the South 462 Stack Group, Anglesey, UK: U-Pb SIMS Detrital Zircon Data. Journal of the Geological Society, London – Special, 161, pp. 743-746.

Cook, A.C., Sherwood, N.R., 1991. Classification of oil shales, coals, and other organic rich rocks. Organic Geochemistry 17, pp. 211–222.

Cordani, U., Nutman, A., Andrade A., Santos J., Azevedo M., Mendes, M., Pinto, M., 2006. New U-Pb SHRIMP zircon ages for pre-variscan orthogneisses from Portugal and their bearing on the evolution. Anais da Academia Brasileira de Ciências do Mar, 78(1), pp. 133-49.

Corfu, F., 2012. A century of U-Pb geochronology: The long quest towards concordance. Geological Society of America Bulletin.

Dallmeyer, R., Fonseca, P., Quesada, C., Ribeiro, A., 1993. $^{40}Ar/^{39}Ar$ mineral age constraints to the tectonothermal evolution of the Variscan Suture in SW Iberia, Tectonophysics, v. 222, pp. 177-194.

De la Rosa, J., Jenner, G., Castro, A., 2002. A study of inherited zircons in granitoid rocks from the South Portuguese and Ossa-Morena Zones, Iberian Massif: support for the exotic origin of the South Portuguese Zone. Tectonophysics 352, pp. 245-255.

Delgado, M., Liñan, E., Pascual, E., Perez, F., 1977. Criterios para la diferenciación de Domínios en Sierra Morena Central. Estud. Geol. 12, pp. 75–90.

Dercourt, J., Ricou, L.E., Vrielynck, B. (eds.), 1993. Atlas Tethys Palaeoenvironmental Maps. Gauthier-Villars, Paris, 307 p.

Donelick, R.A., Ketcham, R., Carlson, W., 1999. Variability of apatite fission-track annealing kinetics: II. Crystallographic orientation effects. American Mineralogist, 84, pp. 1224-1234.

Donelick, R.A., O'Sullivan, P. B., Ketcham, R.A., 2005. Apatite Fission-Track eviews in Mineralogy and Geochemistry. 58, pp. 49-94.

Dow, W. & O'Connor, D., 1982. Kerogen maturity and type by reflected light microscopy applied to petroleum exploration. In: Staplin, F. Dow, W., Milner, C., O'Connor, D., Van Gijzel, P. Welte, P., Yukler, M. (eds) How to assess maturation and palaeotemperatures. Society of economic Paleontologists and Mineralogists, Short Course, 7, pp. 133-157.

Dunning, G., Díez, A., Matas, J., Martín, L., Almarza, J., Donaire, M., 2002. Geocronología U/Pb del volcanismo ácido y granitoides de la Faja Pirítica Ibérica (Zona Surportuguesa). Geogaceta 32, pp. 127–130.

Eden, C., 1991. Tectonostratigraphic analysis of the northern extent of the oceanic exotic terrane, Northwestern Huelva Province, Spain. PhD thesis, University of Southampton.

Ehlers, T. & Farley, K. 2003. Apatite (U-Th)/He thermochronometry: methods and applications to problems in tectonics and surface processes. Earth and Planetary Science Letters, 206, pp. 1-14.

Farley, K., Wolf, R., Silver, L., 1996. The effects of long alpha-stopping distances on (U-Th)/He ages. Geochimica et Cosmochimica Acta, 60, pp. 4223-4229.

Farley, K., 2000. Helium diffusion from apatite: General behavior as illustrated by Durango fluorapatite. Journal of Geophysical Research 105(B2), pp. 2903-2914.

Faure, G. & Mensing, T., 2005. Isotopes: principles and applications. Wiley, Hoboken, New Jersey.

Fermont, J., 1988. Possible causes of abnormal vitrinite reflectance values in paralic deposits of the Carboniferous in the Achterhoek área, The Netherlands. Organic Geochemistry 12, pp. 401-411.

Fernandes, P.M.C., 2000. Investigation of the stratigraphy, maturation and source-rock potential of Carboniferous black shales in the Dublin Basin. Unpublished Ph.D. thesis, University of Dublin.

Fernandes, P., Rodrigues, B., Matos, V., Borges, M., Clayton, G., *2012*. Organic maturation of the Algarve Basin (southern Portugal) and its bearing on thermal history and hydrocarbon exploration. Marine and Petroleum Geology.

Fernandes, P., Rodrigues, B., Matos, V., Borges, M., Clayton, G., 2013. Organic maturation of the Algarve Basin (southern Portugal) and its bearing on thermal history and hydrocarbon exploration. Marine and Petroleum Geology.

Fleischer, R. L. & Hart, H. R., 1972. Fission track dating: techniques and problems. In: Bishop, W., Miller, J. and Cole, S. (Eds), Calibration of Hominoid Evolution. Scottish Academic Press, pp. 135-170.

Frakes, L., Francis, J., Syktus, J., 1992. Climates modes of the Phanerozoic: the history of the Earth's climate over the Past 600 millinon years. Cambridge University press, Cambridge, 310p.

Frietsch, R. & Perdahl, J., 1995. Rare earth elements in apatite and magnetite in Kiruna-type iron ores and some other iron ore types. Ore Geol. Rev. 9, pp. 489– 510.

Fyffe, L., Barr, S., Johnson, S., McLeod, M., McNicoll, V., Valverde-Vaquero, P., Van Staal, C., White, C., 2009. Detrital zircon ages from Neoproterozoic and Early Paleozoic conglomerate and sandstone units of New Brunswick and coastal Maine: implications for the tectonic evolution of Ganderia. Atlantic Geology, 45, pp. 110–144.

Gallagher, K., Brown, R., Johnson, C., 1998 Fission track analysis and its applications to geological problems. Annual Review of Earth and Planetary Sciences, 26, pp. 519-572

García-Navarro, E. & Sierra, S., 1998. Evolución tectónica del borde oriental de la Cuenca del Viar (ZSP). Rev. Soc. Geol. Esp. 11 (3–4), pp. 223–232.

Gleadow, A., Duddy, I.R., Green, P.F., Lovering, J.F. 1986. Confined fission track lengths in apatite: a diagnostic tool for thermal history analysis. Contributions to Mineralogy and Petrology, 94: pp. 405–415.

Gleadow, A. & Brown, R.W., 2000. Fission-track thermochronology and the long-term denudational response to tectonics. In M. A. Summerfield, editor, Geomorphology and Global Tectonics, New York, Wiley, pp. 57–76

Green, P., Duddy, I., Gleadow, A., Tingate, P., Laslett, G., 1986 Thermal annealing of fission tracks in apatite. A qualitative description. Chemical Geology, 59, pp. 237-253.

Green, P.F., 1988. The relationship between track shortening and fission track age reduction in apatite: combined influences of inherent instability, annealing anisotropy, length bias and system calibration. Earth and Planetary Science Letters, 89, pp. 335–352.

Gonzáles-clavijo, E. J., Valadares, V. (2003). O Maciço Alcalino de Monchique (SW português): Estrutura e Modelo de Instalação na Crosta Superior. Comunicações do Instituto Geológico e Mineiro, Tomo 90, pp. 43-64.

Hanchar, J.M., & Oskin, P., 2003. Zircon. Reviews in Mineralogy and geochemistry, Vol. 53. Mineralogical Society of America, Washington, DC, 500 p.

Haq, B.U. & Shutter, S., 2008. A chronology of Paleozoic sea-level changes: Science, v. 322, pp. 64-68.

Hasebe, N., Mori, N., Tagami, T., Matsui, R., 2003. Geological partial annealing zone of zircon fission-track system: additional constraints from the deep drilling MITI-Nishikubiki and MITI-Mishima. Chemical Geology, 199, pp. 45-52

Henriques, M.L. 1954. Notas de mineralogia e petrografia portuguesas: chaminé monchiquítica da praia da Senhora da Luz, Algarve Ocidental. Boletim do Museu e Laboratório Mineralógico e Geológico da Faculdade de Ciências da Universidade de Lisboa, 22, pp.19-25

Hillier, S. & Marshall, J., 1988. A rapid technique to make polished thin sections of sedimentary organic matter concentrates. Journal of Sedimentary Petrology 58, pp. 754-755.

Holmes, A., 1913. The Age of the Earth, New York, Harper & Brothers.

Holmes, A., 1954. The oldest dated minerals of the Rhodesian Shield. Nature 173, pp. 612-617.

House, M.A., Wernicke, B.P., Farley, K.A., Dumitru, T.A., 1997. Cenozoic thermal evolution of the central Sierra Nevada, California, from (U–Th)/He thermochronometry. Earth and Planetary Science Letters, 151, pp. 167–169.

House, M., Farley, K., Kohn, B., 1999. An empirical test of helium diffusion in apatite: borehole data from the Otway Basin, Australia. Earth and Planetary Science Letters, 170, pp. 463-474.

Houseman, G.A. & Hurford, A.J., 1991. Uplift and cooling pathways derived from fission track analysis and mica dating: a review. Geologische Rundschau, 80, pp. 349-368.

Hurford, A.J. & Green, P.F., 1983. The zeta age calibration of fission-track dating. Chemical Geology (Isotope Geoscience Section), 1, pp. 285–317.

ICCP-International Committee for Coal and Organic Petrology, 2001. The new inertinite classification (ICCP System 1994). Fuel 80, pp. 459–471.

Jaffey, A.H., Flynn, K.F., Glendenin, L.E., Bentley, W.C., Essling, A.M., 1971. Precision measurement of half-lives and specific activities of ^{235}U and ^{238}U. Physical Reviews, Section C: Nuclear Physics, v. 4, pp. 1889–1906.

Jesus, A., Munhá, J., Mateus, A., Tassinari, C., Nutman, A., 2007. The Beja Layered Gabbroic Sequence (Ossa Morena Zone, Southern Portugal), geochronology and geodynamic implications. Geodinamica Acta 20, pp. 139–157.

Jorge, R.C.G.S., 2009. Caracterização petrográfica, geoquímica e isotópica dos reservatórios metalíferos crustais, dos processos de extracção de metais e dos fluidos hidrotermais envolvidos em sistemas mineralizantes híbridos na Faixa Piritosa Ibérica. PhD Thesis. Faculdade de Ciências da Universidade de Lisboa.

Jorge, R.C.G.S., Fernandes, P., Rodrigues, B., Pereira, Z., Oliveira, J., 2013. Geochemistry and provenance of the Carboniferous Baixo Alentejo Flysch Group, South Portuguese Zone. Sedimentary Geology, volume 284, pp. 133-148.

Ketcham, R., 2005. Forward and inverse modeling of low-temperature thermochronometry data. Reviews in Mineralogy and Geochemistry, 58, pp. 275-314.

Ketcham, R., Donelick, R., Carlson, W., 1999. Variability of apatite fission-track annealing kinetics: III. Extrapolation to geological time scales. American Mineralogist, 84, pp. 1235-1255.

Ketcham, R. & Donelick, M.B., 2000. AFTSolve: A program for multi-kinetic modeling of apatite fission-track data. Geological Materials Research, v.2, n.1.

Ketcham, R., 2011. HeFTy version 1.7.0 Manual. Apatite to Zircon, Incorporated and Richard A. Ketcham. 67 p.

Korn, D., 1997. The Palaeozoic amonoids of the South Portuguese Zone. Memória 33. Instituto Geológico e Mineiro.

Kullberg, J.C., Pais, J., Mannupella, G., 1992. Aspectos gerais da tectónica alpina no Algarve. Ciências da Terra, Universidade Nova de Lisboa, 11, pp. 293-302.

La Rosa, J., Jenner, J., Castro, A., 2002. A study of inherited zircons in granitoid rocks from the South Portuguese and Ossa–Morena Zones, Iberian Massif: support for the exotic origin of the South Portuguese Zone. Tectonophysics 352, pp. 245–256.

Laznicka, P., 1993. Precambrian empirical metallogeny. Developments in Economic Geology. Elsevier, Amsterdam.

Ludwig, K., 2003. User's manual for Isoplot 3.00: a geochronological toolkit for Microsoft Excel. Berkeley Geochronology Center Special Publication 4.

Luis, L., 2007. Mirone: a multi-purpose tool for exploring grid data. Computers & Geosciences 33, pp. 31-41.

Macintyre, R. M. & Berger, G. W., 1982. A note on the geochronology of the Iberian Alkaline Province. Lithos, 15, pp. 133-136.

Mackowsky, M., 1982. Rank determination by measurement of reflectance of vitrinites. In: Stach. E. et al. (eds.) Stach's Textbook of coal Petrology. (3rd edition), Gebruder Borntraeger (Berlin & Stuutgart,), pp. 319-329.

Manuppella, G., 1988. Litoestratigrafia e tectónica da Bacia Algarvia. Geonovas 10, 67-71.

Mannupella, G. (coord.), 1992. Carta Geológica da Região do Algarve, escala 1/100 000, 2 folhas. Serviços Geológicos de Portugal, Lisboa.

Martinez-Catalán, J., Arenas, R., Díaz, F., Abati, J., 1997. Variscan acretionary complex of northwest Iberia: terrane correlation and succession of tectono- thermal events. Geology 25, pp. 1103-1106.

Martins, L., Madeira, J., Youbi, N., Munhá, J., Mata, J., Kerrich, R., 2008. Rift-related magmatism of the Central Atlantic magmatic province in Algarve, southern Portugal. Lithos 101, pp. 102-124.

McCormack, N., 1998. The Thermal History of the South Portuguese Zone (Unpublished Ph.D. thesis). University of Dublin.

McCormack, N., Clayton, G., Fernandes, P., 2007. The thermal history of the Upper Palaeozoic rocks of southern Portugal. Marine and Petroleum Geology, 24, pp. 145-150.

McDonough, W.F. & Sun, S.S., 1995. Composition of the Earth. Chemical Geology 120, pp. 223-253.

McDowell, F.W. & Keizer, R.P., 1977. Timing of mid-Tertiary volcanism in the Sierra Madre Occidental between Durango City and Mazatlan: Geological Society of America Bulletin, v. 88, pp. 1479-1487.

McDowell, F.W., McIntosh, W.C., Farley, K.A., 2005. A precise $^{40}Ar\backslash^{39}Ar$ reference age for the Durango apatite (U-Th)/He and fission-track dating standard. Chemical Geology 214, pp. 249–263.

Mendes, F., 1967. Contribution à l'étude géochronologique, par la méthode au strontium, des formations cristallines du Portugal. PhD Thesis, Université de Clermont-Ferrand, 159 p.

Mendes, F., 1968. Contribution à l'étude géochronologique, par la méthode au strontium, des formations cristallines du PortugalBoletim do Museu e Laboratório Mineralógico e Geológico da Faculdade de Ciências da Universidade de Lisboa. - Vol. 11, fasc. 1 (1967-1968), 155 p.

Miranda, R., Valadares, V., Terrinha, P., Mata, J., Azevedo, M., R., Gaspar, M., Kullberg, J., C., Ribeiro, C., 2009. Age constraints on the Late Cretaceous alkaline magmatism on the West Iberian Margin. Cretaceous Research, 30, pp. 575-586.

Mitjavila, J., Martí, J., Soriano, C., 1997. Magmatic evolution and tectonic setting of the Iberian Pyrite Belt volcanism. Journal of Petrology 38, pp. 727-755.

Moço, L., Rocha, F., Pereira, Z., Lemos de Sousa, M., Gomes, C., Oliveira, J., 1998. Petrologia Orgânica do Sector Sudoeste da Zona Sul Portuguesa. Comunicações do Instituto Geológico e Mineiro, 84, pp. 26-29.

Moreno, C., 1988. Dispositivos turbidíticos sincrónicos en el Carbonífero Inferior de la Faja Pirítica Ibérica (Zona Surportuguesa). Estudios Geológicos 44, pp. 233–244.

Moreno, C. & Sáez, R., 1989. Petrología y procedencia de las areniscas del Culm de la parte occidental de la Faja Pirítica Ibérica (Zona Surportuguesa). Boletín Geológico y Minero 100, pp. 134–147.

Moreno, C., 1993. Postvolcanic Paleozoic of the Iberian Pyrite Belt: an example of basin morphologic control on sediment in a turbidite basin. Journal of Sedimentary Petrology 63, pp. 1118–1128.

Morton, A.C. & Hallsworth, C.R., 1999. Processes controlling the composition of heavy mineral assemblages in sandstones. Sedimentary Geology 124, pp. 3-29.

Moura, D., 1998. Litoestratigrafia do Neogénico terminal e Plistocénico, na Bacia Centro - Algarve. Evolução Paleoambiental. Dissertação de Doutoramento, Universidade do Algarve, 252p.

Mouterde, R., 1971. Esquisse de l'évolution biostratigraphique de la Péninsule Ibérique au Jurassique, Cuad. Geol. Iberica, Madrid, 2, pp. 21-31.

Munhá, J., 1983. Hercynian magmatism in Iberian Pyrite Belt. In: Lemos de Sousa, M.J., Oliveira, J.T. (eds.) The Carboniferous of Portugal, 29. Serviços Geológicos de Portugal, Lisboa, pp. 39–82.

Munhá, J., 1990. Metamorphic evolution of the South Portuguese/Pulo do Lobo Zone. In: Dallmeyer, R., Martínez García, E. (eds.) Pre-Mesozoic Geology of Iberia. Springer, Berlin, 363-368.

Murchison, D., Cook, A., Raymond, A., 1985. Optical properties of organic matter in relation to thermal gradients and structural deformation. Philosophical Transactions of the Royal Society of London, A. 315, pp. 157-186.

Murphy, J., Fernandez-Suarez, J., Keppie, J., Jeffries, T., 2004a. Contiguous rather than discrete Paleozoic histories for the Avalon and Meguma Terranes based on detrital zircon data. Geology, 32, pp. 585-588.

Murphy, J., Fernandez-Suarez, J., Jeffries, T., Strachan, R., 2004b. U-Pb (LA-ICP-M.S.) dating of detrital zircons from Cambrian clastic rocks in Avalonia: erosion of a Neoproterozoic arc along the northern Gondwanan margin. Journal of the Geological Society, 161, pp. 243-254.

Murphy, J., Keppie, J., Nance, R., Dostal, J., 2010. Comparative evolution of the Iapetus and Rheic Oceans: A North America perspective. Gondwana Research, volume 17, Issues 2-3, pp. 482-499.

Nance, R., Murphy, J., Strachan, R., 1991. Late Proterozoic tectonostratigraphic evolution of the Avalonian and Cadomian terranes. Precambrian Research. 53, pp. 41-78.

Nesbit, R., Pascual, E., Fanning, C., Toscano, M., Sáez, R., Almodóvar, G., 1999. First zircon U-Pb dating of stockwork zircons from the eastern Iberian Pyrite Belt, Spain. Journal of Geological Society of London, v. 156, pp. 7-10.

Oliveira, J., Horm, M., Paproth, E., 1979. Preliminary note on the stratigraphy of the Baixo–Alentejo Flysch Group, Carboniferous of Portugal and on the palaeogeographic development compared to corresponding units in NorthWest Germany. Comunicações dos Serviços Geológicos de Portugal, 65, pp. 151–168.

Oliveira, J. & Wagner Genthis, C., 1983. The Mértola and Mira formations boundary between Doguedo and Almada do Ouro, marine Carboniferous of South Portugal. In: Lemos de Sous, M.J. (ed.) Contributions to the Carboniferous Geology and Palaeontology of the Iberian Peninsula. Universidade do Porto, Porto, pp. 1–39.

Oliveira, J.T., 1990. Stratigraphy and syn-sedimentary tectonism in the South Portuguese Zone. In: Dallmeyer, R.D., Martinez García, E. (Eds.), Pre-Mesozoic Geology of Iberia. Springer-Verlag, Berlin Heidelberg, pp. 333–347.

Oliveira, J.T., Oliveira, V., Piçarra, J.M., 1991. Traços gerais da evolução tectono-estratigráfica da Zona de Ossa Morena, em Portugal: síntese crítica do estado actual dos conhecimentos. Comunicações dos Serviços Geológicos de Portugal 77, pp. 3-26.

Oliveira, J.T. (coord.), 1992. Carta Geológica de Portugal à escala 1:200 000, Notícia explicativa da folha 8, Serviços Geológicos de Portugal.

Oliveira, J. & Quesada, C., 1998. A comparison of stratigraphy, structure, and palaeogeography, of the South Portuguese Zone and southwest England, European Variscides. Geoscience in Southwest England. Proceedings of the Ussher Society, 9(3), pp. 141-150.

Oliveira, J.T., Pereira, Z., Carvalho, P., Pacheco, N., Korn, D., 2004. Stratigraphy of the tectonically imbricated lithological succession of the Neves Corvo mine area, Iberian Pyrite Belt, Portugal. Mineralium Deposita 39, 422–436.

Oliveira, J.T., Relvas, J., Pereira, Z., Matos, J., Rosa, D., Munhá, J.M., Jorge, R.C.G.S., Pinto, A., 2006. O Complexo Vulcano-Sedimentar da Faixa Piritosa: estratigrafia, vulcanismo, mineralizações associadas e evolução tectono-estratigráfica no contexto da Zona Sul Portuguesa. In: Dias, R., Araújo, A., Terrinha, P., Kullberg, J.C. (Eds.), Geologia de Portugal no contexto da Ibéria. Univ. Évora, Évora, pp. 207–243.

Oliveira, J., Rosa, C., Rosa, D., Matos, J., Inverno, C., Andersen, T. 2013a. Geology of the Rosário–Neves Corvo antiform, Iberian Pyrite Belt, Portugal: new insights from physical volcanology. Mineralium Deposita.

Oliveira, T., Relvas, J., Pereira, Z., Matos, J., Rosa, C. Rosa, D., Munhá, J. Fernandes, P., Jorge, R., Pinto, A., 2013b. Geologia Sul portuguesa, com ênfase na estratigradia, vulcanologia física, geoquímica e mineralizações da faixa piritosa. In: Dias, R. Araújo, A., Terrinha, P. Kullberg, J. (Eds.) Geologia de Portugal, volume I-Geologia Pré-mesozóica de Portugal, Escolar editora, pp. 673-767.

Onézime, J., Charvet, J., Faure, M., Bourdier, J., Chauvet, A., 2003. A new geodynamic interpretation for the South Portuguese Zone (SW Iberia) and the Iberian Pyrite Belt genesis. Tectonics, 22, pp. 1–16.

Palain, C., 1976. Une série détritiqui terrigène. Les "Grès de Silves": Trias et Lias inférieur du Portugal. Memória dos Serviços Geológicos de Portugal, N. S. 25, 377 p.

Paton, C., Hellstrom, J., Paul, B., Woodhead, J., Hergt, J., 2011. Iolite: Freeware for the visualization and processing of mass spectrometric data. Journal of Analytical Atomic Spectroscopy, 26, pp. 2508–2518.

Paul, T. A. & Fitzgerald, P. G., 1992. Transmission electron microscopy investigation of fission tracks in fluorapatite. American Mineralogist, 77, pp. 336–344.

Pereira, M. F., Chichorro, M. Brandão Silva, J. Ordóñez-Casado, B., Lee, J. Williams, I. 2012a. Early carboniferous wrenching, exhumation of high-grade metamorphic rocks and basin instability in SW Iberia: Constraints derived from structural geology and U–Pb and ^{40}Ar–^{39}Ar geochronology. Tectonophysics 558-559, pp. 28–44.

Pereira, M. F., Chichorro, M., Johnston, S. T., Gutiérrez-Alonso, G., Silva, J. B., Linnemann, U., Drost, K., 2012b. The missing Rheic Ocean magmatic arcs: Provenance analysis of Late Paleozoic sedimentary clastic rocks of SW Iberia. Gondwana Research.v. 22, 3-4, pp. 882-891.

Pereira, Z., 1997. Palinologia e petrologia orgânica do Sector Sudoeste da Zona Sul Portuguesa. Unpublished PhD thesis, Universidade do Porto.

Pereira, Z., 1999. Palinoestratigrafia do Sector Sudoeste da Zona Sul Portuguesa. Comunicações dos Serviços Geológicos de Portugal, 86, pp. 25–57.

Pereira, Z., Oliveira, V., Oliveira, J.T., 2006. Palynostratigraphy of the Toca da Moura and Cabrela Complexes, Ossa Morena Zone, Portugal. Geodynamic implications. Review of Palaeobotany and Palynology 139, pp. 227–240.

Pereira, Z., Matos, J., Fernandes, P., Oliveira, J., 2007. Devonian and Carboniferous palynostratigraphy of the South Portuguese Zone, Portugal: an overview. Comunicações Geológicas 94, pp. 53–79.

Pereira, Z., Matos, J., Fernandes, P., Oliveira, J., 2008. Palynostratigraphy and Systematic Palynology of the Devonian and Carboniferous successions of the South Portuguese Zone, Portugal. Memória do INETI, 34, pp. 129-146.

Pérez-Estaún, A., Bea, F., Bastida, F., Marcos, A., Martínez-Catalán, J. R., Martínez, D., Arenas, R., Díaz, F., Azor, A., Simancas, J., González, F., 2004. Macizo Iberico. In: Vera J. A. (Eds.) Geologia de España. Sociedad Geológica de España, Instituto Geológico y Minero de España, pp. 21-230.

Petrus, J. & Kamber, B., 2012. VizualAge: A Novel Approach to Laser Ablation ICP-MS U-Pb Geochronology Data Reduction. Geostandards and Geoanalytical Research. V 36, Is3, pp 147-150.

Pin, C., Paquette, J.L., Fonseca, P. 1999. (U–Pb zircon) igneous emplacement age and Sr–Nd isotopic study of the Beja Gabbroic complex (S Portugal). XV reunion de Geología del Oeste Península, Univ. Of Extremadura

at Badajoz, Badajoz, Spain.

Pinto, M. & Andrade, A., 1987. Geocronologia dos granitóides da Zona de Ossa-Morena no contexto do Arco Ibero-Armoricano. Geociências, vol. 2, fasc. 1-2, pp. 95-103.

Quesada, C., Fonseca, P., Munhá, J., Oliveira, J., Ribeiro, A., 1994. The Beja–Acebuches Ophiolite (Southern Ibera Variscan fold belt): geological characterization and geodynamic significance. Boletin Geológico y Minero 105, pp. 3–49.

Ravenhurst, C.E. & Donelick, R.A., 1992. Fission track thermochronology. In: Short Course. Handbook on Low Temperature Thermochronology, Zentilli. M. & Reynolds, P. (eds.), pp. 21-42.

Raymond, A. & Murchison, D. 1989. Organic maturation and its timing in a Carboniferous sequence in the central Midland Valley of Scotland: comparisons with northern England. Fuel, 68, pp. 328-324.

Rey, J., 2006. Les Formations Crétacées de l'Algarve Occidental et Central. Com. Geol., 93, pp. 39-80.

Ribeiro, A., Munhá, J., Dias, D., Mateus, A., Pereira, E., Ribeiro, L., Fonseca, P., Araújo, A., Oliveira, J., Romão, J., Chaminé, H., Coke, C., Pedro, J., 2007. Geodynamic evolution of the SW Europe Variscides. Tectonics, 26.

Ribeiro, A., Quesada, C., Dallmeyer, R.D., 1990. Geodynamic evolution of the Iberian Massif. In: Dallmeyer, R.D., García, E.M. ds.), Pre-Mesozoic Geology of Iberia. Springer-Verlag, Berlin Heidelberg, pp. 399–409.

Rock, N., 1978. Petrology and petrogenesis of the alkaline complex, southern Portugal. Journal Petrology 19, pp. 171-214.

Rock, N., 1982. The late Cretaceous alkaline igneous province in the Iberian Peninsula, and its tectonic significance. Lithos 15, pp. 111-131.

Roeder, P., MacArthur, D., Xin-Pei, Ma., Palmer, G., Mariano, A. 1987. Cathodoluminescence and microprobe study of rare earth elements in apatite. American Mineralogist, 72, pp. 801–811.

Rocha, R.B., 1976. Estudo Estratigráfico e Paleontológico do Jurássico do Algarve Ocidental. Ciências da Terra (U.N.L.), vol. 2, pp. 9-179.

Rosa, D., Finch, A., Andersen, T., Inverno, C., 2009. U–Pb geochronology and Hf isotope ratios of magmatic zircons from the Iberian Pyrite Belt. Mineralogy and Petrology, Volume 95, Issue 1-2, pp. 47-69.

Rosas, F., Marques, F., Ballèvre, M., Tassinari, C., 2008. Geodynamic evolution of the SW Variscides: orogenic collapse shown by new tectonometamorphic and isotopic data from western Ossa–Morena Zone, SW Iberia. Tectonics, v. 27, n.6.

Ross, G. & Murphy, D., 1988. Transgressive stratigraphy, anoxia, and regional correlations within the late Precambrian Windermere grit of the southern Canadian Cordillera. Geology, v. 16, pp. 139-143.

Rutherford, E., 1907. Some cosmical aspects of radioactivity. Journal of the Royal Astronomical Society of Canada, pp. 145–165.

Salman, K., 2004. The timing of the Cadomian and Variscan cycles in the Ossa-Morena Zone, SW Iberia: granitic magmatism from subduction to extension. Journal of Iberian Geology, 30, pp. 119-132.

Sánchez-carretero, R., Eguíluz, L., Pascual, M. & Carracedo, M., 1990. Igneous rocks of the

Ossa-Morena Zone. In: DALLMEYER, R. & Martínez García, E. (Eds), Pre-Mesozoic Geology of Iberia. Springer, Berlin Heidelberg, p. 292–313.

Santos, J., Mata, J., Gonçalves, F., Munhá, J., 1987. Contribuição para o conhecimento geológico-petrológico da região de Santa Susana: O complexo vulcano-sedimentar da Toca da Moura. Comunicaçoes Serviços Geologico de Portugal 73, pp. 29–48.

Schermerhorn, L., 1971. An outline stratigraphy of the Iberian Pyrite Belt. Bol. Geol. Minero, 82, pp. 239-268.

Schoene, B. & Bowring, S.A., 2007. Determining accurate temperature–time paths from U–Pb thermochronology: An example from the Kaapvaal craton, southern Africa. Geochimica et Cosmochimica Acta, 71 (1), pp. 165–185.

Sha, L. & Chappell, B., 1999. Apatite chemical composition, determined by electron microprobe and laser-ablation inductively coupled plasma mass spectrometry, as a probe into granite petrogenesis. Geochimica et Cosmochimica Acta 63 (22), pp. 3861– 3881.

Sierra, S., Moreno, C., González, F., 1999. Los abanicos aluviales de la cuenca pérmica del Viar (SO de España): caracterización sedimentológica y petrográfica. Geogaceta 25, 195–198.

Sierra, S., Moreno, C., Pascual, E., 2009. Stratigraphy, petrography and dispersion of the lower Permian syn-eruptive deposits in the Viar Basin, Spain. Sedimentary Geology 217, pp. 1–29.

Sierra, S., Moreno, C., González, F., 2000. Vulcanismo pérmico en la cuenca del Viar. Caracterización de la Secuencia Volcanoclástica Gris. Geogaceta 27, 159–162.

Silva, J., Oliveira, J., Ribeiro, A., 1990. Structural outline in Pre-Mesozoic geology of Iberia. In: Dallmeyer, R.D., Martinez Garcia, E. (eds.), Pre-Mesozoic Geology of Iberia. Springer-Verlag, Berlin Heidelberg, pp. 399–410.

Sláma, J., Košler, J, Condon, D., Crowley, J., Gerdes, A., Hanchar, J., Horstwood, M., Morris, G., Nasdala, L., Norberg, N., Schaltegger, U., Schoene, B., Tubrett, M., Whitehouse., M., 2008. Plešovice zircon — A new natural reference material for U–Pb and Hf isotopic microanalysis. Chemical Geology. Volume 249, Issues 1–2, 30, pp. 1–35.

Spear, F.S., 1993. Metamorphic Phase Equilibria and Pressure-Temperature-Time Paths, Mineralogical Society of America, Washington, D. C., 799 p.

Stacey, J.S. & Kramers, J.D., 1975. Approximation of terrestrial lead isotope evolution by a two-stage model. Earth and Planetary Science Letters 26 (2), pp. 207–221.

Stach, E., Mackowsky, M-Th., Teichmuller, M., Taylor, G.H., Chandra, D., Teichmuller, R. (Eds.), 1982. Coal Petrology. Gebruder Borntraeger, Berlin - Stuttgart, p. 535 pp.

Stapel, G. 1999. The Nature of Isostasy in West Iberia and its Bearing on Mesozoic and Cenozoic Regional Tectonics (Unpublished Ph.D. thesis). Vrije Universiteit.

Stockli, D.F., Farley, K.A., Dumitru, T.A., 2000. Calibration of the apatite (U–Th)/He thermochronometer on an exhumed fault block, White Mountains, California. Geology, 28, pp. 961–1056.

Stopes, M.C., 1935. On the petrology of banded bituminous coal: Fuel, v. 14, p. 4-13.

Storetvedt, K.M., Mogstad, H., Abranches, M.C., Mitchell, J.G., Serralheiro, A., 1987. Paleomagnetism and isotopic age data from Upper Cretaceous igneous rocks of W Portugal; geological correlation and plate tectonic aspects. Geophysical Journal Royal Astronomical Society 88, pp. 241–263.

Suárez-Ruiz, I., Flores, D., Mendonça Filho, J.G., Hackley, P.C., 2012. Review and update of the applications of organic petrology: Part 1, Geological Applications International Journal of Coal Geology 99, pp. 54-112.

Simancas, J.F., 1983. Geología de la extremidad oriental de la Zona Sudportuguesa. Tesis Doct. Univ. Granada.

Simancas, J.F., 2004. Zona Sudportuguesa. In: Vera, J.A. (Ed.), Geología de España, pp. 199–201. SGE-IGME.

Tagami, T. & O'Sullivan, P.B., 2005. Fundamentals of fission track thermochronology. Reviews in Mineralogy and Geochemistry, 58, pp. 19-47.

Terrinha, P., 1998. Structural Geology and Tectonic Evolution of the Algarve Basin, South Portugal. Unpublished Ph.D. thesis, Department of Geology, Royal School of Mines, Imperial College, London, 430p.

Terrinha, P., Ribeiro, C., Kulberg, J.C., Lopes, C., Rocha, R., Ribeiro, A., 2002. Compressive episodes and faunal isolation during rifting, Southwest Iberia. Journal of Geology ,110, 101-113.

Thomson, S.N., Gehrels, G.E., Ruiz, J., Buchwaldt, R., 2012. Routine low-damage U-Pb dating of apatite using laser ablation-multicollector ICPMS. Geochemistry, Geophysics, Geosystems, 13, Q0AA21.

Toplis, M. & Dingwell, D., 1996. The variable influence of P_2O_5 on the viscosity of melts of differing alkali/aluminium ratio: Implications for the structural role of phosphorus in silicate melts. Geochimica et Cosmochimica Acta, 60 (21), 4107– 4121.

Valadares, V., 2004. O Complexo Alcalino de Monchique-novos dados de cartografia, geoquímica e geocronologia. Tese de mestrado, Lisboa. 171 p.

Verati, C., Rapaille, C., Feraud, G., Marzoli, A., Bertrand, H., Youbi, H., 2007. $^{40}Ar/^{39}Ar$ ages and duration of the Central Atlantic Magmatic Province volcanism in Morocco and Portugal and its relation to the Triassic–Jurassic boundary. Palaeogeography Palaeoclimatology Palaeoecology 244, pp. 308–325.

Von Raumer, F., Stampfli, M., Bussy, F., 2003. Gondwana-derived microcontinents-the constituents of the Variscan and Alpine collisional orogens. Tectonophysics 365, pp. 7–22.

Wagner, G.A. & Van den Haute, P., 1992. Fission Track Dating, Amsterdam, Elsevier.

Wagner, R.H., Mayoral, E.J., 2007. The Early Permian of Valdeviar in Sevilla province, SW Spain: basin history and climatic/palaeogeographic implications. J. Iberian Geol. 33,pp. 93–124.

Warnock, A.C., Zeitler, P.K., Wolf, R.A., Bergman, S.C., 1997. An evaluation of low-temperature apatite U–Th/He thermochronometry. Geochimica et Cosmochimica Acta, 61:pp. 5371–5377.

Wiedenbeck, M., Allé, P., Corfu, F., Griffin, W., Meeir, M., Oberli, F. Von Quadt, A., Roddick, J., Spiegel, W., 1995. Three natural zircon standards for U–Th–Pb, Lu–Hf, trace element and REE analyses. Geostandards Newsletter 19(1), pp. 1–23.

Wolf, R.A., Farley, K.A., Silver, L.T., 1996. Helium diffusion and low-temperature thermochronometry of apatite. Geochimica et Cosmochimica Acta, 60, pp. 4231-4240.

Wolf, R.A., Farley, K.A., Kass, D.M., 1998. A sensitivity analysis of the apatite (U-Th)/He thermochronometer. Chemical Geology. 148, 105-114.

Young, E., Myers, A., Munson, E., Conklin, N., 1969. Mineralogy and geochemistry of fluorapatite from Cerro De Mercado, Durango, Mexico. U. S. Geol. Surv. Prof. Pap. 650-D, D84-D93.

Zeitler, P., Herczig, A., McDougall, I., Honda, M., 1987. U-Th-He dating of apatite: A potential thermochronometer. Geochim Cosmochim Acta 51, pp. 2865-2868.

Ziegler, P.A. (1990): Permo-Triassic development of Pangea. In: P.A. Ziegler (ed): Geological Atlas of Western and Central Europe. Shell International Petroleum Maatschappij B.V., The Hague, 68-90.

ANNEX I

Publications in peer review journals

Marine and Petroleum Geology 46 (2013) 210–233

Contents lists available at SciVerse ScienceDirect

Marine and Petroleum Geology

journal homepage: www.elsevier.com/locate/marpetgeo

Organic maturation of the Algarve Basin (southern Portugal) and its bearing on thermal history and hydrocarbon exploration

Paulo Fernandes [a,*], Bruno Rodrigues [a], Marisa Borges [a,b,1], Vasco Matos [a,2], Geoff Clayton [c]

[a] Universidade do Algarve, CIMA, Campus de Gambelas, 8005-139 Faro, Portugal
[b] LNEG, Rua da Amieira, 4465-965 S. Mamede Infesta, Portugal
[c] Department of Geology, Trinity College, University of Dublin, Dublin 2, Ireland

ARTICLE INFO

Article history:
Received 25 August 2012
Received in revised form
17 June 2013
Accepted 18 June 2013
Available online 27 June 2013

Keywords:
Algarve Basin
Mesozoic
Portugal
Vitrinite reflectance
Maturation
Thermal history
Hydrocarbons

ABSTRACT

The Algarve Basin, southern Portugal is under-explored in terms of petroleum geology. Organic maturation levels and the thermal history of this basin have been ascertained, together with their implications for future exploration. Maturity was determined using vitrinite reflectance and spore fluorescence/colour. The succession was extensively sampled (158 onshore samples and 20 samples from two offshore wells). Thermal history was modelled using 1D PetroMod®.

A palynostratigraphic study of two offshore wells was also completed, showing thick marl–limestone sequences of Middle and Upper Jurassic age. Hiatuses were identified in the offshore wells within the Jurassic section and between the Jurassic and the Miocene sections.

The Mesozoic rocks of the Algarve Basin lie within the oil window. Vitrinite reflectance ranges from 0.52–0.7%R_r in the Lower Cretaceous to 1–1.1%R_r in the Upper Triassic–Hettangian. Miocene rocks that unconformably overlie the Mesozoic strata are immature (0.42–0.47%R_r). Maturation levels increase with increasing age of the strata, indicating that burial was the main process controlling maturation. Thick marl–limestone sequences of the Middle Jurassic (Callovian) and the Upper Jurassic (Oxfordian) are the main source rock intervals. The Miocene successions of both offshore wells contains reworked vitrinite and palynomorphs with maturation levels similar to the Mesozoic rocks of the basin, suggesting exposure and erosion of these rocks during Miocene times.

Palaeogeothermal gradients in the onshore Algarve Basin range from 52 °C/km to 24.7 °C/km with pre-Miocene exhumation estimated at 2000–2500 m. The probable age for the removed cover is Upper Cretaceous to Lower Palaeocene(?) and peak temperatures in the Mesozoic rocks were attained during latest Cretaceous–Early Palaeocene times. Modelled palaeotemperatures suggest that the Jurassic entered the oil-window at the beginning of the Cretaceous with peak oil generation in late Cretaceous time.

1. Introduction

The Algarve Basin is a Mesozoic to Cenozoic sedimentary basin located in southern Portugal, cropping out along the entire south coast from Cape Saint Vincent in the west to the Guadiana river on the Portuguese–Spanish border in the east (Fig. 1). The basin extends offshore, where it has been recognized in seismic lines and 5 hydrocarbon exploration wells (Fig. 1). The Mesozoic geology of the Algarve Basin is, therefore, better known onshore than offshore and comprises sedimentary rocks ranging in age from Upper Triassic to Lower Cretaceous, constituting a succession over 3 km thick in the depocentre of the basin in the central Algarve.

The development of the Algarve Basin is related to consecutive phases of rifting associated with the break-up of Pangaea. Its origin, location, sedimentary record and evolution during the Mesozoic are closely related to a series of basins that developed during the opening of the North and Central Atlantic Ocean, including, for example, the Lusitanian Basin in central Portugal, the Porcupine Basin in offshore western Ireland and the Scotian, Whale and Jeanne d'Arc basins in offshore eastern Canada (Wilson et al., 1989). Although the main geological features of the Algarve Basin have been summarised in several publications (*e.g.* Manuppella et al., 1988; Terrinha et al., 2013), none of these discuss organic maturation

* Corresponding author. Tel.: +351 919707488.
E-mail address: pfernandes@ualg.pt (P. Fernandes).
[1] Current address: PetroStrat Ltd., Tan-y-Graig, Parc Caer Seion, Conwy, Wales LL32 8FA, UK.
[2] Current address: Petrobras, Portugal, Lagoas Park Edifício 11 – 1° Norte 2740-270 – Porto Salvo, Oeiras, Portugal.

0264-8172/$ – see front matter © 2013 Elsevier Ltd. All rights reserved.
http://dx.doi.org/10.1016/j.marpetgeo.2013.06.015

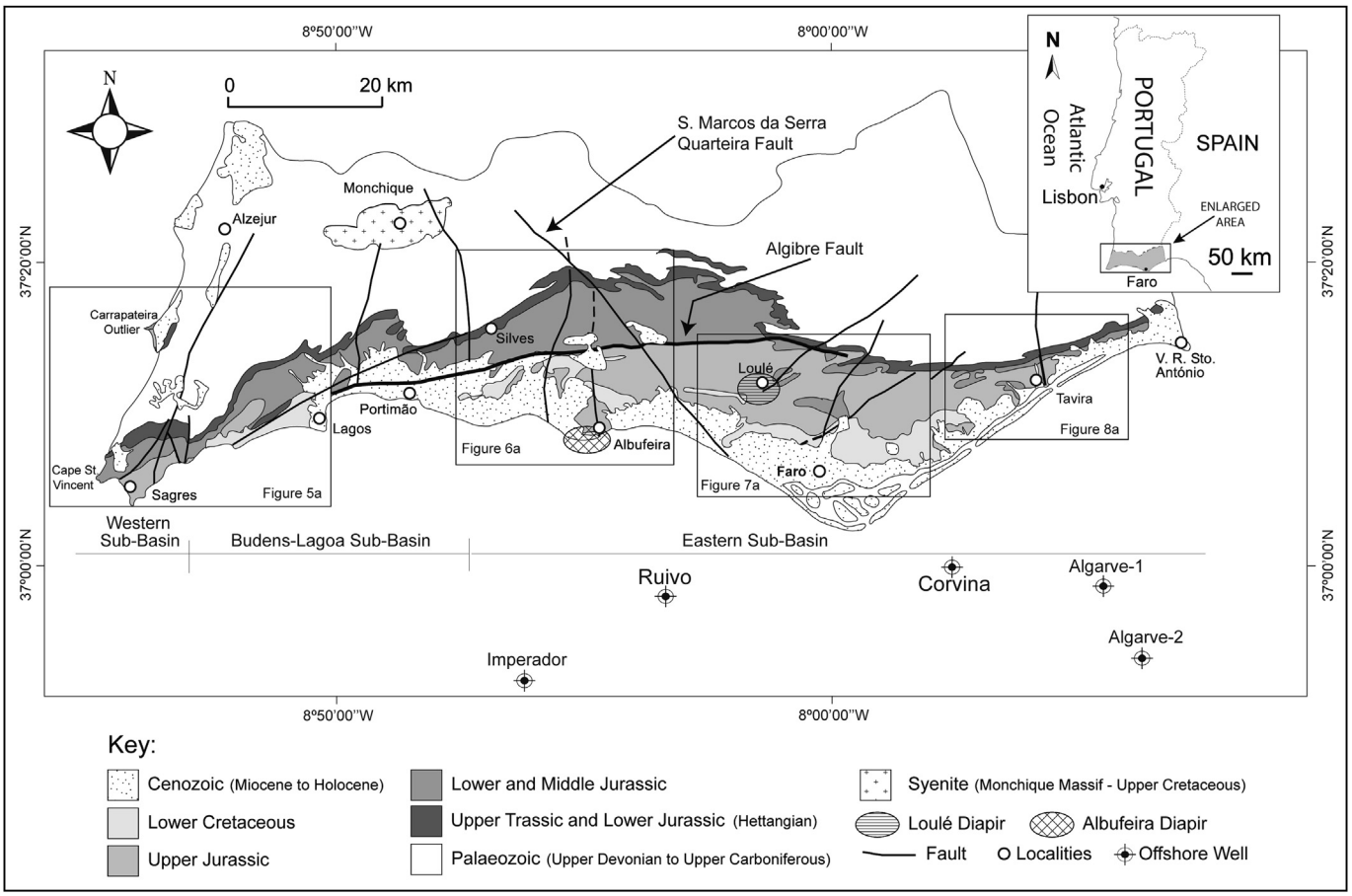

Figure 1. Generalized geology of the Algarve Basin showing the geographical extent of the Western, Budens–Lagoa and Eastern Sub-Basins, the offshore wells and the position of Figures 5a, 6a, 7a and 8a (adapted from Borges et al., 2011).

levels and thermal history, and their implications for the hydrocarbon exploration. Aspects of the petroleum geology are included in unpublished reports produced by oil companies that were active in exploration of the offshore basin between the late 1960s and early 1980s (Chevron, 1975; Challenger, 1976) and in an unpublished Ph.D. thesis (Matias, 2007). However, these summaries contain few data regarding the organic maturation levels of the Algarve Basin and mainly deal with the stratigraphy, micropalaeontology and modelling of exploration wells drilled in the offshore. The few maturation data in these reports are mostly limited to spore colour determinations. In this work, we present vitrinite reflectance (VR) results from 178 rock samples and use these data to estimate their thermal maturity, model the thermal history of the Algarve Basin, and discuss implications for hydrocarbon exploration, especially in the offshore part of the basin.

Thermal history analysis is an indispensable part of any study of sedimentary basins and their hydrocarbon source potential. There are several methods, both optical and geochemical, which can be used to ascertain the temperatures attained by strata during subsidence and interpret their thermal history. VR is an optical method considered a reliable indicator of the organic maturation levels of sedimentary rocks (Hunt, 1996; Robert, 1988; Tissot and Welte, 1978; Bordenave et al. 1993). Since organic maturation levels are largely related to temperature, VR is also a good indicator of peak (palaeo)temperatures, which accounts for its widespread use in basin analysis and hydrocarbon exploration.

Good age control of the sedimentary successions is also fundamental in basin analysis studies related to hydrocarbon exploration and exploitation. This is even more significant in areas where the subsurface geology is mainly recognized by seismic lines (Esso, 1982a,b; Challenger, 1976; Chevron, 1975) and only by five exploration wells, as is the offshore part of the Algarve Basin (Fig. 1). Micropalaeontology and palynology are the staple palaeontological techniques used to determine the age and biostratigraphy in wells and boreholes. In this study, in order to calibrate the ages of offshore geological units of the Algarve Basin and allow correlation with the onshore geology, two wells, Ruivo and Corvina (Fig. 1), were studied for palynology.

2. Geological background of the Algarve Basin

2.1. Onshore geology

Sedimentation in the Algarve Basin was initiated in Late Triassic times with the deposition of continental red beds and evaporites, which unconformably overlie folded and faulted Carboniferous strata (Palain, 1976) (Fig. 2). The red bed succession (Silves Sandstones) consists of sandstones and conglomerates at the base, overlain by variegated mudstones interbedded with siltstones and dolomites (Silves Mudstones – Siltstones and Dolomites). The sandstones were deposited in alluvial environments and the mudstones in alluvial to shallow lacustrine environments. At the top of this sequence, to the south of the E–W trending Algibre Fault (Fig. 1), there are thick evaporitic deposits, whereas north of this major structure, the evaporites are virtually absent. The evaporites mark the first marine incursions into the basin and yield Early

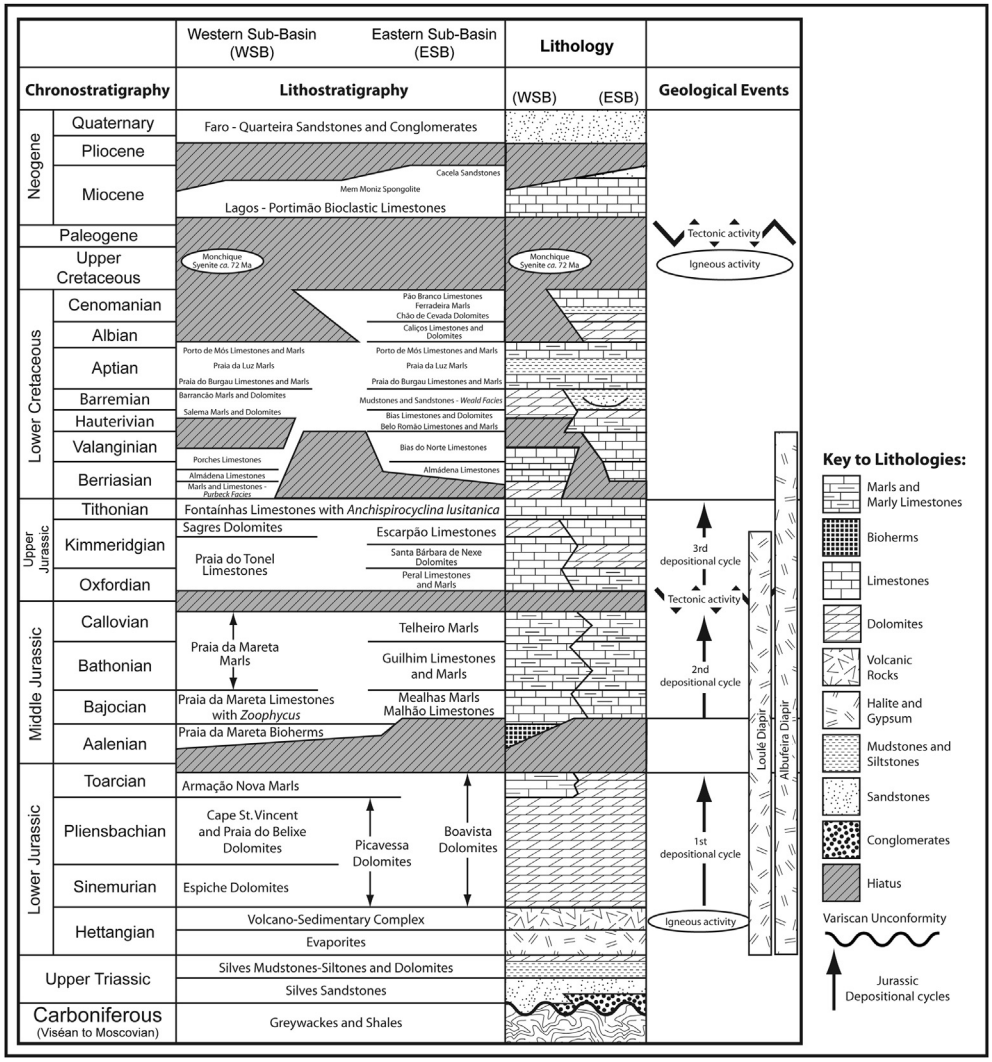

Figure 2. Generalized stratigraphy of the onshore Algarve Basin (adapted from Terrinha, 1998, Rocha, 1976, Rey, 2006, 2009, Manuppella, 1988, Antunes and Pais, 1993 and Pais et al., 2000).

Jurassic (Hettangian) palynomorphs in the Loulé Diapir (Fechner, 1989). These strata are overlain by volcanic rocks associated with the Central Atlantic Magmatic Province (CAMP) (Martins et al., 2008; Verati et al., 2007) and mark the end of the first phase of rifting in the Algarve Basin.

After this important magmatic episode, Sinemurian to Tithonian marine carbonate sedimentation became well-established across the Algarve Basin. Within this interval, the vertical movements of north–south trending faults caused lateral sedimentary facies changes in the limestone across the basin (Manuppella, 1988; Manuppella et al., 1988). These facies changes, together with differences in thicknesses, allow the division of the Algarve Basin into small sub-basins, namely, the Western, the Budens–Lagoa, and the Eastern sub-basins (Fig. 1) (Manuppella et al., 1988).

Three main sedimentary cycles, separated by regional unconformities or hiatuses, are recognized in the Jurassic (Sinemurian to Tithonian) marine carbonates of the Algarve Basin (Fig. 2). These cycles are related either to global sea level variations or to regional tectonic events (Mouterde et al., 1971; Manuppella et al., 1988; Terrinha et al., 2002). The first cycle extends from Sinemurian to lower Toarcian (Fig. 2), and consists mainly of dolomitised limestones that occupy a large area north of the Algibre Fault in the central Algarve. In the Western Sub-Basin, less dolomitised limestones (Cape S. Vincent and Praia do Belixe Dolomites) have yielded Pliensbachian to Lower Toarcian ammonites (Rocha, 1976; Dommergues et al., 2011). Late Sinemurian foraminifera identified in the lower beds of the Picavessa Dolomites confirm the age of this cycle in the Eastern Sub-Basin (Azerêdo et al., 2003).

The second cycle corresponds to the Middle Jurassic (Fig. 2) and is well-exposed at Mareta Beach in the Western Sub-Basin. At this location it is represented by a *ca.* 140 m thick succession at the base of which are coral bioherms with karstified tops that are filled and covered by upper Bajocian limestones with *Zoophycus* and by mid Bathonian marls (Praia da Mareta Marls). The coral bioherms are not dated directly and their age therefore remains problematic. However, the lack of bioherms in the Sinemurian to lower Toarcian succession in the Western Sub-Basin, together with the absence of mid to upper Toarcian strata in the same region, suggested to Rocha (1976) that the most probable age for the Praia da Mareta Bioherms was Aalenian to early Bajocian, and that the karstification episode was pre-late Bajocian. Overlying the mid Bathonian marls are more grey marls that grade upwards into marly limestones that have been affected by several slump events (Gibling and Stuart, 1988; Rocha, 1976). Ammonite faunas and dinoflagellates indicate a Callovian age for this part of the succession (Borges et al., 2011, 2012; Rocha, 1976). In the Eastern Sub-Basin, this cycle is represented by

Bajocian to lower Callovian marls and marly limestones that crop out in the cores of regional anticlines north of Faro (Guilhim) and Tavira (Borges et al., 2012; Marques and Rocha, 1988a, 1988b). The establishment of lower Callovian marl–marly limestone successions across the Algarve Basin suggests that uniform sedimentary conditions prevailed in Callovian time, possibly due to an increase in the rate of subsidence and an associated transgressive episode.

The beds at the base of the third sedimentary cycle rest unconformably on gently-folded Callovian marly limestones and marls (*e.g.* at Cilheta Beach in the Western Sub-Basin). This unconformity marks an important tectonic event that is observed throughout Iberia (Mouterde et al., 1971). Immediately above the unconformity are limestones in the Western Sub-Basin (Praia do Tonel Limestones) and limestone–marl successions in the Eastern Sub-Basin (Peral Limestones and Marls) (Fig. 2). Both lithological units yielded ammonites of mid Oxfordian age. These beds are overlain by a thick succession (over 500 m in the Eastern Sub-Basin) of Upper Jurassic (mid Oxfordian to Tithonian) interbedded limestones, marls, bioherms and dolomites (*e.g.* Manuppella et al., 1987; Oliveira, 1992). Sedimentary conditions became uniform in both sub-basins in the Tithonian with the deposition of shallow water limestones (Fontaínhas Limestones with *Anchispirocyclina lusitanica*) (Fig. 2).

The Lower Cretaceous sedimentary interval is represented by a mixed carbonate and siliciclastic succession (Rey, 1983, 2006, 2009), which attains its maximum thickness (*ca.* 1500 m) in central Algarve in the Eastern Sub-Basin. At its base are Berriasian marls and dolomites that rest conformably on Tithonian limestones (*e.g.* at Ponta da Almádena in the Western Sub-Basin) (Fig. 2). In the eastern Sub-Basin this contact is not observed. The Berriasian strata are followed by Valanginian to Barremian marls, dolomites, sandstones and mudstones that were deposited in nearshore and continental settings. This part of the Lower Cretaceous succession is better represented in the Eastern Sub-Basin. During the Aptian to Albian interval, depositional conditions became more uniform across the basin, resulting in the accumulation of variegated muds of possible lagoonal origin (the Aptian Luz Marls) followed by transgressive limestones and marls (the lower Albian Porto de Mós Limestones and Marls). Upper Albian to Cenomanian strata are only known in the Eastern Sub-Basin and are represented by shallow water limestones interbedded with marls and dolomites.

During the Late Cretaceous–Palaeocene(?), a major uplift episode occurred, related to Alpine tectonism and the emplacement of the Late Cretaceous (Campanian, *ca.* 72 Ma) Monchique Syenite (Fig. 1) (Terrinha et al., 2002; Miranda et al., 2009). Although the main batholith of the Monchique Syenite only intrudes greywackes and shales of Pennsylvanian age, minor intrusions of the Monchique Syenite Massif Dyke Swarm intrude the Algarve Basin Mesozoic succession, especially in the Western Sub-Basin (Martins, 1999; Martins and Munhá, 1993). As a consequence, no Upper Cretaceous to Palaeogene strata are found in the onshore, exhumed Algarve Basin. After this event, sedimentation only resumed during the Miocene (Pais et al., 2000), with bioclastic limestones that grade upwards into silts and fine sands, which unconformably overlie the Jurassic and Lower Cretaceous strata.

2.2. Offshore exploration wells

2.2.1. Ruivo

This well reached a depth of *ca.* 2134 m below sea-bed (Fig. 3). The upper 876 m consists of limestones, sandstones and argillaceous siltstones assigned to the Miocene–Oligocene interval (Chevron, 1975). From 876 to 1087 m depth, sandstones and mudstones lacking any stratigraphically-useful fossils were intersected and tentatively attributed to the Upper Cretaceous (Turonian) (Chevron, 1975). The interval between the 1087 and 1909 m consists of interbedded marls and limestones with microfossils suggesting a Middle Jurassic (Callovian) age. The deepest 225 m of the well, from

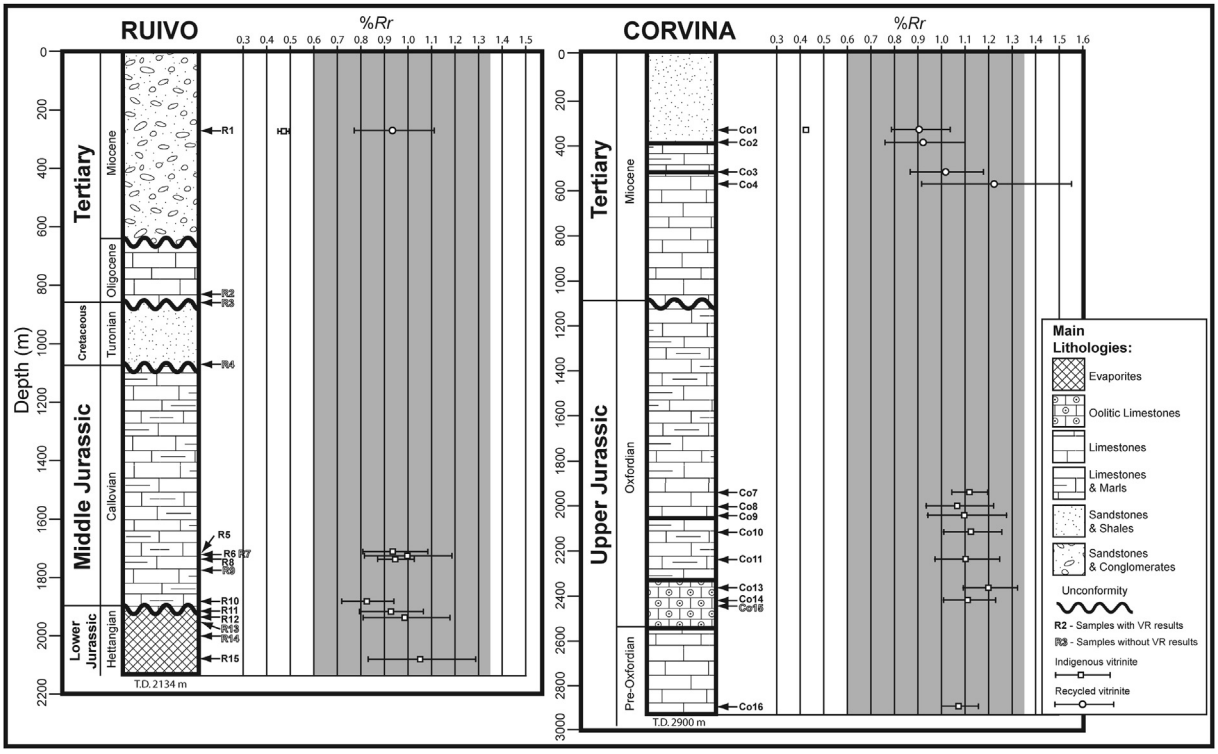

Figure 3. Lithological logs of the offshore wells Ruivo and Corvina with sample position and VR values with respective standard deviations (horizontal bars). Shaded area is the oil window *sensu* Peters and Cassa (1994).

1909 to 2134 m, consists of evaporites (halite and gypsum) with intercalated minor mudstones beds. By lithostratigraphic correlation with the succession in the onshore Algarve Basin, this interval is attributed to the Lower Jurassic (Hettangian).

2.2.2. Corvina

The Corvina well reached a depth of *ca.* 2900 m (Fig. 3). The top 1100 m consists of limestones, siltstones and mudstones assigned to the Miocene–Oligocene. The interval between 1100 and *ca.* 2700 m comprises a thick succession of limestones, marls and dolomites attributed to the Lower Cretaceous and Upper Jurassic on the basis of calcareous nanofossils and foraminifera (Challenger, 1976). Our palynological data from this well interval partially contradict this age determination (see Palynological results). The interval from 2700 m to T.D. consists mainly of limestones lacking any stratigraphically-useful fossils.

2.3. Stratigraphic correlation across the Algarve Basin

From the Lower Jurassic to the Lower Cretaceous, one of the main features of the onshore Algarve Basin was its division into small sub-basins by synsedimentary faults (Manuppella, 1988; Manuppella et al., 1988). One of the main consequences of this partitioning was differing subsidence rates in the sub-basins. The lateral correlation of the Mesozoic Series across the onshore Algarve Basin and its tentative correlation with the two offshore wells studied (Ruivo and Corvina) are summarised in Figure 4. The key measured section for the Western Sub-Basin in the Sagres–Lagos area attains a maximum thickness of *ca.* 1200 m, whereas a maximum thickness of *ca.* 3500 m was measured in the Faro area in the Eastern Sub-Basin. The greater thickness in the latter is mainly due to its thick Upper Jurassic to Lower Cretaceous succession, which is more attenuated in the other two areas that characterize the Eastern Sub-Basin (Albufeira and Tavira), and in the Western Sub-Basin, where subsidence rates were more constant throughout the Mesozoic.

The stratigraphy of offshore Algarve Basin revealed by the wells Ruivo and Corvina shows more hiatuses when compared with the onshore part of the Algarve Basin (Fig. 4), precluding age and lithological correlation of the stratigraphic units between the two parts of the basin. However, it is clear from analysis of the two wells that major unconformities are present in the offshore which are not observed in the onshore succession of the basin. In well Ruivo, the bulk of the Jurassic succession is of Callovian age (see Palynological results section). The basal beds were intruded in places by Hettangian evaporites (possibly a major diapir structure), and the upper part is unconformably overlain by Upper Cretaceous sandstones. In the offshore well Corvina, a very thick Upper Jurassic (Oxfordian) succession of over 1000 m was penetrated (see Palynological results section), which is unconformably overlain by, an equally thick (*ca.* 1000 m) succession consisting of limestones, sandstones and mudstones of Miocene age. Exceptionally thick Upper Jurassic and Miocene successions such as those observed in the well Corvina, are unknown either in the onshore part of the basin or in the well Ruivo.

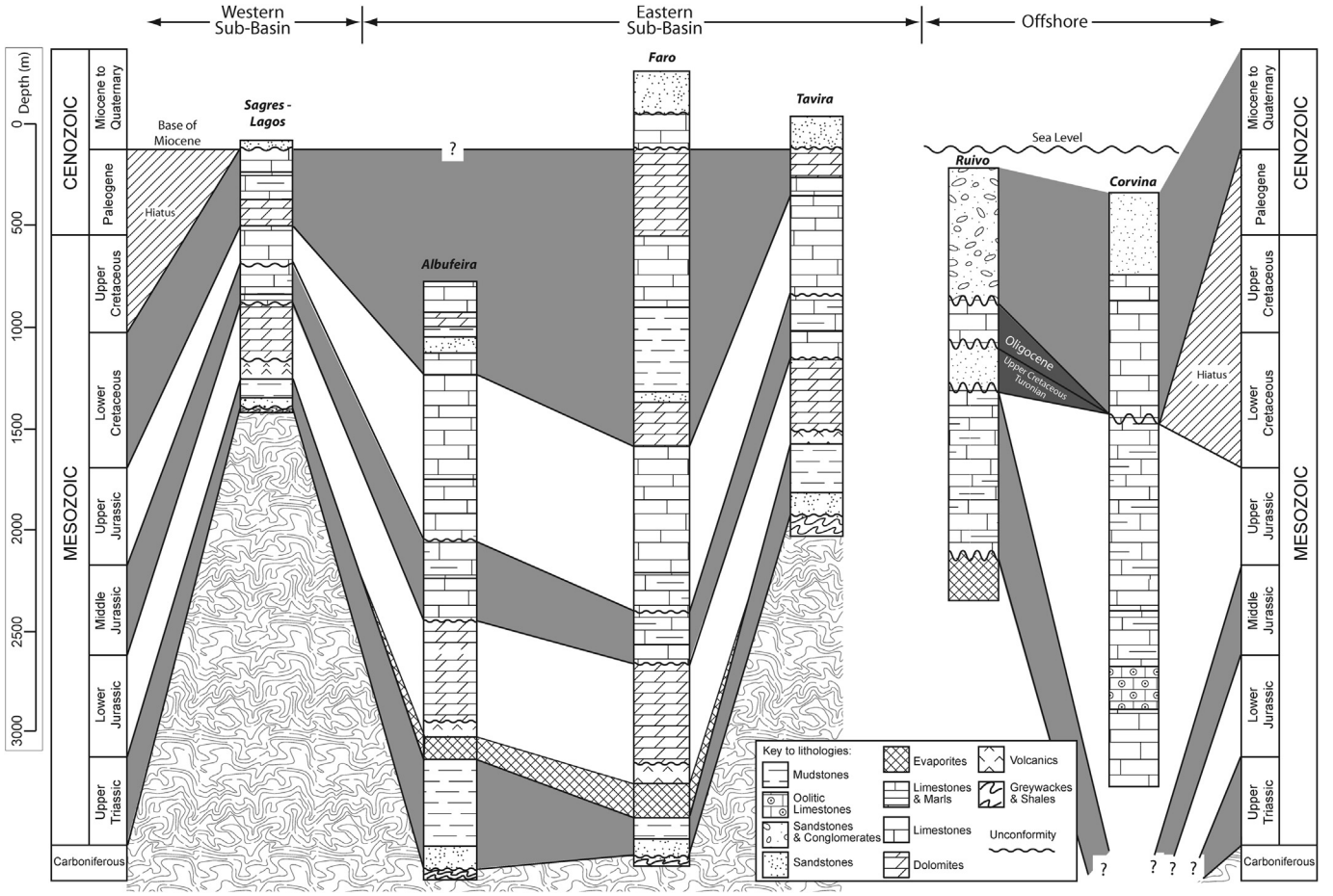

Figure 4. Lateral correlation of the measured stratigraphic sections in the Western (Sagres–Lagos) and Eastern Sub-Basins (Albufeira, Faro and Tavira) of the Algarve Basin and the offshore wells Ruivo and Corvina (adapted from Manuppella, 1988). Datum for the onshore sections is the base of the Miocene and for the offshore wells is the sea level (Ruivo well 91 m water depth and Corvina well 189 m water depth).

3. Materials and methods

VR was determined from 178 samples in order to determine the regional maturity and to elucidate the thermal evolution of the Algarve Basin (Tables 1 and 2). The samples analysed in this study were obtained from various sources: outcrops, two groundwater exploration boreholes (NR and JK), the Loulé Salt Mine, and two offshore hydrocarbon exploration wells (Ruivo and Corvina) (Figs. 1 and 3). Figures 5a, 6a, 7a and 8a show the geographical distribution of the outcrop samples analysed. The lithologies used were grey to dark grey marls, non-calcareous mudstones, siltstones and clay-rich evaporites. Two thin coal lenses in the late Jurassic Peral Limestones and Marls at Cerro da Rocha (Table 1, sample 112) and in the early Cretaceous Mudstones and Sandstones (*Weald Facies*) near Tunes (Table 1, sample 59) were also sampled.

Not all stratigraphic intervals in the Algarve Basin contain lithologies that are suitable for maturation studies. The Upper Triassic to Lower Jurassic (Hettangian) red beds are generally poor in organic matter and maturation results from this stratigraphic interval are confined to a few mudstone beds above the Silves Sandstones and clay-rich evaporites in the Loulé and Albufeira diapirs (Figs. 1 and 2). Pliensbachian to Toarcian maturation results are confined to the Sagres area in the Western Sub-Basin (Fig. 2). In the Eastern Sub-Basin this stratigraphic interval is dominated by dolomitised limestones of the Picavessa and Boavista Dolomites (Fig. 2), which proved to be barren. The majority of data from the Middle Jurassic is from the Callovian marl–limestone successions which are widespread in the Algarve Basin (Praia da Mareta Marls and Telheiro Marls) (Fig. 2). Most of the Upper Jurassic maturation results are from the marl–limestone successions that straddle the Oxfordian–Kimmeridgian boundary in the central Algarve (Peral Limestones and Marls) (Fig. 2). Lower Cretaceous maturation results were recorded essentially from Berriasian to Barremian shallow marine to continental deposits and from the widespread Aptian to Albian lagoon-nearshore to shallow continental shelf sedimentary facies of the Luz Mudstones and Porto de Mós Limestones and Marls (Fig. 2).

The Ruivo and Corvina wells were drilled for hydrocarbon exploration in the offshore part of the Algarve Basin by Chevron and Challenger in 1975 and 1976 respectively. The stratigraphic position of the samples analysed in the wells and the maturation results are shown in Figure 3 and Table 2, respectively. The cuttings sampled were marls, mudstones and siltstones. It was not possible to sample the two wells systematically due to the lack of preserved material through large intervals and to a lesser extent, to the presence of unsuitable lithologies (crystalline limestones). The lithological and biostratigraphic information provided here is from unpublished reports (Chevron, 1975; Challenger, 1976) and from palynological investigations completed during this study.

3.1. Extraction techniques and methods of study

Organic residues were extracted from the rock samples and cuttings using standard cold hydrochloric (HCl) and hydrofluoric acid (HF) techniques. The organic residues used for the maturation studies were then mounted and polished using a method adapted from that described by Hillier and Marshall (1988). Part of the organic residue extracted from the samples was also mounted on slides for spore fluorescence and spore colour determination. Part of the organic residues from the Ruivo and Corvina well samples was also mounted for palynology.

Mean random vitrinite reflectance (%R_r) was the vitrinite reflectance (VR) parameter chosen for maturation assessment of the Algarve Basin because the mounting technique used provides non-oriented vitrinite particles and also because %R_r is the most widely used organic maturation parameter in the oil industry and is readily correlated with other maturity parameters. VR measurements on all of the samples were made in the University of the Algarve using an Olympus BX 51 microscope with a 50× oil-immersion objective lens and equipped with a black and white digital camera. The black and white (8-bit) digital images of vitrinite particles were analysed using a graphical tool, named VITRINITE, that runs within the Mirone Suite (Luis, 2007) and calibrates the scale of 256 grey levels with standards of known reflectivity (Fernandes et al., 2010). The reflectance values of the standards used in this study were: 0.428%, 0.595%, 1.715%, 3.15% and 5.37%. VR was measured in incident light with a wavelength of 546 nm and immersion oil with a refractive index of 1.518 at 20 °C room temperature.

When possible, 100 random reflectances were measured across the slides and their arithmetic mean and standard deviation were calculated (Tables 1 and 2). The arithmetic mean was considered to be the true R_r for the sample. The accuracy of vitrinite reflectance measurements depends on the precision of the reflectance microscope and the number of grains measured. Mackowsky (1982) regarded 100 measurements as a statistically valid size for a population and noted that 900 measurements would be required to give three times the accuracy. McCormack (1998) concluded that only 97 measurements are necessary for each sample to have a precision of 0.1% with a 95% confidence interval with a standard deviation of 0.5%R_r. If the number of measurements decreases to 30, the same confidence interval and standard deviation implies a precision of 0.18%. Therefore, the minimum number of VR measurements regarded as statically valid in this study was 30. Not all samples were rich in indigenous vitrinite and in some cases, the reflectance of fewer than 30 particles was measured. However, most of these relatively vitrinite poor samples belonged to stratigraphic intervals that also included samples with VR measurements based on more than 30 particles. In these cases and in order to have a VR value characteristic of the stratigraphic sections, the VR values measured from all samples of the same stratigraphic sections were combined. In section 6. Organic maturation results, the statistical procedures that were used in the treatment of VR results from the same stratigraphic units are described. Tables 1 and 2 show all organic maturation results, both measured and statistically treated. Figure 9 shows representative VR histograms for the different stratigraphic units onshore and in the offshore wells. The analysis of the VR results shown in some of the histograms is discussed in the following sections.

Fluorescence microscopy is used to differentiate source rocks from non-source rocks and to estimate the level of maturation from fluorescence colours and spectra (Van Gijzel, 1967, 1971, 1975, 1979; McPhilemy, 1988). Organic maturation causes a gradual shift in fluorescence colours (red shift) from the shorter to the longer wavelengths, that is, blue and green to yellow, orange and finally red. Of all the sub-macerals of the liptinite–exinite group, sporinite is the one that shows the most consistent changes in fluorescence colour spectra and intensity with increasing organic maturation. Under fluorescence excitation, it changes colour from green through yellow to orange and finally red, with increasing maturity to the top of the oil-window, after which is no longer fluoresces. Despite some differences in fluorescence colours and intensity for different spore taxa, spore fluorescence is an important parameter of organic maturation for low-rank material.

For this study, qualitative spore fluorescence colour analyses of the samples were completed in the Department of Geology, Trinity College Dublin using a Leitz Dialux 20 microscope with Ploemopak 2.4 incident fluorescent tube with a violet and blue +12 filter block, giving a wavelength band of 390–490 nm. This system was allowed to stabilize for 30 min prior to any observation of the fluorescence properties of the samples.

Table 1
Organic maturation results and calculated palaeotemperatures (°C) (calculated using method described by Barker, 1988) for the onshore samples of the Algarve Basin. All samples are marls or mudstones with the exception of samples 59 and 112, which are thin coal lenses. R_r(%), vitrinite reflectance values, SD, standard deviation, *n*, number of vitrinite particles measured, med., medium VR value for the selected stratigraphic units, std., standard deviation for the selected stratigraphic units, Fluo., spore fluorescence colour (B – blue, G – green, Y – yellow, DY – dark yellow, O – orange, DO – dark orange and R – red) and spore colour, TAI (Thermal Alteration Index).

Sample	R_r (%)	SD	*n*	Fluo.	TAI	Med.	Std.	Lithostratigraphy	Age	Palaeotemp.*	Lat. (N)			Long. (W)		
											°	′		°	′	
Sagres–Lagos																
1	0.52	0.04	57	Y	2–/2	0.58	0.1	Porto de Mós	Albian	80.0	37	6	20.3	8	41	47.2
2	0.68	0.1	39	Y	2			Limestones & Marls		107.9	37	5	8.3	8	41	31.8
3	0.58	0.09	19	Y	2					91.3	37	5	8.3	8	41	31.8
4	1.01	0.06	71	–	–	1.03	0.17	Praia da Luz Marls	Aptian	149.0	37	5	8.1	8	43	6.4
5	1.02	0.22	83	DO	3–/3					150.1	37	5	8.1	8	43	6.4
6	0.98	0.15	83	DO	3–/3					145.9	37	5	8.1	8	43	6.4
7	1.04	0.18	41	DO	3–/3					152.1	37	5	8.1	8	43	6.4
8	0.94	0.1	16	DO	3–/3					141.6	37	5	8.1	8	41	6.4
9	1.11	0.17	86	DO	3–/3					158.9	37	5	8.1	8	41	6.4
10	1.24	0.32	9	DY	2+/3–	1.31	0.32	Porto de Mós	Albian	170.4	37	5	7.0	8	42	54.2
11	1.21	0.17	28	DY	2+/3–			Limestones & Marls		167.8	37	5	7.0	8	42	54.2
12	1.1	0.22	54	DY	2+/3–					157.9	37	5	7.0	8	42	54.2
13	1.12	0.17	28	DY	2+/3–					159.8	37	5	7.0	8	42	54.2
14	1.68	0.15	54	–	4–/4					202.0	37	5	7.0	8	42	54.2
15	0.7	0.05	52	–	–	0.66	0.1	Almádena Limestones	Berriasian	110.9	37	3	47.1	8	47	28.9
16	0.62	0.13	37	–	–					98.3	37	3	47.1	8	47	28.9
17	0.61	0.02	22	DY	2/2+					96.6	37	3	47.1	8	47	28.9
18	0.75	0.12	11	DY	2+					118.1	37	3	47.1	8	47	28.9
19	0.88	0.1	100	DY/O	3–	0.88	0.1	Três Angras Marls	Early Kimmeridgian	134.7	37	11	16.7	8	54	35.1
20	0.82	0.1	72	–	–	0.81	0.1	Praia do Tonel Limestones	Mid Oxfordian	127.4	37	2	22.1	8	53	42.4
21	0.8	0.09	81	–	–					124.8	37	2	22.1	8	53	42.4
22	0.8	0.11	90	–	–					124.8	37	2	22.1	8	53	42.4
23	0.76	0.13	59	–	–	0.89	0.18	Praia da Mareta Marls	Callovian	119.5	37	0	20.3	8	56	22.1
24	1	0.12	70	DY/O	2+/3–					148.0	37	0	20.3	8	56	22.1
25	1.01	0.12	42	O	2+/3–					149.0	37	0	20.3	8	56	22.1
26	0.98	0.09	32	–	–					145.9	37	0	20.3	8	56	22.1
27	1.06	0.1	77	O	2+/3–					154.1	37	0	20.3	8	56	22.1
28	0.93	0.15	16	–	–					140.5	37	0	20.3	8	56	22.1
29	1.01	0.11	31	–	–					149.0	37	0	30.3	8	55	36.7
30	0.91	0.12	49	O	2+/3–					138.2	37	0	30.3	8	55	36.7
31	1.06	0.12	34	DY/O	2+					154.1	37	0	30.3	8	55	36.7
32	0.73	0.08	95	DY/O	2+					115.3	37	0	30.3	8	55	36.7
33	0.99	0.15	84	O	2+/3–					147.0	37	0	30.3	8	55	36.7
34	0.76	0.12	38	–	–					119.5	37	0	30.3	8	55	36.7
35	0.7	0.07	59	–	–					110.9	37	0	30.3	8	55	36.7
36	0.69	0.1	74	–	–					109.4	37	0	30.3	8	55	36.7
37	0.72	0.11	24	–	–					113.8	37	0	30.3	8	55	36.7
38	1.05	0.15	26	O	2+/3–					153.1	37	0	30.3	8	55	36.7
39	0.86	0.18	32	DY/O	2+					132.3	37	0	29.0	8	56	55.4
40	0.88	0.11	25	DY/O	2+					134.7	37	0	29.0	8	56	55.4
41	1.09	0.12	16	DY/O	2+					157.0	37	0	29.0	8	56	55.4
42	0.89	0.2	21	DY/O	2+					135.9	37	0	29.0	8	56	55.4
43	1.04	0.12	55	O	3–	0.96	0.15	Praia da Mareta	Bathonian	152.1	37	0	20.3	8	56	22.1
44	0.87	0.11	82	–	–			Limestones with *Zoophycus*		133.5	37	0	20.3	8	56	22.1
45	1.03	0.12	26	–	–					151.1	37	0	20.3	8	56	22.1
46	0.96	0.15	92	O	3–					143.8	37	0	20.3	8	56	22.1
47	0.99	0.17	59	O	3–	0.99	0.17	Armação Nova Marls	Toarcian	147.0	37	1	48.9	8	59	15.4
48	0.95	0.17	44	–	–	0.95	0.17	Cape St. Vincent Dolomites	Pliensbachian	142.7	37	1	29.5	8	59	35.9
49	1.12	0.19	39	O	3–/3	1.07	0.2	Silves Mudstones –	Late Triassic	159.8	37	9	40.1	8	54	21.3
50	0.99	0.18	26	O	3–/3			Siltstones & Dolomites		147.0	37	9	40.1	8	54	21.3
Albufeira																
51	0.58	0.07	48	–	–	0.60	0.08	Praia da Luz Marls	Aptian	91.3	37	8	17.5	8	24	21.2
52	0.65	0.08	16	–	–					103.2	37	8	17.5	8	24	21.2
53	0.63	0.06	49	–	–	0.58	0.08	Mudstones &	Barremian	99.9	37	9	8.45	8	18	7.0
54	0.55	0.05	100	–	–			Sandstones – *Weald Facies*		85.8	37	9	8.45	8	18	7.0
55	0.6	0.1	95	Y	2+					94.9	37	9	50.7	8	13	38.8
56	0.64	0.04	24	–	–					101.6	37	9	50.7	8	13	38.8
57	0.6	0.08	33	–	–					94.9	37	9	50.7	8	13	38.8
58	0.66	0.1	18		–					104.8	37	9	53.8	8	14	53.2
59	0.57	0.03	5	–	–					89.5	37	9	53.8	8	14	53.2
60	0.53	0.06	29	–	–					82.0	37	9	43.9	8	15	5.5
61	0.56	0.08	81	Y	2+					87.7	37	9	53.8	8	14	53.2
62	0.78	0.11	8	Y	2+/2	0.65	0.09	Almádena Limestones	Berriasian	122.2	37	4	36.3	8	16	35.3
63	0.61	0.05	14	Y	2+/2					96.6	37	4	36.3	8	16	35.3
64	0.6	0.08	39	Y	2+/2					94.9	37	4	36.3	8	16	35.3
65	0.68	0.06	43	–	–					107.9	37	7	16.4	8	13	26.5

Table 1 (*continued*)

Sample	R_r (%)	SD	*n*	Fluo.	TAI	Med.	Std.	Lithostratigraphy	Age	Palaeotemp.*	Lat. (N)			Long. (W)		
											°		′	°		′
66	0.77	0.09	100	–	–	0.80	0.11	Escarpão Limestones	Kimmeridgian/Tithonian	120.8	37	10	12.2	8	15	18.3
67	0.83	0.11	100	–	–					128.6	37	10	12.2	8	15	18.3
68	0.88	0.08	97	–	–					134.7	37	10	12.2	8	15	18.3
69	0.78	0.07	85	–	–					122.2	37	8	15	8	23	5.3
70	0.81	0.1	90	–	–					126.1	37	8	15	8	23	5.3
71	0.65	0.13	23	–	–					103.2	37	8	15	8	23	5.3
72	0.67	0.05	33	–	–					106.4	37	8	15	8	23	5.3
73	0.71	0.09	71	–	–	0.79	0.11	Peral Limestones & Marls	Oxfordian/Kimmeridgian	112.4	37	5	43	8	15	19.8
74	0.74	0.07	98	–	–					116.7	37	5	50.8	8	15	22.3
75	0.88	0.1	30	O	2+					134.7	37	8	19.7	8	11	21.9
76	0.86	0.09	100	–	–					132.3	37	8	26.4	8	11	22.0
77	1.15	0.15	67	O	3–	1.15	0.15	Albufeira Diapir – Evaporites	Hettangian	162.5	37	4	58.2	8	15	44.7
78	0.94	0.15	67	O	3–	1.00	0.15	Silves Mudstones –	Late Triassic	141.6	37	15	25.5	8	18	24.3
79	1.12	0.1	75	–	–			Siltstones & Dolomites		159.8	37	15	38.4	8	19	11.5
80	0.95	0.09	70	–	–					142.7	37	15	14.7	8	20	25.6
81	0.96	0.15	100	DO	3–					143.8	37	15	14.7	8	20	25.6
82	1.03	0.14	53	DO	3–					151.1	37	15	14.7	8	20	25.6
Faro																
83	0.69	0.03	57	–	–	0.69	0.04	Ferradeira Marls	Cenomanian	109.4	37	4	28	7	58	50.6
84	0.69	0.03	43	–	–					109.4	37	4	28	7	58	50.6
85	0.69	0.08	25	–	–					109.4	37	4	28	7	58	50.6
JK1	0.69	0.08	44	BY/Y	2/2+	0.69	0.08	Almádena Limestones	Berriasian	109.4	37	6	27.8	7	55	4.35
86	0.76	0.08	58	–	–	0.78	0.17	Fontaínhas Limestones with	Tithonian	119.5	37	6	1.23	7	49	47.8
87	0.76	0.11	87	2–/2	Y			*Anchispirocyclina Lusitanica*		119.5	37	5	56.3	7	50	54.9
88	0.67	0.08	77	–	–					106.4	37	6	5.99	7	50	53.2
89	0.67	0.13	68	Y	2–/2					106.4	37	6	5.99	7	50	53.2
90	0.61	0.12	73	–	–					96.6	37	5	52.7	7	50	5.0
91	0.94	0.13	68	–	–					141.6	37	5	52.7	7	50	5.0
92	0.68	0.09	33	–	–					107.9	37	5	52.7	7	50	5.0
93	0.75	0.09	46	–	–					118.1	37	5	52.7	7	50	5.0
94	0.75	0.11	50	–	–					118.1	37	5	52.7	7	50	5.0
95	0.89	0.16	38	–	–					135.9	37	5	52.7	7	50	5.0
96	0.9	0.18	100	O	3–					137.0	37	10	34.8	8	4	48.4
97	0.91	0.15	86	O	2+/3–					138.2	37	10	34.8	8	4	48.4
98	0.72	0.06	57	–	–	0.81	0.13	Escarpão Limestones	Oxfordian/Kimmeridgian	113.8	37	6	7.71	7	48	38.1
99	0.89	0.15	52	DY/O	2+/3–					135.9	37	9	0.96	8	7	20.2
100	0.87	0.16	66	DY/O	2+/3–					133.5	37	9	0.96	8	7	20.2
101	0.99	0.13	40	DY	2+/3–					147.0	37	9	7.4	8	6	57.4
102	0.84	0.16	62	DY/O	2+/3–					129.9	37	9	7.4	8	6	57.4
103	0.89	0.14	54	DY	2+/3–					135.9	37	9	7.4	8	6	57.4
104	0.97	0.11	70	O	2+/3–					144.8	37	9	7.4	8	6	57.4
105	0.97	0.17	89	DY/O	2+/3–					144.8	37	9	7.4	8	6	57.4
106	0.68	0.07	33	–	–					107.9	37	8	57.5	8	7	11.8
107	0.79	0.19	38	DY	2+					123.5	37	9	0.76	8	7	9.6
108	0.79	0.13	62	DY	2+					123.5	37	7	50.5	7	54	38.0
109	0.86	0.08	65	DY	2+					132.3	37	7	50.5	7	54	38.0
110	0.86	0.08	24	DY	2+					132.3	37	8	0	7	54	38.0
111	0.84	0.15	31	DY	2+					129.9	37	8	17.4	7	54	36.5
112	0.74	0.05	30	–	–			Peral Limestones & Marls		116.7	37	8	14.3	7	51	48.8
113	0.8	0.11	44	DY/O	2+/3–					124.8	37	8	14.3	7	51	48.8
114	0.82	0.1	77	DY/O	2+/3–					127.4	37	8	14.3	7	51	48.8
115	0.7	0.1	43	DY/O	2+/3–					110.9	37	8	14.3	7	51	48.8
116	0.84	0.11	35	DY/O	2+/3–					129.9	37	8	14.3	7	51	48.8
117	0.77	0.08	63	DY/O	2+/3–					120.8	37	8	14.3	7	51	48.8
118	0.71	0.11	100	DY/O	2+/3–					112.4	37	8	14.3	7	51	48.8
119	0.81	0.09	87	O	3–/3					126.1	37	7	50	7	52	30.0
120	0.81	0.11	77	O	3–					126.1	37	8	7.35	7	52	7.2
121	0.8	0.09	77	O	3–					124.8	37	7	50	7	52	30.0
122	0.79	0.1	73	DY	2+					123.5	37	8	18.6	7	59	48.4
123	0.79	0.09	88	–	–			Peral Limestones &l Marls	Oxfordian	123.5	37	6	11.5	7	49	42.7
124	0.81	0.09	95	–	–					126.1	37	6	11.5	7	49	42.7
125	0.83	0.09	100	O	2+/3					128.6	37	6	11.5	7	49	42.7
126	0.72	0.08	78	–	–					113.8	37	6	23.8	7	50	52.3
127	0.72	0.11	78	–	–					113.8	37	5	45.5	7	54	55.9
128	0.74	0.08	51	–	–					116.7	37	5	45.5	7	54	55.9
129	0.81	0.06	30	O	3–					126.1	37	5	45.5	7	54	55.9
130	0.75	0.08	78	–	–					118.1	37	5	45.5	7	54	55.9
131	0.84	0.08	20	–	–					129.9	37	5	45.5	7	54	55.9
132	0.77	0.09	100	O	3–					120.8	37	5	45.5	7	54	55.9
133	1.02	0.09	72	DO	3–	0.95	0.12	Telheiro Marls	Callovian	150.1	37	6	44.8	7	55	52.1
134	0.93	0.13	55	DO	3					140.5	37	6	44.8	7	55	52.1
135	0.95	0.07	21	–	–					142.7	37	6	44.8	7	55	52.1
136	0.89	0.14	50	–	–					135.9	37	6	44.8	7	55	52.1
137	0.93	0.11	81	DO	3–					140.5	37	6	44.8	7	55	52.1

(*continued on next page*)

Table 1 (*continued*)

Sample	R_r (%)	SD	*n*	Fluo.	TAI	Med.	Std.	Lithostratigraphy	Age	Palaeotemp.*	Lat. (N)			Long. (W)		
											°	′		°	′	
138	1.03	0.16	86	O	3–	1.02	0.18	Loulé Diapir – Evaporites	Hettangian	151.1	37	8	8.37	8	0	18.5
139	1.14	0.17	100	O	3–					161.6	37	8	8.37	8	0	18.5
140	1.05	0.14	100	O	3–					153.1	37	8	8.37	8	0	18.5
141	1	0.17	63	O	3–					148.0	37	8	8.37	8	0	18.5
142	0.91	0.16	100	O	3–					138.2	37	8	8.37	8	0	18.5
143	0.95	0.16	86	O	3–					142.7	37	8	8.37	8	0	18.5
Tavira																
144	0.42	0.05	38	–	–	0.42	0.01	Cacela Formation	Miocene	57.8	37	9	29	7	32	37.31
145	0.85	0.08	75	–	–	0.82	0.10	Escarpão Limestones	Kimmeridgian/Tithonian	131.1	37	8	40.6	7	39	15.6
146	0.86	0.1	65	–	–					132.3	37	8	40.6	7	39	15.6
147	0.79	0.1	74	–	–					123.5	37	8	40.6	7	39	15.6
148	0.83	0.09	100	–	–					128.6	37	8	40.6	7	39	15.6
149	0.79	0.1	100	–	–					123.5	37	8	40.6	7	39	15.6
150	0.87	0.19	42	O	3–	0.85	0.16	Telheiro Marls	Callovian	133.5	37	8	22.4	7	39	25.2
151	0.79	0.1	22	O	3–					123.5	37	8	22.4	7	39	25.2
152	0.84	0.18	76	O	3–					129.9	37	8	22.4	7	39	25.2
153	0.88	0.11	45	O	3–					134.7	37	8	22.4	7	39	25.2
154	0.97	0.2	67	–	–	0.97	0.20	Silves Mudstones – Siltstones & Dolomites	Late Triassic/Hettangian	144.8	37	8	57.8	7	44	59.9
155	0.94	0.09	94	O	3–/3	0.94	0.09	Silves Mudstones – Siltstones & Dolomites	Late Triassic	141.6	37	9	2.5	7	43	59.3
NR1	1.19	0.16	21	O	3–	1.10	0.19	Silves Mudstones –	Late Triassic	166.1	37	10	9.7	7	33	51.4
NR2	1.06	0.19	42	O	3–			Siltstones & Dolomites		154.1	37	10	9.7	7	33	51.4

Suitable miospore species were subjected to 1 min of excitation, after which their fluorescence colours were recorded. The terminology used for describing fluorescent colours was: blue (B), green (G), yellow (Y), dark yellow (DY), orange (O), dark orange (DO) and red (R).

Palynologists have noted that spore colour in transmitted light changes with increasing burial depth from light to dark. They also noted, that these changes were progressive and irreversible. Using colour changes of spores and pollen, Staplin (1969, 1977, 1982) developed the Thermal Alteration Index (TAI) as a relatively simple and rapid technique for evaluating maturation levels in palynological organic residues. The colour indices in Staplin's TAI scale range from 1 to 5 and represent spore colour changes from light yellow to dark yellow, light brown, brown, dark brown and finally

Table 2
Organic maturation results and calculated palaeotemperatures (°C) (calculated using method described by Barker, 1988) for the offshore wells Ruivo and Corvina. R_r (%), vitrinite reflectance values, SD, standard deviation, *n*, number of vitrinite particles measured, Fluo., spore fluorescence colour (B – blue, G – green, Y – yellow, DY – dark yellow, O – orange, DO – dark orange and R – red) and, TAI (Thermal Alteration Index), spore colour.

Sample	Depth (m)	Indigenous vitrinite			Recycled vitrinite			Fluo. indigenous palynomorphs	Fluo. recycled palynomorphs	TAI indigenous palynomorphs	TAI recycled palynomorphs	Age	Palaeotemperature indigenous vitrinite*
		R_r (%)	SD	*n*	R_r (%)	SD	*n*						
Ruivo offshore well													
R1	269	0.47	0.01	4	0.94	0.17	72	B/G	DY/O	1/1+	2+/3–	Miocene	69.5
R2	834	–	–	–	–	–	–	B/G	DY	1/1+	2+		–
R3	854	–	–	–	–	–	–	B/G	DY	1/1+	2+		–
R5	1714	0.94	0.15	39	–	–	–	DY/O	–	2+/3–	–	Callovian	141.6
R6	1724	1	0.19	29	–	–	–	DY/O	–	2+/3–	–		148.0
R7	1729	–	–	–	–	–	–	DY/O	–	3–	–		–
R8	1734	0.95	0.08	49	–	–	–	DY/O	–	3–	–		142.7
R9	1773	–	–	–	–	–	–	DY/O	–	3–	–		–
R10	1884	0.83	0.11	87	–	–	–	O	–	3–	–		128.6
R11	1909	0.93	0.14	25	–	–	–	O	–	3	–		140.5
R12	1934	0.99	0.19	23	–	–	–	DY/O	–	3–	–	Hettangian	147.0
R13	1959	–	–	–	–	–	–	DY/O	–	3–	–		–
R14	2004	–	–	–	–	–	–	DY/O	–	3–	–		–
R15	2079	1.06	0.23	6	–	–	–	DY/O	–	3–	–		154.1
Corvina offshore well													
Co1	344	0.42	0	5	0.91	0.13	48	B/G	O	1/1+	3–/3	Miocene	57.8
Co2	399	–	–	–	0.92	0.18	65	B/G	O	1/1+	3–/3		–
Co3	527	–	–	–	1.02	0.16	87	G/Y	O	2–	3–/3		–
Co4	581	–	–	–	1.23	0.33	100	B/G	DY/O	1+	2+/3–		–
Co7	1896	1.12	0.08	46	–	–	–	DO	–	3–/3	–	Oxfordian	159.8
Co8	1946	1.07	0.15	61	–	–	–	O/DO	–	3–/3	–		155.0
Co9	2006	1.1	0.18	86	–	–	–	DY/O	–	3–	–		157.9
Co10	2046	1.13	0.13	87	–	–	–	DY/O	–	2+/3–	–		160.7
Co11	2121	1.11	0.14	95	–	–	–	DY/O	–	2+/3–	–		158.9
Co13	2306	1.2	0.12	81	–	–	–	DY/O	–	3	–		167.0
Co14	2366	1.11	0.12	91	–	–	–	DY/O	–	3	–		158.9
Co15	2421	–	–	–	–	–	–	DY/O	–	3–/3	–		–
Co16	2891	1.07	0.09	71	–	–	–	DY/O	–	3	–	Pre-Oxfordian	155.0

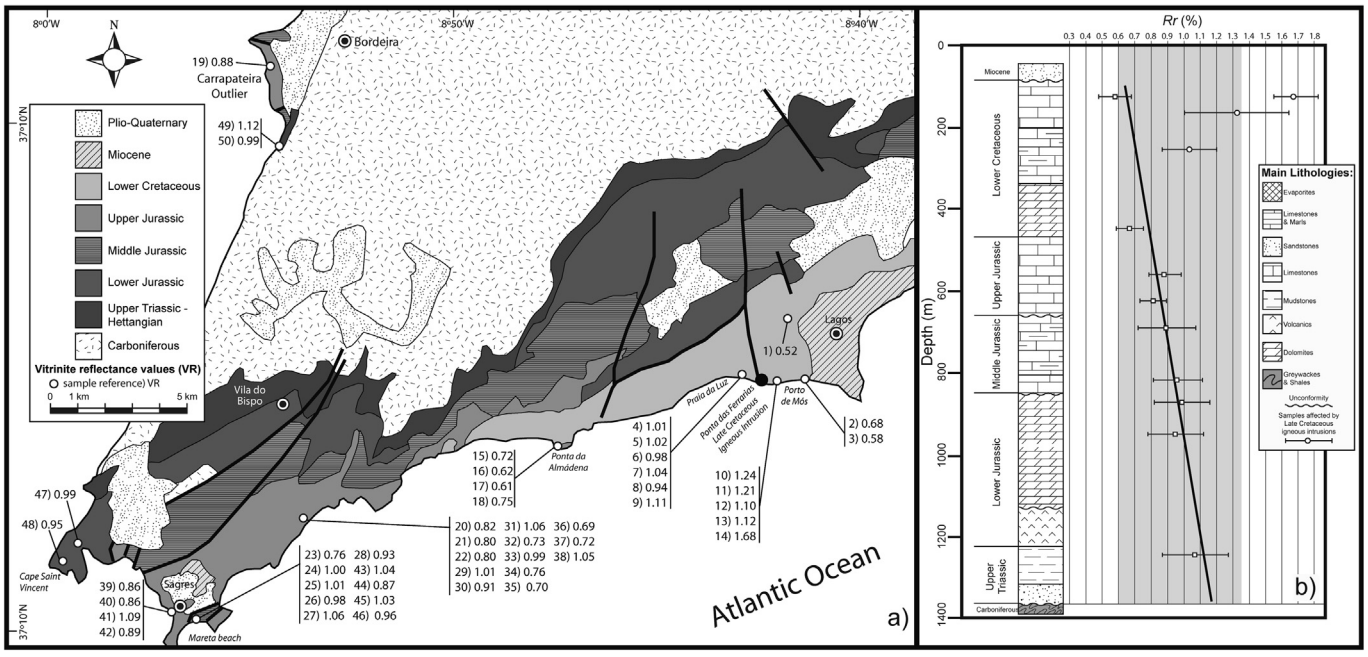

Figure 5. (a) Geology of the Sagres–Lagos area with the location of the samples and VR results, (b) VR profile (horizontal bars are the standard deviation), shaded area is the oil window *sensu* Peters and Cassa (1994).

to black. Organic residues with spores with yellow colours represent immature source rocks with regard to oil. The light browns and brown are mature; dark browns and black indicate overmature source rocks.

In this study, spore colours were recorded using the 'Phillips Petroleum Colour Standard', version no. 2 (1984), which is an adaptation of Staplin's initial TAI chart and includes more shades for the same colour index. In order to determine true spore colour for a sample, the dominant and palest spore colour was recorded and compared with the Phillips Petroleum Colour chart. The index number from this chart was then attributed to the sample. Results of TAI determinations are present together with fluorescence colours and vitrinite reflectance values for each sample (Tables 1 and 2).

Not all spore species are suitable for TAI determinations. When possible, thin walled or delicately ornamented spores were avoided. Thick walled and heavily ornamented spores were also avoided. The species best suited for TAI determinations were acamerate, azonate spores with a smooth exine of medium thickness such as *Cyathidites* spp., which occur throughout the Mesozoic

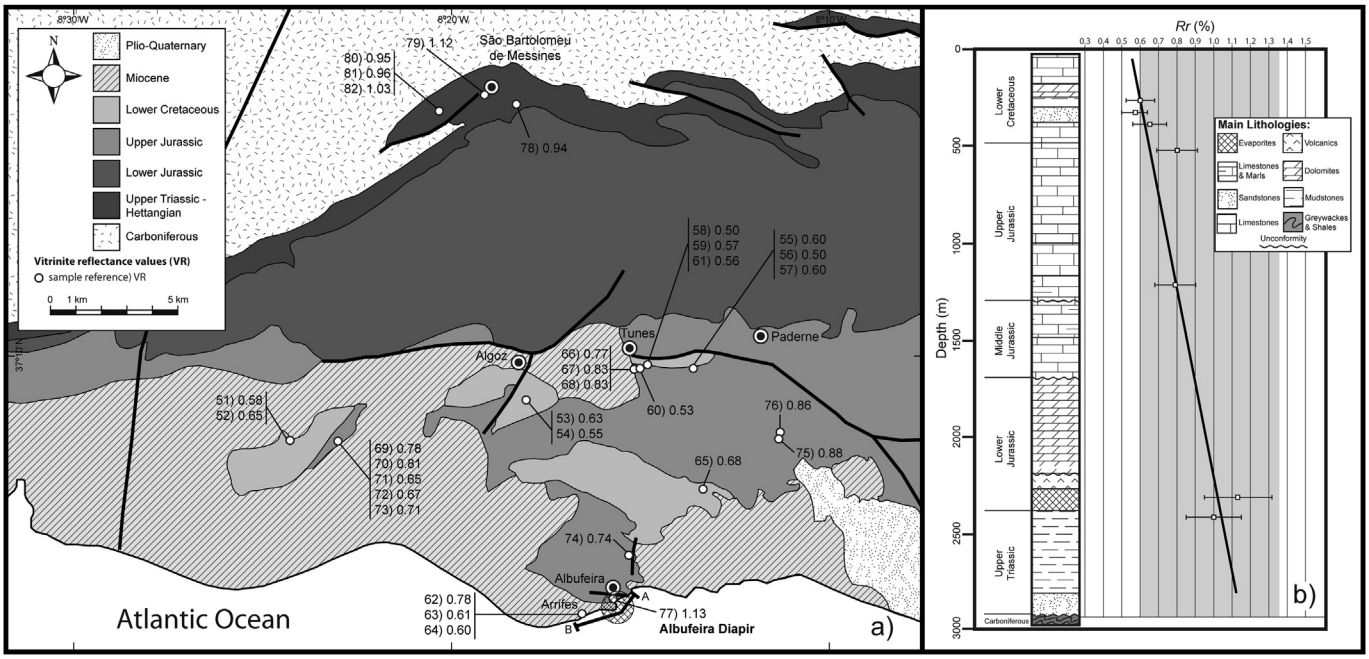

Figure 6. (a) Geology of the Albufeira area with the location of the samples and VR results, (b) VR profile (horizontal bars are the standard deviation). A and B indicates the position of the cross-section illustrated in Figure 12. Shaded area is the oil window *sensu* Peters and Cassa (1994).

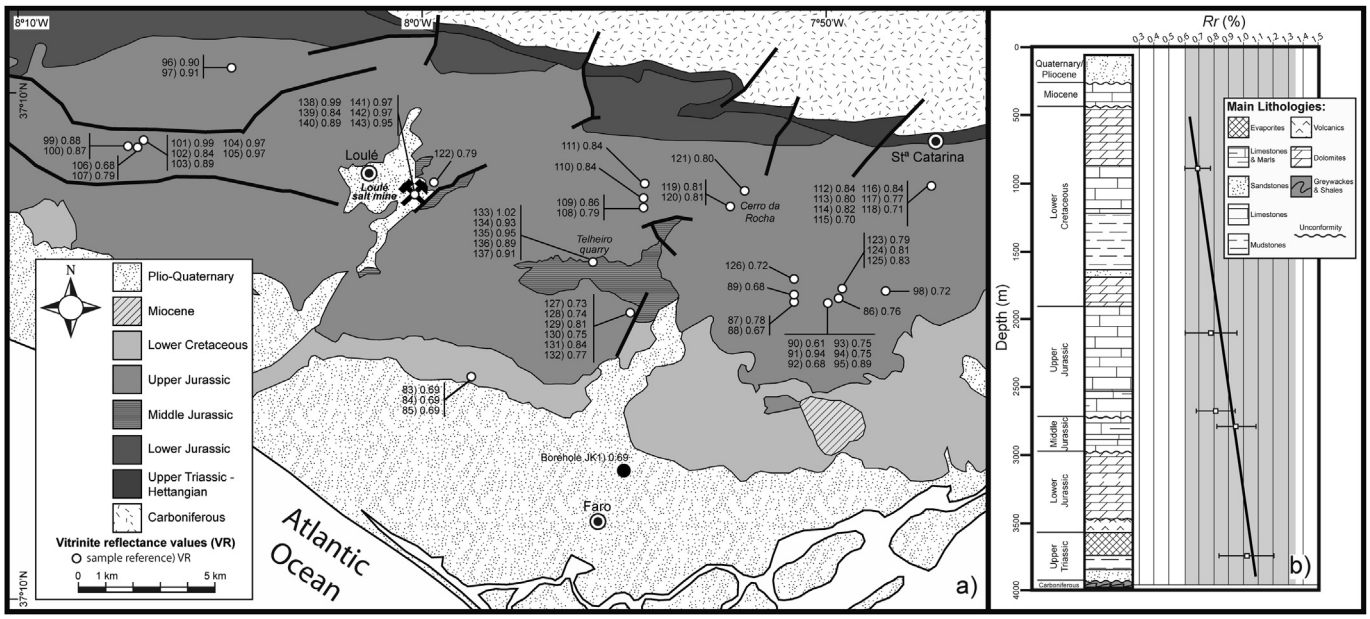

Figure 7. (a) Geology of the Faro area with the location of the samples and VR results, (b) VR profile (horizontal bars are the standard deviation), shaded area is the oil window *sensu* Peters and Cassa (1994).

succession of the Algarve Basin (Borges et al., 2011, 2012). In samples where this type of spore was absent, TAI was assessed using pollen grains of *Classopollis* spp. because of its abundance throughout the Algarve Basin succession, enabling correlation between the different sections and areas of the Algarve Basin.

4. Palynological results

4.1. Ruivo well, offshore

Samples R1 and R2 from the Miocene–Oligocene interval yielded low diversity palynomorph assemblages dominated by dinoflagellates (Table 3). As with the foraminifera and calcareous nanofossils (Chevron, 1975), the palynological assemblage recorded herein, does not give a precise age for this section.

The organic residues from the samples between 1714 and 1909 m (R5 to R11) are rich in phytoclasts, pollen and dinoflagellates that are moderately to well-preserved. The most abundant dinoflagellate taxa recorded in this interval include de genera *Ctenidodinium* and *Systematophora*. Other taxa which are consistently present include, *Compositosphaeridium polonicum* (Plate 1, a), *Gonyaulacysta jurassica* subspecies *adecta*, *Korystocysta gochtii*, *Meiourogonyaulax caytonensis* group (Plate 1, h), *Pareodinia ceratophora* (Plate 1, f), This assemblage permits samples between

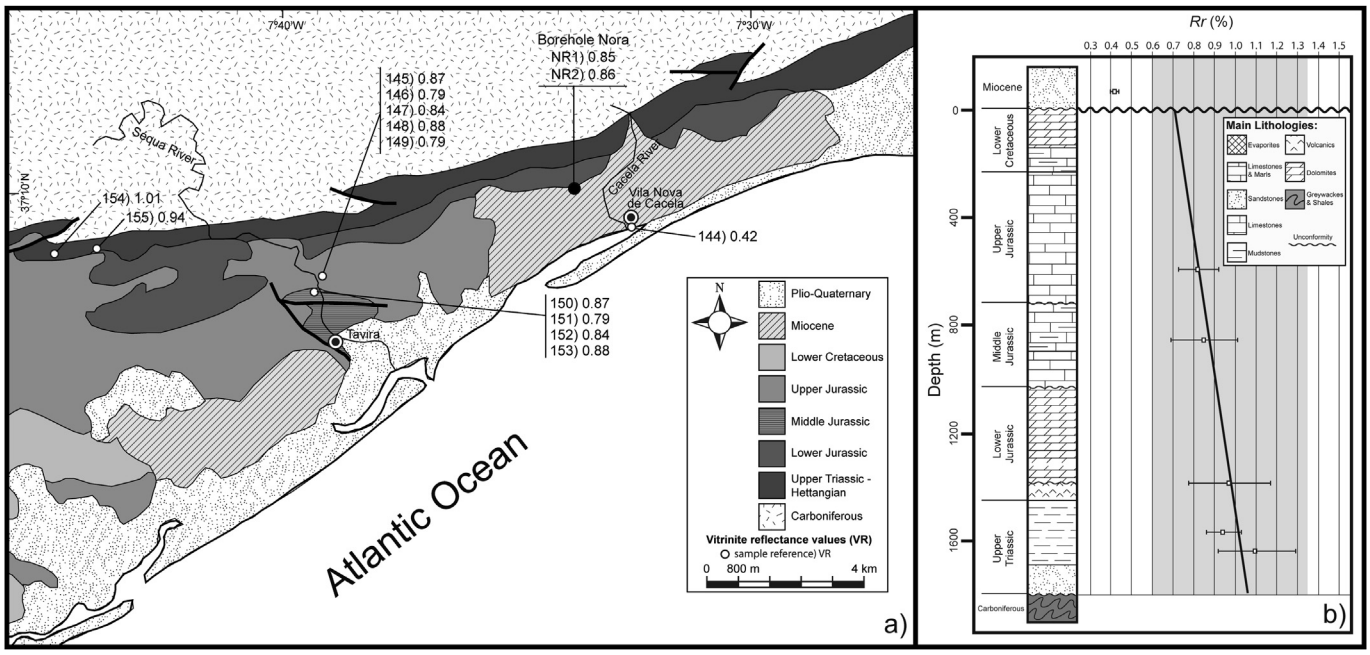

Figure 8. (a) Geology of the Tavira area with the location of the samples and VR results, (b) VR profile (horizontal bars are the standard deviation), shaded area is the oil window *sensu* Peters and Cassa (1994).

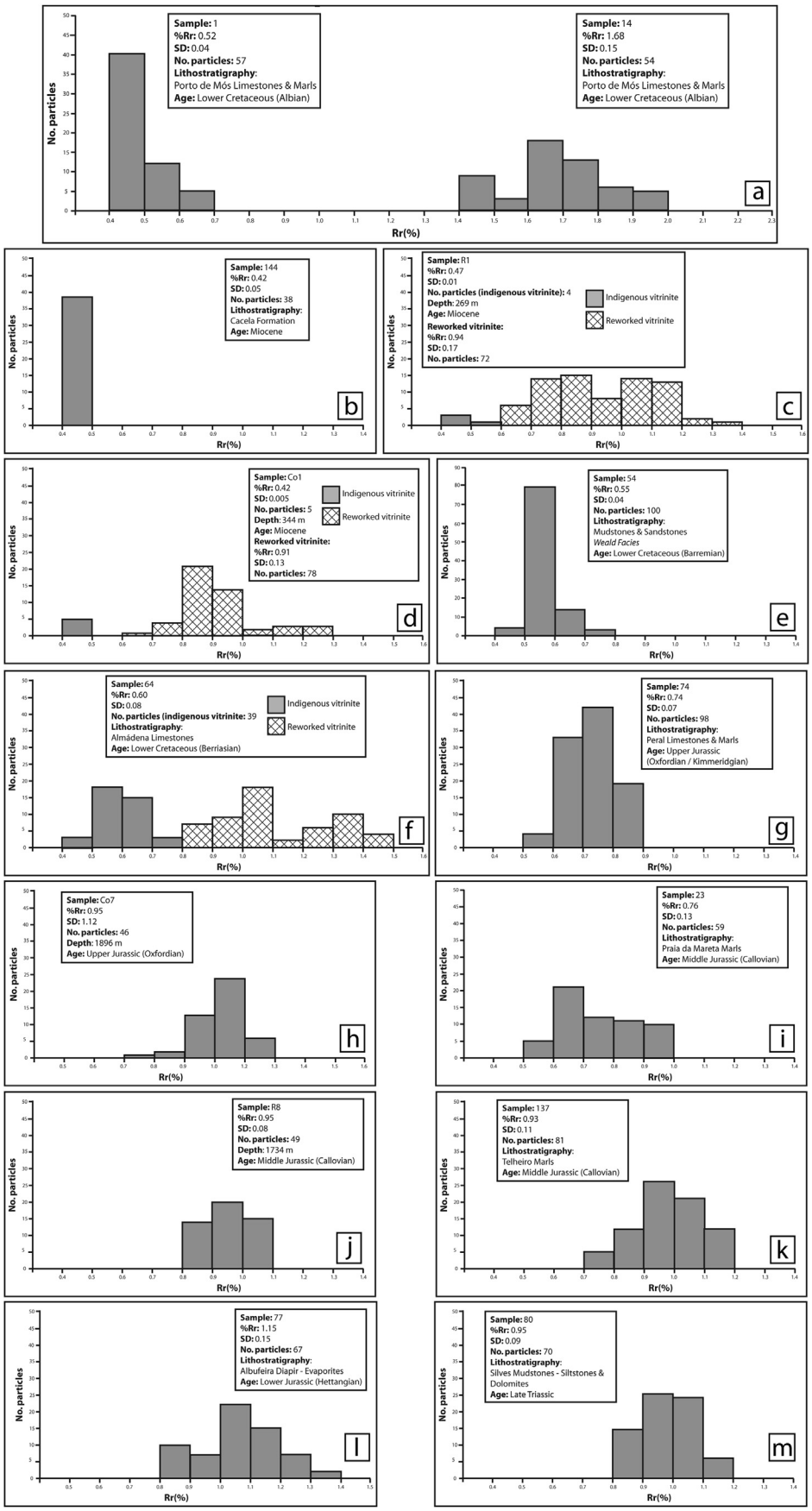

Figure 9. Selected histograms of samples from the onshore Algarve Basin and the offshore wells Ruivo and Corvina characteristic of the main stratigraphic units.

Table 3
The overall palynomorph assemblages of the offshore well Ruivo.

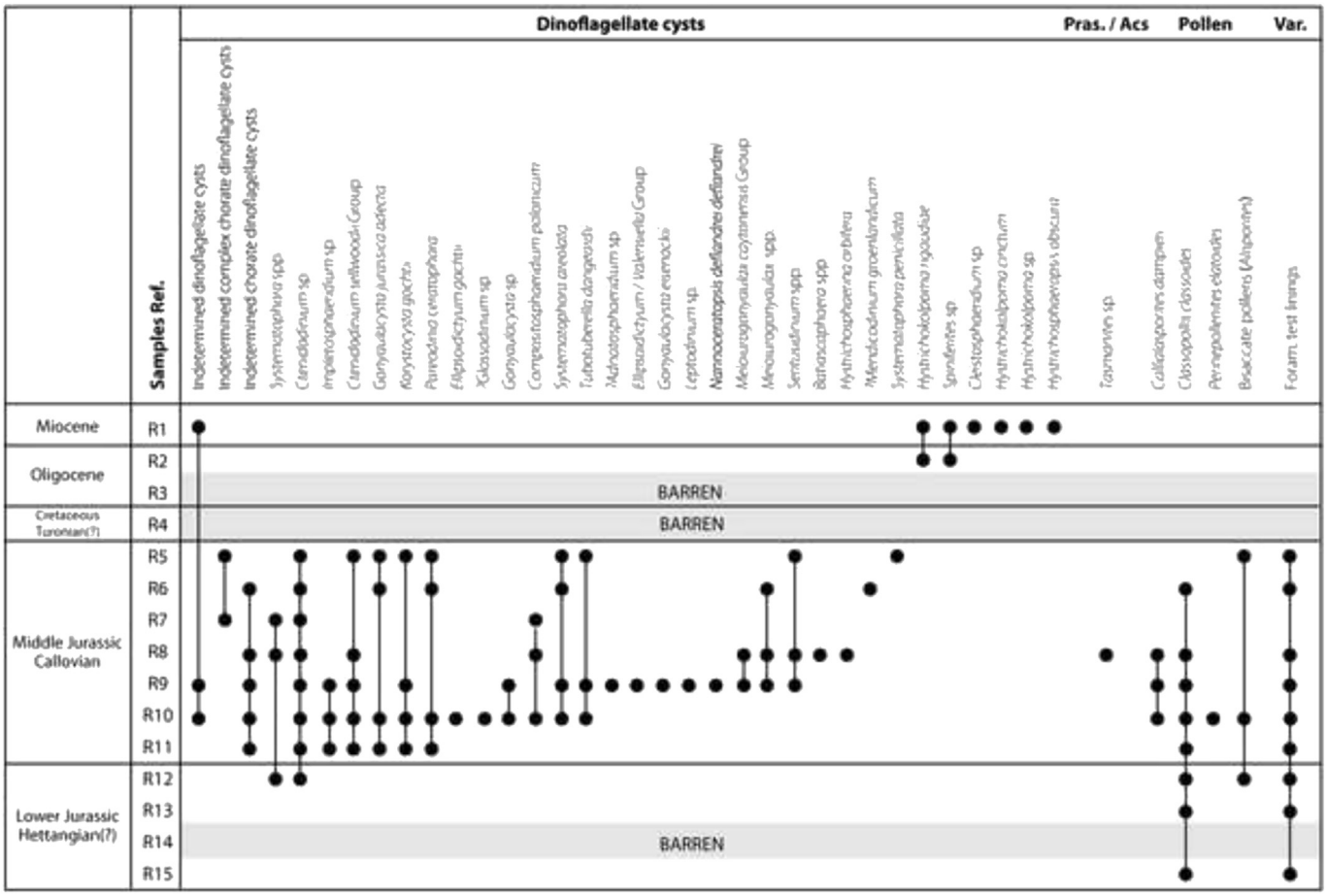

ca. 1700 and 1900 m to be assigned to the mid to late Callovian (Riding, 2005; Riding and Thomas, 1992) (Table 3). The occurrence of *Nannoceratopsis deflandrei* subspecies *deflandrei* (Plate 1, l) in sample R9 is considered reworked, since the range of this species is restricted to the late Pliensbachian–early Bajocian interval, being more common in the Toarcian–Aalenian. These data suggest exposure and erosion of Lower Jurassic rocks in parts of the Algarve Basin during the Callovian.

The four samples between 1934 and 2079 m that had been assigned to the Hettangian by means of lithological correlation were poor in palynomorphs. Long-ranging pollen such as *Classopolis classoides* and *Alisporites* spp. were the only palynomorphs recorded in this interval (Table 3).

4.2. Corvina well, offshore

In all, 16 samples were studied for palynology. The organic residues obtained were rich in phytoclasts and palynomorphs. Dinoflagellates were the most abundant palynomorphs, followed by pollen, prasynopytes, internal linings of foraminifera and acritarchs (indeterminate and *Micrhystridium* spp.).

The dinoflagellate cyst assemblage recovered from samples Co1–Co4, confirms the Miocene age for this interval that was initially provided by other microfossil groups (Challenger, 1976).

The 12 samples between 1806 m and 2891 m yielded a moderately diverse dinoflagellate cyst assemblage. The species *Endoscrinium luridum*, *Hystrichosphaerina orbifera*, *Systematophora* spp., *Gonyaulacysta jurassica* subsp. *adecta* (Plate 1, c) and *Gonyaulacysta jurassica* subsp. *jurassica* are typical of the Oxfordian. The chorate cysts *Compositosphaeridium polonicum* and *Rigaudella aemula* are good markers for the mid Callovian–mid Oxfordian interval, the latter being more common from the late Callovian onwards, and becoming extinct in mid Oxfordian times. *Ctenidodinium ornatum* (Plate 1, e) is a species that is typical of the late Callovian–mid Oxfordian interval, whereas the last occurrence of *Wanaea acollaris* (Plate 1, k) is at the boundary between the Callovian and the Oxfordian stages. Small numbers of specimens of *Stephanelytron redcliffense* (Plate 1, i) were identified in sample Co5. The occurrence of this taxon is limited to the Callovian–early Kimmeridgian. Therefore, the most likely age for the interval between 1806 and 2891 m is early to mid Oxfordian (*e.g.* Riding, 2005; Riding and Thomas, 1992) (Table 4) and not the Lower Cretaceous to Jurassic intervals as proposed in the report Challenger (1976).

5. Composition of the organic matter

This section is not a comprehensive account of the nature and composition of the organic matter in the Algarve Basin. Our goal is to describe the main trends observed in the composition of the organic matter in the basin.

Although the stratigraphic succession of the Algarve Basin records a great variety of sedimentary environments spanning a considerable time, the composition of the dispersed organic matter does not vary greatly between the different lithological units. Overall, the dispersed organic matter in the Algarve Basin is dominated by terrestrially-derived particles such as phytoclasts,

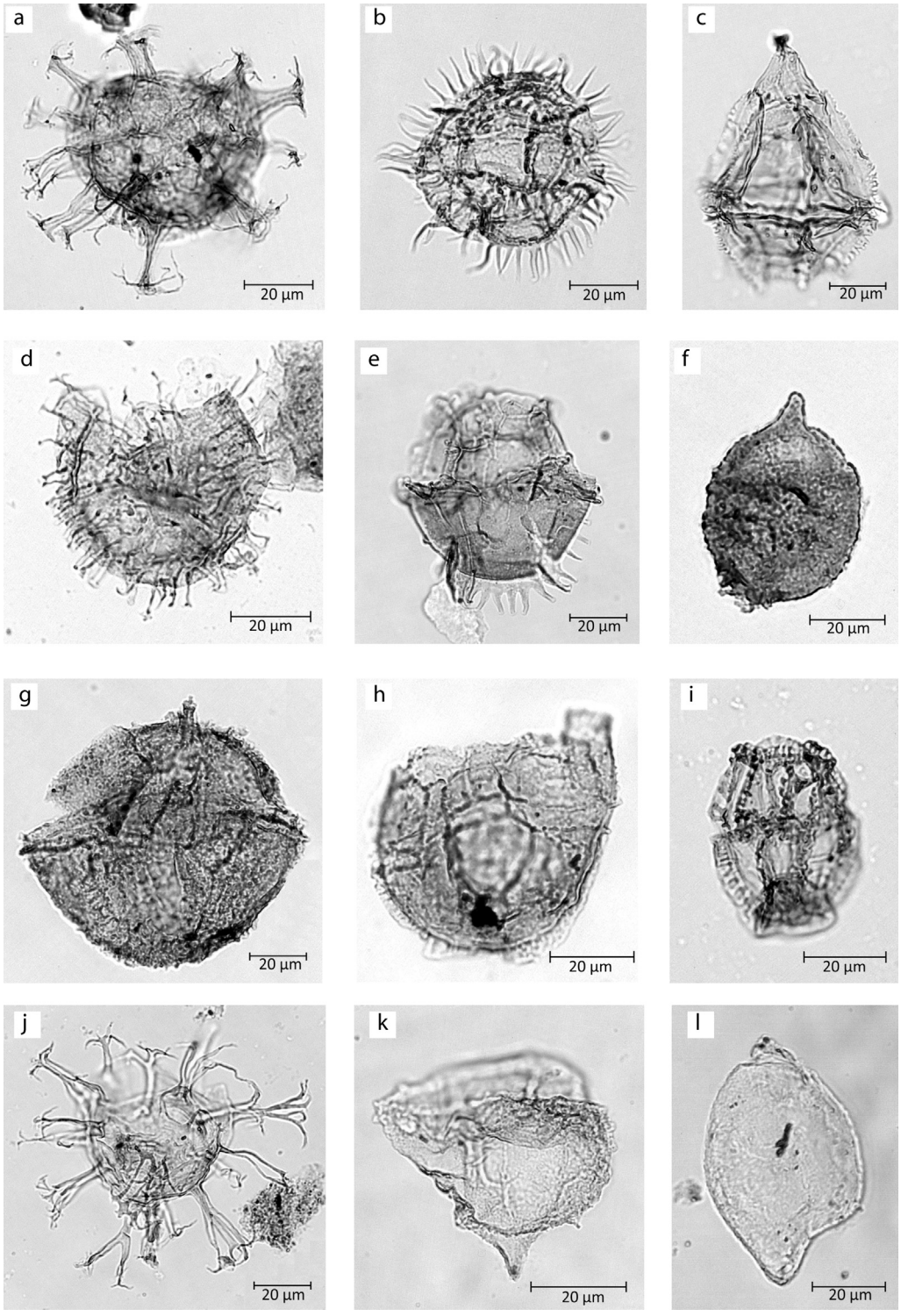

Plate 1. Selected dinoflagellate cysts from the Ruivo and Corvina wells. The sample reference and England Finder coordinates are provided. **a**. *Compositosphaeridium polonicum* (Górka 1965) Lentin and Williams 1981. Ruivo well, Sample R8, P11/2. **b**. *Ctenidodinium sellwoodii* (Sarjeant 1975) Stover and Evitt 1978. Corvina well, Sample Co11, S33. **c**. *Gonyaulacysta jurassica* (Deflandre 1939) Norris and Sarjeant 1965 subsp. *adecta* Sarjeant 1982. Corvina well, Sample Co5, F44/4. **d**. *Impletosphaeridium* spp. Ruivo well, Sample R9, T39/3. **e**. *Ctenidodinium ornatum* (Eisenack 1935) Deflandre 1939. Corvina well, Sample Co9, N7/2. **f**. *Pareodinia ceratophora* Deflandre 1947. Ruivo well, Sample R10, K23. **g**. *Korystocysta gochtii* (Sarjeant 1976) Woollam 1983. Corvina well, Sample Co11, Q32. **h**. *Meiourogonyaulax caytonensis* (Sarjeant 1959) Sarjeant 1969. Ruivo well, Sample R8, U35. **i**. *Stephanelytron redcliffense* Sarjeant. 1961. emend. Stover et al. 1977. Corvina well, Sample Co5, J26/1. **j**. *Surculosphaeridium vestitum* (Deflandre 1939) Davey et al. 1966. Corvina well, Sample Co9, N21/4. **k**. *Wanaea acollaris* Dodekova 1975. Corvina well, Sample Co14, M22/1. **l**. *Nannoceratopsis deflandrei* Evitt 1961 subsp. *deflandrei* (autonym). Ruivo well, Sample R9, Q35/3.

Table 4
The overall palynomorph assemblages of the offshore well Corvina.

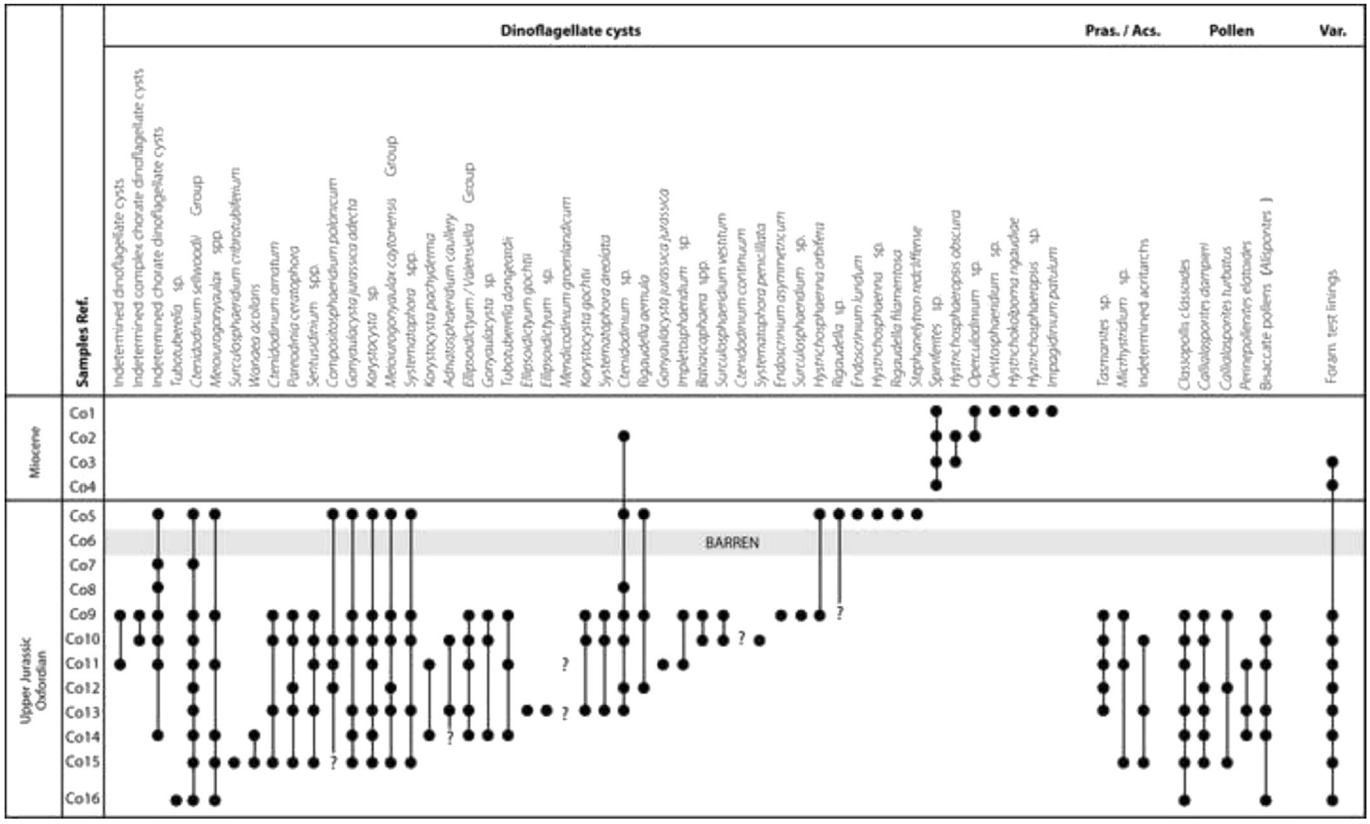

spores and pollen. Black phytoclasts (inertinite) become more important in the Cretaceous strata, possibly related to environmental degradation by aridity, enhanced erosion rates, reworking and oxidation of the organic matter in the continental source areas (Tyson, 1993, 1995). Pollen and spores are also very common and well-preserved, with the gymnosperm pollen *Classopolis classoides* occurring commonly throughout the whole Mesozoic succession of the Algarve Basin. Marine palynomorphs (dinoflagellates and acritarchs) are not distributed evenly through the Algarve Basin succession and never dominate the dispersed organic matter. However, dinoflagellates are common and are invaluable stratigraphically in the Bajocian to Callovian marl–limestone intervals of the basin (Borges et al., 2011, 2012).

Amorphous organic matter (AOM) is never a major constituent of the dispersed organic matter in any of the samples analysed, on average constituting 15–20%. Even in the more marine marl–limestone succession with ammonoids, AOM rarely exceeds 50% of total organic matter. Pyrite is common and appears as inclusions, normally associated with palynomorphs and AOM.

6. Organic maturation results

In order to characterize the true thicknesses of the sections studied and the accurate position of the VR values measured within the stratigraphic succession, the Algarve Basin was divided into 4 areas, each with its own stratigraphy. Although the general stratigraphic architecture of the Algarve Basin is similar in the 4 areas, this division reflects the partition of the basin and the lateral changes in thickness across the basin more accurately (Fig. 4). It also facilitates better understanding of its thermal history. Thus, we follow the partition of the Algarve Basin published by Manuppella et al. (1988) with the key measured stratigraphic successions that characterize each sub-basin, integrated with our own field measured sections. The 4 areas considered are: Sagres–Lagos, Albufeira, Faro and Tavira. The first area belongs to the Western Sub-Basin whereas the other three areas belong to the Eastern Sub-Basin. Figure 1 shows the limits of the areas considered and Figures 5a, 6a, 7a and 8a the geographical location of the samples studied of each area. The VR values shown in the stratigraphic columns for each area are the mean values of all samples from the time interval in the area considered (Table 1). The VR mean (med.) and standard deviation (std.) for each stratigraphic interval in the different areas were calculated from the equations:

$$\text{med.} = \sum(x_i n_i)/\sum n_t$$

$$\text{std.} = \sqrt{(\text{variance})}$$

where, x_i is the mean of each sample, n_i the number of vitrinite particles of each sample and n_t the total number of vitrinite particles measured for each stratigraphic interval considered in the four areas of the Algarve Basin (Sagres–Lagos, Albufeira, Faro and Tavira) (Table 1).

The position of the calculated VR value in the stratigraphic column for each area was placed at approximately the middle of the lithostratigraphic units, when more than three VR samples were measured. In stratigraphic sections with only one sample measured, its position in the stratigraphic column was the measured thickness between the sample and the closest stratigraphic boundary, either the base or the top contact. For example, in the Sagres–Lagos area, VR was measured from 20 samples in the Callovian Praia da Mareta Marls. The calculated mean and standard

deviation value of these 20 samples are 0.89% and 0.18%, respectively (Table 1). Since this unit is approximately 70 m thick (Rocha, 1976; Borges et al., 2011) and through this thickness the VR values does not change significantly, the position of the calculated mean VR value was placed at the mid point of the unit, *i.e.*, at *ca.* 35 m from both the top (the plane of unconformity between the Middle and Upper Jurassic) and the base of this unit (the contact between the Praia da Mareta Marls and the underlying Praia da Mareta Marls with *Zoophycus*) (Fig. 2). In the same area, the three samples studied from the mid Oxfordian Praia do Tonel Limestones (samples 20, 21 and 22; Table 1) have a calculated VR mean of 0.81% and a standard deviation of 0.10%. The samples are from the same outcrop which is positioned 40 m above the Middle Jurassic–Upper Jurassic unconformity in the stratigraphic column.

The following comments apply to the VR results from all Algarve Basin samples, regardless the age of strata or geographic position where the samples are grouped only in terms of the main sedimentary cycles (Upper Triassic–Hettangian, Lower Jurassic, Middle Jurassic, Upper Jurassic and Lower Cretaceous). There is a clear correlation between R_r values and the age of the strata. R_r increases with the age of the rocks as follows: Lower Cretaceous 0.58–0.69%; Upper Jurassic 0.78–0.88%; Middle Jurassic 0.85–0.95%; Lower Jurassic 0.95–0.99% and Upper Triassic–Hettangian 0.94–1.15%. In calculating mean R_r for the Lower Cretaceous rocks, some of the values measured from the Praia da Luz Marls and Porto de Mós Limestones and Marls in the Sagres–Lagos area were not used, because they are regarded as clearly anomalous (see section below).

6.1. Sagres–Lagos

The Sagres–Lagos area corresponds to the part of the Algarve Basin between Cape St. Vincent and Lagos, together with the Carrapateira Outlier, located approximately 20 km north of Sagres, which is considered a northern extension of the main outcrop (Fig. 1). VR was measured from Upper Triassic to Lower Cretaceous (Albian) rocks (Fig. 5a). The composite stratigraphic thickness for this area is *ca.* 1300 m (Manuppella, 1988; Rocha, 1976). Figure 5b shows the mean R_r and standard deviation values for the different stratigraphic levels sampled plotted against the depth of burial. The mean R_r increases from 0.58% in the Albian Porto de Mós Limestones and Marls, to 1.07% in the Upper Triassic Silves Mudstones. Some VR values from samples collected between 50 and 200 m from the intrusion contact at Praia da Luz and Praia de Porto de Mós, are anomalously high for rocks of this age (Aptian/Albian) and are interpreted as the product of heating by the Upper Cretaceous igneous intrusive rocks that outcrop at Ponta das Ferrarias (Fig. 5a). The effects of this rapid heating event are shown in the VR histograms of the samples 1 and 14 (Fig. 9a and Table 1) belonging to the same stratigraphic interval (Porto de Mós Limestones and Marls). Sample 14 was collected from a bed less than 1 m from the contact with the intrusion at Ponta das Ferrarias, whereas sample 1 was collected from an outcrop far from any intrusives. VR increases from 0.52%R_r in sample 1 to 1.68%R_r in sample 14. Spore fluorescence shows yellow colours in sample 1, but spores in sample 14 do not show any fluorescence, which is consistent with the VR results. TAI also show the effect of heating, changing from values of 2 in sample 1 to a TAI value of 4 in sample 14 (Table 1). The effects of Late Cretaceous igneous intrusions on the maturation of the Sagres–Lagos area are more pronounced than predicted and require further study.

Spore fluorescence and spore colour were also observed in the samples analysed and, in general, agree well with the VR results. Fluorescence changes from yellow in the Upper Cretaceous samples, to dark yellow/orange in the Middle Jurassic, and finally to orange in the Upper Triassic–Lower Jurassic samples. TAI for the same stratigraphic interval increases from 2/2+ in the Lower Cretaceous to 2+/3− in the Middle Jurassic and 3−/3 in the Upper Triassic (Table 1).

6.2. Albufeira

The outcrops in this area are located between the town of Silves and the São Marcos da Serra–Quarteira Fault (Figs. 1 and 6a). The stratigraphic succession is *ca.* 3000 m thick and consists of rocks that range in age from Upper Triassic to Lower Cretaceous. Some of the key outcrops in this area are located around the coastal town of Albufeira and include the outcrop of the Albufeira Diapir. This structure is situated adjacent to the E–W trending Baleeira Fault, "an inverted Jurassic normal fault, which was intruded by the Albufeira Salt Diapir during extension of the basin" (Terrinha, 1998). VR, spore fluorescence and colour were measured from Upper Triassic mudstones situated in the S. Bartolomeu de Messines–Vale Fuzeiros area, from Hettangian evaporites of the Albufeira Diapir, from mid Oxfordian–Kimmeridgian marls cropping out near Albufeira town, from inland Lower Cretaceous mudstones and marl outcrops between Paderne and Algoz and from the coastal section at Praia dos Arrifes (Fig. 6a).

VR increases progressively with increasing age of the strata (Fig. 6b), from a mean value of 0.60% in the Aptian Praia da Luz Marls to a mean value of 1.0% in the Late Triassic Silves Mudstones – Siltstones and Dolomites. Sample 64 (Table 1) of Lower Cretaceous contains clearly reworked vitrinite particles (Fig. 9f) with VR above 0.8%R_r. This VR value was adjusted to include only the indigenous vitrinite particles.

Spore fluorescence is consistent with VR and with fluorescence colour and intensity. It also gradually changes with the increasing age of the rocks. The samples from the Upper Cretaceous are characterized by intense bright yellow spore fluorescence, whereas dark orange and orange fluorescence colours were recorded in the Upper Triassic and Hettangian samples, respectively (Table 1). TAI values increase from 2+ in the Upper Cretaceous to 3− in the Upper Triassic.

6.3. Faro

Figure 7a shows the VR results for the Faro area, which corresponds to a large area in the central – east Algarve, south of the Algibre Fault, where Upper Jurassic carbonates crop out extensively (Fig. 1). The stratigraphic succession in this area is the thickest in all the Algarve Basin at *ca.* 3500 m, suggesting that this area was the depocentre of the onshore part of the basin (Fig. 4). Of particular significance in this area are the Lower Cretaceous sediments that are more than 1000 m thick and which extend up into the Cenomanian (Rey, 2009) indicating that sedimentation in the Algarve Basin continued through Late Cretaceous time.

Samples for maturation studies were collected from Late Triassic (?) – Hettangian evaporites in the underground Loulé Salt mine, from early Callovian marls in the disused Telheiro quarry, from numerous Upper Jurassic (late Oxfordian to Tithonian) marl outcrops and also from outcrops of Albian–early Cenomanian (?) marls. The ages of the Cretaceous samples are not very well constrained but field relations suggest a stratigraphic position close to the top of the Cretaceous succession (Fig. 7b). A core of mudstone from depth 46 m in a shallow groundwater exploration borehole (JK) was also sampled, providing additional Early Cretaceous VR data.

VR values from this area show a linear increase with the age of the strata with a mean of 0.69% for the Early Cretaceous rocks and 1.02% for the Hettangian evaporites of the Loulé Diapir (Fig. 7b). The

observed spore fluorescence is consistent with the VR results with fluorescence ranging from intense bright yellow in the majority of the of the Lower Cretaceous samples, to orange – dark orange in the Middle Jurassic and Hettangian. TAI values from the Faro area increase from 2/2+ in the Upper Cretaceous rocks to a 3– in the Hettangian evaporites of the Loulé Diapir (Table 1).

6.4. Tavira

This area corresponds essentially to the *ca.* 1800 m thick section that crops out north of Tavira, along the banks of the Séqua river (Fig 8a). In this section, maturation studies were completed on samples of Callovian marls, Kimmeridgian to Tithonian marls and Upper Triassic–Hettangian mudstones. In addition, two Upper Triassic mudstone core samples from a shallow groundwater exploration borehole (NR) were sampled (NR1 and NR2 at depths of 156 and 158 m respectively).

VR results show a similar pattern to the other three areas. R_r values increase linearly with age and depth of burial from a mean R_r of 0.82% in the Lower Cretaceous to 1.10% in the Upper Triassic, near the base of the local succession (Fig. 8b). Spore fluorescence and colour results (Table 1) from the Upper Triassic and Callovian rocks are fully consistent with the organic maturation levels determined by VR. Orange spore fluorescence colours and TAI of 3– were recorded in the Callovian samples. Orange spore fluorescence colours and TAI of 3/3 were also observed in the Upper Triassic samples.

In a single sample collected from the Miocene argillaceous siltstones of the Cacela Formation, near Ribeira de Cacela, a R_r value of 0.42% was determined. This value is considerably lower than the values measured for the Mesozoic rocks and lies off the regression line defined by the Mesozoic samples (Fig. 8b). Although this result is only from a single sample, it is significant to understanding the timing of maturation for the Mesozoic succession in the Algarve Basin.

6.5. Offshore wells

The offshore wells, Ruivo and Corvina, intersected different Mesozoic stratigraphic intervals in the Algarve Basin succession. In the Ruivo well, a thick Middle Jurassic section (Callovian) overlies Hettangian evaporites, whereas in the Corvina well, a thick Upper Jurassic (Oxfordian) section was encountered (Fig. 3). The Mesozoic strata in both wells are unconformably overlain by Tertiary clastic rocks. This unconformity is also observed in the onshore part of the Algarve Basin where Miocene bioclastic limestones of the Lagos–Portimão Formation generally rest unconformably on rocks of Cretaceous, Jurassic or locally Carboniferous age. The presence of Hettangian evaporites at the base of the Ruivo well indicates the presence of a diapir that intruded the Middle Jurassic rocks.

Figure 3 shows the VR results from in both wells. Unfortunately, the lack of continuous sampling precluded the estimation of maturation gradients and detailed consideration of the thermal history of the offshore part of the Algarve Basin. In the well Ruivo, VR was measured in Callovian and Hettangian rocks from the lower section in the well. In this interval R_r ranges from 0.94% to 1.06% indicating that this part of the well section is within the late oil-window. The orange to dark yellow spore fluorescence colours and TAI ranging from 2+ to 3– (Table 2) that were recorded from this interval confirm this conclusion. Moreover, the VR values determined compare closely with the Middle Jurassic sections in the onshore part of the Algarve Basin, especially the Middle Jurassic sections of the Eastern Sub-Basin.

The VR of the Tertiary sample analysed at the top of the well (R1) is complex. This sample shows two different populations of vitrinite: one with a mean VR value similar to that of the Mesozoic rocks (0.94%R_r) interpreted as reworked, and a second with a much lower mean VR value of 0.47%R_r, regarded as the true indigenous vitrinite population for this stratigraphic interval (Fig. 9). Although indigenous vitrinite is rare in this sample (only 4 grains were measured, Table 2), it is rich in palynomorphs, together with the other Miocene samples (R2 and R3), whose fluorescence and TAI colours are consistent with the two VR maturity populations in sample R1. These samples show two different populations of palynomorphs, one consisting essentially of spores with brown to dark brown exines (TAI: 2+/3–) and showing dark yellow and orange fluorescence colours; the second consisting of spores, bissacate pollen and dinoflagellates with transparent to light yellow exine colours (TAI: 1/1+) and intense blue/green fluorescence. This clearly indicates the presence of an important reworked population of palynomorphs and possibly also of vitrinite, since the indigenous population of palynomorphs (the Miocene dinoflagellates prove the age of this interval) indicates immaturity with regard to the oil-window. Therefore, the highest VR population of sample R1 in this well interval is interpreted as representing a reworked vitrinite population. The possibility of the lowest VR population being caved material can be discounted because the samples are from the upper part of the well with negligible overlying strata.

In the well Corvina (Fig. 3), the most extensively sampled interval comprises *ca.* 600 m of mid Oxfordian marls between 1800 and 2400 m. VR was also measured in Miocene mudstones and from a marl sample located at T.D. VR for all Upper Jurassic samples ranged between 1.07%R_r and 1.2%R_r and does not show any clear increase with depth of burial. The values determined indicate a position in late oil-window. Palynomorph fluorescence in this interval varies from dark yellow, orange to dark orange, whereas TAIs are 2+/3–/3. These two organic maturation parameters suggest a slightly lower maturation level than the VR results. The VR results from the Upper Jurassic samples in this well are also higher than those from the same stratigraphic levels in the onshore part of the basin, especially in the Eastern Sub-Basin.

VR in the Miocene sample Co1, at the top of the well, shows a bimodal population of vitrinite, a situation very similar to that found in the Miocene samples of the Ruivo well. The VR value of the indigenous population is 0.42%R_r, whereas the reworked population is 0.91%R_r. The other Miocene samples in this well (Table 2) only have reworked vitrinite populations. However, as observed in the well Ruivo, they contain abundant palynomorphs which can be divided in two populations on the basis of their fluorescence and spore colours. A population of light-coloured palynomorphs that includes the dinoflagellate species that provides the age for this interval of the well, has intense blue/green fluorescence colours and TAI of 1/1+/2–, indicating immaturity with regard to the oil-window. Dark-brown to brown palynomorphs (spores) are also present showing dark yellow, orange and dark orange fluorescence and a TAI of 2+/3/3–. The organic maturation results from the Miocene strata in both wells are very similar, with two populations of organic particles, one indigenous with low maturation levels and a second with reworked material indicating higher maturation levels.

7. Thermal history

7.1. Palaeogeothermal gradients estimates

The VR results from the Mesozoic rocks of the onshore Algarve Basin indicate that there is a clear relationship between maturity and age (Fig. 5a, 6a, 7a and 8a) with maturation levels increasing with increasing age of the strata, suggesting that burial was the main process controlling organic maturation. Overall, the results

strongly suggest that the conductive heating caused by burial was the main cause of organic maturation in the onshore Algarve Basin. The R_r values measured also indicate that most of the Mesozoic rocks in the Algarve Basin are within the oil-window or the late oil-window (*sensu* Peters and Cassa, 1994).

VR values from the same age strata are similar, regardless of geographical location within the onshore Algarve Basin. Subsidence rates during the Upper Triassic–Lower Cretaceous interval varied across the Algarve Basin with the highest rates recorded in the Eastern Sub-Basin (Faro area) and the lowest in the Sagres Sub-Basin (Terrinha, 1998; Terrinha et al., 2013) (Fig. 3). Therefore, for this time interval, these two sub-basins of the Algarve Basin must have experienced different geothermal gradients in order to produce the maturation levels measured.

Palaeogeothermal gradients have been modelled using the empirical equation of Barker (1988) that computes peak palaeotemperature from VR value ($[T(°C) = 104\ln(R_o) + 148]$, where T(°C) is the maximum palaeotemperature attained by the rock and R_o the VR value measured in the rock). The calculated palaeotemperatures were used to estimate geothermal gradients and also the amount of the eroded sedimentary sections of the areas studied.

The calculated palaeotemperatures for all samples are shown in Tables 1 and 2, and the modelled palaeogeothermal gradients for the four areas of the onshore Algarve Basin are shown in Figure 10. Palaeotemperatures used for constructing the palaeogeothermal gradients were calculated using the mean VR values that were used to construct the VR profiles of each area (Figs. 5b, 6b, 7b and 8b).

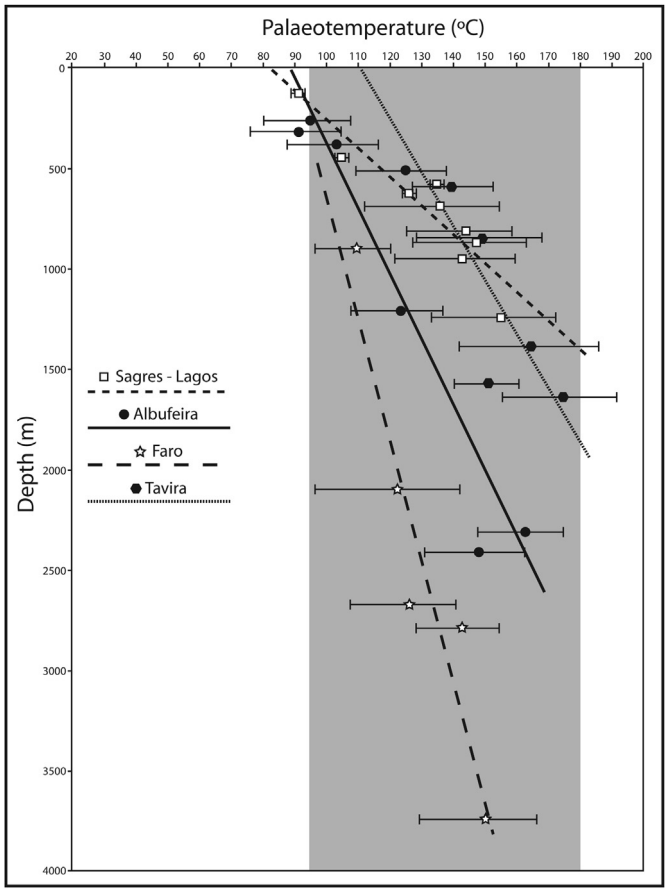

Figure 10. Calculated palaeogeothermal gradients of the four areas studied in the onshore Algarve Basin.

Calculation of palaeogeothermal gradients is based on data from the Upper Triassic through Lower Cretaceous interval, in order to calculate geothermal gradients when sediments were at their maximum burial depth and the amount of sediment removed. Hence, a relatively high palaeogeothermal gradient of *ca.* 70 °C/km was calculated for the Sagres–Lagos area whereas the other three areas, all belonging to the Eastern Sub-Basin, have lower palaeogeothermal gradients of *ca.* 17 °C/km in the Faro area, *ca.* 31 °C/km in the Albufeira area, and *ca.* 37 °C/km in the Tavira area. The relatively low palaeogeothermal gradient in the Faro area could be due possible to erroneous positioning of VR samples in the composite stratigraphic column, especially in the case of the Cretaceous value, the precise age of which is uncertain.

The palaeogeothermal gradients calculated for the Eastern Sub-Basin are within the range of geothermal gradients that characterize sedimentary basins developed in passive margin settings (Allen and Allen, 2005; McKenzie, 1978). The much higher palaeogeothermal gradient in the Western Sub-Basin is more difficult to interpret. Locally elevated VR values observed in the Aptian–Albian sediments at Praias da Luz and Porto de Mós in the Sagres–Lagos area are attributed to conductive heating related to a localized Late Cretaceous igneous intrusion at Ponta das Ferrarias (see Section 6.1), although outcrops close to igneous intrusions were avoided during sampling in this area. With the exception of the two outcrops cited above, this area is characterized by numerous intrusions that are related to the Monchique Syenite Massif dyke swarm (Rock, 1978, 1982; Martins, 1999). The possibility that the elevated palaeogeothermal gradient in this area has been produced by concealed igneous intrusions cannot be discounted. Regional elevation in the geothermal gradient related to the intrusion of the Upper Cretaceous Monchique Syenite igneous body (González-Clavijo and Valadares, 2003) is less probable, since it only intrudes Late Carboniferous rocks and is located approximately 10 km from the Algarve Basin (Fig. 1), though the geometry of its underground extension is unknown. On the basis of the maturation data presented in this study for the Sagres–Lagos area, it is impossible to determine whether the magnitude of the Late Cretaceous igneous activity related to the Monchique Massif was sufficient to elevate the local geothermal gradient, or if the high gradient was due to other causes, such as close proximity to the North Atlantic rifting axis. This requires further investigation.

7.2. Eroded cover estimates

The calculated palaeogeothermal gradients have also been used to estimate the amount of eroded sedimentary cover in the area studied. The method employed is after Bray et al. (1992) and is summarised in Figure 11. It utilises the value of the palaeogeothermal gradient $(dT/dY)_{pal}$, the value of the palaeotemperature measured at today's surface (T_i at 0 m) and the likely surface palaeotemperature at the time of maturation (T_s). The amount of the eroded cover is obtained, assuming that the palaeogeothermal gradient was constant through time, by dividing the difference ($T_i - T_s$) for the value of the palaeogeothermal gradient (Fig. 11). One problem of this method is estimation of the palaeosurface temperature (T_s). Since the Algarve Basin was located in the tropical zone for most of Mesozoic time (Rocha, 1976; Terrinha et al., 2013) where mean temperatures are normally *ca.* 20 °C, this value has been used.

Applying this methodology for the Mesozoic palaeothermal gradients calculated, the exhumation in the onshore Algarve Basin before the deposition of Miocene sediments is estimated at a maximum of *ca.* 4000 m in the Faro area and a minimum of 880 m in the Sagres–Lagos area. In the Albufeira and Tavira areas, the removed cover has similar thicknesses of 2225 m and 2430 m, respectively. The most probable age for the removed cover is Upper

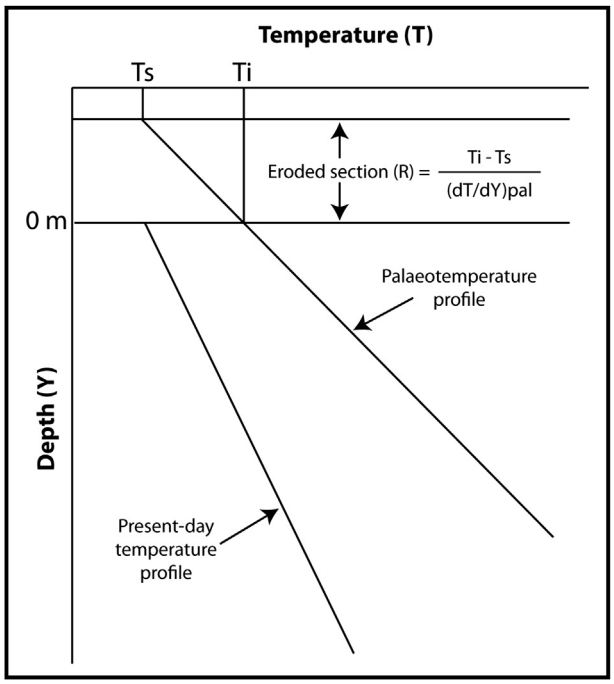

Figure 11. Method for estimating the amount of eroded cover when the value of the palaeogeothermal gradient is constrained and a palaeosurface temperature Ts is assumed. (After Bray et al., 1992.)

Cretaceous (post-Cenomanian) to Palaeocene(?). The estimated thicknesses of cover removed suggest either continuous sedimentation in the Algarve Basin through much of Upper Cretaceous time or a substantial section eroded at the base of the Miocene unconformity.

7.3. Timing of maturation

The timing of maturation in the Mesozoic rocks in the Algarve Basin is constrained by several lines of evidence. The first of these is the break in the maturation trends between the mature Mesozoic succession and the immature Miocene. This discontinuity was found in both the onshore (Tavira area) (Fig. 8b) and offshore sedimentary records (Fig. 3) implying that the timing of oil generation in the Algarve Basin is pre-Miocene. In the onshore Algarve Basin Miocene rocks unconformably overlie tilted and folded Upper Triassic, Jurassic, Cretaceous and even Late Carboniferous basement rocks (Terrinha et al., 2013). No Palaeogene rocks are recognized onshore, and if they were ever deposited here, they were eroded prior to the deposition of the Miocene strata. In the offshore, Palaeogene sediments were recognized in two wells, Algarve-1 and Algarve-2 (Fig. 1). In well Algarve-1, Eocene to Oligocene limestones and dolomites unconformably overlie Lower Cretaceous clastic rocks, whereas in well Algarve-2, a Palaeocene to mid Eocene 500 m thick succession of limestones and marls is unconformably overlain by Pliocene clays (Terrinha et al., 2013). This evidence indicates that there was no continuous sedimentation in the Algarve Basin through the Cretaceous–Palaeogene and Palaeogene–Neogene intervals. However, the lack of maturation data from the Palaeocene rocks precludes better constraint of the timing of maturation and the possibility that peak temperatures, and oil generation were attained during Palaeocene times cannot be totally discarded. However, we do not favour this last hypothesis on the basis of our maturation data and other regional geological evidence. Firstly, there is a lack of proven thick Palaeocene sequences in the Algarve Basin, both onshore and offshore of the order of magnitude that was estimated (Section 7.2. Eroded cover estimates). Secondly, apatite fission track studies of the Carboniferous rocks located north of the Algarve Basin boundary and the Monchique Syenite Massif, indicate cooling ages of 113–111 Ma (Stapel, 1999) and 72 Ma (Terrinha et al., 2006) respectively. In the case of the Monchique Syenite Massif the apatite fission track age is approximately the same age of the emplacement (Miranda et al., 2009), indicating that the intrusion of the batholith occurred at shallow crustal depths and the Pennsylvanian greywackes and shales intruded were between 60 °C and 90 °C (Terrinha et al., 2013). This suggests that during latest Cretaceous–Early Palaeocene times basement rocks that surround the Algarve Basin, and probably the Algarve Basin were subjected to active uplift and erosion and not enhanced subsidence. Therefore, we suggest that peak temperatures in the Mesozoic rocks of the Algarve Basin were attained in Late Cretaceous times but prior to 72 Ma (Campanian), episode that coincide with the intrusion of the Monchique Syenite Massif.

Other evidence for this interpretation includes the presence of reworked organic particles (vitrinite and palynomorphs) in the Miocene strata of the offshore wells. The reworked VR particles have similar values to the Mesozoic successions, implying that some the Mesozoic succession of the Algarve Basin was exposed and eroded during Miocene time. Possible extrabasinal sources for the reworked organic particles are the Mesozoic rocks of the Lusitanian Basin located in central littoral Portugal and the Mesozoic rocks exposed in the Betic Cordillera in southern Spain.

The Albufeira and Loulé diapirs also provide information on the timing of maturation. In the case of the Albufeira Diapir, salt movement was controlled by the east–west trending Baleeira Fault (Terrinha, 1998). The evaporites (halite and anhydrite) crop out in the hangingwall block of the fault and were injected across the fault zone, resulting in tectonic contact with Upper Jurassic and Lower Cretaceous rocks. Halokinesis of the Albufeira Diapir was responsible for the tilting and rotation to the vertical of the Lower Cretaceous rocks in contact with the evaporites at Praia dos Arrifes (Fig. 12). VR measured in the Hettangian evaporites of the diapir is 1.15%R_r but is *ca.* 0.65%R_r in the Lower Cretaceous, implying that the main halokinesis movement post-dates organic maturation. A similar situation occurs in the Loulé Diapir, where the VR for the Upper Jurassic rocks around Loulé is 0.78%R_r, whereas the Hettangian evaporites have a value of *ca.* 1.03%R_r, again suggesting that the movement of the salt post-dates organic maturation. The main phase of salt movement occurred in relation to the principal episode of inversion of the Algarve Basin, which structural evidence, both onshore and offshore, indicates is Late Cretaceous–Palaeogene in age. It also suggests that the Algarve Basin was substantially uplifted during Neogene times and a great deal of Mesozoic sediments was exhumed (Terrinha, 1998; Terrinha et al., 1990, 2013).

7.4. 1D thermal modelling

The burial and thermal histories of the onshore Algarve Basin were modelled using Schlumberger PetroMod 1D® software. The basic data concerning the lithology, age and thickness of each rock unit were taken from the key measured sections in the four areas and from our own field observations. Input of the correct lithologies into the model is very important since it controls parameters such as compaction rates and thermal conductivities. Palaeoheat flow (PHF) is another important parameter for modelling the temperature–time curve. The palaeoheat flow over time used in modelling was after the work of Matias (2007) for the offshore Algarve Basin. Palaeoheat flows were calculated for two episodes of rifting with lithospheric stretching factors of $\beta = 1.5$ for the Upper Triassic and

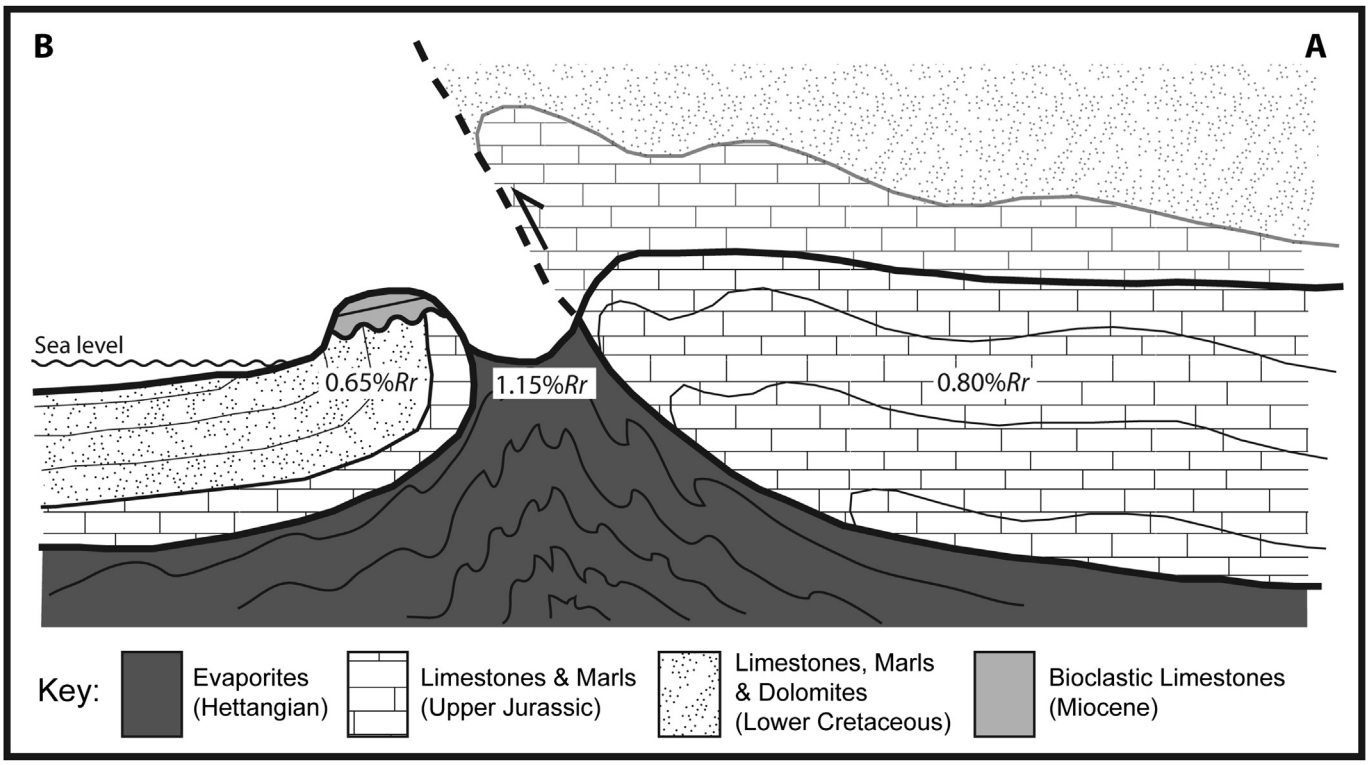

Figure 12. Schematic geological cross section perpendicular to the Baleeira Fault, showing the position of the Albufeira Diapir and VR results. The location (A and B) of the cross-section is shown in Figure 6a (adapted from Terrinha, 1998).

$\beta = 1.4$ for the Cretaceous, values considered by Matias (2007) as appropriate for the evolution of this basin.

The other boundary conditions that were used in modelling were the palaeo-water depth (PWD) and the temperature at the sediment–water interface (SWIT). Depositional environment was the only feature of the rocks that was taken into account to define the PWD (in metres). SWIT was calculated from the palaeolatitude of the Algarve Basin during the Mesozoic. As the Algarve Basin was located within the tropical belt in Upper Triassic–Lower Cretaceous times, a temperature of 20 °C was adopted as the SWIT value for the shallow water carbonate rock units, whereas a temperature of 10 °C was used for marl–limestone sequences, representing deposition in deeper and colder shelf areas (*ca.* 50–100 m water depth).

A critical point in the thermal history of the Algarve Basin revealed by the analysis and interpretation of the VR data is that a considerable Late Cretaceous sedimentary succession was eroded prior to the deposition of the Miocene strata (see Section 7.2). Moreover, peak temperatures were probably also attained in latest Cretaceous times (see Section 7.3). These two considerations were taken into account in the 1D thermal modelling rather than unrealistically high palaeoheat flows (and palaeogeothermal gradients) that would be needed to fit the VR values if present day stratigraphic thicknesses were used. An additional sedimentary cover of Upper Cretaceous age between 100 Ma (Cenomanian) and 72 Ma (Campanian), consisting of a carbonate sequence similar to the preserved Lower Cretaceous with PWD of 10 m and SWIT of 20 °C was added to the stratigraphic column of each area until the VR values and temperatures modelled fitted the VR values measured. The other limit applied to the model was that peak temperatures in the Mesozoic succession were attained in latest Cretaceous times (*ca.* 72 Ma). Modelling of the two offshore wells was not attempted due to their limited stratigraphy compared to the onshore Algarve Basin.

Figure 13a–d, shows the burial curves, together with the VR values and palaeotemperatures modelled with the 1D PetroMod model. For the burial curve of the Sagres–Lagos area (Fig. 13a), the value for the Late Cretaceous palaeoheat flow was increased in relation to the other areas to conform with the VR data from this area. The values for the 'best-fit' Late Cretaceous cover thicknesses and palaeogeothermal gradients derived from the modelled burial curves for each area are: Sagres–Lagos area 2500 m and 52 °C/km; Albufeira area 2200 m and 27.5 °C/km; Faro area 2000 m and 24.7 °C/km and Tavira area 4000 m and 25.8 °C/km.

For the areas situated in the Eastern Sub-Basin, the modelled palaeogeothermal gradients are very similar and, with the exception of the Tavira area, a similar thickness of Upper Cretaceous succession was also estimated. This does not imply a higher rate of subsidence for the Tavira area, rather that more exhumation took place here because part of the Lower Cretaceous succession present in the Faro and Albufeira areas is missing. According to the modelled burial curves, 2000–2200 m of Upper Cretaceous sedimentary rocks must have been deposited to account for the VR values measured in the Eastern Sub-Basin.

In the Western Sub-Basin, the modelled palaeogeothermal gradient is approximately double (52 °C/km) that in the Eastern Sub-Basin (24.7–27.5 °C/km) but the thickness of the Upper Cretaceous sedimentary pile is 2500 m, of similar magnitude to that in the Eastern Sub-Basin. This suggests that the process responsible for the elevated regional palaeogeothermal gradient did not enhance the subsidence rate in this sub-basin.

Comparison of the modelled palaeogeothermal gradients with those calculated directly from the VR profiles by the Barker (1988) equation for the Algarve Basin indicates that the latter are overestimated by *ca.* 5–10 °C/km. The exception to this is the Faro area, where the calculated VR palaeogeothermal gradient is lower. However, this may be due to an incorrect positioning of samples in the composite stratigraphic column, as mentioned previously (Section 6.3). Thus, the values of the modelled palaeogeothermal gradients are better constrained when compared

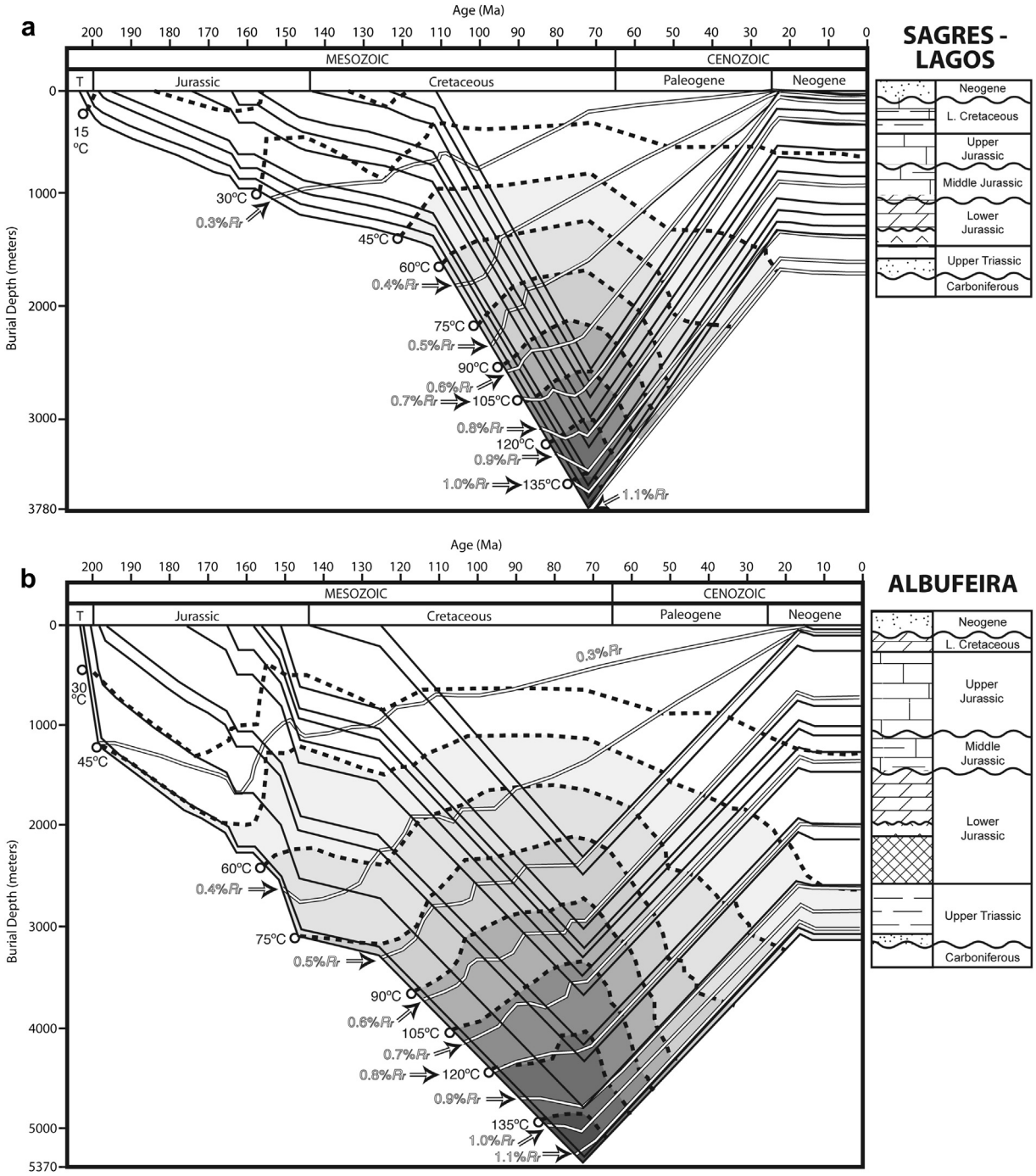

Figure 13. Burial histories curves modelled for the areas studied in the onshore Algarve Basin, a) Sagres-Lagos, b) Albufeira, c) Faro and d) Tavira.

with the calculated by the VR profiles using the Barker (1988) equation, implying that the modelled thicknesses for eroded Upper Cretaceous sedimentary pile are also more realistic. This is also due to the fact that the model computes the evolution of the palaeoheat flow and the petrophysical parameters (compaction, rock thermal conductivities, etc.) over time, factors that are not taking into account in computations using only the VR profiles.

8. Implications for hydrocarbon exploration

VR, qualitative spore fluorescence and TAI determinations indicate that the Mesozoic succession in the onshore Algarve Basin lies within the oil-window. The Hettangian evaporites have R_r *ca.* 1.1% and the Lower Cretaceous sediments *ca.* 0.52–0.7%. The Mesozoic succession in the offshore wells, Hettangian and Callovian strata in the well Ruivo, and Oxfordian rocks in the well Corvina, all lie within the late oil-window. Modelled burial curves indicate that palaeogeothermal gradients for the onshore successions vary between 24.7 and 27.5 °C/km in the Eastern Sub-Basin, but a higher gradient of 52 °C/km has been calculated for the Western Sub-Basin. The cause of local elevation in the regional palaeogeothermal gradients remains uncertain. These results, together with regional geological evidence indicate that peak palaeotemperatures were probably attained in late Cretaceous

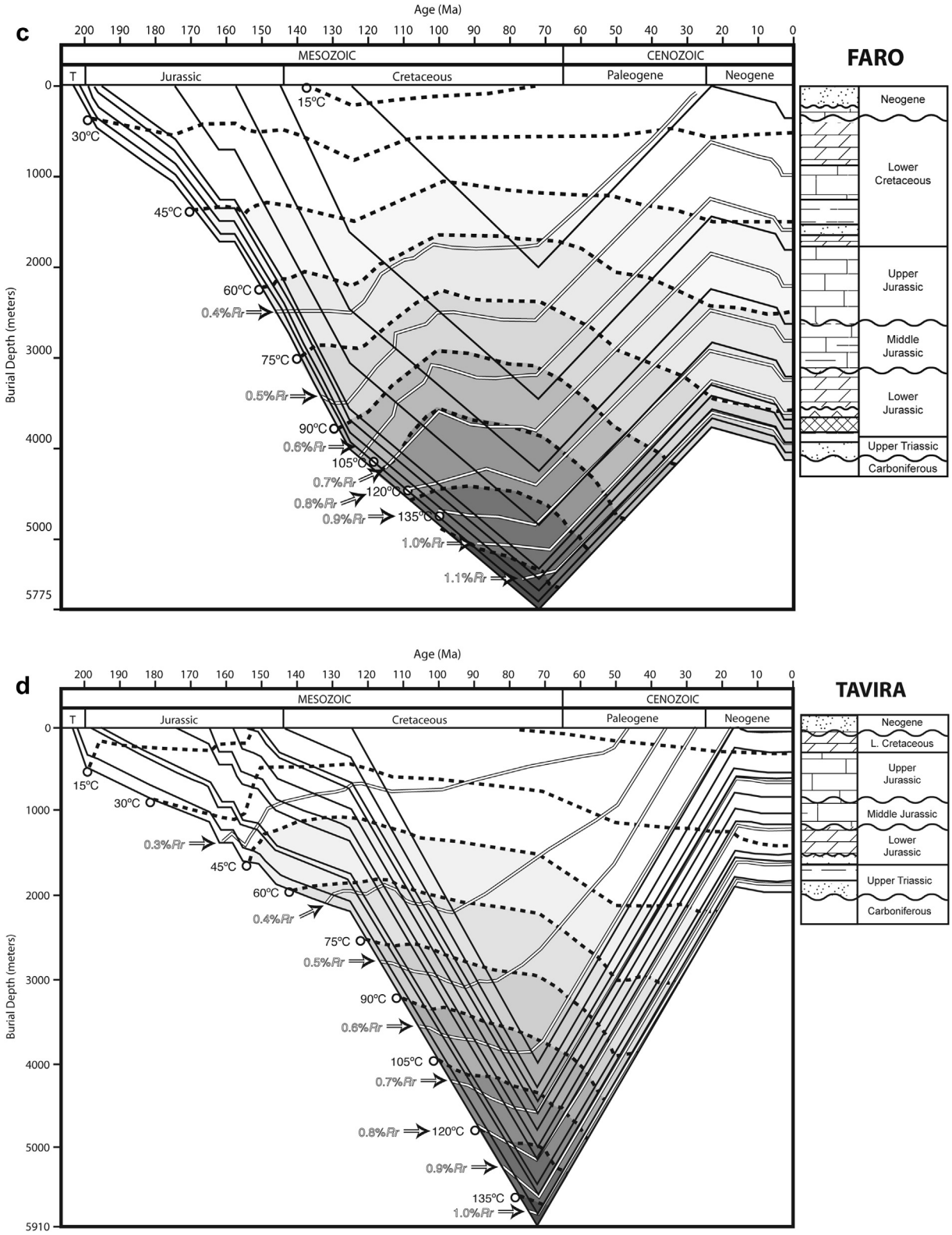

Figure 13. (*continued*).

time. However, the potential source rock intervals probably stopped generating from the moment the uplift of the onshore area began, *ca.* 72 Ma. Modelled burial curves suggest that the Lower Jurassic succession across the Algarve Basin entered the oil window at the beginning of the Cretaceous and that peak oil generation occurred in late Cretaceous time. Therefore, some of the Jurassic and Lower Cretaceous sections in the Algarve Basin have considerable potential as targets for future oil exploration.

Between 2000 and 2500 m of cover must have been deposited and subsequently eroded in the onshore area in order to account for the maturation levels measured. This implies continuous subsidence and sedimentation during Late Cretaceous time up to 72 Ma. Tectonic inversion of the Algarve Basin probably occurred during the Palaeogene and was related to the onset of the alpine tectonism and the emplacement of the Monchique Syenite (Terrinha et al., 2002; Miranda et al., 2009). The low maturity of the Miocene sediments (immature with respect to the oil-window) both onshore and offshore proves that Miocene–Pleistocene reburial of the Mesozoic succession did not increase its maturity.

Even though the Mesozoic succession lies within the oil-window, oil shows are virtually absent in the Algarve Basin. The presence of small amounts of oil filling fractures and pores in a sample of jet recently found in the Kimmeridgian–Tithonian Escarpão Limestones in the Eastern Sub-Basin (Fig. 2) confirms to some extent the maturation levels established by our study (Costa et al., 2010). The absence of oil shows may be due to the type of organic matter observed in the organic residues of the rocks of the Algarve Basin. The most abundant organic particles found in the organic residues of the Algarve Basin are terrestrially derived (vitrinite and inertinite). This type of organic matter (kerogen type III–II) is gas prone type rather than oil prone. However, another likely explanation was that oil generated and trapped during burial escaped from the reservoirs during the uplift events in the latest Cretaceous and early Tertiary. Investigation of source rock quality and quantity is beyond the scope of this work but a comprehensive study is clearly needed in order to ascertain the stratigraphic distribution of the organic facies and source rock potential.

9. Summary and conclusions

VR results from 175 samples demonstrate that the Mesozoic succession in the Algarve Basin lies within the oil window. VR ranges from 0.52–0.70%R_r in the Lower Cretaceous to 1–1.1%R_r in the Upper Triassic–Hettangian section. Miocene carbonates and mudrocks that unconformably overlie the Mesozoic strata are immature with regard to the oil window. The Mesozoic successions in the Ruivo and Corvina wells in the offshore part of the Algarve Basin lie within the late oil-window. As in the onshore Algarve Basin, Miocene rocks in these offshore wells are immature.

Palynological study of the offshore Ruivo and Corvina wells has provided new stratigraphic information. In the Ruivo well, most of the palynological productive Mesozoic section consists of thick marls and limestones that yielded a dinoflagellate assemblage of Callovian age. These rocks overlie evaporites of Hettangian age. The Mesozoic section in the Corvina well yielded a dinoflagellate assemblage of mid to upper Oxfordian age.

Modelled palaeogeothermal gradients in the Eastern Sub-Basin range from 24.7 to 27.5 °C/km, whereas a higher gradient of 52 °C/km was modelled for the Western Sub-Basin. Peak temperatures in the Algarve Basin were attained during Late Cretaceous–Early Palaeocene(?) time. To account for the maturation levels determined in the onshore Algarve Basin, 2000–2500 m of cover must have been eroded. This erosion occurred during much of Palaeogene time and was due to the onset of the Alpine Orogeny. Evidence for this event is provided by the considerable amount of reworked vitrinite particles and palynomorphs found together with the indigenous organic particles in the Miocene succession of the offshore wells Ruivo and Corvina. The maturation levels of the reworked organic material are similar to the levels of the Mesozoic rocks of the Algarve Basin suggest, therefore, that parts of the basin were already exposed and were being eroded during Miocene times. Modelled burial curves suggest that the Upper Triassic–Hettangian section entered the oil window in Early Cretaceous time and that peak temperatures of all the stratigraphic units were attained in latest Cretaceous time.

Acknowledgements

This work is a contribution to the project PTDC/CTE-GEX/72694/2006 financed by the Portuguese Foundation for Science and Technology (Fundação para a Ciência e a Tecnologia – FCT). P. Fernandes wishes to thanks: Dr. Teresinha Abecassis from the DPEP – Lisbon, for facilitating access to the core and data for the offshore wells Ruivo and Corvina, and Eng. Alexandre Araújo from the Loulé Salt Mine (Campina de Cima, Loulé – CUF) for allowing the access to the mine and guidance during sampling in the mine. The authors also wish to thank the associated editor Dr. Nicholas Harris and the two anonymous reviewers, whose comments greatly improved the final manuscript.

References

Allen, P.A., Allen, J.R., 2005. Basin Analysis: Principles and Applications, second ed. Blackwell Publishing, Oxford.
Antunes, M., Pais, J., 1993. The Neogene of Portugal. Ciências da Terra (UNL) 12, 7–22.
Azerêdo, A., Duarte, L., Henriques, M., Manuppella, G., 2003. Da dinâmica continental no Triásico aos mares do Jurássico Inferior e Médio. Cadernos de Geologia de Portugal. Instituto Geológico e Mineiro, Lisboa.
Barker, C., 1988. Geothermics of petroleum systems: implications of the stabilization of kerogen thermal maturation after a geologically brief heating duration at peak temperature. In: Magoon, L.B. (Ed.), Petroleum Systems of the United States, U.S. Geological Survey Bulletin, 1870, pp. 26–29.
Bordenave, M., Espitalié, J., Laplat, P., Oudin, J., Vandenbrouke, M., 1993. Screening techniques for source rock evaluation. In: Bordenave, M. (Ed.), Applied Petroleum Geochemistry. Editions Technip, Paris, pp. 217–279.
Borges, M., Riding, J., Fernandes, P., Pereira, Z., 2011. The Jurassic (Pliensbachian to Kimmeridgian) palynology of the Algarve Basin and the Carrapateira outlier, southern Portugal. Review of Palaeobotany and Palynology 163, 190–204.
Borges, M., Riding, J., Fernandes, P., Matos, V., Pereira, Z., 2012. Callovian (Middle Jurassic) dinoflagellate cysts from the Algarve Basin, southern Portugal. Review of Palaeobotany and Palynology 170, 40–56.
Bray, R., Green, P., Duddy, I., 1992. Thermal history reconstruction using apatite fission track analysis and vitrinite reflectance: a case study from the UK East Midlands and the Southern North Sea. In: Hardman, R. (Ed.), Exploration Britain: Geological Insight for the Next Decade, Geological Society of London Special Publication, vol. 67, pp. 3–25.
Challenger Portugal Inc., 1976. Geological Completion Report-Corvina.
Chevron Overseas Petroleum Inc., 1975. Evaluation Report Ruivo-1.
Costa, A., Suarez-Ruiz, I., Fernandes, P., Flores, D., 2010. First Results of a Perhydrous Coal from the Mesozoic Algarve Basin, Portugal, pp. 35–36. Abstracts of 62nd Meeting of the International Committee for Coal and Organic Petrology (ICCP), Belgrade.
Dommergues, J.L., Meister, C., Rocha, R., 2011. The Pliensbachian ammonites of the Algarve Basin (Portugal) and their palaeobiogeographical significance for the "Iberia-Newfoundland" conjugate margins. Swiss Journal of Geosciences 104, 81–96.
Esso Exploration Inc., 1982a. Geological Completion Report Algarve-1.
Esso Exploration Inc., 1982b. Geological Completion Report Algarve-2.
Fechner, G., 1989. Eine unterliassische Mikroflora aus dem Salzdiapir bei Loulé (Süd-Portugal). Berliner Geowissenschaftliche Abhandlungen Reihe A 106, 37–47.
Fernandes, P., Luis, J., Rodrigues, B., Marques, M., Valentim, B., Flores, D., 2010. The measurement of vitrinite reflectance with MatLab. In: Oliwkiewicz-Miklasinka, M., Stempien-Salek, M., Iaptas, A. (Eds.), CIMP Poland General Meeting, September 2010. Institute of Geological Sciences, Polish Academy of Sciences, Warsaw, pp. 11–13.
González-Clavijo, E., Valadares, V., 2003. O Maciço Alcalino de Monchique (SW Português) estrutura e modelo de instalação na crosta superior. Comunicações do Instituto Geológico e Mineiro 90, 43–64.
Gibling, M., Stuart, C., 1988. Carbonate slide deposits in the Middle Jurassic of Portugal. Sedimentary Geology 57 (1–2), 59–73.
Hillier, S., Marshall, J., 1988. A rapid technique to make polished thin sections of sedimentary organic matter concentrates. Journal of Sedimentary Petrology 58, 754–755.
Hunt, J., 1996. Petroleum Geochemistry and Geology. W.H. Freeman and Co., New York.
Luis, L., 2007. Mirone: a multi-purpose tool for exploring grid data. Computers & Geosciences 33, 31–41.
Mackowsky, M.T., 1982. Rank determination by measurement of reflectance of vitrinites. In: Stach, E., Mackowsky, M., Teichmuller, M., Taylor, G., Chandra, D., Teichmuller, R. (Eds.), Stach's Textbook of Coal Petrology, third ed. Gebrüder Borntraeger, Berlin & Stuttgart, pp. 319–329.
Manuppella, G., Ramalho, M., Antunes, A., Pais, J., 1987. Carta Geológica de Portugal na escala 1:50 000, Notícia Explicativa da Folha 53-A (Faro). Serv. Geol. Port., p. 52.

Manuppella, G., 1988. Litoestratigrafia e tectónica da Bacia Algarvia. Geonovas 10, 67–71.
Manuppella, G., Marques, B., Rocha, R.B., 1988. Évolution tectono-sédimentaire du bassin de l' Algarve pendant le Jurassique. In: 2nd International Symposium on Jurassic Stratigraphy, Lisboa, pp. 1031–1046.
Marques, B., Rocha, R., 1988a. O Caloviano do flanco norte do Guilhim (Algarve oriental): biostratigrafia e paleobiogeografia. Ciências da Terra (UNL) 9, 19–26.
Marques, B., Rocha, R., 1988b. Evolução paleogeográfica e paleobiogeográfica do Caloviano-Kimmeridgiano do Algarve. Ciências da Terra (UNL) 9, 33–40.
Martins, L., Munhá, J., 1993. Magmatismo cretácico do Algarve litoral: zonamento inverso em clinopiroxenas e suas implicações petrogenéticas. In: Mem. Mus. Lab. Min. Geol. Fac. Ciênc. Univ. Porto, vol. 3, pp. 105–106.
Martins, L., 1999. Cretaceous alkaline magmatism in Algarve litoral (South Portugal): a basanite – lamprophyre suite. Geolines 9, 84–91.
Martins, L., Madeira, J., Youbi, N., Munhá, J., Mata, J., Kerrich, R., 2008. Rift-related magmatism of the Central Atlantic magmatic province in Algarve, southern Portugal. Lithos 101, 102–124.
Matias, H., 2007. Hydrocarbon Potential Od the Offshore Algarve Basin (PhD thesis). Lisbon University.
McCormack, N., 1998. The Thermal History of the South Portuguese Zone (Unpublished Ph.D. thesis). University of Dublin.
McKenzie, D., 1978. Some remarks on the development of sedimentary basins. Earth and Planetary Science Letters 40, 25–32.
McPhilemy, B., 1988. The value of fluorescence microscopy in routine palynofacies analysis: Lower Carboniferous successions from Counties Armagh and Roscommon, Ireland. Review of Palaeobotany and Palynology 56, 345–359.
Miranda, R., Valadares, V., Terrinha, P., Mata, J., Azevedo, M.R., Gaspar, M., Kullberg, J., Ribeiro, C., 2009. Age constraints on the Late Cretaceous alkaline magmatism on the West Iberian Margin. Cretaceous Research 30, 575–586.
Mouterde, R., Ramalho, R., Rocha, R., Ruget, C., Tintant, H., 1971. Le Jurassique du Portugal. Esquisse stratigraphique et zonale. Boletim da Sociedade Geológica de Portugal 18, 73–104.
Oliveira, J.T. (Coord.), 1992. Carta Geológica de Portugal na escala 1:200 000, Notícia Explicativa da Folha 8. Serviços Geológicos de Portugal, 91 pp.
Palain, C., 1976. Une série détritique terrigène, les "Grés de Silves". Trias et Lias Inférieur du Portugal. In: Memórias dos Serviços Geológicos de Portugal, N.S., vol. 25, p. 377.
Pais, J., Legoinha, P., Elderfield, H., Sousa, L., Estevens, M., 2000. The Neogene of Algarve (Portugal). Ciências da Terra 14, 277–288.
Peters, K.E., Cassa, M.R., 1994. Applied source rock geochemistry. In: Magoon, L.B., Dow, W.G. (Eds.), The Petroleum System – From Source to Trap, American Association of Petroleum Geologists Memoir 60, pp. 93–117.
Rey, J., 1983. Le Cretacé de l'Algarve: Essay de Synthèse. Comunicações dos Serviços Geológicos de Portugal 69 (1), 87–101.
Rey, J., 2006. Les Formations Crétacées de l'Algarve Occidental et Central. Comunicações Geológicas 93, 39–80.
Rey, J., 2009. Les Formations Crétacées de l'Algarve Oriental. Comunicações Geológicas 96, 19–38.
Riding, J., Thomas, J.E., 1992. Dinoflagellate cysts of the Jurassic System. In: Powell, A.J. (Ed.), A Stratigraphic Index of Dinoflagellate Cysts, British Micropalaeontological Society Publications Series, pp. 7–97.
Riding, J.B., 2005. Middle and Upper Jurassic (Callovian to Kimmeridgian) palynology of the onshore Moray Firth Basin, northeast Scotland. Palynology 29, 87–142.
Robert, P., 1988. Organic Metamorphism and Geothermal History. ELF Aquitaine and D. Reidl, Dordrecht.
Rocha, R., 1976. Estudo estratigráfico e paleontológico do Jurássico do Algarve ocidental. Ciências da Terra 2, 178.
Rock, N., 1978. Petrology and petrogenesis of the alkaline complex, southern Portugal. Journal Petrology 19, 171–214.
Rock, N., 1982. The late Cretaceous alkaline igneous province in the Iberian Peninsula, and its tectonic significance. Lithos 15, 111–131.
Stapel, G., 1999. The Nature of Isostasy in West Iberia and its Bearing on Mesozoic and Cenozoic Regional Tectonics (Unpublished Ph.D. thesis). Vrije Universiteit.
Staplin, F., 1969. Sedimentary organic matter, organic metamorphism and oil and gas occurrence. Bulletin of Canadian Petroleum Geology 17, 47–66.
Staplin, F.L., 1977. Interpretation of thermal history from colour of particulate organic matter – a review. Palynology 1, 9–18.
Staplin, F., 1982. How to assess maturation and palaeotemperatures: introduction. In: Staplin, F., et al. (Eds.), How to Assess Maturation and Palaeotemperatures, Society of Economic Paleontologists and Mineralogists Short Course No. 7, pp. 1–5.
Terrinha, P., Coward, M., Ribeiro, A., 1990. Salt Tectonics in the Algarve Basin: The Loulé Diapir. In: Comun. Sev. Geol. Port., vol. 76, pp. 33–40.
Terrinha, P., 1998. Structural Geology and Tectonic Evolution of the Algarve Basin, South Portugal (Unpublished Ph.D. thesis). Department of Geology, Imperial College of Science, Tecnhology and Medicine, University of London.
Terrinha, P., Ribeiro, C., Kulberg, J.C., Lopes, C., Rocha, R., Ribeiro, A., 2002. Compressive episodes and faunal isolation during rifting, Southwest Iberia. Journal of Geology 110, 101–113.
Terrinha, P., Rocha, R., Rey, J., Cachão, Moura, D., Roque, C., Martins, L., Valadares, V., Cabral, J., Azevedo, M.R., Barbero, L., Clavijo, E., Dias, R.P., Gafeira, J., Matias, H., Matias, L., Madeira, J., Marques da Silva, C., Munhá, J., Rebelo, L., Ribeiro, C., Vicente, J., Youbi, N., 2006. A Bacia do Algarve: Estratigrafia, paleogeografia e tectónica. In: Dias, R., Araújo, A., Terrinha, P., Kullberg, J.C. (Eds.), Geologia de Portugal no contexto da Ibéria. Universidade de Évora, pp. 247–316.
Terrinha, P., Rocha, R., Rey, J., Cachão, M., Moura, D., Roque, C., Martins, L., Valadares, V., Cabral, J., Azevedo, M.R., Barbero, L., Clavijo, E., Dias, R.P., Matias, H., Madeira, J., Silva, C.M., Munhá, J., Rebelo, L., Ribeiro, C., Vicente, J., Noiva, J., Youbi, N., Bensalah, M.K., 2013. A Bacia do Algarve: Estratigrafia, paleogeografia e tectónica. In: Dias, R., Araújo, A., Terrinha, P., Kullberg, J.C. (Eds.), Geologia de Portugal, Geologia Meso-cenozóica de Portugal, vol. II, pp. 29–166.
Tissot, B., Welte, D., 1978. Petroleum Formation and Occurrence, a New Approach to Oil and Gas Exploration. Sringer-Verlag, Berlin Heidelberg, New York.
Tyson, R., 1993. Palynofacies analysis. In: Jenkins, D.J. (Ed.), Applied Micropaleontology. Kluwer Academic Publishers, Dordrecht, pp. 153–191.
Tyson, R., 1995. Sedimentary Organic Matter, Organic Facies and Palynofacies. Chapman & Hall, London.
Van Gijzel, P., 1967. Palynology and fluorescence microscopy. Review of Palaeobotany and Palynology 2, 49–79.
Van Gijzel, P., 1971. Review of the UV-fluorescence microphotometry of fresh and fossil exines and exosporia. In: Brooks, J., et al. (Eds.), Sporopollenin. Academic Press, London & New York, pp. 659–685.
Van Gijzel, P., 1975. Polychromatic UV-fluorescence microscope-photometry of fresh and fossil plant substances with special reference to the location and identification of dispersed organic material in rocks. In: Alpern, B. (Ed.), Pétrographie de la matière organique des sédiments, relations avec la paléotemperature et le potentiel pétrolier. Colloque International, Centre National de la Recherche Scientifique, Paris, pp. 67–91.
Van Gijzel, P., 1979. Manual of the Techniques and Some Geological Applications of Fluorescence Microscopy. American Association of Stratigraphical Palynologists Foundation, Dallas.
Verati, C., Rapaille, C., Féraud, G., Marzoli, A., Bertrand, H., Youbi, N., 2007. $^{40}Ar/^{39}Ar$ ages and duration of the Central Atlantic Magmatic Province volcanism in Morocco and Portugal and its relation to the Triassic–Jurassic boundary. Palaeogeography, Palaeoclimatology, Palaeoecology 344, 308–325.
Wilson, R., Hiscott, R., Willis, M., Gradstein, E., 1989. The Lusitanian Basin of west central Portugal: Mesozoic and Tertiary tectonic, stratigraphy and subsidence history. In: Tankard, A., Balkwill, H. (Eds.), Extensional Tectonics and Stratigraphy of the North Atlantic Margins, AAPG Memoir 46, pp. 341–361.

Sedimentary Geology 284–285 (2013) 133–148

Contents lists available at SciVerse ScienceDirect

Sedimentary Geology

journal homepage: www.elsevier.com/locate/sedgeo

Geochemistry and provenance of the Carboniferous Baixo Alentejo Flysch Group, South Portuguese Zone

R.C.G.S. Jorge [a,*], P. Fernandes [b], B. Rodrigues [b], Z. Pereira [c], J.T. Oliveira [d]

[a] CREMINER (LA-ISR), Universidade de Lisboa, Faculdade de Ciências, Departamento de Geologia, Edificio C6, Piso 4, Campo Grande, 1749-016 Lisboa, Portugal
[b] CIMA, Centro de Investigação Marinha e Ambiental, Universidade do Algarve, Campus de Gambelas, 8005-139 Faro, Portugal
[c] LNEG-LGM, Unidade de Geologia e Cartografia Geológica, Rua da Amieira, 4465-965S. Mamede Infesta, Portugal
[d] LNEG-LGM, Unidade de Recursos Naturais e Geofísica, Apartado 7586, 2611-901 Alfragide, Portugal

ARTICLE INFO

Article history:
Received 2 February 2012
Received in revised form 21 November 2012
Accepted 7 December 2012
Available online 19 December 2012

Editor: G.J. Weltje

Keywords:
Baixo Alentejo Flysch Group
South Portuguese Zone
Carboniferous
Whole-rock geochemistry
Provenance analysis

ABSTRACT

This work is focused on the turbiditic sediments from the Carboniferous Baixo Alentejo Flysch Group (BAFG) in the South Portuguese Zone, an external zone of the Iberian Variscides. The aim of this work is to constrain the provenance and tectonic setting of these sediments in a context of a complex evolution of SW Iberian Variscides. For this purpose, we performed a systematic study of petrographical and geochemical signatures of greywackes and shales from the three BAFG formations: Mértola, Mira and Brejeira. Major and trace element composition and ratios suggest heterogeneous source area composition for BAFG shales and greywackes. For the oldest Mértola Formation greywackes, source area is dominated by granitoid rocks with minor mafic input. The latter becomes residual in the Mira Formation. The youngest Brejeira Formation greywackes show clear felsic affiliation associated with an increase in recycled components. The shales of all three BAFG formations denote a granodioritic affiliation. Chemical Index of Alteration (CIA) and Plagioclase Index of Alteration (PIA) values suggest moderate weathering in the source areas of Mértola and Mira formations. These indices, together with A–CN–K relations, point out to steady-state weathering conditions in the source areas of both formations. In contrast, both CIA and PIA values for the Brejeira Formation indicate variable conditions of palaeoweathering, from moderate to intense, as a consequence of non-steady-state conditions probably triggered by tectonic instability in the provenance area. Compared to the greywackes, the shales of all three BAFG formations exhibit higher CIA and PIA values, as well as low K_2O/Al_2O_3 (~0.2) and index of compositional variability (<1), reflecting the cumulative effect of multiple cycles of sedimentary recycling and prolonged chemical weathering history. Major and trace element distribution and upper continental crust-normalized multi-element plots suggest that the sediments of BAFG were derived mainly from a continental arc/active margin with minor contribution from old continental crust. Together, our geochemical data are compatible with BAFG sediments derived mainly from SW border of the Ossa Morena Zone (Gondwanan affinity), with possible contribution from an external (Avalonian) source.

1. Introduction

Provenance analysis of siliciclastic sediments is a powerful tool in elucidating the evolution of ancient sedimentary basins. Diverse techniques based on petrographic and geochemical criteria have been successfully used for this purpose (*e.g.*, Dickinson and Suczek, 1979; Ingersoll et al., 1984; Taylor and McLennan, 1985; Wronkiewicz and Condie, 1987; McLennan, 1989; McLennan et al., 1990, 1993; Zuffa, 1991; McLennan and Hemming, 1992). Geochemistry of major and trace elements of siliciclastic rocks provides valuable information regarding the composition of the sediment source areas, palaeoweathering conditions, hydraulic selection, recycling and, in some cases, the tectonic setting of the sedimentary basins (*e.g.*, Nesbitt and Young, 1982; Bhatia and Crook, 1986; Fedo et al., 1995; Bauluz et al., 2000; Cullers and Podkovyrov, 2002; McLennan et al., 2003; Armstrong-Altrin et al., 2004; Slack et al., 2004; Veizer and Mackenzie, 2005; Etemad-Saeed et al., 2011). A main premise relies on the assumption that certain trace elements (*e.g.*, Th, Sc, Rare Earth Elements (REE)) tend to stay in a particulate phase during weathering, erosion and transport, and thus are transferred to a sedimentary record proportionally to their abundances in the source area (McLennan et al., 1990).

Geodynamic and palaeogeographic reconstructions place the South Portuguese Zone (SPZ, Fig. 1) as an external zone of the Iberian Variscides and thus a possible western equivalent of the northern Variscan belt (*i.e.* southwest England and Ireland, and Rhenohercynian Zone of northwest Germany; Ribeiro et al., 1990, 2007; Oliveira and Quesada, 1998; Franke, 2000; von Raumer et al., 2003; Nance et al.,

* Corresponding author.
E-mail addresses: rjorge@fc.ul.pt (R.C.G.S. Jorge), pfernandes@ualg.pt (P. Fernandes), bmgrodrigues@sapo.pt (B. Rodrigues), zelia.pereira@lneg.pt (Z. Pereira), tomas.oliveira@lneg.pt (J.T. Oliveira).

0037-0738/$ – see front matter © 2012 Elsevier B.V. All rights reserved.
http://dx.doi.org/10.1016/j.sedgeo.2012.12.005

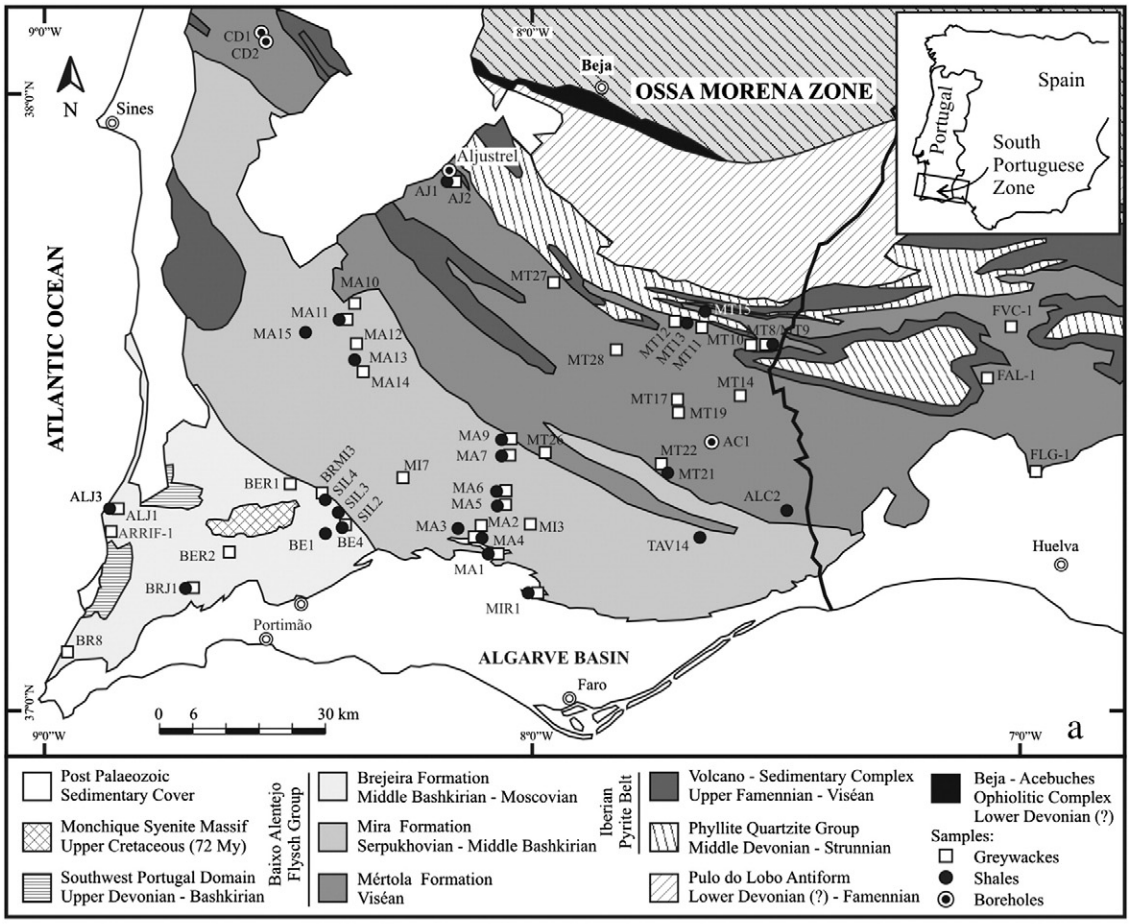

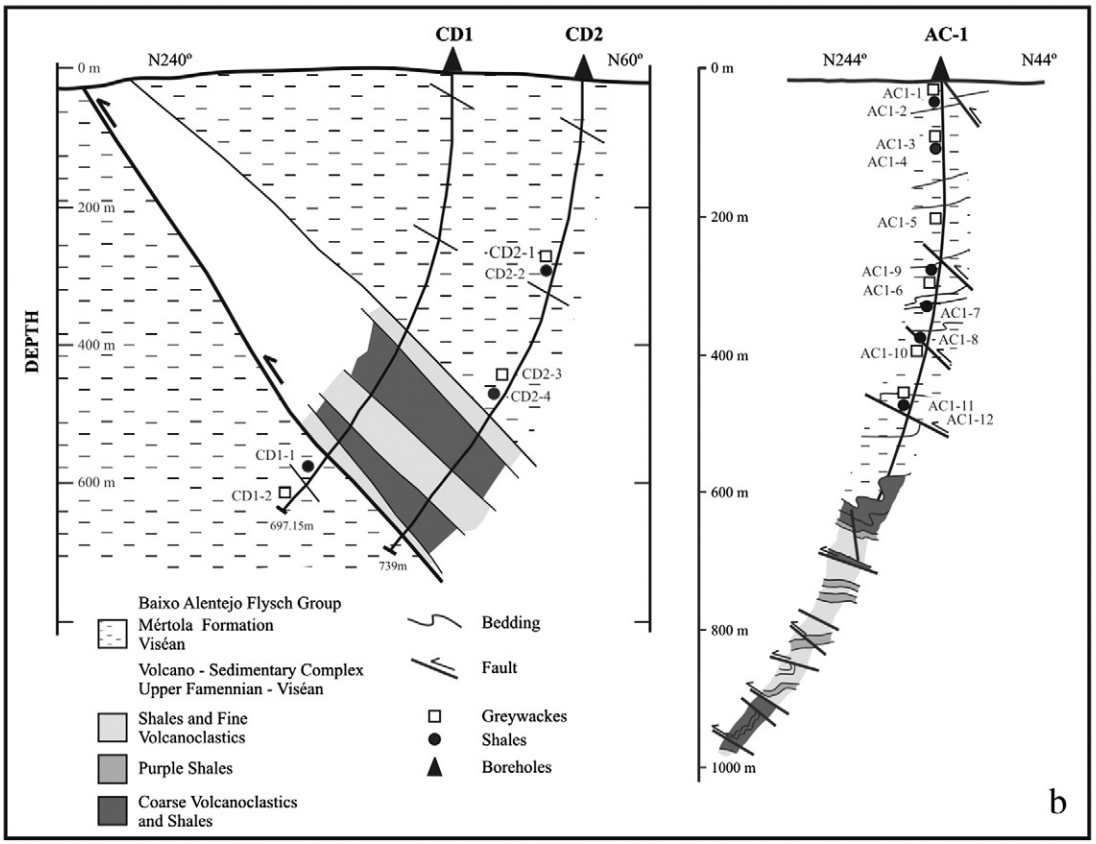

Fig. 1. General geology of the South Portuguese Zone with location of the boreholes and samples used in this work (a); and the sub-surface geology given by the boreholes AC-1, CD1 and CD2 (b).

2010). Within the SPZ, several domains can be recognized, among them a thick siliciclastic succession of the Baixo Alentejo Flysch Group (BAFG). The BAFG is made up, from base to top, by three formations, Mértola, Mira and Brejeira, deposited between Middle Viséan to Moscovian times (Oliveira, 1983, 1990; Pereira, 1999; Pereira et al., 2007, 2008). The deposition of the BAFG has been interpreted as a consequence of the oblique collision between the SPZ, of Avalonian affinity, and the Ossa Morena Zone, of Gondwanan affinity (Oliveira, 1990; Silva et al., 1990; von Raumer et al., 2003; Ribeiro et al., 2007; Jorge et al., 2012).

Previous provenance studies of BAFG have been limited mostly to the paleocurrents and petrographic analyses of the Viséan Mértola Formation (van den Boogaard, 1967; Schermerhorn, 1971; Oliveira, 1983, 1988; Moreno, 1988, 1993; Moreno and Sáez, 1989). The source area for the Mértola Formation sediments has been considered to derive from terranes located to the north of the basin (so called Beja Geanticline, SW border of the Ossa Morena Zone), actively uplifted during Lower and Middle Carboniferous (Schermerhorn, 1971). An opposing view of van den Boogaard (1967) and Oliveira (1983, 1988), proposes the Iberian Pyrite Belt (IPB), together with limited input from external sources, as a main source for Mértola Formation sediments. Moreno (1988, 1993), and Moreno and Sáez (1989) favor the contribution of two coeval turbidite systems fed from two different sources, the OMZ and the IPB.

In this work we present the first systematic study of the detrital modes and major, trace and rare earth element distribution in greywackes and shales of all three formations of the BAFG. The aim of this study is to assess the potential variations in the palaeoweathering conditions, source area composition and sedimentary recycling, to further constrain the tectonic setting of basin in the context of evolution of SW Iberian Variscides.

2. Geological and stratigraphic setting

The northern contact between the SPZ and the Precambrian–Palaeozoic rocks of the OMZ is marked by the presence of the Beja–Acebuches Ophiolite Complex, an important variscan suture. To the south the SPZ is unconformably overlain by the Mesozoic rocks of the Algarve Basin (Fig. 1). The SPZ comprises rocks ranging from Middle Devonian (or older?) to Pennsylvanian in age, which are organized into four geological domains, from north to south: the Pulo do Lobo Antiform (PLA), the IPB, the BAFG and the Southwest Portugal Domain (SPD) (Oliveira, 1990; Oliveira et al., 2006). The core of the PLA comprises highly deformed phyllites, quartzites, minor felsic volcanics and metabasalts with MORB-type geochemical affinities (Munhá, 1983; Quesada et al., 1994). In the northern and southern limbs of this antiform occur siliclastic successions dated by palynomorphs from Lower Frasnian to Upper Famennian (Pereira et al., 2006a). The geological setting of the PLA within the SPZ is still controversial and is interpreted by some authors as an accretionary prism related to a northward dipping subduction of late Palaeozoic Rheic ocean under the OMZ (Munhá et al., 1986; Silva et al., 1990; Fonseca and Ribeiro, 1993; Quesada et al., 1994; Nance et al., 2010) and by others as a complex antiform structure resulting from the superimposition of an accretionary prism by a discordant sedimentary basin contemporaneous to the IPB detritic substrate (Oliveira et al., 2006; Pereira et al., 2006a).

The IPB is formed by the Phyllite–Quartzite Group (PQ) at the base and the Volcano-Sedimentary Complex (VSC) at the top of the succession. The PQ comprises of a detrital sequence of shales and sandstones with occasional bioclastic limestones in the upper levels (Oliveira, 1990). The PQ was laid down in a shallow water environment, possibly a large marine siliciclastic platform affected by wave and storm events (Moreno and Sáez, 1990; Oliveira, 1990; Moreno et al., 1996; Jorge et al., 2007). The compositional maturity of the PQ sediments and their geochemical and isotope signatures are consistent with a passive continental margin depositional setting (Jorge et al., 2006, 2012). The PQ's thickness is in excess of 1000 m and its base is not known. The upper levels are dated as Middle to Upper Devonian (Givetian to Famennian) based on various palaeontological indicators (Lake et al., 1988; Oliveira, 1990; González, 2005; Pereira et al., 2008).

The VSC represents a submarine volcanic succession interbedded with abundant siliciclastic rocks and minor Si–Fe–Mn exhalites (Barriga, 1990; Oliveira, 1990). The magmatism in the IPB was generated within an intracontinental environment affected by transtensil tectonics and is represented by a bimodal, predominantly felsic suite (Munhá, 1983; Silva et al., 1990; Mitjavila et al., 1997). The architecture of the felsic volcanic centers is defined by lava–cryptodome–pumice cone volcanoes (Rosa et al., 2010). The volcanic rocks are subordinate, comprising only about 25% of the succession of the VSC (Tornos, 2006). The siliciclastic rocks are represented by black shales, purple shales and siltstones. The VSC hosts the world's largest province of volcanic-hosted massive sulfides, of more than 88 deposits including several giants and world class units (*e.g.*, Barriga, 1990; Saez et al., 1999; Tornos, 2006). The thickness of the VSC varies from few tens of meters to more than 1000 m. Sediments interbedded with the volcanics yielded palynomorphs (and rare conodonts) that date the VSC from Upper Devonian to Upper Viséan (Oliveira, 1990; Oliveira et al., 2004; Pereira et al., 2008).

The deposition of the BAFG turbiditic sediments resulted from the inversion in the tectonic regime of the SPZ that started in the Middle Viséan, as a consequence of the oblique collision between the SPZ and the OMZ which created a major compressive regime. During this phase the tectonic stacking created by south verging folds and thrust faults allowed a development of a basin, probably a foreland, where the BAFG accumulated (Oliveira, 1990; Ribeiro et al., 1990, 2007; Silva et al., 1990).

The Middle to Upper Viséan Mértola Formation of the BAFG consists of greywackes interbedded with shales, siltstones, rare conglomerates and mudflow deposits. The majority of the greywackes exhibit sedimentary features typical of proximal turbiditic deposits, organized in several thinning-upward sequences resulting from lateral lobe migration and avulsion. Palaeocurrent studies in the Mértola region indicate progradation of the turbidite lobes to S–SW (Oliveira, 1983, 1988). Thick shaley intervals within the Mértola Formation turbiditic lobes contain Upper Viséan ammonoids fauna and miospores. The Mértola Formation is in excess of 1000 m thick (Oliveira, 1983, 1988). At the boundary between the Mértola and the younger Mira Formation occurs a laterally continuous 50–100 m thick belt of black shales and siltstones. Uppermost Viséan ammonoids from these sediments may indicate a period of major transgression *ca.* 330–328 My.

The Mira Formation comprises greywackes interbedded with shales and rare conglomerate beds. The turbidites of the Mira Formation are generally thinner bedded and have fewer sand-rich horizons than those from the Mértola Formation. The few available palaeocurrent data indicate southwest progradation of sedimentary lobes. Ammonoid faunas from the Mira Formation shale beds point out a Serpukhovian to Middle Bashkirian age (Oliveira, 1990).

The Brejeira Formation is made up by greywackes, shales and quartzwackes, and, similarly to the other two formations, exhibits an overall turbiditic character. The basal part of this formation comprises a 5 to 10 km wide belt, exhibiting thick beds of matrix poor quartzwackes interbedded with shales (Oliveira et al., 1979; Oliveira, 1990). Another belt comprising thick-bedded matrix rich greywackes and shales occupies a vast area to the southwest. Coarse-grained greywackes of this last belt overlie the lithologies of the SPD, in some places on an erosional contact. Palaeocurrents measured in the northern quartz-rich turbiditic belt exhibit complex flow patterns with directions to SE and E and, at a lesser extent, to the SW (Oliveira, 1983). In the coastal sections of the Brejeira Formation flow directions of palaeocurrents are to the N. Detailed studies of the palynomorphs and ammonoid fauna of the Brejeira Formation indicate ages ranging from the Upper Bashkirian (miospore biozone FR), near the contact with the Mira Formation, to Lower Moscovian (miospore biozone OT), in the coastal sections to the north

of Cape Saint Vincent (Pereira, 1999; Pereira et al., 2008). In Upper Bashkirian–Moscovian times the progradation of the turbiditic deposition reached the SPD.

3. Sampling and analytical techniques

A total of 78 representative samples of shales and greywackes from Mértola, Mira and Brejeira Formations were collected from outcrops (60) and from mineral exploration boreholes (18) in the Portuguese and Spanish sectors of the SPZ (Fig. 1a and b, respectively). Borehole samples were collected from three mineral exploration boreholes (AC1, CD1 and CD2) in the Portuguese sector of the SPZ. Figs. 1 and 2 show the geographic distribution of the samples and their stratigraphic position within the BAFG units. The borehole samples all belong to the lower levels of the Mértola Formation in close relation to the VSC. Borehole AC1 (Alcaria da Cova) has a total depth of *ca.* 1000 m. The first 590 m of this borehole cut lithologies from the Mértola Formation below which occurs stratigraphic contact with the VSC rocks. Boreholes CD1 (Cidrão 1) and CD2 (Cidrão 2) show a *ca.* 200 m thick VSC succession thrusted over the Mértola Formation Greywackes and shales of the Mértola Formation occur stratigraphically above the VSC succession, in the hanging wall of the thrusted block. Thus, the samples collected from borehole CD1 are from the Mértola Formation in the footwall of the thrust block whereas the samples from the borehole CD2 are from the hanging wall block (Fig. 1).

The studied samples were classified into greywacke and shale based on regional geological comparison (*e.g.* Oliveira et al., 1979; Oliveira, 1983, 1990) and petrographic study. A group of 41 thin sections of BAFG greywackes were studied in detail, of those 20 from Mértola, 13 from Mira and 8 from Brejeira Formations. Point counting of an average of 320 framework grains per sample was performed according to the method of Gazzi–Dickinson (Ingersoll et al., 1984). The cement and matrix (pseudomatrix) were not counted.

A group of 74 samples from boreholes (14) and outcrops (60) were selected for the whole-rock geochemistry analysis. This group includes 41 greywackes (5 borehole samples, 36 from outcrops) and 33 shales (9 borehole samples, 24 from outcrops). All samples were cleaned and all weathering coats removed. Samples were ground in an agate mill at the Geology Department of Faculty of Sciences of Lisbon University.

The analytical procedures used were inductively coupled plasma-optical emission spectrometry (ICP-OES) for major elements analysis plus Ba, Sr and Zr; and inductively coupled plasma-mass spectrometry (ICP-MS) for the majority of trace elements. All analyses were

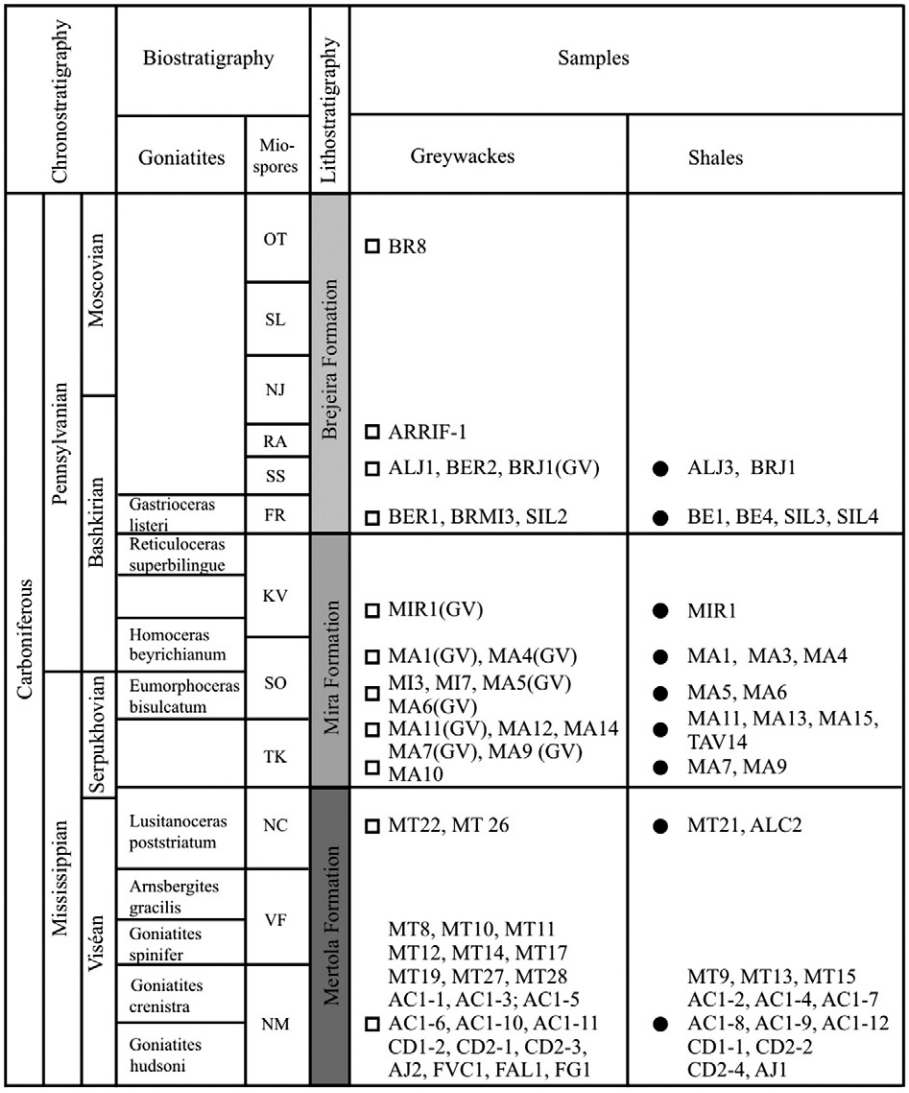

Fig. 2. Stratigraphic position of the BAFG greywackes and shales.

performed at Activation Laboratories Ltd. (ACTLABS, Ontario, Canada) following standard procedures for each method. Alkaline dissolution with lithium metaborate/tetraborate followed by nitric acid dissolution was performed for all analyses, except for the determination of Cu, Ni and Zn, for which acid digestion was carried out. The standards used were: NIST 694, DNC-1, BIR-1, FK-N, NIST 1633b, SY-3, W-2, NIST 696, JSD-3, CTA-AC-1, WMG-1, GXR-1, MICA-FE, GXR-2, LKSD-3 and MAG-1. Appendix 1 shows the analyses for three standard reference materials (BIR-1, W-2a and DNC-1) and detection limits for each element. The calculated reproducibility is better than 3% for major-element contents (SiO_2, TiO_2, Al_2O_3; Fe_2O_3, MnO, MgO, CaO, Na_2O, K_2O and P_2O_5), <4% for rare earth elements (REE) and ≈5% for high field strength elements (HFSE). Additional information on analytical procedures is available at http://www.actlabs.com. For the weight/weight conversion from major oxides to atoms conversion factors were used, according to Ragland (1989).

4. Petrography

The greywackes of the Mértola, Mira and Brejeira Formations exhibit differences in the relative abundances of their major components, quartz, feldspar and lithoclasts (Appendix 2). The average modal compositions of greywackes from the Mértola, Mira and Brejeira Formations are $Qt_{46.2}F_{26.9}L_{26.9}$, $Qt_{61.7}F_{7.6}L_{30.7}$, and $Qt_{83.1}F_{6.7}L_{10.1}$, respectively, where Qt is the total quartz, F the sum of plagioclases and K-feldspar and L is the sum of all lithic fragments (volcanic, sedimentary and metasedimentary). Matrix constitutes 20–30% of all greywackes studied. The major clastic component of the Mértola Formation is quartz, which shows rounded to sub-rounded forms. Quartz grains often show diffuse boundaries and irregular contacts due to some degree of dissolution into the matrix. In all samples, the contents in feldspar and lithic components, mainly represented by volcanic rocks, vary significantly (Fig. 3a, b). The abundance of opaque minerals, mainly diagenetic

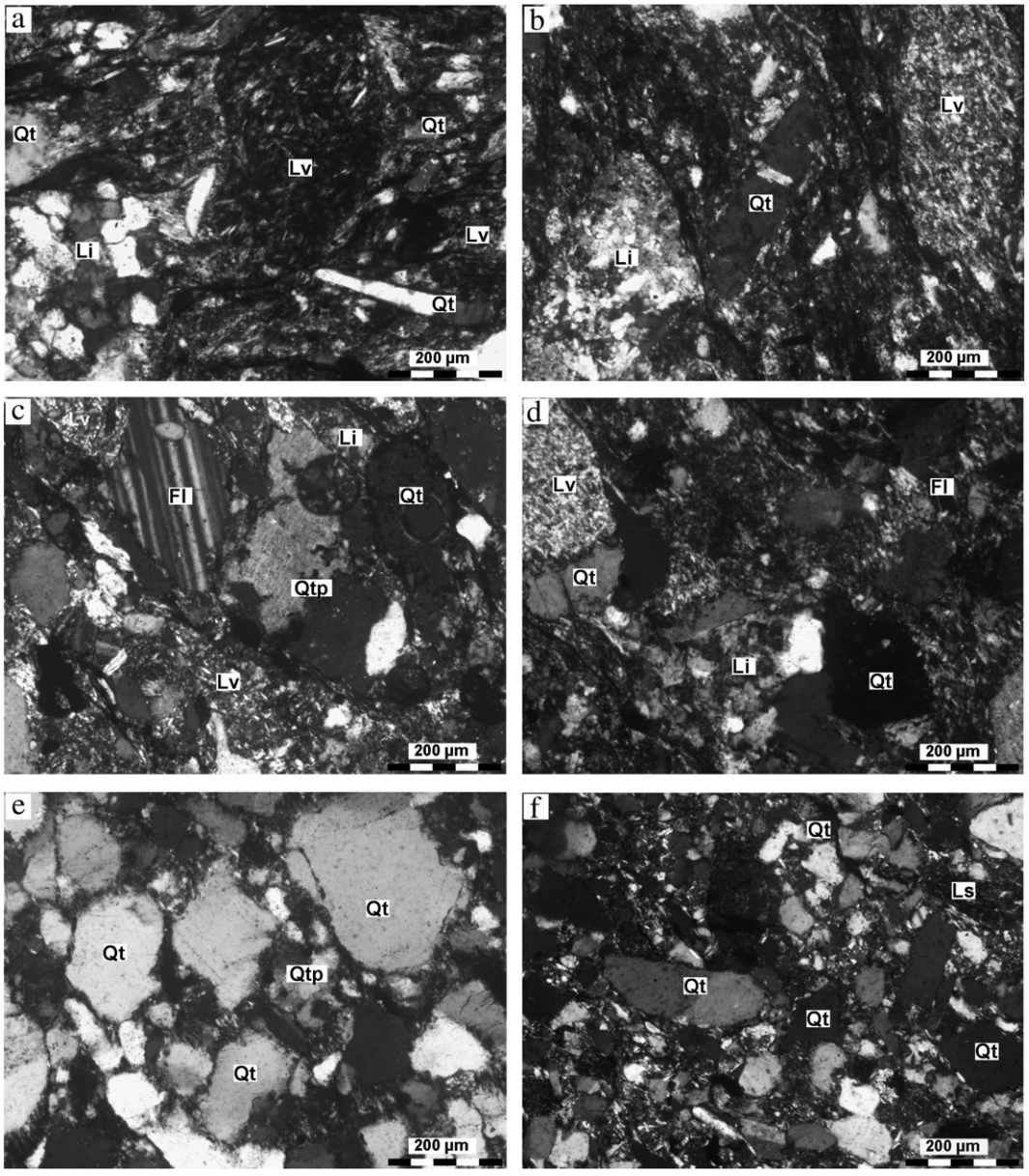

Fig. 3. Photomicrographs of detrital components in the Baixo Alentejo Flysch Group greywackes under cross-polarized light. (a–b) Samples from the Mértola Formation show large rock fragments and several types of subangular quartz with low esfericity. (b–c) Mira Formation samples exhibit fewer lithoclast fragments. (e–f) Brejeira Formation samples show very well calibrated clasts mainly composed of quartz. Abbreviations: Qt — monocrystaline quartz; Qtp — polycrystaline quartz: Pl — plagioclase; Ls — siliciclastic rock fragment; Lv — vulcanic rock fragment; and Li — igneous rock fragment.

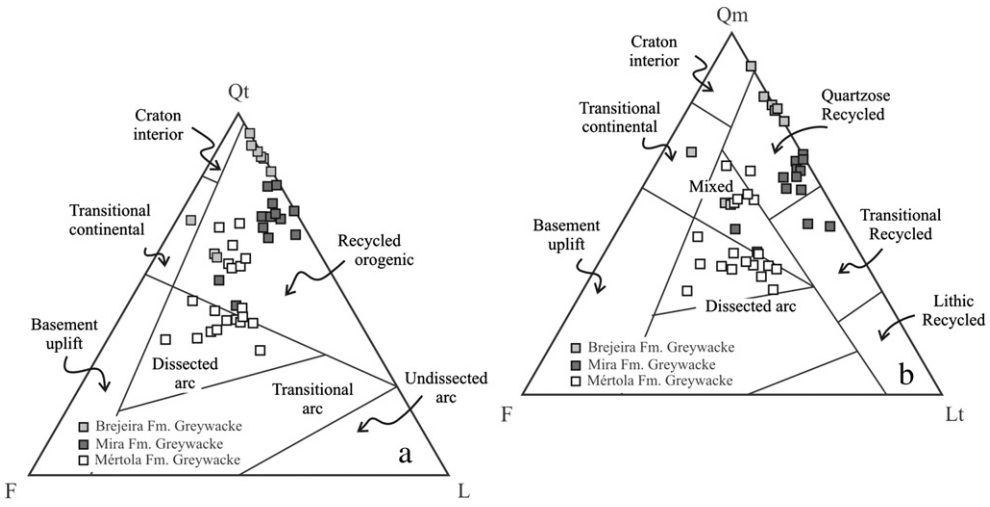

Fig. 4. Plots of BAFG greywackes on triangular QtFL (a) and QmFLt (b) discriminant provenance diagrams. After Dickinson et al. (1983).

pyrite, is relatively high. Tourmaline and zircon are observed as the main accessory minerals. In Mira greywackes, quartz is the major component, occurring with rounded to angular forms. Lithoclasts of volcanic grains are the second most abundant modal grains, with few exceptions (Fig. 3c, d). Feldspars, as average, represent less than 10% of the clastic grains. The occurrence of opaque minerals is relatively high. Accessory heavy minerals are represented by zircon, rutile and tourmaline. Brejeira greywackes are mainly composed of quartz and exhibit well-sorted grains. Abundant quartz grains assume rounded to sub-rounded forms, often with sutured contacts and showing the effects of pressure solution. Lithoclasts are mostly composed by sedimentary and metasedimentary grains. Volcanic grains are rare (Fig. 3e, f). Opaque minerals are relatively abundant. Tourmaline, zircon and rutile are more abundant in the Brejeira than both the Mértola and Mira greywackes.

In the QtFL provenance ternary diagram (Dickinson et al., 1983) the greywackes from the BAFG do not fall into the same field (Fig. 4a). The Mértola greywackes plot in the field of dissected magmatic arc and recycled orogenic sources whereas the Brejeira greywackes plot almost exclusively in the field of recycled orogenic sources. Mira samples plot mainly in the recycled orogenic field, showing a distribution stretching from Brejeira to Mértola samples. On the QmFLt triangular diagram (monocrystalline quartz, feldspar and total lithic fragments) the Mértola, Mira and Brejeira greywackes all exhibit a similar distribution patterns (Fig. 4b; after Dickinson et al., 1983). These data suggest the initial derivation of the BAFG sediments from the dissected magmatic arc, with gradual increase in recycled components, most pronounced in the youngest Brejeira Formation.

5. Whole-rock geochemistry

Mean chemical composition, variation range and standard deviation for shales and greywackes from the three BAFG formations are listed in Table 1, and Appendix 3 contains geochemistry analyses for all samples. The geochemistry data for borehole and outcrop samples are presented together, since no statistically significant compositional differences between these two groups were found. Fig. 5 shows plots of average major and trace elements from the BAFG greywackes and shales normalized to UCC values (Taylor and McLennan, 1985).

5.1. Major elements

The geochemistry of major elements clearly reflects the mineralogy of the greywackes from the three BAFG formations (Table 1). Average SiO_2 and Al_2O_3 in Mértola greywackes are $64.8 \pm 3.4\%$ and $15.8 \pm 1.8\%$, respectively. Similar values are recorded for the Mira Formation ($SiO_2 = 68.8 \pm 5.8\%$ and $Al_2O_3 = 13.2 \pm 1.7\%$). The Brejeira greywackes show higher SiO_2 ($78.1 \pm 5.7\%$) and lower Al_2O_3 ($9.0 \pm 1.2\%$) contents reflecting a greater amount of detrital quartz in these rocks. Shales from Mértola, Mira and Brejeira have average SiO_2 content of $58.1 \pm 1.6\%$, $55.3 \pm 3.3\%$ and $54.1 \pm 2.8\%$, respectively. The Al_2O_3 contents for these rocks are similar (Mértola $= 19.0 \pm 0.9\%$, Mira $= 22.2 \pm 2.0\%$, Brejeira $= 24.0 \pm 1.9\%$).

The index of compositional variability (ICV) $[(Fe_2O_3 + K_2O + Na_2O + CaO + MgO + MnO + TiO_2)/Al_2O_3]$ can be used as a measure of compositional maturity of mudstones (Cox et al., 1995). Immature mudstones rich in non-clay silicate minerals show ICV values greater than one. In contrast, more mature mudstones exhibit values below one, reflecting mineralogy with the predominance of clay minerals (Cullers and Podkovyrov, 2002). The average values of ICV for the Mértola, Mira and Brejeira shales are 0.9 ± 0.05 (1.0–0.8), 0.7 ± 0.1 (0.8–0.5) and 0.6 ± 0.03 (0.7–0.6), respectively. The mean K_2O/Al_2O_3 ratio for all groups of analyzed shales is ~0.2. Together, the ICV values and the K_2O/Al_2O_3 ratios suggest compositional maturity of the BAFG shales (Table 2).

Greywackes of Mértola, Mira and Brejeira Formation have average K_2O/Na_2O ratios of 0.7 ± 0.7 (3–0.3), 0.9 ± 0.5 (2.5–0.5) and 2.6 ± 2.2 (6.4–1.0), respectively Table 2. In the ternary plot $(Fe_2O_3 + MgO) - Na_2O - K_2O$ of Blatt et al. (1980) Mértola and Mira greywackes plot along the fields of sodic and ferromagnesian potassic (Fig. 6). All but one Brejeira greywackes are limited to the field of ferromagnesian potassic.

Compared with the UCC values, all analyzed greywackes, with the exception of Brejeira ones, exhibit similar MgO contents and have slightly higher TiO_2, Fe_2O_3 and MnO. Variable depletion in CaO, Na_2O and K_2O is observed (Fig. 5a). Shales show a similar pattern, with a generalized slight enrichment in K_2O and variable depletion in MgO (except for the Mértola Formation), CaO and Na_2O (Fig. 5b).

SiO_2 exhibits variable negative correlation with Al_2O_3, TiO_2, Fe_2O3, K_2O, MnO, MgO and P_2O_5 for all analyzed greywackes, reflecting the quartz dilution effect (Fig. 7a–d). Al_2O_3 correlates well with K_2O, Fe_2O_3 and TiO_2 (Fig. 7e). In the shales, SiO_2 also shows negative correlation with a majority of major elements, and Al_2O_3 shows positive correlation with K_2O, MgO, Fe_2O_3 and TiO_2 (Fig. 7a–e). This suggests that chemical weathering in the source area was a dominant factor controlling the mineralogy of weathered products. In fact, during

Table 1
Average whole-rock composition of the BAFG greywackes and shales.

Lithology	Greywackes											
Formation	Mértola				Mira				Brejeira			
	n = 20	σ	Max.	Min.	n = 13	σ	Max.	Min.	n = 8	σ	Max.	Min.
wt.%												
SiO_2	64.76	3.40	69.76	57.19	68.84	5.79	75.83	55.00	78.09	5.69	86.33	66.74
TiO_2	0.80	0.10	0.96	0.63	0.74	0.09	0.84	0.54	0.66	0.06	0.72	0.56
Al_2O_3	15.80	1.78	20.21	13.79	13.20	1.67	14.91	8.78	8.96	1.20	10.75	7.43
$Fe_2O_{3(T)}$	6.25	1.18	7.95	3.49	5.73	1.37	8.49	3.71	4.38	2.80	10.36	0.48
MnO	0.08	0.02	0.14	0.04	0.13	0.15	0.51	0.03	0.11	0.20	0.58	0.00
MgO	2.27	0.43	3.31	1.31	2.09	1.26	5.73	1.16	1.01	0.64	2.39	0.16
CaO	0.88	0.61	1.88	0.24	0.86	2.34	8.61	0.05	0.26	0.39	1.11	0.01
Na_2O	3.30	0.92	4.52	1.22	2.05	0.58	2.88	0.57	0.87	0.51	1.48	0.19
K_2O	1.84	0.72	3.63	1.05	1.65	0.25	2.16	1.37	1.32	0.16	1.62	1.15
P_2O_5	0.18	0.03	0.23	0.13	0.12	0.04	0.19	0.06	0.09	0.03	0.13	0.04
LOI	3.94	1.04	6.73	2.72	4.71	3.56	15.42	2.73	3.43	1.90	7.92	2.14
Total	100.09	0.58	100.90	98.84	100.12	0.53	100.90	99.26	99.00	0.72	99.99	97.89
ppm												
Sc	15.4	3.3	23.0	11.0	12.4	2.1	16.0	8.0	7.6	1.5	10.0	6.0
V	122.6	24.1	169.0	79.0	94.6	15.9	117.0	62.0	62.1	14.9	89.0	46.0
Cr	70.0	15.9	120.0	40.0	78.5	15.2	100.0	50.0	55.0	14.1	80.0	40.0
Co	13.8	3.0	20.0	7.0	12.8	4.4	22.0	7.0	10.6	5.6	21.0	1.0
Ni	30.5	9.4	50.0	20.0	23.1	7.5	40.0	20.0	22.5	4.6	30.0	20.0
Cu	27.0	27.9	130.0	10.0	10.8	2.8	20.0	10.0	16.3	17.7	60.0	10.0
Zn	83.0	18.7	120.0	50.0	79.2	14.4	100.0	50.0	71.3	29.0	110.0	30.0
As	8.1	3.4	16.0	5.0	7.7	4.3	18.0	5.0	31.5	55.1	164.0	5.0
Rb	74.5	32.8	160.0	44.0	72.0	9.5	90.0	57.0	59.1	9.2	76.0	48.0
Sr	245.9	76.6	345.0	118.0	97.5	38.0	194.0	60.0	53.4	9.0	72.0	42.0
Y	21.2	5.1	31.2	13.8	23.0	3.0	28.3	18.0	24.5	3.1	28.7	19.4
Zr	162.4	18.7	206.0	131.0	220.0	47.7	278.0	148.0	286.4	47.6	389.0	233.0
Nb	8.0	2.3	15.4	6.0	9.8	1.0	10.8	7.2	10.7	1.1	12.4	9.3
Sn	1.3	0.8	3.0	0.5	73.3	252.6	914.0	2.0	3.3	3.6	12.0	1.0
Cs	3.8	1.5	7.0	2.1	2.9	0.7	4.3	1.8	2.1	0.4	2.7	1.5
Ba	373.7	84.4	503.0	228.0	266.3	46.7	336.0	200.0	213.5	43.3	302.0	168.0
Hf	4.6	0.5	5.4	3.4	5.8	1.2	7.4	3.8	7.1	1.2	9.2	5.5
Ta	0.7	0.2	1.3	0.5	0.9	0.1	1.1	0.7	0.9	0.1	1.0	0.8
Pb	15.7	4.4	23.0	9.0	8.4	3.2	14.0	5.0	42.1	81.2	241.0	5.0
Th	9.0	1.8	13.5	6.3	9.0	1.7	11.6	5.7	7.3	0.5	8.2	6.7
U	2.8	0.5	3.6	2.2	2.9	0.5	3.7	2.1	2.2	0.3	2.6	1.7
La	29.1	5.5	42.1	22.4	26.4	4.5	36.0	18.2	26.9	3.2	32.4	22.8
Ce	58.5	10.6	78.0	46.7	54.2	9.3	74.4	37.2	57.0	6.0	66.0	48.7
Pr	6.7	1.3	9.4	5.0	6.7	1.2	9.3	4.4	6.8	0.7	8.3	6.1
Nd	24.6	4.2	33.0	18.3	23.3	3.8	30.8	16.4	24.3	2.7	29.3	20.6
Sm	4.8	0.9	6.4	3.5	4.7	0.7	6.0	3.5	4.9	0.6	6.0	4.1
Eu	1.3	0.2	1.8	1.0	1.1	0.2	1.4	0.9	1.1	0.1	1.3	0.9
Gd	4.3	0.9	6.2	2.6	4.2	0.5	5.1	3.5	4.5	0.6	5.6	3.6
Tb	0.7	0.2	1.0	0.4	0.7	0.1	0.8	0.6	0.7	0.1	0.9	0.6
Dy	3.8	0.9	5.6	2.6	4.0	0.5	4.9	3.2	4.3	0.5	4.9	3.5
Ho	0.7	0.2	1.0	0.5	0.8	0.1	1.0	0.6	0.9	0.1	1.0	0.7
Er	2.1	0.5	3.2	1.5	2.4	0.3	2.9	1.8	2.5	0.3	2.9	2.1
Tm	0.3	0.1	0.5	0.2	0.4	0.0	0.4	0.3	0.4	0.0	0.4	0.3
Yb	2.1	0.5	3.0	1.6	2.3	0.3	2.7	1.7	2.4	0.3	2.8	2.0
Lu	0.3	0.1	0.5	0.2	0.3	0.0	0.4	0.3	0.4	0.0	0.4	0.3
Lithology	Shales											
Formation	Mértola				Mira				Brejeira			
	n = 15	σ	Max.	Min.	n = 12	σ	Max.	Min.	n = 6	σ	Max.	Min.
wt.%												
SiO_2	58.13	1.64	61.26	55.05	55.30	3.33	61.96	50.46	54.10	2.77	56.63	49.52
TiO_2	0.91	0.04	0.96	0.82	1.03	0.08	1.15	0.92	1.03	0.12	1.13	0.82
Al_2O_3	18.97	0.87	20.81	17.82	22.24	2.00	27.16	19.16	23.96	1.92	27.60	22.37
$Fe_2O_{3(T)}$	7.03	0.56	7.98	5.97	6.76	1.13	8.21	4.50	6.55	0.77	7.49	5.42
MnO	0.10	0.04	0.22	0.06	0.09	0.07	0.28	0.03	0.04	0.03	0.11	0.01
MgO	2.69	0.25	3.15	2.19	2.02	0.43	2.96	1.33	1.54	0.27	1.88	1.11
CaO	0.70	0.51	2.06	0.26	0.17	0.19	0.73	0.02	0.09	0.06	0.19	0.04
Na_2O	1.42	0.43	2.49	0.81	0.79	0.23	1.18	0.43	0.69	0.19	0.87	0.34
K_2O	3.79	0.44	4.60	2.81	4.28	0.60	5.44	3.68	4.73	1.01	6.75	3.99
P_2O_5	0.20	0.06	0.39	0.14	0.16	0.13	0.56	0.06	0.14	0.02	0.16	0.10
LOI	5.13	0.74	6.84	4.32	6.86	0.95	8.17	5.55	7.32	0.98	8.76	6.34
Total	99.10	0.51	99.91	98.29	99.69	0.51	100.80	99.01	100.19	0.35	100.60	99.78

(continued on next page)

Table 1 (*continued*)

Lithology	Shales											
Formation	Mértola				Mira				Brejeira			
	n = 15	σ	Max.	Min.	n = 12	σ	Max.	Min.	n = 6	σ	Max.	Min.
ppm												
Sc	22.5	2.0	27.0	18.0	24.0	2.7	29.0	19.0	23.0	2.4	27.0	20.0
V	160.8	15.5	197.0	139.0	180.2	19.1	224.0	144.0	192.0	19.7	215.0	164.0
Cr	84.0	10.6	110.0	70.0	119.2	13.8	150.0	100.0	130.0	8.9	140.0	120.0
Co	18.5	4.5	28.0	10.0	13.2	5.8	25.0	3.0	16.0	11.1	36.0	7.0
Ni	36.7	16.3	70.0	20.0	37.5	31.9	130.0	20.0	26.7	16.3	60.0	20.0
Cu	51.3	10.6	70.0	30.0	44.2	14.4	60.0	10.0	38.3	14.7	60.0	20.0
Zn	111.3	17.3	140.0	70.0	103.3	21.9	140.0	70.0	131.7	47.9	210.0	80.0
As	10.6	4.9	20.0	5.0	14.6	7.0	27.0	5.0	13.0	9.1	25.0	5.0
Rb	151.9	21.7	211.0	119.0	196.3	25.9	250.0	175.0	224.5	36.9	298.0	201.0
Sr	150.1	42.4	209.0	77.0	151.7	33.6	216.0	110.0	110.7	17.1	127.0	80.0
Y	29.6	2.7	33.9	26.1	37.2	12.5	75.8	29.5	38.7	1.0	40.2	37.3
Zr	149.7	9.0	167.0	133.0	179.1	22.5	215.0	138.0	183.5	22.5	208.0	145.0
Nb	10.6	0.9	12.6	9.5	15.4	1.8	17.7	11.7	19.1	1.8	20.5	16.8
Sn	1.2	1.1	3.0	0.5	3.5	1.6	7.0	0.5	4.2	0.4	5.0	4.0
Cs	7.7	1.5	10.9	5.8	9.3	1.7	12.0	6.6	10.7	1.7	13.0	7.7
Ba	767.7	113.9	975.0	557.0	684.7	117.4	867.0	520.0	740.2	267.0	1226.0	541.0
Hf	4.4	0.3	4.8	4.1	5.0	0.6	6.0	4.2	5.1	0.7	5.8	3.8
Ta	1.0	0.1	1.1	0.9	1.3	0.1	1.5	1.0	1.5	0.2	1.7	1.1
Pb	20.7	7.0	36.0	11.0	13.9	9.4	33.0	5.0	19.3	17.3	50.0	5.0
Th	12.3	1.2	15.0	10.6	14.9	1.3	17.0	12.8	16.2	0.9	17.8	15.0
U	3.5	0.4	4.6	2.9	4.2	0.8	5.8	3.2	4.3	0.5	5.4	3.9
La	35.8	4.1	47.0	32.0	46.3	6.2	57.7	37.2	51.6	5.2	61.5	46.5
Ce	74.4	6.7	87.5	63.9	95.2	13.4	119.0	75.1	106.7	10.8	128.0	97.3
Pr	8.4	0.8	10.3	7.5	12.0	1.8	15.5	9.3	12.9	0.6	13.9	12.2
Nd	31.2	2.5	36.0	27.9	41.2	7.2	58.1	33.4	44.5	2.5	49.0	41.4
Sm	6.1	0.6	7.2	5.3	8.4	1.9	13.4	6.8	9.1	0.6	10.2	8.5
Eu	1.3	0.1	1.5	1.0	1.9	0.6	3.8	1.5	2.0	0.1	2.2	1.9
Gd	5.8	0.8	7.2	4.9	7.1	2.2	14.0	5.4	7.5	0.6	8.5	6.7
Tb	1.0	0.1	1.1	0.8	1.1	0.3	2.2	0.9	1.2	0.1	1.3	1.1
Dy	5.2	0.5	6.0	4.5	6.6	2.0	12.6	5.2	7.0	0.4	7.7	6.6
Ho	1.0	0.1	1.2	0.9	1.3	0.4	2.4	1.0	1.4	0.1	1.5	1.3
Er	3.0	0.3	3.5	2.6	3.9	1.0	6.8	3.0	4.1	0.2	4.3	3.9
Tm	0.5	0.0	0.5	0.4	0.6	0.1	0.9	0.4	0.6	0.0	0.6	0.6
Yb	2.9	0.2	3.4	2.5	3.6	0.7	5.4	2.9	3.9	0.2	4.1	3.6
Lu	0.4	0.0	0.5	0.4	0.6	0.1	0.8	0.4	0.6	0.1	0.7	0.5

chemical weathering Al and Ti tend to be stable or residual; K and Mg are fixed in clay minerals, while Ca is usually bleached (Feng and Kerrich, 1990).

5.2. Trace elements

As expected, average trace elements concentrations of the BAFG greywackes are lower than those in the shales, due to the quartz dilution effect. With the exception of the Brejeira, all other greywackes exhibit variable enrichment in transition trace elements (TTE) Sc, V, Cr, Ni and Co relative to the UCC (Fig. 5c). In Mértola and Mira greywackes, the degree of enrichment undergoes great sample-to-sample variability, although this is more pronounced in the Mértola Formation. Large Ion Lithophile Elements (LILE) concentration in greywackes is generally lower than in the UCC. The BAFG shales exhibit enrichment in TTE similar to those observed in greywackes (Fig. 5d). The enrichment in Rb, Ba and Cs, together with the depletion in Sr, is consistent with the geochemical behavior of K and Ca.

Sc, V and Cr in shales and greywackes show moderate to strong positive correlation with Al_2O_3 and K_2O (Fig. 7f–h), suggesting that abundances of these elements are controlled by K-bearing phyllosilicates. With the exception of Mértola Formation, all analyzed greywackes exhibit variable enrichment in Zr compared to the UCC (190 ppm; Taylor and McLennan, 1985), best pronounced in Brejeira greywackes, where average Zr content is 286 ± 48 ppm (389–233 ppm), probably reflecting an increased influence of hydraulic selection and/or sedimentary recycling. All greywackes and shales exhibit high positive correlation between Zr–Hf and Nb–Ta indicating that both pairs of elements are fixed in zircon and rutile. Additionally, Th and Al_2O_3 show positive correlation in all analyzed rocks, once again pointing out the importance of phyllosilicates in controlling their abundances.

5.3. Rare earth elements

The average of total of REE (∑REE) contents for Mértola, Mira and Brejeira greywackes (139, 131 and 137 ppm respectively) are slightly less than the UCC (146.4 ppm; Taylor and McLennan, 1985). Shales from the three formations have variable enrichment in ∑REE (Mértola = 177, Mira = 230 and Brejeira = 253 ppm) relatively to the UCC.

As illustrated in Fig. 8, average chondrite-normalized REE patterns (Taylor and McLennan, 1985) of analyzed rocks are enriched in light REE (LREE) ($La_n/Sm_n < 5$), with the flattened patterns of heavy REE (HREE) (Gb_n/Yb_n: 1.5–2). The Eu anomaly (Eu/Eu*) is variable. For Mértola, Mira and Brejeira greywackes the values of Eu/Eu* are 0.84 ± 0.10, 0.75 ± 0.08, and 0.68 ± 0.01, respectively. In shales these values are 0.66 ± 0.07 for Mértola, 0.73 ± 0.05 for Mira, and 0.72 ± 0.02 for Brejeira Formation.

∑LREE and ∑HREE of analyzed shales show weak positive correlation with Al_2O_3. Additionally, ∑HREE of Mira and Brejeira shales show strong positive correlation with Y (r = 0.99 and r = 0.73, respectively) reflecting the role of Y-rich minerals in the control of REE contents of these rocks. ∑LREE and ∑HREE of Mértola greywackes exhibit significative positive correlation with Al_2O_3 (r = 0.74 and r = 0.89), TiO_2 (r = 0.63 and r = 0.80) and Y (r = 0.90 and r = 0.99). ∑HREE in these rocks do not correlate with P_2O_5. ∑LREE and ∑HREE of Mira greywackes show positive correlation with Al_2O_3 (r = 0.55 for both) and P_2O_5 (r = 0.55 and r = 0.66). In the

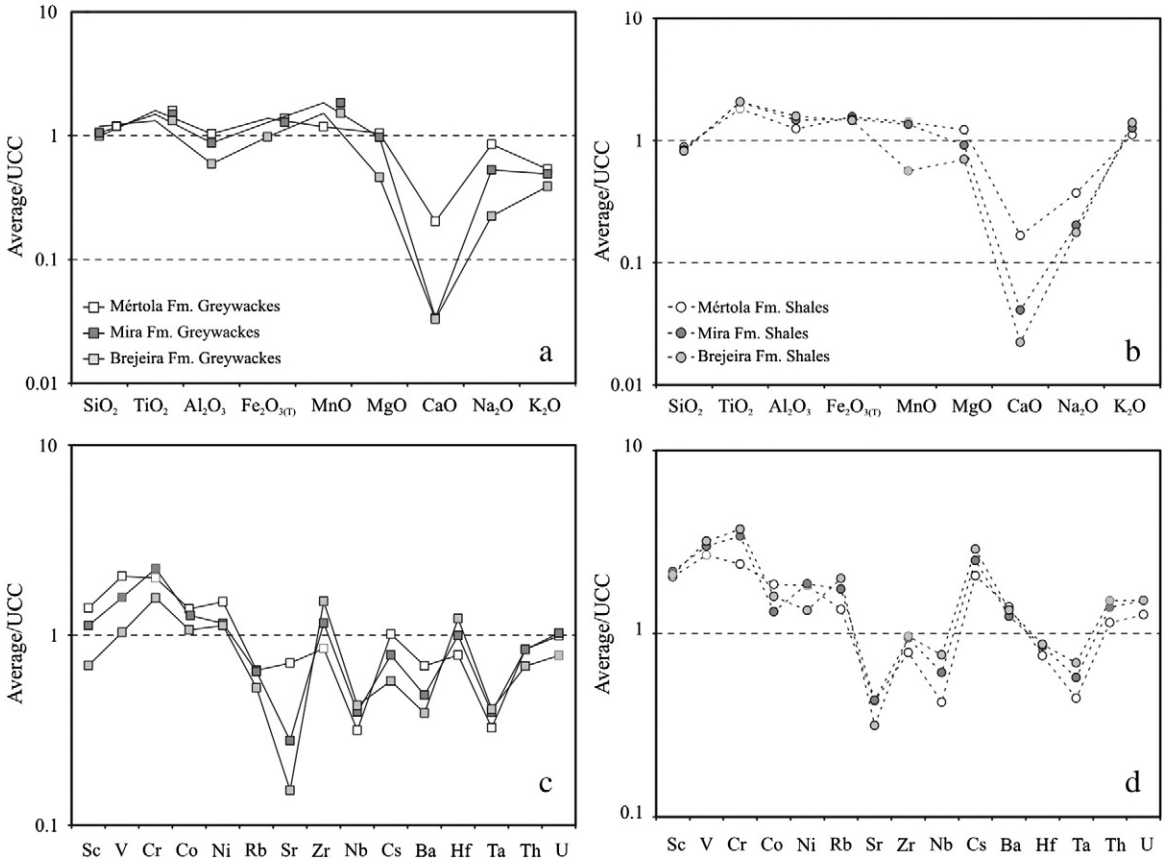

Fig. 5. UCC-normalized average major (a, b) and trace (c, d) elements composition in different groups of the BAFG greywackes (a, c) and shales (b, d). Normalizing values of UCC after Taylor and McLennan (1985).

Table 2
Elemental ratios in the BAFG greywackes and shales.

Lithology	Greywackes											
Formation	Mértola				Mira				Brejeira			
	n = 20	σ	Max.	Min.	n = 13	σ	Max.	Min.	n = 8	σ	Max.	Min.
CIA	66.25	3.98	74.02	61.54	71.16	2.79	76.57	66.99	74.61	6.95	83.00	63.34
PIA	69.89	6.50	85.07	63.16	76.36	4.25	86.12	70.10	82.48	9.91	94.61	67.24
ICV	–	–	–	–	–	–	–	–	–	–	–	–
K_2O/Na_2O	0.72	0.67	2.98	0.28	0.92	0.49	2.46	0.51	2.62	2.23	6.37	1.01
K_2O/Al_2O_3	0.11	0.03	0.20	0.07	0.13	0.02	0.16	0.11	0.15	0.01	0.16	0.14
∑REE	139.32	24.91	190.97	108.30	131.43	19.81	173.29	93.03	136.96	13.63	162.14	122.29
∑LREE	123.71	22.00	168.67	97.41	115.28	19.10	156.52	79.77	119.88	12.79	142.04	103.82
∑HREE	14.36	3.11	20.94	9.90	15.04	1.69	17.85	12.15	16.02	1.89	18.81	13.09
Eu/Eu*	0.84	0.10	1.02	0.65	0.75	0.08	0.92	0.62	0.68	0.01	0.70	0.67
La/Sm_n	3.84	0.38	4.85	3.34	3.54	0.42	4.41	2.86	3.44	0.30	3.97	2.94
Gb/Yb_n	1.67	0.25	2.08	1.25	1.53	0.17	1.83	1.25	1.51	0.10	1.68	1.41
Lithology	Shales											
Formation	Mértola				Mira				Brejeira			
	n = 15	σ	Max.	Min.	n = 12	σ	Max.	Min.	n = 6	σ	Max.	Min.
CIA	71.09	3.46	74.84	64.49	78.14	1.81	81.19	74.68	78.93	0.99	80.17	77.26
PIA	80.53	5.44	88.47	70.38	91.67	2.36	94.85	87.82	93.53	1.65	96.14	91.49
ICV	0.88	0.05	0.97	0.81	0.69	0.08	0.81	0.53	0.61	0.03	0.67	0.59
K_2O/Na_2O	2.94	1.10	5.68	1.37	5.83	1.73	8.84	3.22	8.19	5.80	19.85	4.93
K_2O/Al_2O_3	0.20	0.02	0.23	0.15	0.19	0.02	0.22	0.16	0.20	0.02	0.24	0.18
∑REE	176.91	14.85	211.93	160.43	229.66	35.06	312.70	185.25	253.08	17.97	285.80	233.68
∑LREE	155.85	13.80	187.78	139.05	202.95	29.58	263.70	163.54	224.74	17.14	255.65	205.86
∑HREE	19.77	1.82	22.81	17.19	24.81	6.64	45.17	20.10	26.35	0.88	28.13	25.90
Eu/Eu*	0.66	0.07	0.79	0.56	0.73	0.05	0.85	0.66	0.72	0.02	0.74	0.70
La/Sm_n	3.71	0.33	4.24	2.92	3.54	0.42	4.38	2.71	3.57	0.33	4.18	3.21
Gb/Yb_n	1.61	0.20	1.95	1.30	1.58	0.25	2.09	1.20	1.58	0.19	1.93	1.37

$CIA = [Al_2O_3/(Al_2O_3 + CaO^* + Na_2O + K_2O)] \times 100$ (Nesbitt and Young, 1982).
$PIA = [(Al_2O_3 - K_2O)/(Al_2O_3 + CaO^* + Na_2O - K_2O)] \times 100$ (Fedo et al., 1995).
$ICV = [(Fe_2O_3 + K_2O + Na_2O + CaO + MgO + MnO + TiO_2)/Al_2O_3]$ (Cox et al., 1995).

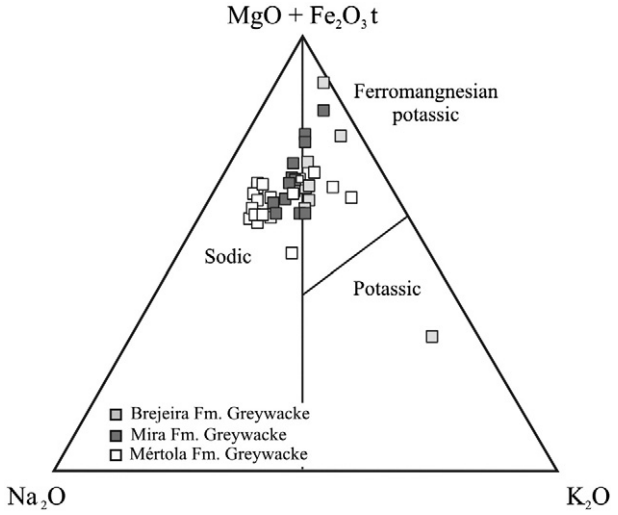

Fig. 6. Classification of the BAFG greywackes according to Blatt et al. (1980).

Brejeira greywackes, ∑LREE show weak correlation with TiO_2 (r = 0.45) while ∑HREE correlate weakly with Al_2O_3 (r = 0.44) and P_2O_5 (r = 0.67). Only in these greywackes that strong correlation of ∑HREE with TiO_2 (r = 0.91), Zr (r = 0.75) and Y (r = 0.98) is observed. Collectively, these correlations suggest the variable influence of several mineralogical phases, such as phyllosilicates, phosphates and zircon, on the control of REE contents of BFGA lithologies.

6. Palaeoweathering conditions

Weathering intensity at the source area is one of the main factors which influence both the mineralogy and the alkaline and alkaline earth element concentration of siliciclastic rocks. Large ionic radius cations such as Cs, Rb and Ba are preferentially fixed in weathering profiles through adsorption on clays, while smaller cations like Na, Ca and Sr are selectively leached from them (Nesbitt et al., 1980). The Chemical Index of Alteration (CIA) proposed by Nesbitt and Young (1982) is particularly useful because it reflects the intensity of chemical weathering in the source area while also allowing a quantitative measure of the amount of chemically weathered materials included in siliciclastic rocks (Nesbitt, 2003). CIA varies from ≈50 for unweathered igneous rocks to near 100 for residual clays enriched in kaolinite and Al oxi-hydroxides. This index is calculated using molar proportions of the following oxides: $CIA = [Al_2O_3/(Al_2O_3 + CaO^* + Na_2O + K_2O)] \times 100$, where CaO* is the amount of CaO incorporated in the silicate fraction of the sample only, after correction for Ca contained in carbonate (McLennon, 1993; Fedo et al., 1995).

The CO_2 contents were not analyzed in this study. Majority of studied samples show very low average CaO content (<2%, Table 1 and Appendix 3). In few samples, where petrographic examination revealed a presence of carbonates, the CIA value was corrected according to McLennon (1993).

Mértola and Mira greywackes exhibit average CIA values of 66.3 ± 4.0 and 71.2 ± 2.8, respectively Table 2. Within each formation, CIA values for greywackes show reduced variation, ranging from 61.5 to 74.0 in Mértola greywackes and from 67.0 to 76.6 in Mira. Average CIA values for Mértola and Mira shales are higher as compared to greywackes (71.1 ± 3.5 and 78.1 ± 1.8, respectively) and also show a reduced range of variation (64.5–74.8 and 74.7–81.2, respectively). The increased CIA values for shales of both formations should have resulted from prolonged chemical weathering associated with multiple cycles of sedimentary recycling (see below). All together, CIA values for Mértola and Mira greywackes and shales point out to moderate weathering conditions at the source area. The reduced range of variation of CIA values suggests steady-state weathering conditions in source area resulting from stable rates of chemical weathering and erosion over time (Nesbitt et al., 1997; Nesbitt, 2003).

Brejeira Formation shales exhibit average CIA values of 78.9 ± 1.0 (77.3–80.2). CIA values for Brejeira greywackes show an average of 74.6 ± 6.9 and vary from 63.3 to 83.0. Within this range, the highest CIA values are associated with samples from the base of the Brejeira Formation, while lower values belong to the top of this unit. Collectively, these values suggest moderate to intense chemical weathering conditions. The range of CIA values is clearly reflected in the A–CN–K $(Al_2O_3 - (CaO^* + Na_2O) - K_2O)$ diagram, where Brejeira greywackes project continuously along the ideal weathering trend parallel to A–CN line (Fig. 9). The data point out to the non steady-state conditions of the source area weathering for the Brejeira Formation rocks, resulting from changing rates of chemical alteration and physical erosion over time, probably as a consequence of tectonic instability in the source area (*e.g.*, Nesbitt et al., 1997; Nesbitt, 2003; Lee, 2009).

The degree of source weathering and elemental distribution during diagenesis can also be estimated using the related Plagioclase Index of Alteration (PIA) (Fedo et al., 1995), calculated using molar proportions of the following oxides: $PIA = [(Al_2O_3 - K_2O)/(Al_2O_3 + CaO^* + Na_2O - K_2O)] \times 100$, where CaO* is the amount of CaO incorporated in the silicate fraction of the rock only. Unweathered plagioclase has PIA value of 50, while Post Archaen Average Shale (PAAS) has PIA values of 79.

Mértola and Mira greywackes exhibit average PIA values of 69.9 ± 6.5 (63.2–85.1) and 76.4 ± 4.3 (70.1–86.1), respectively. The Brejeira greywackes show average PIA values of 82.5 ± 9.9 (67.2–94.6), indicating an increase in PIA values from the base to the top of the BAFG succession. The range of PIA values in these greywackes is a consequence of a variable degree of conversion of feldspars to clay minerals. As expected, Mértola, Mira and Brejeira shales exhibit higher PIA values compared to greywackes, respectively, 80.5 ± 5.4 (70.4–88.5), 91.7 ± 2.4 (87.8–94.9) and 93.5 ± 1.6 (91.5–96.1), reflecting phyllosilicate-dominated mineralogy. Both CIA and PIA values suggest that from Middle Viséan to Moscovian times, the source area of the BAFG experienced variable chemical weathering conditions, which become more severe to the top of stratigraphic succession, probably related to the tectonic instability in the provenance area (see discussion below).

7. Source rock composition

The chemical composition of the source area for siliciclastic sediments can be inferred from the triangular diagram A–CN–K $(Al_2O_3 - (CaO^* + Na_2O) - K_2O)$; where CaO* is the amount of CaO incorporated in the silicate-bearing minerals. As the weathering trends are parallel to the A–CN boundary, a regression can be made by backward projection relatively to the feldspar join line, to infer the composition of the source area (Nesbitt and Young, 1984, 1989; Fedo et al., 1995).

On the A–CN–K diagram (Fig. 9) the Mértola greywacke samples project in several trends parallel to the A–CN, where regression lines intercept plagioclase–alkali feldspar join mainly along granodioritic and granitic source and to a lesser extent, basaltic source. Mira and Brejeira greywackes exhibit lower degree of dispersion, and the regression lines project between the fields of granodioritic and granitic composition. The shales from all three BAFG formations project along the "trend" defined by PAAS and North American Shale Composition (NASC), within a granodioritic source composition (Fig. 9). The low degree of dispersion between analyzed shales may also represent a cumulative effect of multiple phases of sedimentary recycling (*cf.* McLennan et al., 1993). Accordingly, the shales from three BAFG formations exhibit low values of ICV (<1) and K_2O/Al_2O_3 (~0.2) consistent with the predominance of clay minerals that may have resulted from a lower input of first cycle detritus coupled with the recycling of sedimentary material (Cox et al., 1995). This conclusion is also

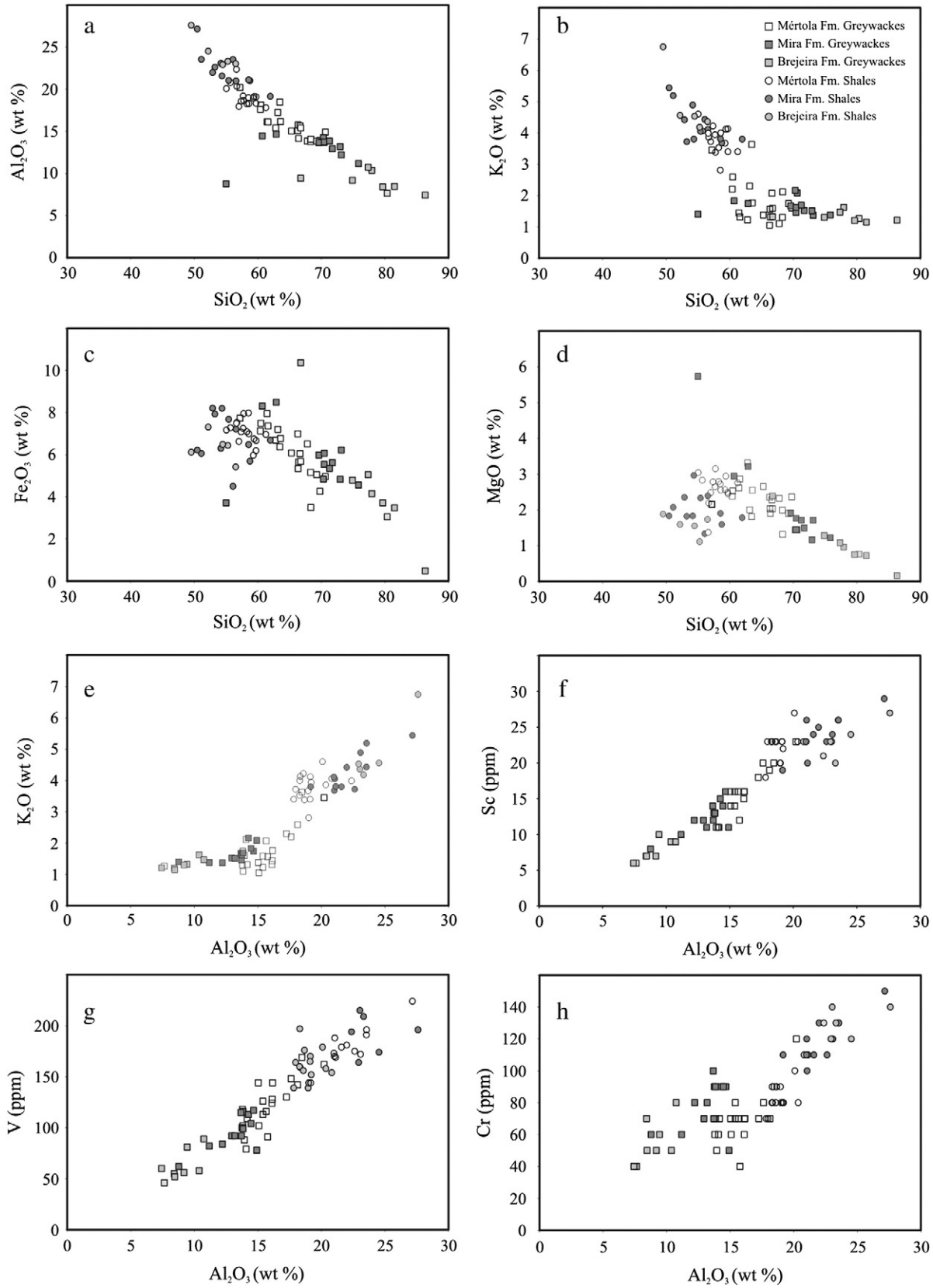

Fig. 7. Variations of SiO_2 *versus* Al_2O_3, K_2O, Fe_2O_3 and MgO (wt.%), and of Al_2O_3 *versus* K_2O (wt.%), Sc, V and Cr (ppm) for the BAFG rocks.

supported by consistently higher CIA values for BAFG shales when compared with associated greywackes. In fact, as shown by McLennan et al. (1990), in turbiditic sequences muds tend to have higher CIA values than associated sands, as a consequence of extensive history of chemical weathering coupled to multiple cycles of sedimentary recycling.

The provenance of BAFG sediments can be also inferred from the geochemistry of selected trace elements. This is based on the fact

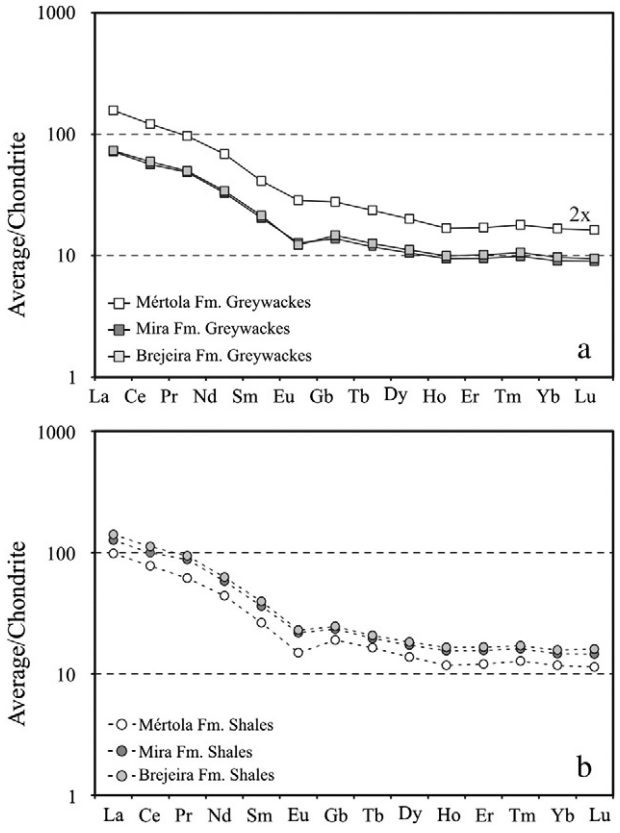

Fig. 8. Chondrite-normalized average REE patterns in the BAFG greywackes (a) and shales (b). Average REE contents for Mértola greywackes are doubled (2×) for the ease of observation.
Normalizing values of chondrite after Taylor and McLennan (1985).

that during weathering, erosion and transport, certain trace elements stay virtually insoluble and are transferred almost quantitatively to the sedimentary record and, consequently, bear the signature of the parental rock (McLennan et al., 1983, 1993; Taylor and McLennan, 1985; Bhatia and Crook, 1986; Feng and Kerrich, 1990; Cullers, 1995; Armstrong-Altrin et al., 2012). Among all useful trace elements (*e.g.* Th, Sc and HFSE), the REE have the advantage of not being easily fractionated during the sedimentation process, allowing to consider the REE pattern of siliciclastic rocks as an average representative of the source area composition (McLennan, 1989; Cullers, 1995; Mongelli et al., 1996; Bauluz et al., 2000). Additionally, the LREE/HREE ratio and the Eu anomaly value vary according to the chemical composition of the source. A majority of felsic rocks have variable degree of negative Eu anomalies, while basic rocks show a small or inexistent negative Eu anomaly (Cullers et al., 1987; Cullers, 1995). The fine-grained sediments seem to preserve the size of the negative Eu anomalies (Cullers et al., 1987).

The normalized patterns of shales and greywackes from three BAFG formations are characterized by a sharp enrichment in LREE and the flattened HREE patterns (see Fig. 8 and Table 1 and 2). The Eu/Eu* ratio ranges between 1.02–0.65 and 0.92–0.62 in greywackes of Mértola and Mira formations, respectively. However, in greywackes from both formations only a limited number of samples exhibit small or absent negative Eu/Eu* ratios. In shales, the Eu/Eu* values are 0.79–0.56 (0.66 ± 0.07) in the Mértola Formation and 0.85–0.66 (0.73 ± 0.05) in the Mira Formation The range of Eu/Eu* values for both lithologies is compatible with a heterogeneous source area of mostly felsic composition with a minor contribution from basic rocks (see discussion below). The Brejeira shales and greywackes exhibit less variable Eu/Eu* ratios, 0.74–0.70 and 0.70–0.67, respectively, compatible with a plutonic felsic and/or reworked sedimentary source.

According to Feng and Kerrich (1990) and McLennan et al. (1990), Th and Sc are particularly useful to constrain source area composition of siliciclastic rocks, largely because no fractionation is known to be associated to these elements in the sedimentary cycle. Th and Sc are enriched in felsic and basic rocks, respectively, and their elemental ratio is very sensitive to compositional variations associated to the provenance area (McLennan et al., 1990). In addition, the Zr/Sc ratio is a reliable index of sedimentary recycling processes, because of the resistance of zircon to chemical weathering and erosion. In first cycle sediments, Th/Sc and Zr/Sc ratios tend to correlate positively, depending on the source rock composition, while in more mature or recycled rocks Zr/Sc varies considerably, contrasting with the small

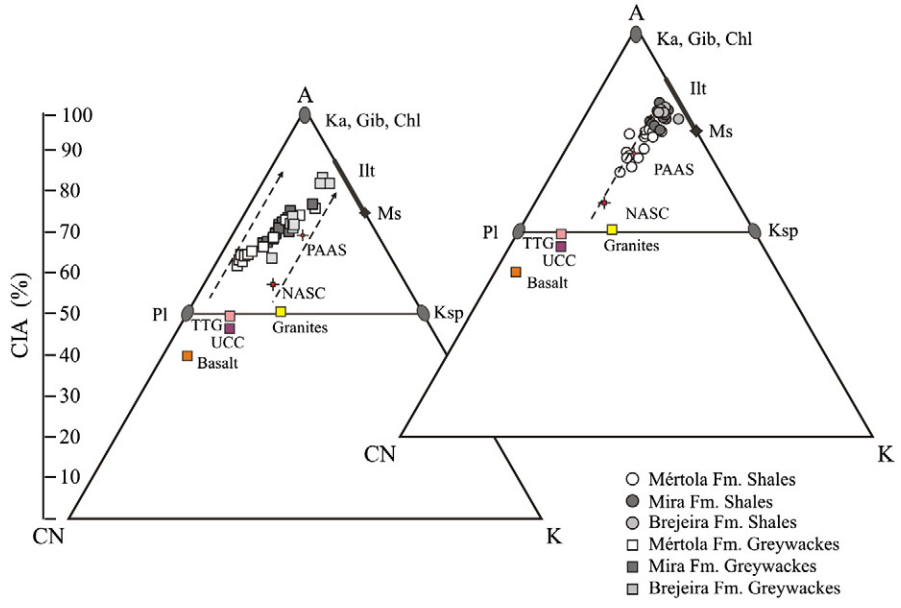

Fig. 9. A–CN–K diagrams (after Nesbitt and Young, 1982) for studied greywackes (a) and shales (b). CIA = Chemical Index of Alteration; A = Al_2O_3; CN = $CaO^* + Na_2O$; K = K_2O (molar proportions); CaO^* is the amount of CaO incorporated in the silicate fraction of the sample; Pl = plagioclase; Ksp = K-feldspar; Ka = kaolinite; Gib = gibbsite; Chl = chlorite; Ms = muscovite; and Ilt = Illite. Dotted lines indicate the direction of ideal weathering trends for these protoliths.

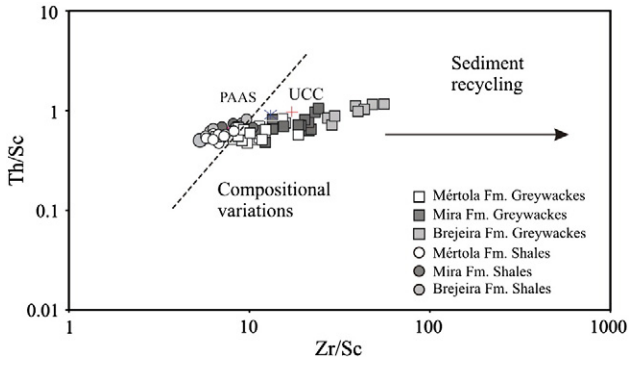

Fig. 10. Th/Sc *vs.* Zr/Sc plot showing the trend of the BAFG siliciclastic rocks and possible effects of the sediment recycling.
After McLennan et al. (1993).

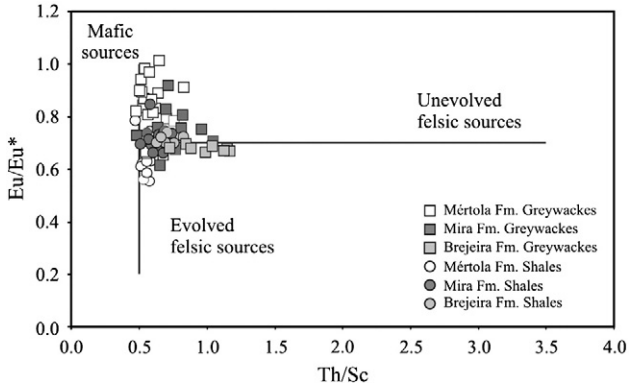

Fig. 11. Eu/Eu* *vs.* Th/Sc plot showing the distribution of the BAFG siliciclastic rocks to fields for stream sediments derived from mafic and felsic igneous sources.
After McLennan et al. (1990), Cullers (2000), and Slack et al. (2004).

variation in the Th/Sc ratio (McLennan et al., 1993). On the Th/Sc *versus* Zr/Sc plot (Fig. 10) the BAFG rocks show considerable variation in Zr/Sc ratio, with a group of samples clustering close to the UCC and PAAS. Higher Zr/Sc ratios of Mira and Brejeira greywackes reflect Zr enrichment as a result of higher degree of sedimentary recycling, most pronounced in the case of the Brejeira rocks.

To assess the degree of felsic *vs.* mafic contribution in the BAFG sediments, all samples were projected on Eu/Eu* *versus* Th/Sc diagram (Fig. 11). On this diagram, the majority of samples plot within the fields of unevolved felsic source and to a lesser extent, on evolved felsic source. A small number of greywacke and shale samples from Mértola and Mira Formation fall into the field of mafic source (Th/Sc < 0.5 and Eu/Eu* > 0.7) or on the boundary between the two fields. Samples with higher Th/Sc ratios do not seem to contain any mafic contribution (Slack et al., 2004).

The La/Sc, Th/Sc, La/Co and Cr/Th ratios of different igneous and sedimentary rocks are shown in Table 3, in comparison to the BAFG rocks analyzed in this study. The diverse critical provenance ratios suggest the predominance of felsic over mafic sources in the source area of the BAFG, with many of values close to the UCC.

8. Paleotectonic setting

To identify the tectonic setting of ancient sedimentary basins, several geochemical indicators and discriminating diagrams based on major and trace elements have been proposed (*e.g.* Bhatia, 1983; Bhatia, and Crook, 1986; Roser and Korsch, 1986, 1988). In these diagrams, sediments are grouped into three or four categories based on their bulk geochemical signal (*e.g.*, oceanic island arc, continental arc, active continental margin, Bhatia, and Crook, 1986). The widespread applicability of these geochemical indicators for the interpretation of palaeotectonic settings has been favored by some authors and questioned by others (*e.g.* Winchester and Max, 1989; McLennan et al., 1990, 1993; Floyd et al., 1991; Slack and Stevens, 1994; Toulkeridis et al., 1999; Armstrong-Altrin and Verma, 2005; Ryan and Williams, 2007).

To infer the palaeotectonic setting of the BAFG, all analyzed samples were projected on the La–Th–Sc diagram proposed by Bhatia and Crook (1986), where the majority of shales and greywackes consistently project within the continental island arc field, indicating a dissected magmatic arc as a source terrane (Fig. 12). However, a small number of Brejeira greywackes plot outside the pre-defined fields.

Floyd et al. (1991) proposed multi-element diagrams normalized to UCC to assess tectonic settings for coarse siliciclastic rock deposition, using as a reference the average data for greywackes from common tectonic environments (Fig. 13). On these diagrams, the elements are arranged, from right to left, in order of increasing ocean residence times and fall into two groups, a more stable (Th–Ta) and more mobile (Ni–K) one. This approach allows the recognition of a number of source- and tectonic environment discriminating features: (i) the Nb/Nb* ratio (actual normalized Nb abundance divided by predicted normalized Nb abundance based on extrapolation between Ni and Ti), which is typically low for sources derived from subduction-related magmatic rocks; the anomaly is less pronounced for passive margins involving reworked continental crust and is influenced by the contribution of mafic material in the source area; (ii) relative abundance of V, Cr, Ni, Ti and Sc: typical values for this anomaly are >1 for active margins and <1 for passive margins; and (iii) relative abundance of Ti, Hf, Zr and Y: positive values of Ti–Hf–Zr–Y anomaly reflect heavy mineral input (mainly zircon), and for passive margins the values are >1 (Floyd et al., 1991).

Using the normalization proposed by Floyd et al. (1991, Fig. 13), the greywackes of the three BAFG formations exhibit a generalized depletion in Ta–Nb and variable enrichment in V–Cr–Ni–Ti–Sc. V and Ni values for Brejeira greywackes are close to 1. The same is true for the Ni in the Mira greywackes. With the exception of Mértola greywackes, a positive anomaly in Hf–Zr–Y is observed, consistent with the enrichment in heavy minerals. The enrichment in Hf–Zr–Y

Table 3
Elemental ratios of the BAFG rocks compared to those of sediments derived from basic and silicic rocks, granites, andesites, basalts, UCC and PAAS.

Elemental ratio	Granites[a]	Andesites	Basalts[a]	UCC[b]	PAAS[b]	Coarse fractions from		Fine fractions from		Greywackes			Shales		
						Silicic sources[c]	Basic sources[c]	Silicic sources[c]	Basic sources[c]	Mértola Fm.	Mira Fm.	Brejeira Fm.	Mértola Fm.	Mira Fm.	Brejeira Fm.
La/Sc	8.00	0.90	0.32	2.73	2.38	2.50–16.30	0.43–0.86	0.7–27.7	0.4–1.1	1.40–2.55	1.34–2.64	2.28–4.63	1.42–2.16	1.49–2.68	1.93–2.68
Th/Sc	3.60	0.22	0.07	0.97	0.91	0.84–20.50	0.05–0.22	0.64–18.1	0.05–0.4	0.47–0.83	0.48–1.05	0.72–1.17	0.47–0.63	0.51–0.74	0.63–0.83
La/Co	13.33	0.90	0.32	3.00	1.65	1.8–13.8	0.14–0.38	1.4–22.2	–	1.24–3.39	0.98–3.00	1.25–25.90	1.25–3.23	1.64–17.5	1.44–7.09
Cr/Th	0.44	9.77	61.25	3.27	7.53	0.5–7.7	22–100	–	–	5.16–9.55	5.55–11.72	5.81–10.09	5.74–8.33	6.96–9.35	7.55–8.64
Eu/Eu*	0.34	0.66	1.09	0.65	0.66	0.40–0.94	0.71–0.95	0.32–0.83	0.7–1.02	0.65–1.02	0.62–0.92	0.67–0.70	0.56–0.74	0.66–0.85	0.70–0.74

[a] Condie (1993).
[b] Taylor and McLennan (1985).
[c] Cullers (2000).

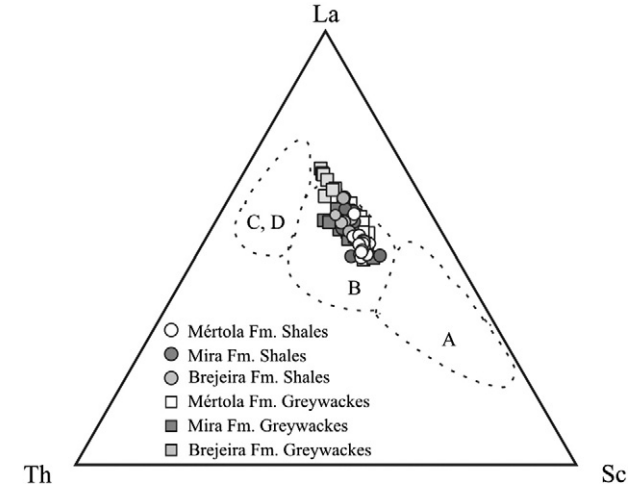

Fig. 12. Plot of the BAFG siliciclastic rocks composition in tectonic setting discriminant diagram La–Th–Sc. A = oceanic island arc; B = continental island arc; C = active continental margin and D = passive continental margin.
After Bhatia and Crook (1986).

is observed from the base to the top of BAFG succession, accompanied by the gradual depletion in Sr. Normalized multi-elemental patterns of different analyzed greywackes point out a geodynamic setting of continental arc/active margin, despite the enrichment in Hf–Zr–Y and pronounced negative anomaly in Sr, typical of passive margins

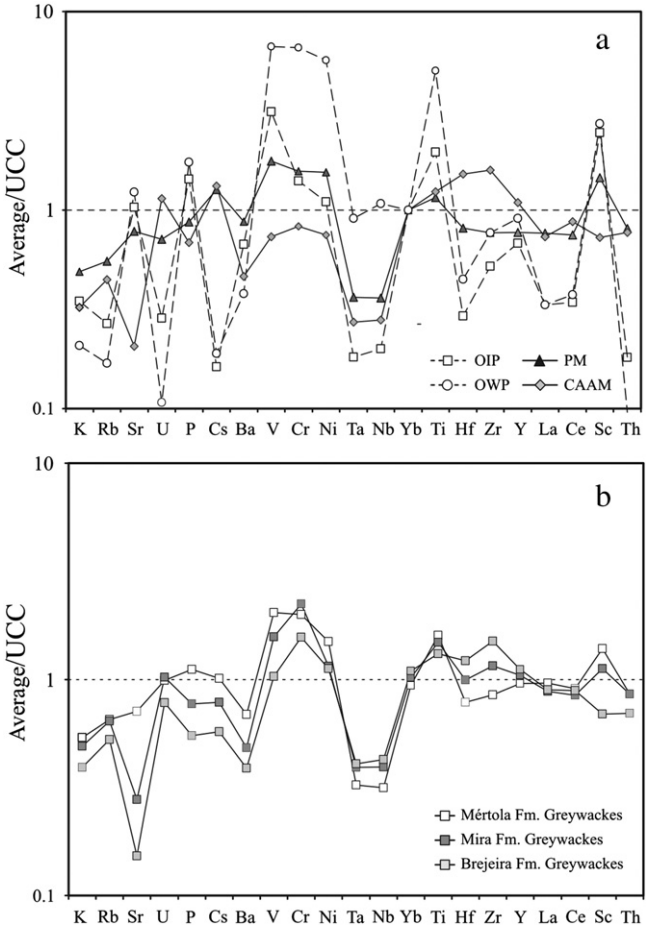

Fig. 13. UCC-normalized multi-element plots of (a) average greywacke abundance from oceanic island arc (OIA), oceanic within-plate (OWP), passive margin (PM) and continental arc/active continental margin; and (b) average composition of the BAFG greywackes.
After Floyd et al. (1991).

where sedimentary recycling processes play an important role (McLennan et al., 1990). The presence of these two types of signatures is common in active margins, where sedimentation is characterized by a mixture of young arc-derived material of variable composition and old upper crustal material (McLennan et al., 1990, 1993). The UCC-normalized multi-elemental patterns observed in the three BAFG formations indicate the contribution of the SW border of the OMZ as an important source for these sediments, in agreement with the environment of oblique collision between the SPZ and the SW border of the OMZ. As a consequence of this collision, the SW border of the OMZ was rapidly uplifted during Carboniferous times (Oliveira et al., 2006; Jesus et al., 2007; Rosas et al., 2008). The rapid uplift and intense erosion to which this region was subjected since the late Tournaisian are well documented in the Cabrela and Toca da Moura sedimentary basins (Pereira et al., 2006b). However, an intrabasinal (*i.e.*, the IPB) input of sediments for the BAFG cannot be ruled out. As documented in this work, the geochemical signatures of the Mértola and Mira sediments indicate source area(s) dominated by granitoid composition with minor contribution from mafic rocks. This granitoid signature could have had origin in the predominantly acidic volcanism of the IPB. The presence of acid and basic volcanic clasts in the greywackes also suggests a provenance from the Pyrite Belt (Schermerhorn, 1971; Oliveira, 1988; Moreno and Saez 1989, Moreno, 1993). However, previous studies denote the lack of evidence for large gravity sliding, olistrostomes and slump scars rooted in the IPB, and, together with the palaeocurrents data in the Mértola and Mira Formations (Oliveira, 1990), suggest a limited provenance from the IPB, not enough to account for the huge volume (more than 3 km in thickness) of the Mértola and Mira sediments. In agreement, the UCC-normalized multi-elemental patterns of the BAFG greywackes bear continental arc/active margin signatures, also implying limited input from intrabasinal component.

The detrital modes and geochemistry of the Brejeira Formation sediments indicate an additional contribution from old upper continental crustal source. These data can have two alternative interpretations: i) an internal orogen source alone, or ii) with a contribution of an external source. At present, the petrographic and geochemical data alone are not sufficient to distinguish between the two alternatives; however, combined with the palaeocurrents measured in the Brejeira Formation, and with the stratigraphy of the SPD, they are more consistent with the latter. In fact, the mixed mud/carbonate platform of the SPD was involved in the flysch sedimentation only in the late Bashkirian and Moscovian times and the palaeocurrents of the Brejeira Formation indicate more varied directions of sediment transport, with flows from NNW to SSE and from S to N (Oliveira, 1990).

It has been suggested that the IPB and the SPD were part of the Avalonia Plate (*e.g.*, Martinez-Catalán et al., 1997; Oliveira and Quesada, 1998; la Rosa et al., 2002; von Raumer et al., 2003; Ribeiro et al., 2007; Jorge et al., 2012). The collision of this plate with the western (present coordinates) margin of the OMZ (an outboard part of Gondwanan Iberia) in late Viséan times brought to an end the volcanism in both plates, and was followed by tectonic inversion, uplifting in the OMZ and the development of a SW prograding trough in the Avalonia side. Our data are compatible with the view that, until the early Bashkirian, this trough should have received eroded sediments from the exhumed OMZ (*e.g.*, Precambrian gneisses, Lower Palaeozoic granites and metasediments), and from Mississippian volcanic rocks from both sutured plates. These sources contributed, in different proportions, to the bulk of the Mértola and Mira rocks. From early Bashkirian onwards the trough received a stronger contribution from the continental crust of the Avalonia Plate as indicated by the predominantly felsic and recycled signature of the Brejeira Formation sediments.

9. Conclusions

The greywackes from the Mértola and Mira formations show similar modal compositions, while Brejeira greywackes are more enriched in

quartz and have lithoclasts composed mostly by sedimentary and metasedimentary grains.

Compared to UCC values, the analyzed greywackes, with the exception of those from the Brejeira Formation, exhibit similar MgO concentrations and have slightly higher TiO_2, Fe_2O_3 and MnO, with variable depletion in CaO, Na_2O and K_2O and variable enrichment in TTE (Sc, V, Cr, Ni and Co). LILE contents in greywackes are generally lower than the UCC. Shales show a similar pattern, with generalized slight enrichment in K_2O and variable depletion in MgO (except for the Mértola Formation), CaO and Na_2O, enrichment in Rb, Ba and Cs, and depletion in Sr.

A–CN–K diagrams and CIA and PIA values suggest that Mértola and Mira Formations underwent moderate weathering in the source areas, where reduced variation of both palaeoweathering indices indicates steady-state weathering conditions. The youngest Brejeira Formation shows greater CIA and PIA variation, reflecting moderate to intense weathering as a consequence of a non-steady-state conditions. High CIA and PIA values of shales from the three BAFG formations, and low ICV (<1) and K_2O/Al_2O_3 (~0.2) ratios suggest a more complex history of chemical weathering associated with multiple cycles of sedimentary recycling. These data indicate that during Middle Viséan to Moscovian times, weathering conditions of source area(s) of BAFG sediments changed from moderate to intense probably as a consequence of tectonic instability in the area.

The source area of Mértola greywackes is heterogeneous, dominated by rocks with granitoid composition and minor mafic input. The mafic component becomes residual in greywackes of Mira Formation, where granitoid source predominates. Greywackes from the Brejeira Formation exhibit a clear felsic signature with significant increase in recycled components. All analyzed shales show geochemical features compatible with provenance areas of mostly granodioritic composition.

Petrographic analyses, geochemical signatures of major and trace elements and multi-element tectonic discriminant diagrams suggest a continental arc/active margin as the most prominent origin for BAFG sediments. These data also indicate that an old upper continental crust contributed to the sediments of the Mira and Brejeira formations, more pronouncedly to the latter. Collectively, geochemical signatures of three BAFG formations are compatible with provenance from the SW border of Ossa Morena mostly, with possible contribution of an external (Avalonian) source.

Supplementary data to this article can be found online at http://dx.doi.org/10.1016/j.sedgeo.2012.12.005.

Acknowledgements

This work is a contribution to the project POCI/CTE-GEX/60278/2004 financed by the Portuguese Foundation for Science and Technology (Fundação para a Ciência e a Tecnologia — FCT). The authors wish to thank J. Matos from the LNEG — Beja for the access to the boreholes AC-1, CD1 and CD2 cores and data. We would like to thank R. Goodhue from the Department of Geology, Trinity College, for critical reading of the manuscript. We greatly appreciate constructive and helpful reviews by J. S. Armstrong-Altrin, G. Shellnutt and comments by Editor G.J. Weltje that considerably improved this manuscript.

References

Armstrong-Altrin, J.S., Verma, S.P., 2005. Critical evaluation of six tectonic setting discrimination diagrams using geochemical data of Neogene sediments from known tectonic setting. Sedimentary Geology 177 (1–2), 115–129.

Armstrong-Altrin, J.S., Lee, Y.I., Verma, S.P., Ramasamy, S., 2004. Geochemistry of sandstones from the Upper Miocene Kudankulam Formation, Southern India: implications for provenance, weathering, and tectonic setting. Journal of Sedimentary Research 74 (2), 285–297.

Armstrong-Altrin, J.S., Lee, Y.I., Kasper-Zubillaga, J.J., Carranza-Edwards, A., Garcia, D., Eby, G.N., Balaram, V., Cruz-Ortiz, N.L., 2012. Geochemistry of beach sands along the western Gulf of Mexico, Mexico: implication for provenance. http://dx.doi.org/10.1016/j.chemer.2012.07.003.

Barriga, F., 1990. Metallogenesis in the Iberian Pyrite Belt. In: Dallmeyer, R.D., Martinez García, E. (Eds.), Pre-Mesozoic Geology of Iberia. Springer Verlag, Berlin Heidelberg, pp. 369–379.

Bauluz, B., Mayayo, M.J., Fernandez-Nieto, C., Lopez, J.M.G., 2000. Geochemistry of Precambrian and Paleozoic siliciclastic rocks from the Iberian Range (NE Spain): implications for source-area weathering, sorting, provenance, and tectonic setting. Chemical Geology 168, 135–150.

Bhatia, M.R., 1983. Plate-tectonics and geochemical composition of sandstones. Journal of Geology 91, 611–627.

Bhatia, M.R., Crook, K.A.W., 1986. Trace-element characteristics of graywackes and tectonic setting discrimination of sedimentary basins. Contributions to Mineralogy and Petrology 92, 181–193.

Blatt, H., Middleton, G.V., Murray, R.C., 1980. Origin of Sedimentary Rocks. Prentice-Hall, Englewood Cliffs, NJ.

Condie, K.C., 1993. Chemical-composition and evolution of the upper continental-crust — contrasting results from surface samples and shales. Chemical Geology 104, 1–37.

Cox, R., Lowe, D.R., Cullers, R.L., 1995. The influence of sediment recycling and basement composition on evolution of mudrock chemistry in the southwestern United States. Geochimica et Cosmochimica Acta 59, 2919–2940.

Cullers, R.L., 1995. The controls on the major-element and trace-element evolution of shales, siltstones and sandstones of Ordovician to Tertiary age in the Wet Mountains Region, Colorado, USA. Chemical Geology 123, 107–131.

Cullers, R.L., 2000. The geochemistry of shales, siltstones and sandstones of Pennsylvanian–Perminian age, Colorado, USA: implication for provenance and metamorphic studies. Lithos 51, 181–203.

Cullers, R.L., Podkovyrov, V.N., 2002. The source and origin of terrigenous sedimentary rocks in the Mesoproterozoic Ui group, southeastern Russia. Precambrian Research 117, 157–183.

Cullers, R.L., Barrett, T., Carlson, R., Robinson, B., 1987. Rare-earth element and mineralogic changes in Holocene soil and stream sediment: a case study in the Wet Mountains, Colorado, USA. Chemical Geology 63, 275–297.

Dickinson, W.R., Suczek, C.A., 1979. Plate-tectonics and sandstone compositions. American Association of Petroleum Geologists Bulletin 63, 2164–2182.

Dickinson, W.R., Beard, L.S., Brakenridge, G.R., Erjavec, J.L., Ferguson, R.C., Inman, K.F., Knepp, R., Lindberg, F.A., Ryberg, P.T., 1983. Provenance of North American Phanerozoic sandstones inrelation to tectonic setting. Geological Society of America Bulletin 94, 222–235.

Etemad-Saeed, N., Hosseini-Barzi, M., Armstrong-Altrin, J.S., 2011. Petrography and geochemistry of clastic sedimentary rocks as evidences for provenance of the Lower Cambrian Lalun Formation, Posht-e-badam block, Central Iran. Journal of African Earth Sciences 61, 142–159.

Fedo, C.M., Nesbitt, H.W., Young, G.M., 1995. Unraveling the effects of potassium metasomatism in sedimentary-rocks and paleosols, with implications for paleoweathering conditions and provenance. Geology 23, 921–924.

Feng, R., Kerrich, R., 1990. Geochemistry of fine-grained clastic sediments in the Archean Abitibi greenstone-belt, Canada — implications for provenance and tectonic setting. Geochimica et Cosmochimica Acta 54, 1061–1081.

Floyd, P.A., Shail, R., Leveridge, B.E., Franke, W., 1991. Geochemistry and provenance of Rhenohercynian synorogenic sandstones: implications for the tectonic environment discrimination. In: Morton, A.C., Todd, S.P., Haughton, P.D.W. (Eds.), Developments in Sedimentary Provenance StudiesGeological Society Special Publication 57, 173–188.

Fonseca, P., Ribeiro, A., 1993. Tectonics of the Beja–Acebuches Ophiolite: a major suture in the Iberian Variscan Foldbelt. Geologische Rundschau 82, 440–447.

Franke, W., 2000. The mid-European segment of the Variscides: tectonostratigraphic units, terrane boundaries and plate tectonic evolution. In: Franke, W., Haak, V., Oncken, O., Tanner, D. (Eds.), Orogenic Processes, Quantification and Modelling in the Variscan Belt. Geological Society of London. Special Publications 179, 35–61.

González, F., 2005. Las pizarras negras del límite Devónico/carbonífero de la Faja Pirítica Ibérica (S.O. de España). Estúdio bioestratigráfico e implicaciones sobre la paleogeografía de la cuenca y el origen de las mineralizaciones de sulfuros. PhD Thesis, Facultad de Ciencias Experimentales, Departamento de Geologia, Área de Estratigrafia, Universidad de Huelva, Spain.

Govindaraju, K., 1994. Compilation of working values and sample description for 383 geostandards Geostandards Newsletter (18) (Suppl. S1) 1–158.

Ingersoll, R.V., Bullard, T.F., Ford, R.L., Grimm, J.P., Pickle, J.D., Sares, S.W., 1984. The effect of grain-size on detrital modes — a test of the Gazzi–Dickinson point-counting method. Journal of Sedimentary Petrology 54, 103–116.

Jesus, A., Munhá, J., Mateus, A., Tassinari, C., Nutman, A.P., 2007. The Beja Layered Gabbroic Sequence (Ossa Morena Zone, Southern Portugal), geochronology and geodynamic implications. Geodinamica Acta 20, 139–157.

Jorge, R.C.G.S., Relvas, J.M.R.S., Matos, J.X., 2006. Geochemistry of metasediments from the Phyllite–Quartzite Group, Iberian Pyrite Belt: provenance, source-area weathering and geotectonic implications. Geochimica et Cosmochimica Acta 70 (18) (Suppl. 1), A298.

Jorge, R.C.G.S., Fernandes, P., Pereira, Z., Oliveira, J.T., Relvas, J., 2007. A Late Fammenian age storm-dominated succession at Berrocal (Iberian Pyrite Belt-Spain). In: Pereira, Z., Oliveira, J.T., Wicander, R. (Eds.), CIMPLISBON'07, pp. 83–87.

Jorge, R.C.G.S., Relvas, J.M.R.S., Meffre, S., Tassinari, C.C.G., Fernandes, P., Pereira, Z., 2012. U–Pb detrital zircon age and Nd–Pb isotopic composition of sediments from the Phyllite–Quartzite Group, Iberian Pyrite Belt. European Mineralogical Conference, vol. 1 . (EMC2012-275-2).

la Rosa, J., Jenner, J., Castro, A., 2002. A study of inherited zircons in granitoid rocks from the South Portuguese and Ossa–Morena Zones, Iberian Massif: support for the exotic origin of the South Portuguese Zone. Tectonophysics 352, 245–256.

Lake, P.A., Oswin, W.M., Marshall, J.E.A., 1988. Apalynological approach to terrane analysis in the South Portuguese Zone. Trabajos de Geologia 17, 125–131 (Oviedo).

Lee, Y.I., 2009. Geochemistry of shales of the Upper Cretaceous Hayang Group, SE Korea: implications for provenance and source weathering at an active continental margin. Sedimentary Geology 215, 1–12.
Martinez-Catalán, J.R., Arenas, R., Díaz García, F., Abati, J., 1997. Variscan acretionary complex of northwest Iberia: terrane correlation and succession of tectonothermal events. Geology 25, 1103–1106.
McLennan, S.M., 1989. Rare-earth elements in sedimentary-rocks — influence of provenance and sedimentary processes. Reviews in Mineralogy 21, 169–200.
McLennan, S.M., Hemming, S., 1992. Samarium neodymium elemental and isotopic systematics in sedimentary-rocks. Geochimica et Cosmochimica Acta 56, 887–898.
McLennan, S.M., Taylor, S.R., Eriksson, K.A., 1983. Geochemistry of Archean shales from the Pilbara Supergroup, Western Australia. Geochimica et Cosmochimica Acta 47, 1211–1222.
McLennan, S.M., Taylor, S.R., McCulloch, M.T., Maynard, J.B., 1990. Geochemical and Nd–Sr isotopic composition of deep-sea turbidites — crustal evolution and plate tectonic associations. Geochimica et Cosmochimica Acta 54, 2015–2050.
McLennan, S.M., Hemming, S., McDaniel, D.K., Hanson, G.N., 1993. Geochemical approaches to sedimentation, provenance, and tectonics. In: Basu, M.J.J.a.A. (Ed.), Processes Controlling the Composition of Clastic SedimentsThe Geological Society of America 21–40.
McLennan, S.M., Bock, B., Hemming, R., Hurowitz, J.A., Lev, S.M., McDaniel, D.K., 2003. The roles of provenance and sedimentary processes in the geochemistry of sedimentary rocks. In: Lentz, D.R. (Ed.), Geochemistry of Sediments and Sedimentary RocksGeological Association of Canada 7–38.
McLennon, S.M., 1993. Weathering and global denudation. Journal of Geology 101, 295–303.
Mitjavila, J., Marti, J., Soriano, C., 1997. Magmatic evolution and tectonic setting of the Iberian Pyrite Belt volcanism. Journal of Petrology 38 (6), 727–755.
Mongelli, G., Cullers, R.L., Muelheisen, S., 1996. Geochemistry of Late Cretaceous Oligocenic shales from the Varicolori Formation, southern Apennines, Italy: implications for mineralogical, grain-size control and provenance. European Journal of Mineralogy 8 (4), 733–754.
Moreno, C., 1988. Dispositivos turbidíticos sincrónicos en el Carbonífero Inferior de la Faja Pirítica Ibérica (Zona Surportuguesa). Estudios Geológicos 44, 233–244.
Moreno, C., 1993. Postvolcanic Paleozoic of the Iberian Pyrite Belt: an example of basin morphologic control on sediment in a turbidite basin. Journal of Sedimentary Petrology 63, 1118–1128.
Moreno, C., Sáez, R., 1989. Petrología y procedencia de las areniscas del Culm de la parte occidental de la Faja Pirítica Ibérica (Zona Sur-Portuguesa). Boletín Geológico y Minero 100, 134–147.
Moreno, C., Sáez, R., 1990. Sedimentación marina somera en el devónico del anticlinorio de Puebla de Guzmán, Faja Pirítica Ibérica. Geogaceta 8, 62–64.
Moreno, C., Sierra, S., Saez, R., 1996. Evidence for catastrophism at the Famennian–Dinantian boundary in the Iberian Pyrite Belt. In: Strogen, P., Somervilee, I.D., Jones, G.L. (Eds.), Recent Advances in Lower Carboniferous GeologyGeological Society of London, Special Publication 107, 153–162 (London).
Munhá, J., 1983. Hercynian magmatism in Iberian Pyrite Belt. In: Lemos de Sousa, M.J., Oliveira, J.T. (Eds.), The Carboniferous of Portugal, 29. Serviços Geológicos de Portugal, Lisboa, pp. 39–82.
Munhá, J., Oliveira, J.T., Ribeiro, A., Oliveira, V., Quesada, C., Kerrich, R., 1986. Beja–Acebuches ophiolite: characterization and geodynamic significance. Maleo 2 (13), 31.
Nance, R.D., Gutiérrez-Alonso, G., Keppie, J.D., Linnemann, U., Murphy, J.B., Quesada, C., Strachan, R.A., Woodcock, N., 2010. Evolution of the Rheic Ocean. Gondwana Research 17, 194–222.
Nesbitt, H.W., 2003. Petrogenesis of siliciclastic sediments and sedimentary rocks. In: Lentz, D.R. (Ed.), Geochemistry of Sediments and Sedimentary RocksGeological Association of Canada 39–51.
Nesbitt, H.W., Young, G.M., 1982. Early Proterozoic climates and plate motions inferred from major element chemistry of lutites. Nature 299, 715–717.
Nesbitt, H.W., Young, G.M., 1984. Prediction of some weathering trends of plutonic and volcanic-rocks based on thermodynamic and kinetic considerations. Geochimica et Cosmochimica Acta 48, 1523–1534.
Nesbitt, H.W., Young, G.M., 1989. Formation and diagenesis of weathering profiles. Journal of Geology 97, 129–147.
Nesbitt, H.W., Markovics, G., Price, R.C., 1980. Chemical processes affecting alkalis and alkaline-earths during continental weathering. Geochimica et Cosmochimica Acta 44, 1659–1666.
Nesbitt, H.W., Fedo, C.M., Young, G.M., 1997. Quartz and feldspar stability, steady and non-steady state weathering, and petrogenesis of siliciclastic sands and muds. Journal of Geology 105, 173–191.
Oliveira, J.T., 1983. The marine Carboniferous of South Portugal: a stratigraphic and sedimentological approach. In: Lemos de Sousa, M.J., Oliveira, J.T. (Eds.), The Carboniferous of South Portugal, 29, pp. 3–38 (Lisboa).
Oliveira, J.T., 1988. Estratigrafia, sedimentologia e estrutura do Flysch da Formação de Mértola, na região de Mértola. Comunicações dos Serviços Geológicos de Portugal 74, 3–19.
Oliveira, J.T., 1990. Stratigraphy and syn-sedimentary tectonism in the South Portuguese Zone. In: Dallmeyer, R.D., Martinez García, E. (Eds.), Pre-Mesozoic Geology of Iberia. Springer-Verlag, Berlin Heidelberg, pp. 333–347.
Oliveira, J.T., Quesada, C., 1998. A comparison of stratigraphy, structure, and palaeogeography, of the South Portuguese Zone and southwest England, European Variscides. Geoscience in South-West England 9, 141–150.
Oliveira, J., Horm, M., Paproth, E., 1979. Preliminary note on the stratigraphy of the Baixo–Alentejo Flysch Group, Carboniferous of Portugal, and on the palaeogeographic development compared to corresponding units in NorthWest Germany. Comunicações dos Serviços Geológicos de Portugal 65, 151–168.
Oliveira, J.T., Pereira, Z., Carvalho, P., Pacheco, N., Korn, D., 2004. Stratigraphy of the tectonically imbricated lithological succession of the Neves Corvo mine area, Iberian Pyrite Belt, Portugal. Mineralium Deposita 39, 422–436.
Oliveira, J.T., Relvas, J., Pereira, Z., Matos, J., Rosa, D., Munhá, J.M., Jorge, R.C.G.S., Pinto, A., 2006. O Complexo Vulcano-Sedimentar da Faixa Piritosa: estratigrafia, vulcanismo, mineralizações associadas e evolução tectono-estratigráfica no contexto da Zona Sul Portuguesa. In: Dias, R., Araújo, A., Terrinha, P., Kullberg, J.C. (Eds.), Geologia de Portugal no contexto da Ibéria. Univ. Évora, Évora, pp. 207–243.
Pereira, Z., 1999. Palinoestratigrafia do Sector Sudoeste da Zona Sul Portuguesa. Comunicações dos Serviços Geológicos de Portugal 86, 25–57.
Pereira, Z., Fernandes, P., Oliveira, J.T., 2006a. Palinoestratigrafia do Domínio Pulo do Lobo, Zona Sul Portuguesa. Comunicações Geológicas 93, 23–38.
Pereira, Z., Oliveira, V., Oliveira, J.T., 2006b. Palynostratigraphy of the Toca da Moura and Cabrela Complexes, Ossa Morena Zone, Portugal. Geodynamic implications. Review of Palaeobotany and Palynology 139, 227–240.
Pereira, Z., Matos, J., Fernandes, P., Oliveira, J.T., 2007. Devonian and Carboniferous palynostratigraphy of the South Portuguese Zone, Portugal — an overview. Comunicações Geológicas 94, 53–79.
Pereira, Z., Matos, J., Fernandes, P., Oliveira, J.T., 2008. Palynostratigraphy and systematic palynology of the Devonian and Carboniferous successions of the South Portuguese Zone, Portugal. Memória N.º 34 do INETI, pp. 1–176.
Quesada, C., Fonseca, P., Munhá, J., Oliveira, J.T., Ribeiro, A., 1994. The Beja–Acebuches Ophiolite (Southern Ibera Variscan fold belt): geological characterization and geodynamic significance. Boletin Geológico y Minero 105, 3–49.
Ragland, P.C., 1989. Basic Analytical Petrology. Oxford University Press, New York, Oxford. (369 pp.).
Ribeiro, A., Quesada, C., Dallmeyer, R.D., 1990. Geodynamic evolution of the Iberian Massif. In: Dallmeyer, R.D., García, E.M. (Eds.), Pre-Mesozoic Geology of Iberia. Springer-Verlag, Berlin Heidelberg, pp. 399–409.
Ribeiro, A., Munhá, J., Dias, D., Mateus, A., Pereira, E., Ribeiro, L., Fonseca, P., Araújo, A., Oliveira, J.T., Romão, J., Chaminé, H., Coke, C., Pedro, J., 2007. Geodynamic evolution of the SW Europe Variscides. Tectonics 26.
Rosas, F.M., Marques, F.O., Ballèvre, M., Tassinari, C., 2008. Geodynamic evolution of the SW Variscides: orogenic collapse shown by new tectonometamorphic and isotopic data from western Ossa–Morena Zone, SW Iberia. Tectonics 27, TC6008.
Rosa, C., McPhie, J., Relvas, J., 2010. Type of volcanoes hosting the massive sulfide deposits of the Iberian Pyrite Belt. Journal of Volcanology and Geothermal Research 194, 107–126.
Roser, B.P., Korsch, R.J., 1986. Determination of tectonic setting of sandstone–mudstone suites using SiO_2 and K_2O/Na_2O ratio. Journal of Geology 94, 635–650.
Roser, B.P., Korsch, R.J., 1988. Provenance signatures of sandstone mudstone suites determined using discriminant function analysis of major element data. Chemical Geology 67, 119–139.
Ryan, K.M., Williams, D.M., 2007. Testing the reliability of discrimination diagrams for determining the tectonic depositional environment of ancient sedimentary basins. Chemical Geology 242 (1–2), 103–125.
Saez, R., Pascual, E., Toscano, M., Almodovar, G., 1999. The Iberian type of volcano-sedimentary massive sulphide deposits. Mineralium Deposita 5–6, 549–570.
Schermerhorn, L.J.G., 1971. An outline stratigraphy of the Iberian Pyrite Belt. Boletin Geologico y Minero LXXXII–III–IV, 239–268.
Silva, J.B., Oliveira, J.T., Ribeiro, A., 1990. Structural outline in Pre-Mesozoic geology of Iberia. In: Dallmeyer, R.D., Martinez Garcia, E. (Eds.), Pre-Mesozoic Geology of Iberia. Springer-Verlag, Berlin Heidelberg, pp. 399–410.
Slack, J.F., Stevens, B.P.J., 1994. Clastic metasediments of the Early Proterozoic Broken-Hill Group, New-South-Wales, Australia — geochemistry, provenance, and metallogenic significance. Geochimica et Cosmochimica Acta 58, 3633–3652.
Slack, J.F., Dumoulin, J.A., Schimidt, J.M., Young, L.E., Rombach, C.S., 2004. Paleozoic sedimentary rocks in the Red Dog Zn-Pb-Ag district and vicinity, western Brooks Range Alaska: provenance, deposition, and metallogenic significance. Economic Geology 99, 1385–1414.
Taylor, S.R., McLennan, S.M., 1985. The Continental Crust: Its Composition and Evolution. Balckwell, Oxford . (312 pp.).
Tornos, F., 2006. Environment of formation and styles of volcanogenic massive sulfides: the Iberian Pyrite Belt. Ore Geology Reviews 28, 259–307.
Toulkeridis, T., Clauer, N., Korfner, A., Reimer, T., Todt, W., 1999. Characterization, provenance, and tectonic setting of Fig Tree greywackes from the Archaean Barbertone Belt, South Africa. Sedimentary Geology 124, 113–129.
van den Boogaard, M., 1967. Geology of the Pomarão region, Southern Portugal. PhD thesis, Rotterdam, Netherlands.
Veizer, J., Mackenzie, F.T., 2005. Evolution of sedimentary rocks. In: Holland, H.D., Turekian, K.K. (Eds.), Treatise on Geochemistry, 7. Elsevier, pp. 369–407.
von Raumer, J.F., Stampfli, G.A., Bussy, F., 2003. Gondwana-derived microcontinents — the constituents of the Variscan and Alpine collisional orogens. Tectonophysics 365, 7–22.
Winchester, J., Max, M., 1989. Tectonic setting discrimination in clastic sequences: an example from the Late Proterozoic Erris Group, NW Ireland. Precambrian Research 45, 191–201.
Wronkiewicz, D.J., Condie, K.C., 1987. Geochemistry of Archean shales from the Witwatersrand Supergroup, South Africa — source-area weathering and provenance. Geochimica et Cosmochimica Acta 51, 2401–2416.
Zuffa, G.G., 1991. On the use of turbidite arenites in provenance studies: critical remarks. In: Morton, A.C., Todd, S.P., Haughton, P.D.W. (Eds.), Developments in Sedimentary Provenance Studies. Geological Society Special Publication, 57. The Geological Society, London, pp. 23–29.

Journal of the Geological Society, London, Vol. **169**, 2012, pp. 647–654. doi: 10.1144/jgs2011-156.

New evidence concerning the thermal history of Devonian and Carboniferous rocks in the South Portuguese Zone

PAULO FERNANDES[1*], JENNIFER A. MUSGRAVE[2], GEOFF CLAYTON[2], ZÉLIA PEREIRA[3], JOSÉ TOMÁS OLIVEIRA[4], ROBBIE GOODHUE[2] & BRUNO RODRIGUES[1]

[1]*Universidade do Algarve, Centro de Investigação Marinha e Ambiental, Campus de Gambelas, 8005-139 Faro, Portugal*

[2]*Department of Geology, Trinity College, University of Dublin, Dublin 2, Ireland*

[3]*Laboratório de Nacional de Geologia e Energia, Rua da Amieira, 4465-965 S. Mamede Infesta, Portugal*

[4]*Laboratório de Nacional de Geologia e Energia, Estrada Portela, Zambujal Alfragide, Ap.7586, 2720-866 Amadora, Portugal*

**Corresponding author (e-mail: pfernandes@ualg.pt)*

Abstract: The Late Palaeozoic rocks of southern Portugal have a complex thermal history. Vitrinite reflectance determinations from 90 samples confirm that the organic maturity of Late Palaeozoic rocks in SW Portugal is very high, mainly corresponding to meta-anthracite coal rank. The optic fabric of vitrinite in oriented coal samples from the Brejeira Formation suggests maturation under simple, non-tectonic, burial conditions with peak temperatures being attained prior to Variscan deformation. The lack of any increase in vitrinite reflectance with depth through *c*. 1 km of section in borehole AC-1 is not consistent with conductive heat transfer and is interpreted as the result of late synorogenic to post-orogenic advective heating. This heating episode generated temperatures sufficiently high to produce levels of maturity corresponding to meta-anthracite coal rank through much of the terrane now exposed, but not high enough to result in overprinting of the pre-deformation optic fabric of vitrinite in the thin coals. The slightly lower maturity of older, platform-facies rocks in the Aljezur–Bordeira area may reflect either deposition on a basement high followed by less burial than adjacent parts of the basin, or the area being the site of a sink for descending relatively cool fluids.

The South Portuguese Zone is one of the main geological units of the Variscan Iberian Massif (Fig. 1). Its faulted boundary against the Ossa Morena Zone in the north is marked by the Beja Acebuches Ophiolite and to the south it is overlain unconformably by Mesozoic sedimentary rocks of the Algarve Basin (Fig. 1). The Beja Acebuches Ophiolite is interpreted as a remnant of the Rheic Ocean that separated the Euramerican South Portuguese Zone from the Gondwanan Ossa Morena Zone (Oliveira 1990; Quesada *et al*. 1994; Oliveira & Quesada 1998; Oliveira *et al*. 2006).

The South Portuguese Zone is divided into four 'domains' based on lithology, deformation style and age. The domains trend from NW–SE near the coast to east–west inland and generally young towards the SW. These domains are, from NE to SW, the Pulo do Lobo Antiform, the Pyrite Belt, the Baixo Altentejo Flysch Group and the Southwest Portugal Domain.

The Pulo do Lobo Formation crops out in the centre of the antiformal structure of the Pulo do Lobo Antiform. It consists of highly deformed phyllites and quartzites with small intercalations of amphibolites of mid-ocean ridge basalt (MORB)-type geochemical affinity. Detrital zircons from the quartzites suggest a maximum depositional age of 438 Ma (Silurian) for the protolith of this formation (Braid *et al*. 2011). Flysch-type successions crop out on the northern and southern flanks of the antiform. These rocks are dated palynologically as Frasnian to late Famennian (Pereira *et al*. 2006, 2008). However, detrital zircons in the upper unit of the overlying flysch succession (the Santa Íria Formation) located on the northern limb of the Pulo do Lobo Antiform in Spain give a maximum depositional age of Tournaisian (347 ± 5.5 Ma, Braid *et al*. 2011), compared with the late Famennian age provided by palynomorphs for the same unit in Portugal (Pereira *et al*. 2006). This suggests eastward progradation of flysch deposition during late Famennian to Tournaisian time, although this requires further investigation. Vitrinite reflectance (VR) of the organic matter from the flysch successions of the Pulo do Lobo Antiform indicates that meta-anthracite coal rank was attained post-late Devonian (Pereira *et al*. 2006).

The Pyrite Belt succession consists of phyllites and quartzites of the Phyllite Quartzite Group overlain by volcanic rocks and sediments of the Volcano-Sedimentary Complex, which are often mineralized. Palynomorphs present in the uppermost beds of the Phyllite Quartzite Group indicate a Late Devonian age (Pereira *et al*. 2008). The Volcano-Sedimentary Complex is dated as Late Devonian to late Viséan based on palynomorphs and rare conodonts (Boogaard 1963, 1967; Oliveira & Wagner Genthis 1983; Oliveira *et al*. 2004, 2005; Pereira *et al*. 2007, 2008). VR values from the Pyrite Belt in the São Domingos mine area range from 4.6 to 5.2% R_r, indicating a meta-anthracite coal rank (Pereira *et al*. 2006).

The Baixo Altentejo Flysch Group is a turbiditic sequence over 5 km thick that progrades southwards. The flysch sequence in the South Portuguese Zone is divided into three formations based on sedimentology and age. In ascending order these are the Mértola, Mira and Brejeira Formations. These units are dated by ammonoid faunas and palynomorphs as late Viséan, Serpukhovian to early Bashkirian, and late Bashkirian to late Moscovian respectively (Oliveira *et al*. 1979, 1985; Korn 1997; Pereira 1999; Pereira *et al*. 2007, 2008). The Baixo Altentejo Flysch Group represents the development of a foreland basin that formed as a result of the collision of the South Portuguese Zone and the Ossa Morena Zone, with associated tectonic stacking that propagated from NE to SW (Oliveira 1990; Silva *et al*. 1990; Pereira 1997, 1999). Reworked Cambrian to Early Devonian palynomorphs occur commonly in the Brejeira Formation (Pereira 1999), indicating a source area for these clastic sediments outside the South Portuguese Zone, as no rocks older than the Mid-Devonian crop out in the South Portuguese

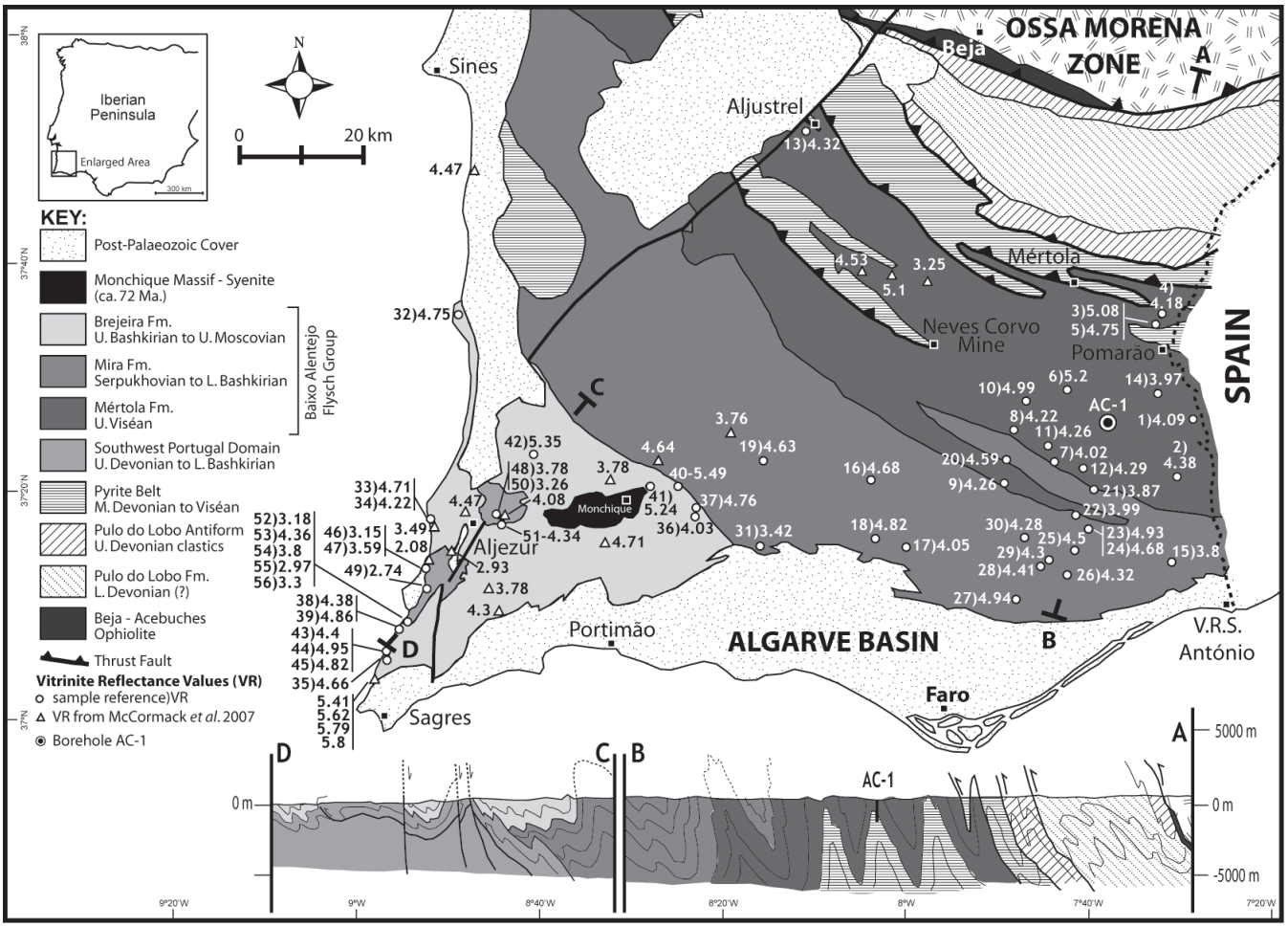

Fig. 1. Generalized geology of SW Portugal, locations of outcrop samples and borehole AC-1, and vitrinite reflectance results.

Zone. McCormack *et al*. (2007) published a comprehensive study of the thermal history of the Baixo Altentejo Flysch Group, determining a mean VR of 4.28% R_r for this domain and suggesting that the timing of maturation was post-Variscan deformation, within the late Carboniferous–late Triassic interval.

The Southwest Portugal Domain succession comprises Late Devonian quartzites and shales (Tercenas Formation) followed by a mud-dominated carbonate platform sequence, the Carrapateira Group, of Tournaisian to late Bashkirian age (Pereira 1999). A few samples from the Tercenas Formation and from the Viséan Murração Formation indicate maturation levels of *c*. 3.2% R_r (McCormack 1998; McCormack *et al*. 2007), which are lower than the mean maturation value of *c*. 4.83% R_r for the younger Brejeira Formation of the Baixo Altentejo Flysch Group. An inversion of the VR values in these strata in the SWP was also described by Moço *et al*. (1998), with the highest values being recorded in the Brejeira Formation (4.5% R_r) and lower values being recorded in the older units of the Carrapateira Group (2.5–4% R_r).

Diagenetic and metamorphic conditions within the South Portuguese Zone have also been studied by means of clay mineral crystallinity (Munhá 1983, 1990; McCormack 1998; Abad *et al*. 2001). These studies show a decrease in crystallinity from epizone conditions in the NE to the late diagenetic zone in the SW. The Pulo do Lobo Formation in the core of the Pulo do Lobo Antiform is of greenschist facies, whereas the clastic units in both limbs attained epizone facies.

Materials and methods

The samples analysed in this study were obtained from outcrops and a mineral exploration borehole (AC-1). Black and grey shales were the main lithologies sampled for maturation studies. A few thin coal lenses in fine-grained turbiditic beds in the Brejeira Formation were also sampled.

The dispersed organic matter in all of the Baixo Altentejo Flysch Group mudrocks studied is dominated by amorphous organic matter and phytoclasts (vitrinite and inertinite). Framboidal pyrite always appears as inclusions, normally associated with amorphous organic matter (AOM). Inertinite is an important constituent of the dispersed organic matter in some samples, although it is always less abundant than vitrinite.

The composition of the organic matter in the Southwest Portugal Domain mudrocks varies greatly between formations. AOM is the dominant constituent in the Quebradas and Bordalete formations. Vitrinite and inertinite are important constituents of the dispersed organic matter in the sandstone-dominated interval at the top of the Tercenas Formation. In the Murração Formation, organic matter is scarce and is dominated by inertinite and AOM.

Borehole AC-1

Borehole AC-1 was drilled by Billiton Portugal Lta. in 1986 for mineral exploration. It reached a depth of *c*. 980 m (1064 m with

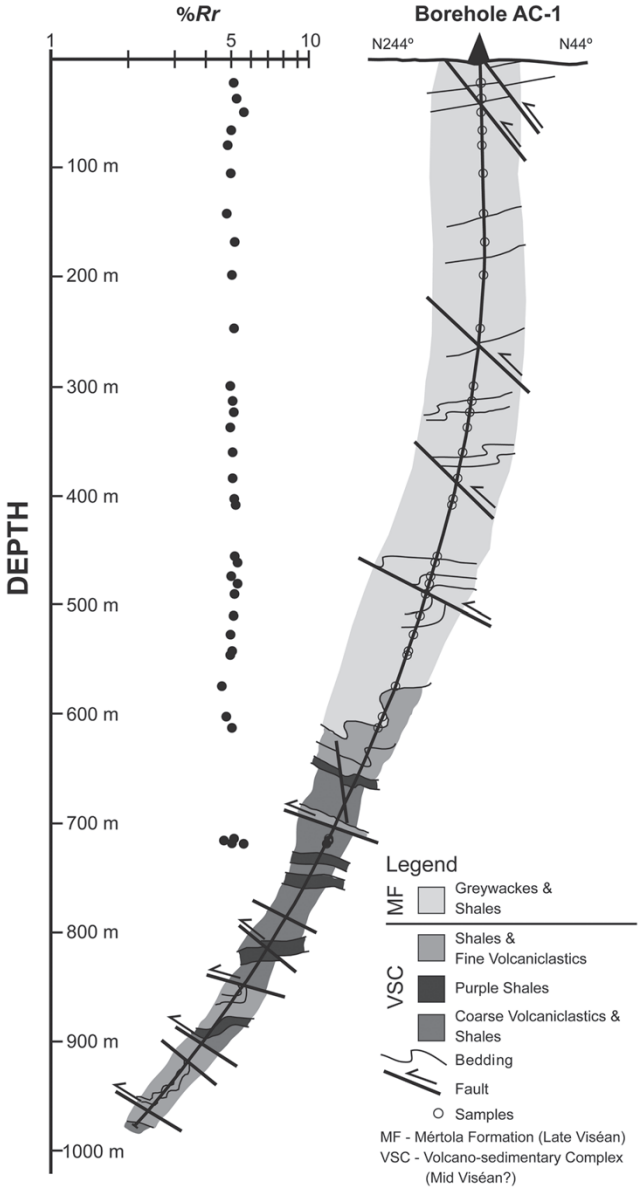

Fig. 2. Vitrinite reflectance results from borehole AC-1.

inclination corrected to vertical). The upper *c*. 600 m consists of interbedded shales and greywackes of the Mértola Formation. Below 600 m, the succession comprises shales and fine and coarse volcaniclastic rocks of the Volcano-Sedimentary Complex of the Iberian Pyrite Belt. The Mértola Formation section was extensively sampled, with shale samples taken at an average spacing of 20 m. Only six samples were taken from grey shales in the Volcano-Sedimentary Complex, the lowest from 729.5 m. The Mértola Formation is assigned to the NM Miospore Biozone, of mid-late Viséan age. Moderately well-preserved specimens of *Raistrickia nigra*, a key species of the miospore biozone are present. Samples from the Volcano-Sedimentary Complex did not provide any stratigraphically useful information.

The structural interpretation of borehole AC-1 suggests that no major fractures were intersected. Rocks of the Mértola Formation and the Volcano-Sedimentary Complex are, generally, subhorizontal or dipping gently to the SW, suggesting a non-faulted contact between the two units (Fig. 2). The faults penetrated were considered to be late reverse faults, with correlation of beds across the faults suggesting very limited displacements (Fig. 2). Tectonic cleavage was also observed in the shaly intervals, dipping 30–40° to the NE. Structural analysis of the data suggests that the borehole penetrated the normal limb of a regional anticline. These structural features are typical of the southern branch of the Iberian Pyrite Belt, which is characterized by rooted folds (Silva *et al*. 1990).

Outcrop samples

VR was determined from 54 shale and two coal samples from outcrops in the Baixo Altentejo Flysch Group and Southwest Portugal Domain to determine the regional maturity and to elucidate the thermal evolution of the South Portuguese Zone.

At Pedras das Ameias, at the western end of the Arrifana harbour section (Fig. 3), interbedded greywackes and shales of the Brejeira Formation include occasional very thin (<1 cm) coal lenses. The section is dominated by numerous NW–SE-trending folds from which field-oriented coal samples were taken on both vertical and subhorizontal limbs.

Extraction techniques and methods of study

Organic particles were extracted from the rock samples using standard cold hydrofluoric acid (HF) techniques. The organic residues obtained were then mounted and polished using a method adopted from that described by Hillier & Marshall (1988).

Mean random vitrinite reflectance (%R_r) was the VR parameter chosen for maturation assessment of shales because the mounting technique used provides non-oriented vitrinite particles and also because %R_r is the most widely used organic maturation parameter. VR measurements on most of the samples were made using an Olympus BX 51 microscope equipped with a black and white digital camera. The black and white (8-bit) digital images of vitrinite particles were analysed using a MatLab routine. This routine is a graphical tool that runs within the Mirone suite (Luis 2007) and calibrates the scale of 256 grey levels with standards of known reflectivity (Fernandes *et al*. 2010). The reflectance values of the standards used were 0.428, 0.595, 1.715, 3.150 and 5.370%. VR was measured in incident light with a wavelength of 546 nm and immersion oil with a refractive index of 1.518. Reflectances of the oriented coal samples from Pedras das Ameias were measured using the techniques and equipment described by McCormack *et al*. (1998).

Vitrinite reflectance results

Figure 1 shows the new VR results from outcrop samples together with results from McCormack *et al*. (2007). Results from borehole AC-1 are shown in Figure 2. The Baixo Altentejo Flysch Group rocks cropping out in the South Portuguese Zone do not display great variability in VR, with R_r ranging from 3.80 to 5.55%. The majority of VR values range from 4.0 to 5.0% R_r, corresponding to meta-anthracite coal rank. There is no clear correlation between the R_r means in the three formations investigated. This is even more marked if peak palaeotemperatures calculated by Barker & Goldstein's (1990) empirical equations are compared, with a difference of less than 10 °C between the mean peak palaeotemperature for the three formations (Table 1). The mean peak palaeotemperatures for the Mértola, Mira and Brejeira formations are 311, 302 and 310 °C respectively. The palaeotemperatures do not show any consistent change, in relation to stratigraphic position within the Baixo Altentejo Flysch Group.

The geographical distribution of R_r values for the rocks of the Baixo Altentejo Flysch Group suggests that there is not a clear depocentre for this unit. This is consistent with the synsedimentary tectonic model proposed by Oliveira (1990) for the South

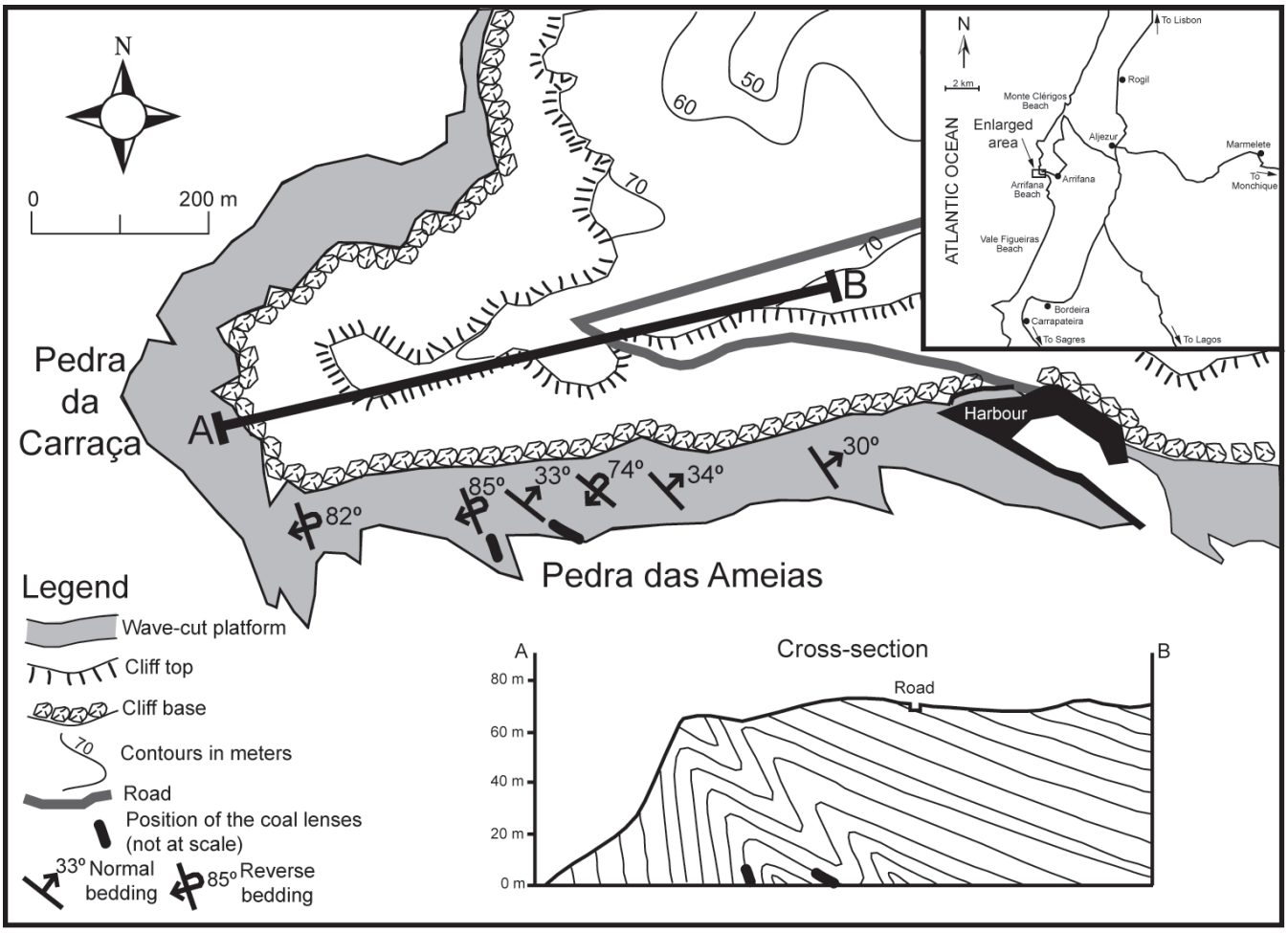

Fig. 3. Geological map and cross-section of the Pedra das Ameias area showing the structure and location of field-oriented coal lenses.

Portuguese Zone, with progradation to the SW of the turbiditic sedimentation in response to thrusting and tectonic stacking to the north.

VR values in borehole AC-1 do not show a clear increase with depth through *c.* 700 m of section; the best-fit line is more or less vertical (Fig. 2). The lack of downhole increase in VR in the borehole precludes the calculation of a meaningful regional palaeogeothermal gradient in the Baixo Alentejo Flysch Group.

For optic fabric determination of the coal lenses at Pedra das Ameias (Fig. 3), three orthogonal faces were cut and polished on each sample; (a) parallel to bedding; (b) perpendicular to bedding and parallel to strike; (c) perpendicular to bedding and parallel to dip. Measurements made on these three surfaces revealed uniaxial negative vitrinite reflectance indicatrices (VRIs) with maximum reflectance (R_{max}) parallel to bedding and minimum reflectance (R_{min}) perpendicular to bedding, even where the dip was close to vertical (85°). In the case of a vertical coal lens investigated, R_{max} is 6.29%, R_{min} (b) is 3.72% and R_{min} (c) is 3.83%.

The results from the oriented coal samples support the interpretation published by McCormack *et al*. (2007), but are more convincing as they are based on a more extreme range of dips. The uniaxial negative VRIs recorded are 'typical of coalification in tectonically undeformed subsiding basins' (Taylor *et al*. 1998; after Levine & Davis 1989). There is no trace of later modification producing biaxial positive or negative VRIs that would indicate further coalification during intense or even incipient tectonism. Further coalification during a post-tectonic vertical loading regime (i.e. post-Variscan burial of the section) might be expected to result in complete or partial rotation of the VRIs in the vertical limbs to a position where R_{max} is horizontal but this was not observed. The implication of this evidence is that maximum temperatures were attained prior to initiation of deformation.

The organic maturation of the Southwest Portugal Domain has not been as comprehensively studied as the Baixo Alentejo Flysch Group. The VR measurements from SW Portugal are from rocks cropping out in the Aljezur and Bordeira inliers. Here, the Famennian Tercenas Formation has a mean of 3.37% R_r, the Tournaisian Bordalete Formation a mean of 3.26% R_r, the Viséan Murração Formation 4.34% R_r and the Serpukhovian to Bashkirian Quebradas Formation a mean of 3.52% R_r. With the exception of the Murração Formation, the VR values measured for the Southwest Portugal Domain are in general 1% R_r lower than the average values of the Baixo Alentejo Flysch Group rocks of the same age (Table 1). Although VR suppression could be invoked to explain the low values obtained from the predominantly shaly Quebradas Formation, this is most unlikely at such high levels of maturity and the same mechanism cannot be applied to the other coarser-grained formations. More likely explanations for the low R_r values observed are that either the platform-facies sediments of the Aljezur–Bordeira area were a 'sink' for descending, relatively cool fluids, or that this area was situated on a persistent basement high and was less deeply buried than adjacent areas.

Table 1. *Vitrinite reflectance results and calculated palaeotemperatures (in °C), according to Barker & Goldstein (1990)*

Sample	R_r (%)	SD	*n*	Formation	Stratigraphy	Palaeo-temperature (°C)	Latitude (N)			Longitude (W)			Borehole AC-1						
							°	′	″	°	′	″	Sample	Depth (m)	R_r (%)	SD	*n*	Formation	Stratigraphy	Palaeo-temperature (°C)
1	4.09	0.27	70	Mértola	Mid-Viséan	294.4	37	26	50.2	7	27	36.0	AC-1(1)	21	5.06	0.27	63	Mértola	Mid-Viséan	315.8
2	4.38	0.28	70	Mértola	Mid-Viséan	301.3	37	21	49.8	7	30	7.5	AC-1(2)	35.1	5.19	0.25	70	Mértola	Mid-Viséan	318.4
3	5.08	0.39	100	Mértola	Mid-Viséan	316.2	37	35	11.9	7	32	30.4	AC-1(3)	47.7	5.55	0.31	67	Mértola	Mid-Viséan	325.1
4	4.18	0.45	100	Mértola	Mid-Viséan	296.6	37	35	54.5	7	31	45.4	AC-1(4)	64.3	4.96	0.29	70	Mértola	Mid-Viséan	313.8
5	4.75	0.33	75	Mértola	Mid-Viséan	309.5	37	35	10.6	7	32	29.7	AC-1(5)	77.9	4.8	0.22	70	Mértola	Mid-Viséan	310.5
6	5.2	0.47	100	Mértola	Mid-Viséan	318.6	37	29	46.0	7	42	7.9	AC-1(6)	103.6	4.93	0.29	70	Mértola	Mid-Viséan	313.2
7	4.02	0.39	100	Mértola	Mid-Viséan	292.7	37	23	13.8	7	43	40.9	AC-1(7)	140.6	4.75	0.24	36	Mértola	Mid-Viséan	309.5
8	4.22	0.41	100	Mértola	Mid-Viséan	297.6	37	26	2.4	7	48	8.3	AC-1(8)	166.7	5.1	0.27	70	Mértola	Mid-Viséan	316.6
9	4.26	0.3	70	Mértola	Mid-Viséan	298.5	37	21	16.3	7	49	12.7	AC-1(9)	197.2	4.99	0.29	70	Mértola	Mid-Viséan	314.4
10	4.99	0.3	90	Mértola	Mid-Viséan	314.4	37	28	32.3	7	46	39.8	AC-1(10)	246.2	5.08	0.34	70	Mértola	Mid-Viséan	316.2
11	4.26	0.25	70	Mértola	Mid-Viséan	298.5	37	24	31.2	7	44	24.3	AC-1(11)	299.2	4.9	0.35	70	Mértola	Mid-Viséan	312.6
12	4.29	0.29	70	Mértola	Mid-Viséan	299.2	37	22	36.2	7	40	43.7	AC-1(12)	312.8	5.02	0.37	70	Mértola	Mid-Viséan	315.0
13	4.32	0.42	100	Mértola	Mid-Viséan	299.9	37	53	30.7	8	9	32.9	AC-1(13)	322.6	5.07	0.31	70	Mértola	Mid-Viséan	316.0
14	3.97	0.35	65	Mértola	Serpukhovian	291.4	37	16	46.5	7	30	30.8	AC-1(14)	337.1	4.91	0.34	70	Mértola	Mid-Viséan	312.8
15	3.8	0.32	100	Mira	Serpukhovian	287.0	37	14	16.7	7	30	42.2	AC-1(15)	359.9	5.02	0.25	60	Mértola	Mid-Viséan	315.0
16	4.68	0.31	70	Mira	Serpukhovian	308.0	37	21	42.2	8	3	50.4	AC-1(16)	383.7	5.02	0.22	70	Mértola	Mid-Viséan	315.0
17	4.05	0.42	95	Mira	Serpukhovian	293.4	37	15	45.6	7	59	52.1	AC-1(17)	402.8	5.08	0.28	100	Mértola	Mid-Viséan	316.2
18	4.82	0.33	100	Mira	Serpukhovian	310.9	37	16	25.9	8	3	17.5	AC-1(18)	421.5	5.16	0.42	72	Mértola	Mid-Viséan	317.8
19	4.63	0.55	100	Mira	Serpukhovian	306.9	37	23	13.1	8	15	47.4	AC-1(19)	468.6	5.12	0.31	70	Mértola	Mid-Viséan	317.0
20	4.59	0.28	80	Mira	Serpukhovian	306.0	37	23	11.2	7	48	57.2	AC-1(20)	474.1	5.24	0.3	68	Mértola	Mid-Viséan	319.3
21	3.87	0.26	60	Mira	Serpukhovian	288.9	37	20	55.1	7	39	16.2	AC-1(21)	486.8	4.95	0.32	100	Mértola	Mid-Viséan	313.6
22	3.99	0.23	60	Mira	Serpukhovian	291.9	37	18	53.1	7	40	49.7	AC-1(22)	494	5.24	0.32	100	Mértola	Mid-Viséan	319.3
23	4.93	0.25	70	Mira	Serpukhovian	313.2	37	17	13.9	7	39	49.2	AC-1(23)	503	5.1	0.29	70	Mértola	Mid-Viséan	316.6
24	4.68	0.25	70	Mira	Serpukhovian	308.0	37	17	13.9	7	39	49.2	AC-1(24)	522.2	5.06	0.32	58	Mértola	Mid-Viséan	315.8
25	4.5	0.27	70	Mira	Serpukhovian	304.0	37	15	26.5	7	41	27.4	AC-1(25)	539.4	4.92	0.15	39	Mértola	Mid-Viséan	313.0
26	4.32	0.24	90	Mira	Serpukhovian	299.9	37	13	14.0	7	42	20.7	AC-1(26)	554.7	5	0.21	66	Mértola	Mid-Viséan	314.6
27	4.94	0.43	69	Mira	Serpukhovian	313.4	37	11	11.3	7	47	51.5	AC-1(27)	557.5	4.92	0.25	70	Mértola	Mid-Viséan	313.0
28	4.41	0.35	60	Mira	Serpukhovian	302.0	37	14	3.7	7	45	10.3	AC-1(28)	586.9	4.56	0.24	80	Mértola	Mid-Viséan	305.0
29	4.34	0.23	70	Mira	Serpukhovian	300.4	37	14	33.7	7	44	20.3	AC-1(29)	612.7	4.74	0.26	70	VSC	Early Viséan(?)	309.2
30	4.28	0.24	70	Mira	Serpukhovian	299.0	37	16	34.6	7	46	57.3	AC-1(30)	623.1	4.99	0.25	70	VSC	Early Viséan(?)	314.4
31	3.42	0.28	100	Mira	Serpukhovian	276.4	37	15	54.4	8	16	0.9	AC-1(31)	724.9	5.08	0.34	70	VSC	Early Viséan(?)	316.2
32*	4.75	0.47	47	Brejeira	Moscovian	309.5	37	36	3.2	8	49	1.2	AC-1(32)	726.5	4.65	0.27	63	VSC	Early Viséan(?)	307.3
33	4.71	0.59	30	Brejeira	Moscovian	308.6	37	17	44.8	8	52	16.9	AC-1(33)	728.5	4.99	0.23	70	VSC	Early Viséan(?)	314.4
34	4.22	0.29	80	Brejeira	Moscovian	297.6	37	17	44.8	8	52	16.9	AC-1(34)	729.5	5.54	0.37	67	VSC	Early Viséan(?)	324.9
35	4.66	0.43	100	Brejeira	Moscovian	307.5	37	5	50.5	8	56	53.5								
36	4.03	0.31	54	Brejeira	Moscovian	292.9	37	18	24.4	8	23	11.8								
37	4.76	0.28	35	Brejeira	Moscovian	309.7	37	19	10.3	8	22	59.0								
38	4.38	0.41	52	Brejeira	Moscovian	301.3	37	8	54.0	8	54	51.4								
39	4.86	0.6	100	Brejeira	Moscovian	311.8	37	8	54.4	8	54	52.7								
40	5.49	0.37	100	Brejeira	Moscovian	324.0	37	21	6.6	8	24	53.8								
41	5.24	0.38	100	Brejeira	Moscovian	319.3	37	15	54.4	8	16	0.9								
42	5.35	0.57	100	Brejeira	Moscovian	321.4	37	20	50.8	8	28	35.8								
43	4.4	0.26	100	Brejeira	Moscovian	301.8	37	23	48.2	8	41	1.7								
44	4.95	0.18	34	Brejeira	Moscovian	313.6	37	5	58.2	8	56	43.7								
45	4.82	0.37	100	Brejeira	Moscovian	310.9	37	5	55.7	8	56	23.9								
46	3.15	0.39	95	Tercenas	Famennian	268.2	37	5	55.7	8	56	23.9								
47	3.59	0.52	100	Tercenas	Famennian	281.3	37	13	51.1	8	52	48.2								
48	3.78	0.4	100	Bordalete	Tournaisian	286.5	37	13	51.5	8	52	48.5								
49	2.74	0.43	100	Bordalete	Tournaisian	254.1	37	18	18.0	8	44	48.5								
50	3.26	0.4	76	Bordalete	Tournaisian	271.6	37	12	0.7	8	52	38.8								
51	4.34	0.5	100	Murração	Viséan	300.4	37	18	21.1	8	44	46.8								
52	3.18	0.46	100	Quebradas	Serpukhovian	269.1	37	17	46.2	8	44	23.5								
53	4.36	0.54	100	Quebradas	Serpukhovian	300.8	37	9	1.8	8	54	51.5								
54	3.8	0.54	100	Quebradas	Serpukhovian	287.0	37	9	1.8	8	54	51.5								
55	2.97	0.28	100	Quebradas	Serpukhovian	262.3	37	9	1.8	8	54	51.5								
56	3.3	0.59	100	Quebradas	Serpukhovian	272.8	37	9	1.8	8	54	51.5								

All samples are shale with the exception of sample 32, which is a thin coal lens. R_r, vitrinite reflectance values (%); SD, standard deviation; *n*, number of vitrinite particles measured. Location of Borehole AC1: 37°26′18.29″N, 7°37′49.59″W. VSC, Volcano-Sedimentary Complex.

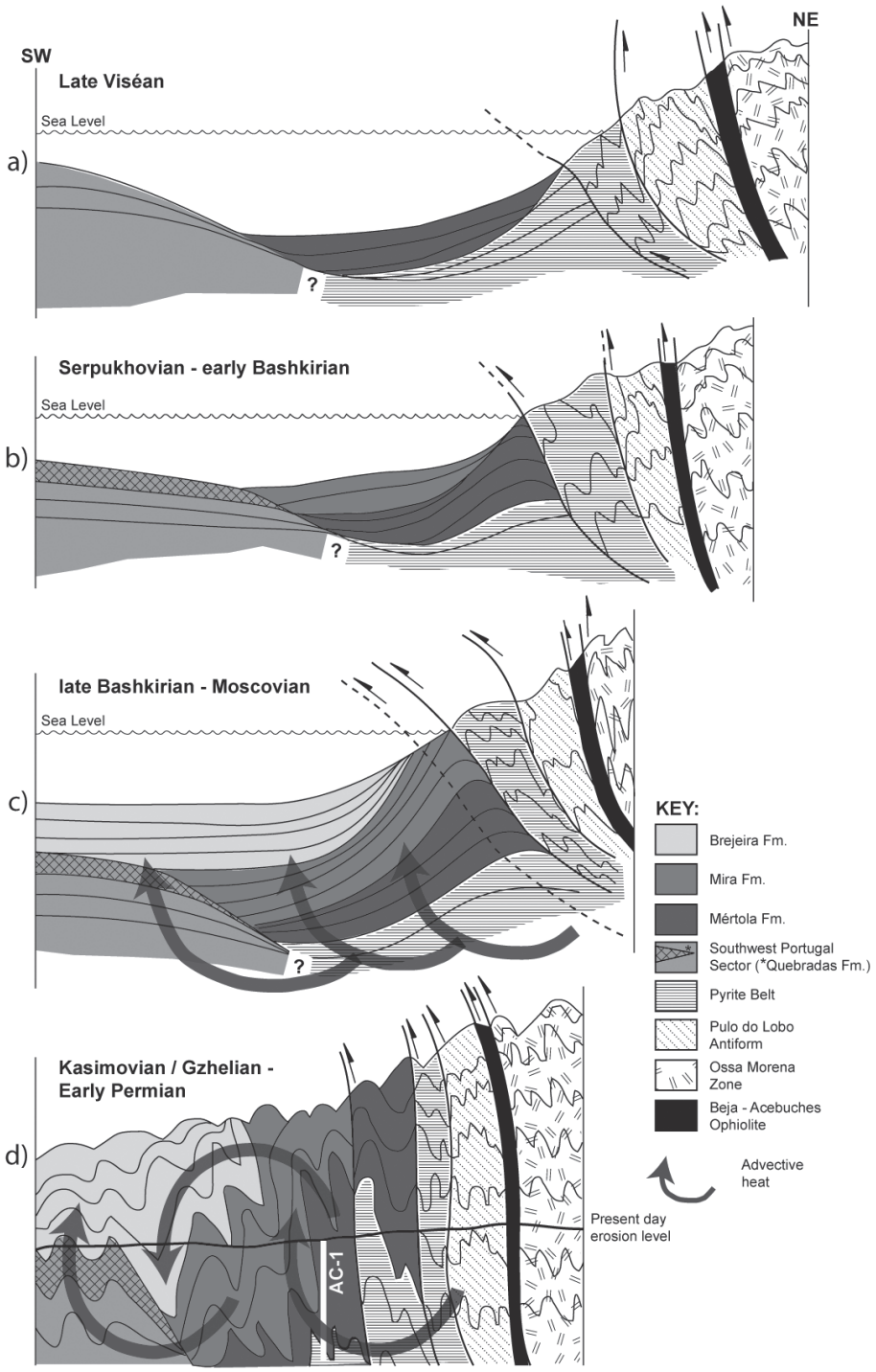

Fig. 4. Schematic cross-sections illustrating the tectonic and thermal evolution of the Late Palaeozoic rocks of the South Portuguese Zone. Figures not to scale. (**a**) Late Viséan. Rapid subsidence (>2 km) and start of turbiditic deposition (Mértola Formation). Early Variscan thrusting in the north involves the Pulo do Lobo and Pyrite Belt. Deposition of muds and limestones (Murração Formation) on the distal part of a carbonate platform in Southwest Portugal Domain. (**b**) Serpukhovian–early Bashkirian. Deposition of the Mira Formation; continuing rapid subsidence. Thrusting continues in the north and propagates southwards. Deposition of muds in anoxic environments in SW Portugal Sector (Quebradas Formation). (**c**) Late Bashkirian–Moscovian. Deposition of the Brejeira Formation, which progrades southwards and onlaps onto the platform-facies rocks in the Southwest Portugal Domain. Thrusting continues in the north and starts to involve the Mértola and Mira Formations. Increasing topographic relief owing to thrust sheet stacking initiates advective heating, which becomes the main mechanism for heat transfer. Enhanced burial maturation at relatively shallow depth in the south caused by high geothermal gradient. (**d**) Kasimovian/Gzhelian–Early Permian. End of main phase of Variscan deformation and maximum relief of mountain ranges. Advective heating homogenizes temperatures across the entire South Portuguese Zone.

Thermal history

High maturity in Western European Late Palaeozoic rocks has been noted by several researchers. For example, Cornford *et al*. (1987), described VR in the Culm Basin of SW England ranging from 4.4 to 5.6%. Those workers attributed the high values to a combination of several factors: burial, Variscan thrusting and the emplacement of the Dartmoor Granite. The Culm succession of turbidites and subsidiary black shales is closely comparable in age, facies and maturity with the Mira and Brejeira formations in SW Portugal (Oliveira & Quesada 1998). Hower & Gayer (2002) drew attention to the importance of advective heating in Palaeozoic foreland basins, based on four case studies from the USA, South Wales and Australia. A model that is consistent with our results in SW Portugal is discussed below and illustrated in Figure 4.

Pre-Variscan

Our data suggest that the attainment of peak temperatures during late Pennsylvanian time was the consequence of simple, pre-tectonic burial. The high maturity of rocks towards the top of the Pennsylvanian succession (Table 1) necessitates a high geothermal

gradient at this time in view of the limited thickness of cover section available at this time.

Based on geophysical evidence, Simancas *et al*. (2006) suggested that magma trapped in the mid-crust within the Iberian Variscides produced high geothermal gradients and postulated the development of a mantle plume in early Carboniferous time. Doblas *et al*. (1998) also inferred the existence of a pan-European mantle plume but based this on the geochemistry of volcanic rocks and suggested that this was a later (latest Carboniferous–early Permian) event. However, if the advective fluid flow system described below was operative in late Carboniferous time, it could have produced a sufficiently high geothermal gradient to explain the observed maturity of the Late Palaeozoic units in SW Portugal, obviating the need for any mantle plume.

Variscan

Temperatures remained high but did not exceed the maximum attained before Variscan deformation. The evidence for this is the optic fabric determined from the oriented coal samples from Arrifana. Advective heating by hot fluids expelled during Variscan folding and thrusting produced relatively uniform high temperatures in the upper crust, overprinting any existing vertical VR gradient.

In the Brejeira Formation (incorrectly identified by Zulauf *et al*. 2011 as the Mértola Formation), fluid inclusions from vertical and horizontal veins genetically related to Variscan folding indicate peak temperatures of 200 ± 20 °C for vertical veins and 230 ± 22 °C for horizontal veins. Palaeotemperatures calculated from VR in the present study are in the range of 276–325 °C with mean 304 °C in the Baixo Altentejo Flysch Group (Table 1), supporting our contention that peak temperatures were achieved prior to Variscan deformation but still remained high during and after deformation.

Post-Variscan

Evidence for high temperatures having been maintained for some time after deformation is provided by the similarity of VR in Carboniferous rocks at the surface throughout SW Portugal, regardless of their stratigraphic age. In borehole AC-1, the lack of any downhole increase in VR through *c*. 700 m of section is not consistent with conductive heating in a 'normal' burial maturation regime but suggests advective heat transfer. Based on hydrogeological modelling, Gayer *et al*. (1998) attributed the anthracite rank of parts of the South Wales Coalfield to 'topographically driven fluid flow systems that developed soon after the climax of the Variscan orogeny'. Those workers also suggested a very short (1–2 Ma) duration for the flow system after maximum uplift.

We suggest that a similar fluid flow regime in the Late Palaeozoic units of SW Portugal was established, driven by thrusting and tectonic stacking to the north in the Pulo do Lobo Antiform and the northern branch of the Pyrite Belt (Silva *et al*. 1990). The anomalously low maturity of platform-facies rocks in the Aljezur–Bordeira antiforms may be a consequence of this area having been a 'sink' for descending, relatively cool fluids.

Variscan deformation was clearly followed by uplift and erosion but the timing of this is poorly constrained. Late Triassic sediments and volcanic rocks unconformably overlie deformed and highly mature Devonian and Carboniferous strata throughout SW Portugal. The much lower maturity of the Triassic units (*c*. 1.1% R_r) is due to Mesozoic burial (McCormack *et al*. 2007). Mesozoic re-burial of the already highly mature Late Palaeozoic rocks did not elevate their temperatures sufficiently to further increase their maturity.

Conclusions

The organic maturity of the Late Palaeozoic rocks of SW Portugal is very high, mainly corresponding to meta-anthracite coal rank. The slightly lower maturity of older, platform-facies rocks in the Aljezur–Bordeira antiforms resulted either from this area having been a sink for desending, relatively cold fluids or from less burial than adjacent parts of the basin. The optic fabric of vitrinite in oriented coal samples from the Brejeira Formation indicates maturation under simple, non-tectonic burial conditions; that is, peak temperatures were attained prior to Variscan deformation. The high maturity of samples from close to the top of the preserved Pennsylvanian (Moscovian) section suggests an anomalously high late Carboniferous geothermal gradient. The lack of any increase in VR through *c*. 700 m of section in borehole AC-1 is not consistent with conductive heat transfer but suggests advective heating. Mesozoic re-burial of the Late Palaeozoic rocks had no effect on their already high maturity.

This work is a contribution to the project POCI/CTE-GEX/60278/2004 financed by the Portuguese Foundation for Science and Technology (Fundação para a Ciência e a Tecnologia; FCT). P.F. wishes to thank J. Matos from the LNEG–Beja for facilitating access to the core and data for borehole AC-1.

References

Abad, I., Mata, M.P., Nieto, F. & Velilla, N. 2001. The phyllosilicates in diagenetic rocks of the South Portuguese Zone, Southwestern Portugal. *Canadian Mineralogist*, **39**, 1571–1589.

Barker, C.E. & Goldstein, R.H. 1990. Fluid-inclusion technique for determining maximum temperature in calcite and its comparison to the vitrinite reflectance geothermometer. *Geology*, **18**, 1003–1006.

Boogaard, M. 1963. Conodonts of Upper Devonian and Lower Carboniferous age from Southern Portugal. *Geologie en Mijnbouw*, **42**, 248–259.

Boogaard, M. 1967. *Geology of Pomarão region (Southern Portugal)*. PhD thesis, University of Amsterdam.

Braid, J., Murphy, J., Quesada, C. & Mortensen, J. 2011. Tectonic escape of a crustal fragment during the closure of the Rheic Ocean: U–Pb detrital zircon data from the Late Palaeozoic Pulo do Lobo and South Portuguese zones, southern Iberia. *Journal of the Geological Society, London*, **168**, 383–392.

Cornford, C., Yarnell, L. & Murchison, D.G. 1987. Initial vitrinite reflectance results from the Carboniferous of north Devon and north Cornwall. *Proceedings of the Ussher Society: Geoscience in South-West England*, **6**, 461–467.

Doblas, M., Oyarzun, R., *et al*. 1998. Permo-Carboniferous volcanism in Europe and northwest Africa: a superplume exhaust valve in the centre of Pangaea? *Journal of African Earth Sciences*, **26**, 89–99.

Fernandes, P., Luís, J., Rodrigues, B., Marques, M., Valentim, B. & Flores, D. 2010. The measurement of vitrinite reflectance with MatLab. *In*: Oliwkiewicz-Miklasinka, M., Stempien-Salek, M. & Laptas, A. (eds) *CIMP Poland General Meeting, September 2010*. Institute of Geological Sciences, Polish Academy of Sciences, Warsaw, 11–13.

Gayer, R., Garven, G. & Rickard, D. 1998. Fluid migration and coal-rank development in foreland basins. *Geology*, **26**, 679–682.

Hillier, S. & Marshall, J. 1988. A rapid technique to make polished thin sections of sedimentary organic matter concentrates. *Journal of Sedimentary Petrology*, **58**, 754–755.

Hower, J.C. & Gayer, R.A. 2002. Mechanisms of coal metamorphism: case studies from Paleozoic coalfields. *International Journal of Coal Geology*, **50**, 215–245.

Korn, D. 1997. *The Palaeozoic ammonoids of the South Portuguese Zone*. Memórias dos Serviços Geológicos de Portugal, **33**.

Levine, J.R. & Davis, A. 1989. The relationship of coal fabrics to the Alleghanian tectonic deformation in the central Appalachian fold-and-thrust belt, Pennsylvania. *Geological Society of America Bulletin*, **101**, 1333–1347.

Luis, J. 2007. Mirone: a multi-purpose tool for exploring grid data. *Computers and Geosciences*, **33**, 31–41.

McCormack, N. 1998. *The thermal history of the South Portuguese Zone*. PhD thesis, University of Dublin.

McCormack, N., Clayton, G. & Fernandes, P. 1998. Poder reflector da vitrinite, mineralogia das argilas e cristalinidade da ilite na Zona Sul Portuguesa. *Comunicações do Instituto Geológico e Mineiro*, **84**, 34–35.

McCormack, N., Clayton, G. & Fernandes, P. 2007. The thermal history of the Upper Palaeozoic rocks of southern Portugal. *Marine and Petroleum Geology*, **24**, 145–150.

Moço, L.P., Rocha, F., Pereira, Z., Lemos de Sousa, M.J., Gomes, C. & Oliveira, J.T. 1998. Petrologia Orgânica do Sector Sudoeste da Zona Sul Portuguesa. *Comunicações do Instituto Geológico e Mineiro*, **84**, 26–29.

Munhá, J. 1983. Hercynian magmatism in Iberian Pyrite Belt. *In*: Lemos de Sousa, M.J. & Oliveira, J.T. (eds) *The Carboniferous of Portugal*. Memórias dos Serviços Geológicos de Portugal, Lisbon, **29**, 39–82.

Munhá, J. 1990. Metamorphic evolution of the South Portuguese/Pulo do Lobo Zone. *In*: Dallmeyer, R.D. & Martínez García, E. (eds) *Pre-Mesozoic Geology of Iberia*. Springer, Berlin, 363–368.

Oliveira, J. & Wagner Genthis, C. 1983. The Mértola and Mira formations boundary between Doguedo and Almada do Ouro, marine Carboniferous of South Portugal. *In*: Lemos de Sousa, M.J. (ed.) *Contributions to the Carboniferous Geology and Palaeontology of the Iberian Peninsula*. Universidade do Porto, Porto, 1–39.

Oliveira, J.T. 1990. Stratigraphy and syn-sedimentary tectonism in the South Portuguese Zone. *In*: Dallmeyer, R.D. & Martínez García, E. (eds) *Pre-Mesozoic Geology of Iberia*. Springer, Berlin, 333–347.

Oliveira, J. & Quesada, C. 1998. A comparison of stratigraphy, structure and paleogeography of the South Portuguese Zone and Southwest England, European Variscides. *Proceedings of the Ussher Society: Geoscience in South-West England*, **9**, 141–150.

Oliveira, J., Horn, M. & Paproth, E. 1979. Preliminary note on the stratigraphy of the Baixo–Alentejo Flysch Group, Carboniferous of Portugal, and on the palaeogeographic development compared to corresponding units in Northwest Germany. *Comunicações dos Serviços Geológicos de Portugal*, **65**, 151–168.

Oliveira, J.T., Horn, M., Kullmann, J. & Paproth, E. 1985. The stratigraphy of the Upper Devonian and Carboniferous sediments of Southwest Portugal. *In: X Congreso Internacional de Estratigrafia e Geología del Carbonífero, Instituto Geológico y Minero de España*. Comisión Nacional de Geología de España, Madrid, **1**, 1–17.

Oliveira, J.T., Pereira, Z., Carvalho, P., Pacheco, N. & Korn, D. 2004. Stratigraphy and tectonically imbricated lithological succession of the Neves–Corvo Mine Region, Iberian Pyrite Belt: implications for the regional basin dynamics. *Mineralium Deposita*, **39**, 422–436.

Oliveira, J.T., Pereira, Z., Rosa, C., Rosa, D. & Matos, J. 2005. Recent advances in the study of the stratigraphy and the magmatism of the Iberian Pyrite Belt, Portugal. *Journal of the Virtual Explorer*, **19/9**, doi:10.3809/jvirtex.2005.00123.

Oliveira, J.T., Relvas, J., *et al.* 2006. O Complexo Vulcano-Sedimentar da Faixa Piritosa: estratigrafia, vulcanismo, mineralizações associadas e evolução tectono-estratigráfica no contexto da Zona Sul Portuguesa. *In*: Dias, R., Araújo, A., Terrinha, P. & Kullberg, J.C. (eds) *Geologia de Portugal no contexto da Ibéria*. University of Évora, Évora, 207–243.

Pereira, Z. 1997. Palinologia e petrologia orgânica do Sector Sudoeste da Zona Sul Portuguesa. PhD thesis, Universidade do Porto.

Pereira, Z. 1999. Palinoestratigrafia do Sector Sudoeste da Zona Sul Portuguesa. *Comunicações dos Serviços Geológicos de Portugal*, **86**, 25–57.

Pereira, Z., Fernandes, P. & Oliveira, J.T. 2006. The upper Devonian palynostratigraphy and organic matter maturation of the Pulo do Lobo Domain, South Portuguese Zone, Portugal. *Comunicações Geológicas*, **93**, 23–38.

Pereira, Z., Matos, J., Fernandes, P. & Oliveira, J.T. 2007. Devonian and Carboniferous palynostratigraphy of the South Portuguese Zone, Portugal—an overview. *Comunicações Geológicas*, **94**, 53–79.

Pereira, Z., Matos, J., Fernandes, P. & Oliveira, J.T. 2008. *Palynostratigraphy and Systematic Palynology of the Devonian and Carboniferous successions of the South Portuguese Zone, Portugal*. Memória do INETI, **34**.

Quesada, C., Fonseca, P., Munhá, J., Oliveira, J.T. & Ribeiro, A. 1994. The Beja–Acebuches Ophiolite (Southern Iberia Variscan fold belt): geological characterization and geodynamic significance. *Boletin Geológico Minero*, **105**, 3–49.

Silva, J.B., Oliveira, J.T. & Ribeiro, A. 1990. The South Portuguese Zone: structural outline. *In*: Dallmeyer, R.D. & Martínez García, E. (eds) *Pre-Mesozoic Geology of Iberia*. Springer, Berlin, 348–362.

Simancas, J.F., Carbonell, R., *et al.* 2006. Transpressional collision tectonics and mantle plume dynamics: the Variscides of southwestern Iberia. *In*: Gee, D.G. & Stephenson, R.A. (eds) *European Lithosphere Dynamics*. Geological Society, London, Memoirs, **32**, 345–354.

Taylor, G.H., Teichmuller, M., Davis, A., Diessel, C.F.K., Littke, R. & Robert, P. 1998. *Organic Petrology*. Borntraeger, Berlin.

Zulauf, G., Gutiérrez-Alonso, G., Kraus, R., Petschick, R. & Potel, S. 2011. Formation of chocolate-tablet boudins in a foreland fold and thrust belt: a case study from the external Variscides (Almograve, Portugal). *Journal of Structural Geology*, **33**, 1639–1649.

Received 14 December 2011; revised typescript accepted 14 May 2012.
Scientific editing by John Marshall.

Discrimination of sediment samples for forensic application using REE

A. RODRIGUES, A. GUEDES*, H. RIBEIRO, B. VALENTIM AND F. NORONHA

Centro de Geologia da Universidade do Porto e Departamento de Geociências, Ambiente e Ordenamento do Território, Faculdade de Ciências, Universidade do Porto, Rua do Campo Alegre 687, Porto, Portugal (*correspondence: aguedes@fc.up.pt)

The geochemical signature of sediments is currently used as trace evidence in forensic investigations. In this research, geochemical studies have been carried out on Portuguese coastal sands aiming to ascertain its use for forensic purposes.

Rare Earth Elements (REE) concentrations were determined on samples collected on three coastal areas surrounded by different geological contexts, namely limestone, granite and metasediment. Eight sand samples were collected along transects perpendicular to the coastline, in beach and dune from each site. Each sample was manually collected with a plastic spade from the surface sediment, at a depth of approximately 0-5cm. From the sediment samples a standardized particle size fraction of <150 μm was obtained by dry sieving method and subsequently grinded to minimise the variation in the geochemical properties due to particle size.

The REE composition fraction was determined using four acid digestions ultratrace ICP-MS analysis at ACME labs (Canada), and concentrations calculated. Although the measured REEs concentrations can be compared directly for forensic purposes a normalisation reported to condrite meteorites was performed [1].

A REEs normalised concentration and a hierarchical cluster analyses were performed to obtain discrimination between samples. They reveal differences between samples associated with different geological context, and permitted the discrimination between samples surrounded by granite from samples surrounded by limestone and metasediments. It was also possible to discriminate some of the samples based on their REE concentration and profile.

This research was supported by Project PTDC/CTE-GEX/67442/2006 of FCT (Portugal).

[1] Taylor & McLennan (1985) Blackwell Scientific Publications, 312p.

Geochemical signatures in detrital tourmalines as indicators for sediment provenance: The Baixo Alentejo Flysch Group, South Portuguese Zone

B. RODRIGUES[1]*, P. DIAS[2], R.C.G.S. JORGE[3] AND P. FERNANDES[1]

[1]CIMA, University of the Algarve, Campus de Gambelas, 8005-139 Faro, Portugal (*correspondence: bmgrodrigues@sapo.pt, pfernandes@ualg.pt)
[2]CIG-R, University of Minho (patriciasdias@gmail.com)
[3]CREMINER LA/ISR, Dep. Geologia, Fac. Ciências da Universidade de Lisboa (rjorge@fc.ul.pt)

Microprobe analyses were made to infer the source of detrital tourmalines from the Mid to Late Carboniferous turbiditic deposits of the Baixo Alentejo Flysch Group (BAFG) of the South Portuguese Zone. A representative group of greywacke samples covering the whole range of the BAFG ages was collected for this study. Tourmalines have brown to brownish gray colors and do not show any optical zonation. In the Fe-Mg-Al diagram, the tourmalines fall into the fields of Ca-poor metapelites, metapsammites and quartz-tourmaline rocks. Microprobe analyses revealed a range of values between schorl and dravite end members, being closer to the latter, with variable contents of X-site vacancies (0.05-0.255 apfu), Ca (0.078-0.2 apfu), Na (0.627-0.924 and Al (5.746-6.622 apfu). The Fe/(Fe+Mg) and Na/(Na+Ca) ratios range from 0.32-0.45 and 0.79-0.91, respectively.

The presence of well-rounded tourmaline grains suggests that they could have derived from a source located at a great distance from the sedimentary basin, or from reworked sedimentary rocks. The occurrence of few euhedral grains indicates minor contribution from first cycle sediments. Together, these data suggest that the detrital BAFG tourmalines derived from multiple sources with the predominance of rocks with a felsic composition.

Bruno Rodrigues holds a PhD grant from the Portuguese Foundation for Science and Technology (n.° SFRH/BD/62213/2009).

ANNEX II

Vitrinite reflectance histograms

ANNEX II

AR2

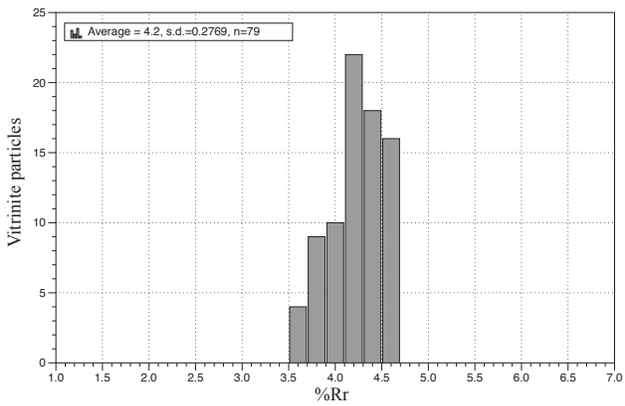

MM3

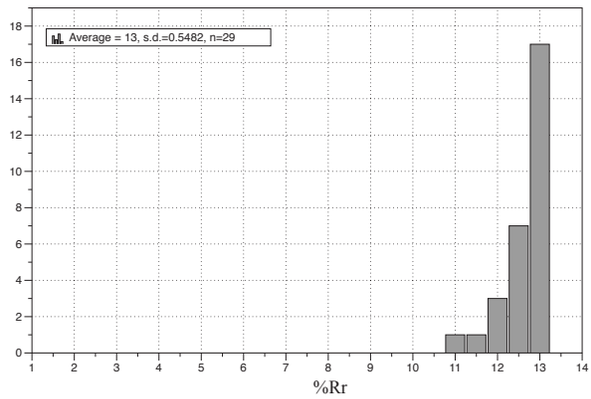

JVN1

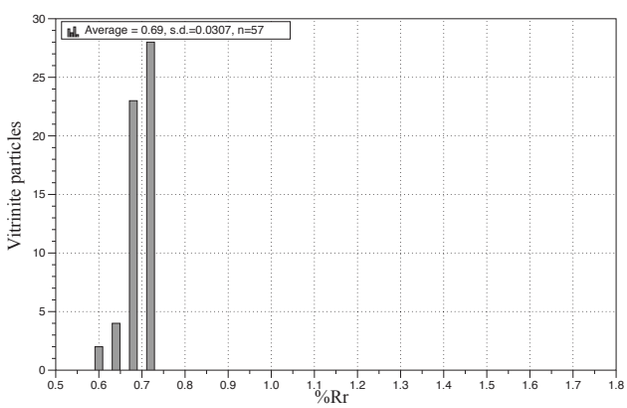

JVN2

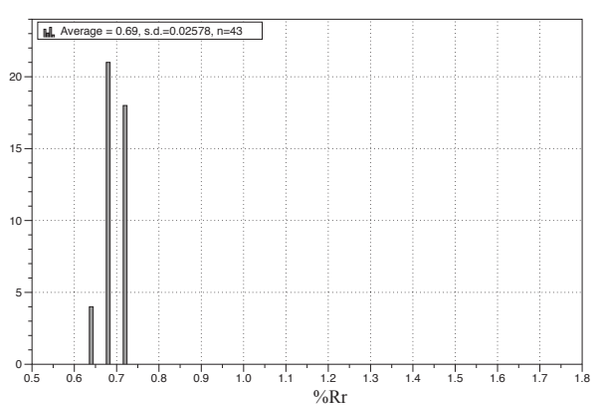

JVN4

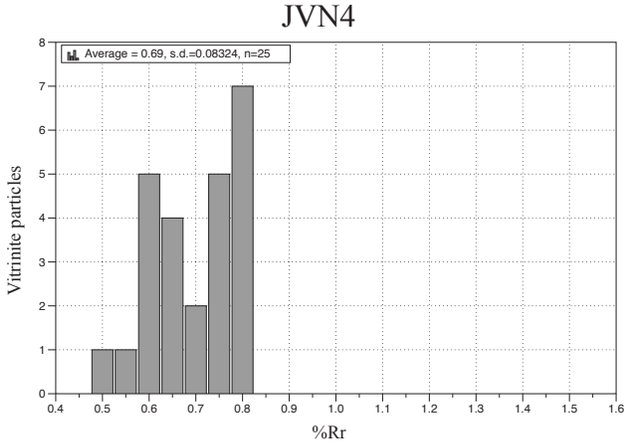

ANNEX II

CST1-475 m

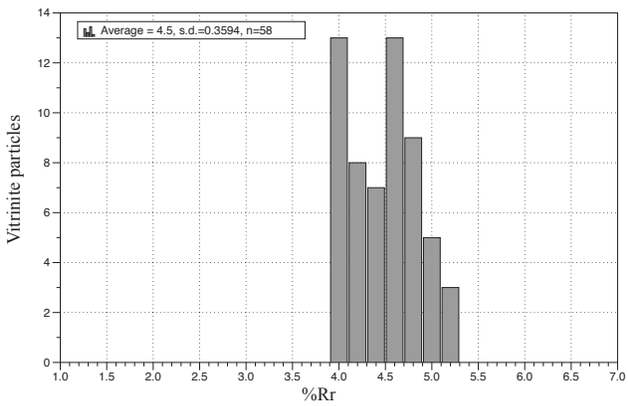

CST1-526 m

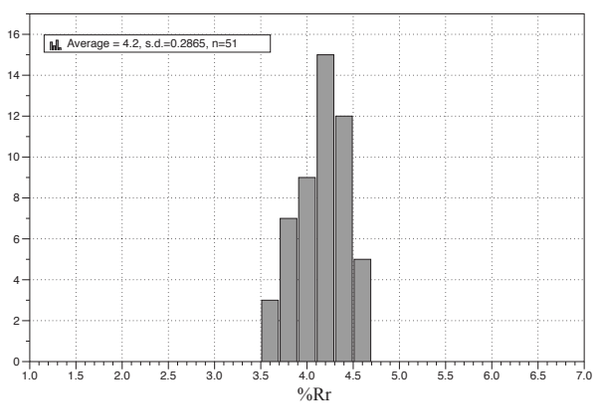

CST1-584 m

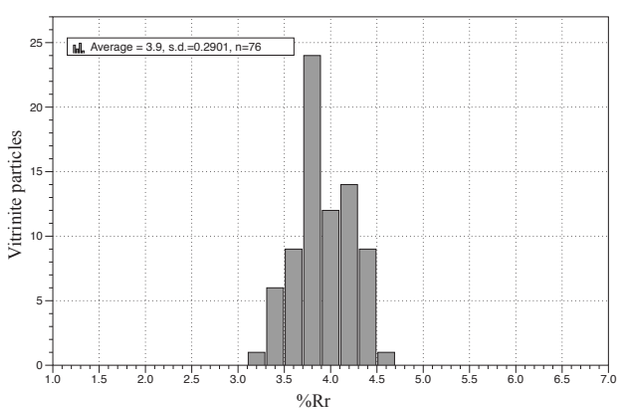

RIT2

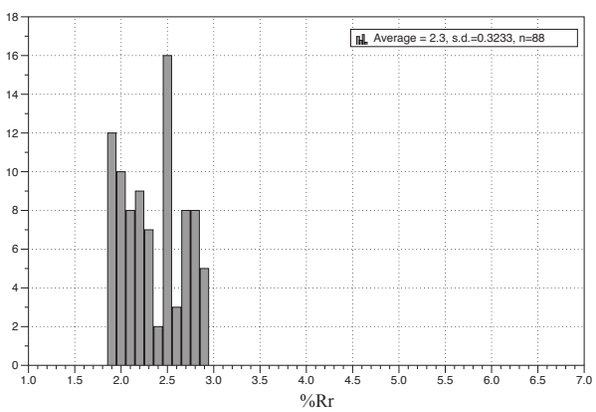

VNC2

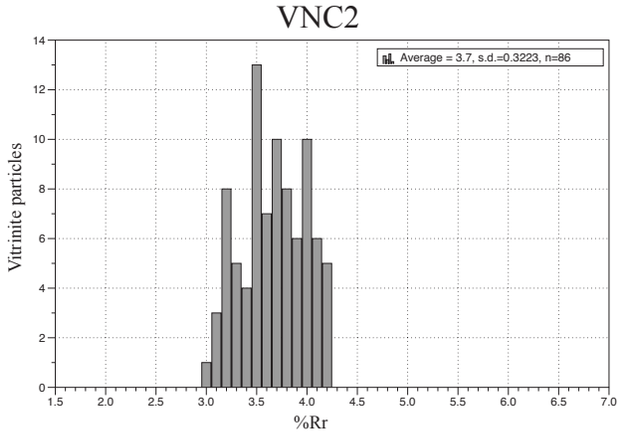

VNC3

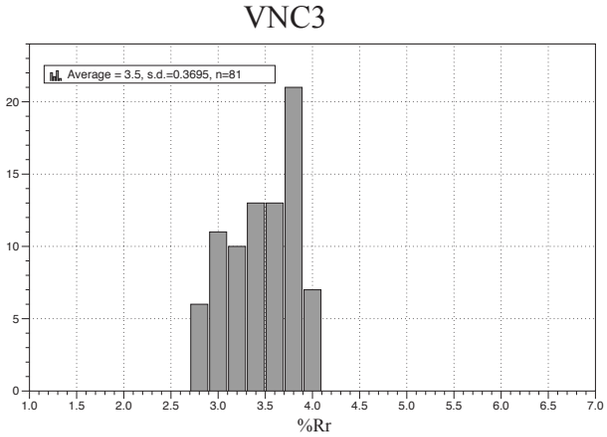

IC1-2

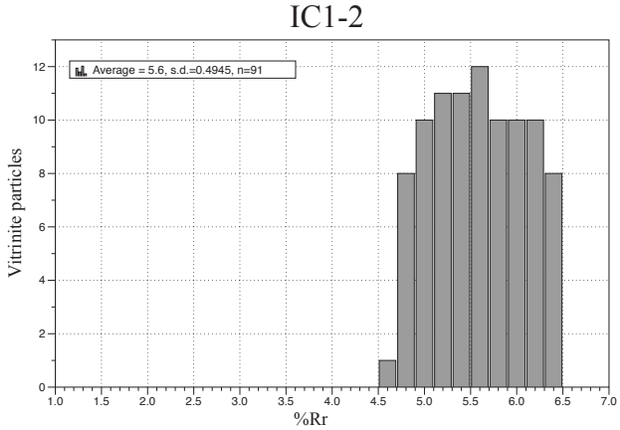

BA1

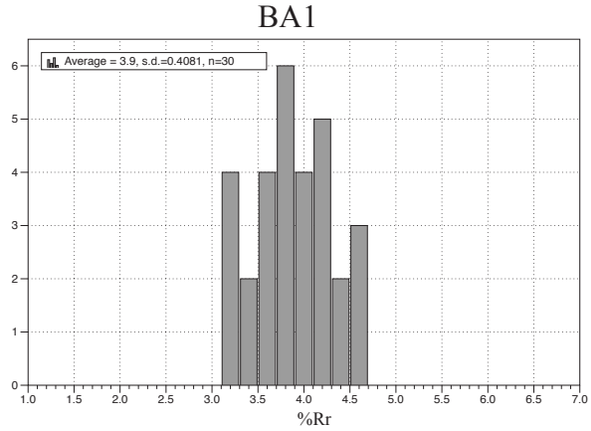

ANNEX II

CST1-582 m

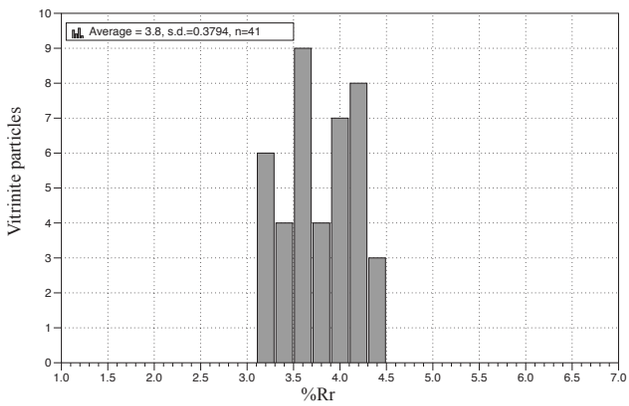

CST1-646 m

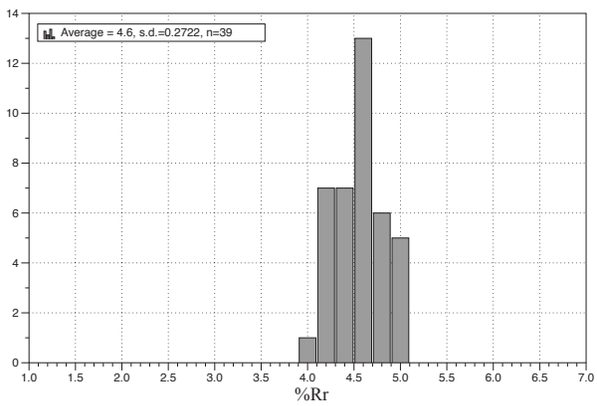

CST1-677 m

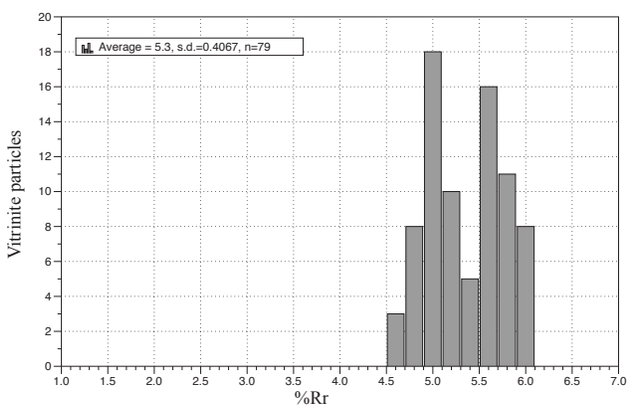

CT1-46 m

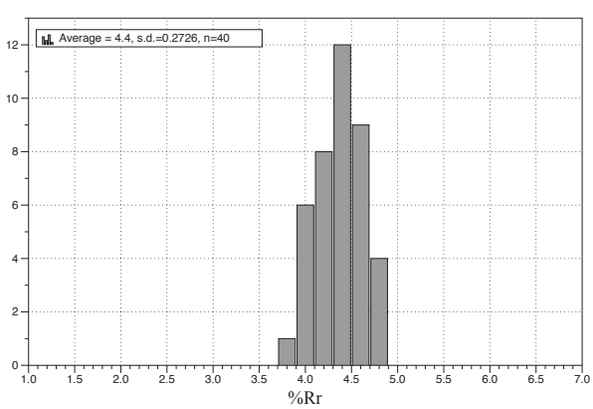

CT1-108 m

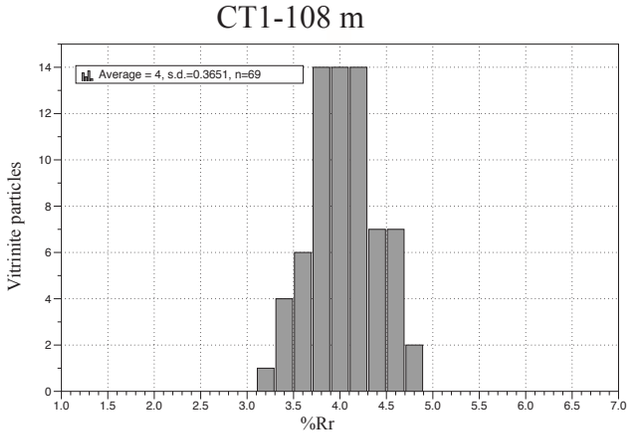

CT1-141 m

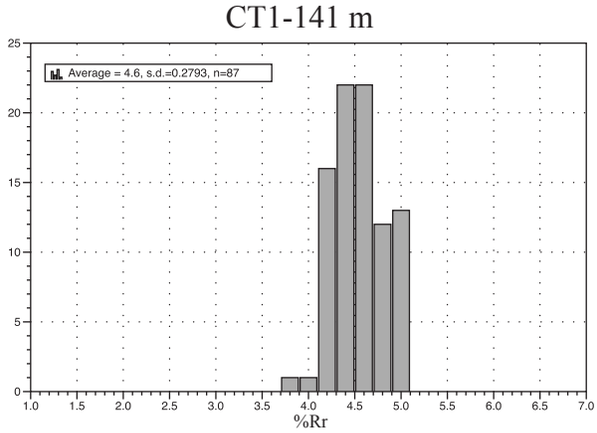

CT1-314 m

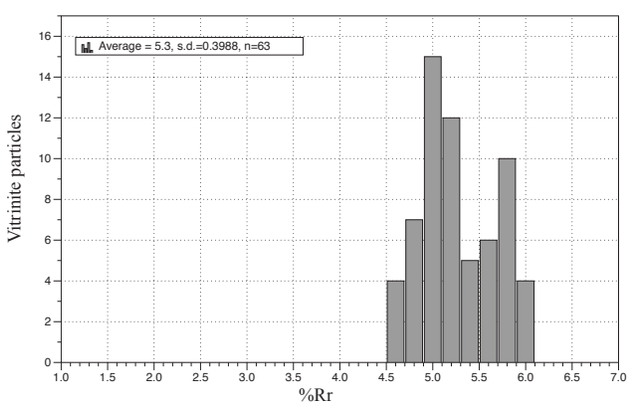

CT1-359 m

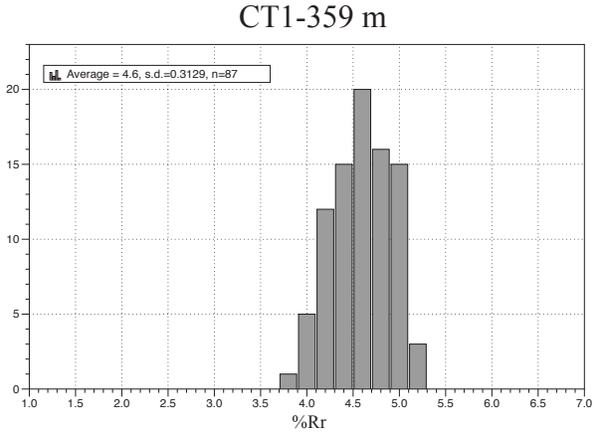

ANNEX II

CST1-13 m

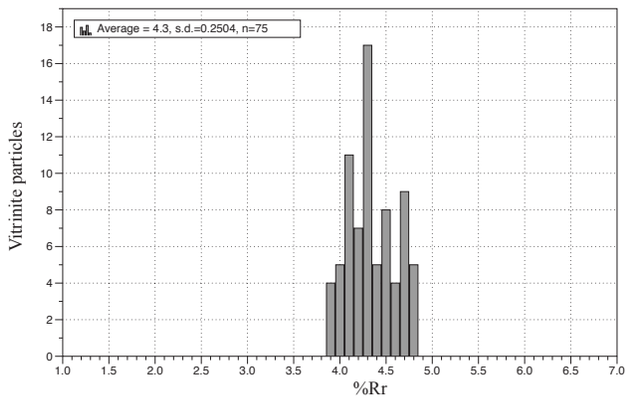

CST1-56 m

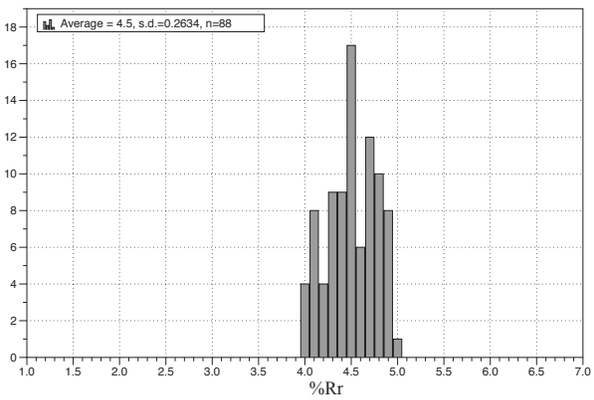

CST1-88 m

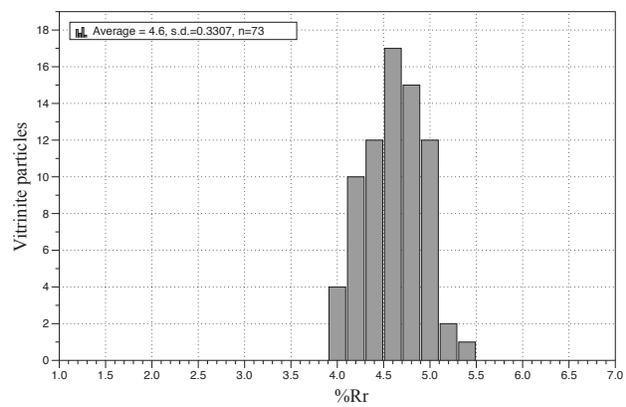

CST1-211 m

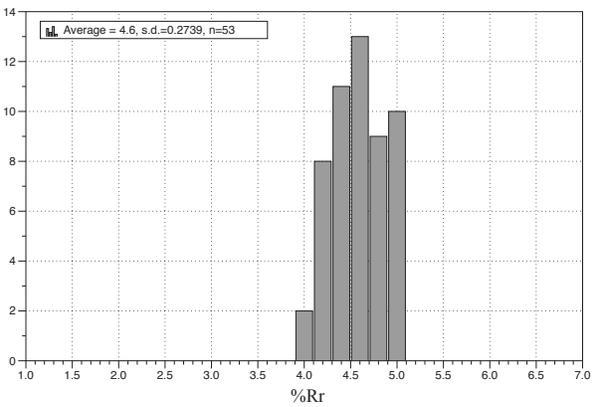

CST1-281 m

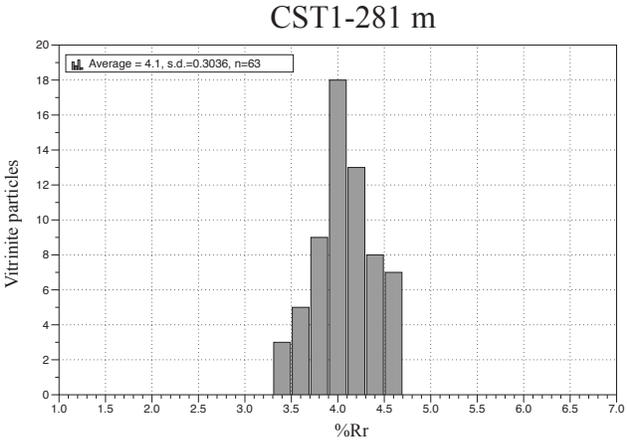

CST1-354 m

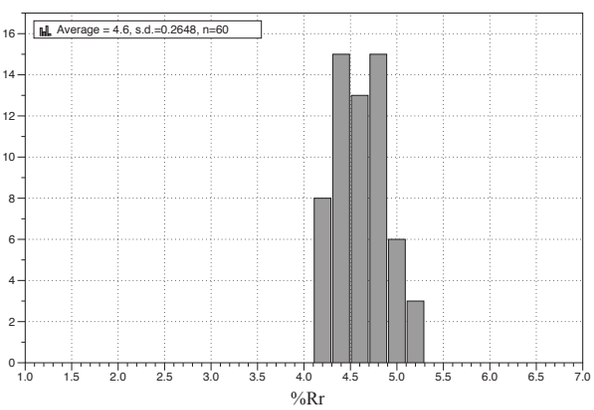

CST1-401 m

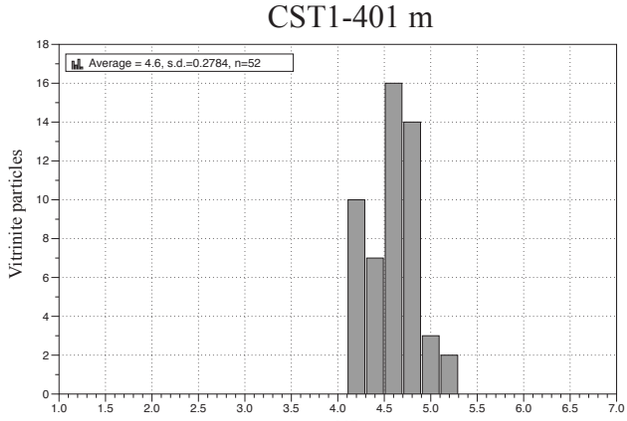

CST1-483 m

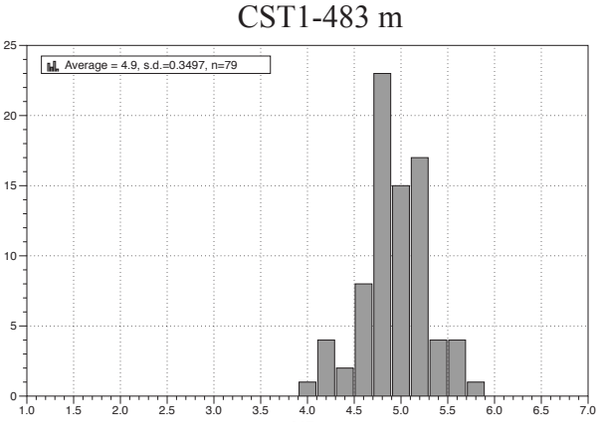

ANNEX III

Detrital zircon U-Pb data

Grain number	$^{207}Pb/^{235}U$ ratio	±(2σ, %)	$^{207}Pb/^{235}U$ age (Ma)	±Ma (2σ)	$^{206}Pb/^{238}U$ ratio	±(2σ, %)	$^{206}Pb/^{238}U$ age (Ma)	±Ma (2σ)	discordance (%)	U conc (ppm)
Mértola Formation (FM1)										
FM1_2	0.401	0.013	190	100	0.0558	0.0017	340	19	4	416
FM1_5	0.454	0.014	170	96	0.0583	0.0017	354	15	5	398
FM1_6	0.419	0.013	219	99	0.0548	0.0016	341	18	7	326
FM1_8	0.947	0.026	513	64	0.0975	0.0029	587	20	8	672
FM1_9	8.17	0.22	2220	34	0.408	0.012	2193	53	4	307
FM1_12	0.403	0.015	173	99	0.0551	0.0018	328	13	6	335
FM1_14	0.661	0.019	377	98	0.0818	0.0024	497	18	4	401
FM1_15	0.394	0.016	80	180	0.0553	0.0017	329	26	7	225
FM1_17	0.419	0.016	20	130	0.0574	0.0017	335	19	7	241
FM1_19	0.419	0.014	171	95	0.0556	0.0017	335	13	5	465
FM1_20	0.604	0.02	220	110	0.0654	0.002	383	17	10	437
FM1_22	0.412	0.016	269	67	0.0552	0.0018	340	12	5	697
FM1_24	6.53	0.18	1985	53	0.398	0.012	2134	57	6	192
FM1_25	0.414	0.032	500	220	0.0591	0.0021	376	28	9	166
FM1_26	0.45	0.015	210	130	0.0605	0.0019	366	20	6	255
FM1_27	0.587	0.018	400	110	0.0822	0.0026	501	20	6	335
FM1_28	0.431	0.016	307	98	0.0585	0.0018	356	15	6	357
FM1_29	0.486	0.014	346	46	0.0581	0.0017	359	12	6	921
FM1_30	0.402	0.023	160	210	0.0569	0.002	348	23	7	243
FM1_32	0.437	0.014	290	100	0.0636	0.002	388	18	6	412
FM1_33	0.421	0.025	170	300	0.06	0.0024	373	29	7	228
FM1_34	0.42	0.027	420	310	0.0612	0.0021	359	51	10	125
FM1_37	0.76	0.025	502	47	0.0959	0.0037	589	21	5	1055
FM1_39	0.63	0.019	415	84	0.0829	0.0025	503	17	5	384
FM1_40	0.388	0.012	198	85	0.0533	0.0016	327	13	5	488
FM1_45	0.714	0.021	575	88	0.0811	0.0024	506	21	6	520
FM1_52	0.631	0.018	424	92	0.0715	0.0021	440	20	7	422
FM1_54	1.637	0.06	810	240	0.1525	0.0047	897	56	7	113
FM1_58	0.673	0.022	380	140	0.078	0.0023	471	26	7	224
FM1_62	5.95	0.16	1810	110	0.393	0.011	2096	61	9	126
FM1_63	0.407	0.012	199	78	0.0579	0.0017	349	14	5	656
FM1_64	0.377	0.016	223	85	0.0534	0.0018	326	16	5	558
FM1_66	0.409	0.016	230	130	0.0574	0.0018	346	23	6	234
FM1_68	0.405	0.015	210	120	0.0618	0.0019	384	22	7	548
FM1_69	0.46	0.015	260	62	0.0584	0.0018	354	14	5	704
FM1_70	0.429	0.028	239	80	0.0621	0.002	370	16	10	362
FM1_71	0.415	0.019	140	150	0.0616	0.002	370	21	8	237
FM1_73	0.406	0.013	257	99	0.0599	0.0018	368	20	6	378
FM1_76	0.415	0.015	250	140	0.057	0.0017	336	30	8	194
FM1_77	0.423	0.017	180	130	0.0582	0.0018	349	24	6	300
FM1_78	0.447	0.029	530	200	0.0623	0.0021	360	42	9	136
FM1_79	0.411	0.015	280	100	0.0558	0.0017	345	15	4	538
FM1_80	0.478	0.022	690	160	0.0598	0.0019	358	36	10	110
FM1_81	0.728	0.028	370	200	0.0899	0.0027	537	35	6	215
FM1_82	0.774	0.023	515	84	0.0919	0.0027	563	23	4	428
FM1_84	0.889	0.024	597	73	0.1016	0.0029	619	21	4	588
FM1_89	0.409	0.015	220	170	0.0542	0.0017	335	19	6	314
FM1_98	0.454	0.012	296	55	0.0552	0.0017	340	11	5	1133
FM1_99	4.93	0.13	1788	45	0.32	0.01	1786	50	4	449
FM1_100	0.407	0.017	300	180	0.0551	0.0018	334	22	7	237
Mira Formation (AO1)										
AO1_4	0.389	0.016	140	100	0.0541	0.0012	326	13	8	264
AO1_7	0.394	0.016	160	120	0.0546	0.0013	330	14	9	234
AO1_10	0.623	0.032	350	150	0.0775	0.002	454	24	9	127
AO1_11	0.404	0.018	150	110	0.0543	0.0014	327	11	9	259
AO1_13	5.19	0.15	1811	54	0.3085	0.0071	1727	37	7	183
AO1_14	0.641	0.023	496	52	0.0823	0.0018	508	14	6	382
AO1_15	5.99	0.17	1920	44	0.3574	0.0082	1978	64	5	258
AO1_17	7.38	0.27	1980	170	0.397	0.011	2049	75	9	26
AO1_19	0.38	0.013	252	62	0.0517	0.0012	317	11	8	432
AO1_24	0.645	0.025	380	97	0.081	0.002	490	17	8	169
AO1_28	0.389	0.013	272	36	0.0534	0.0012	332.2	7.9	4	759
AO1_29	5.99	0.16	1910	59	0.36	0.008	1963	38	4	147
AO1_31	0.382	0.013	261	51	0.053	0.0012	327	10	7	452
AO1_33	0.674	0.034	320	160	0.0868	0.0023	513	22	10	128
AO1_34	0.399	0.019	241	71	0.053	0.0013	325	13	7	480
AO1_37	0.39	0.023	200	130	0.0535	0.0015	323	13	9	181
AO1_41	0.778	0.027	270	130	0.0958	0.0021	538	28	7	173
AO1_46	0.595	0.024	435	53	0.0774	0.0019	477	14	7	271
AO1_47	0.908	0.031	430	100	0.0966	0.0023	575	17	9	183
AO1_49	10.39	0.34	2200	120	0.473	0.012	2413	64	8	32
AO1_51	0.398	0.019	212	76	0.0526	0.0013	322	12	6	511
AO1_52	0.403	0.02	-20	190	0.0565	0.0015	332	15	9	252
AO1_57	0.386	0.015	203	64	0.0529	0.0013	319	11	8	411

ANNEX III Detrital zircon U-Pb Data

Grain number	$^{207}Pb/^{235}U$ ratio	±(2σ, %)	$^{207}Pb/^{235}U$ age (Ma)	±Ma (2σ)	$^{206}Pb/^{238}U$ ratio	±(2σ, %)	$^{206}Pb/^{238}U$ age (Ma)	±Ma (2σ)	discordance (%)	U conc (ppm)
AO1_58	0.399	0.018	321	57	0.0554	0.0015	345	11	8	489
AO1_60	2.612	0.097	1060	130	0.2247	0.0055	1267	37	8	94
AO1_62	0.633	0.023	401	77	0.0817	0.0019	496	15	7	399
AO1_65	0.382	0.016	197	65	0.0534	0.0013	316	18	7	609
AO1_68	0.385	0.013	310	46	0.0534	0.0012	332.3	9.1	7	532
AO1_69	0.852	0.033	627	98	0.102	0.0025	612	21	9	133
AO1_71	0.382	0.018	218	84	0.0531	0.0013	327	12	9	335
AO1_73	0.396	0.019	90	150	0.0559	0.0014	327	17	9	229
AO1_74	0.629	0.025	338	88	0.0809	0.002	486	15	7	265
AO1_75	0.385	0.02	230	100	0.0538	0.0013	325	16	10	260
AO1_79	0.451	0.015	169	78	0.0615	0.0015	369	11	6	517
AO1_81	0.402	0.018	-10	130	0.0557	0.0014	324	11	10	302
AO1_85	0.53	0.024	170	110	0.0679	0.0017	400	15	9	264
AO1_87	0.586	0.024	343	60	0.0761	0.002	465	12	7	362
AO1_90	0.394	0.017	87	91	0.0538	0.0013	320	12	9	267
AO1_92	0.411	0.019	130	120	0.0541	0.0015	318	14	9	247
AO1_94	10.32	0.3	2400	39	0.464	0.012	2428	52	6	150
Brejeira Formation (DZ1)										
DZ_1_1	0.867	0.049	410	170	0.1026	0.0028	606	19	6	103
DZ_1_2	0.924	0.042	619	91	0.1113	0.0029	674	17	4	264
DZ_1_3	0.886	0.049	600	68	0.1074	0.0031	658	19	4	262
DZ_1_4	2.082	0.093	1000	170	0.1929	0.0054	1114	26	4	126
DZ_1_5	0.812	0.042	560	99	0.0994	0.0027	604	20	3	315
DZ_1_6	0.458	0.026	328	94	0.0627	0.0018	383	14	4	274
DZ_1_7	0.514	0.027	401	94	0.0695	0.0019	428	12	5	229
DZ_1_8	0.838	0.054	520	140	0.1013	0.0025	615	15	5	143
DZ_1_9	1.433	0.067	929	59	0.1535	0.003	926	14	2	363
DZ_1_10	3.23	0.13	1453	47	0.256	0.0052	1466	26	3	405
DZ_1_11	5.87	0.27	1939	54	0.362	0.01	1997	49	4	260
DZ_1_12	0.826	0.043	607	85	0.1007	0.0032	614	18	4	258
DZ_1_13	0.914	0.054	530	190	0.108	0.0027	653	20	6	87
DZ_1_14	1.326	0.075	849	99	0.1429	0.0045	856	24	4	118
DZ_1_15	6.71	0.3	2071	40	0.383	0.011	2092	51	4	612
DZ_1_16	0.53	0.026	413	74	0.0691	0.0021	427	13	3	361
DZ_1_17	0.827	0.052	600	170	0.0982	0.0029	601	16	6	90
DZ_1_18	0.906	0.05	440	190	0.1065	0.0024	638	20	6	70
DZ_1_19	0.739	0.046	350	230	0.0929	0.0026	556	21	6	97
DZ_1_20	0.851	0.046	560	170	0.1035	0.0022	633	18	5	102
DZ_1_21	1.811	0.083	1040	110	0.1791	0.0041	1062	25	5	145
DZ_1_22	1.354	0.062	860	120	0.1463	0.0032	879	23	4	161
DZ_1_23	0.879	0.043	520	160	0.1081	0.0023	650	19	5	189
DZ_1_24	0.555	0.03	320	110	0.0737	0.002	447	16	5	238
DZ_1_25	0.846	0.061	400	150	0.0865	0.0025	519	18	10	178
DZ_1_26	0.833	0.042	580	51	0.1004	0.0029	615	16	4	440
DZ_1_27	0.804	0.038	585	86	0.0988	0.0023	605	14	4	279
DZ_1_28	0.52	0.024	424	36	0.0695	0.0016	432.5	9.5	4	757
DZ_1_29	7.24	0.29	2146	36	0.3895	0.0088	2120	41	4	543
DZ_1_30	0.716	0.033	490	120	0.0901	0.0019	550	13	4	211
DZ_1_31	0.511	0.024	400	41	0.0677	0.0013	420.4	8.2	4	629
DZ_1_32	0.712	0.033	544	82	0.0898	0.0021	554	13	5	313
DZ_1_33	5.62	0.24	1909	37	0.3256	0.0083	1812	41	6	490
DZ_1_34	7.49	0.33	2182	48	0.3957	0.0093	2150	44	4	254
DZ_1_35	1.395	0.067	840	120	0.1496	0.0032	900	20	5	122
DZ_1_36	5.96	0.28	1965	34	0.35	0.011	1934	53	4	375
DZ_1_37	0.823	0.037	622	61	0.0994	0.0022	611	13	4	296
DZ_1_38	0.787	0.036	570	65	0.0965	0.0023	599	15	4	486
DZ_1_39	0.89	0.053	700	230	0.1019	0.0026	621	24	7	55
DZ_1_40	0.765	0.041	558	82	0.0929	0.0027	572	17	5	263
DZ_1_41	0.523	0.023	367	75	0.0688	0.0016	425	11	3	400
DZ_1_42	0.924	0.046	634	98	0.1096	0.0026	667	16	5	213
DZ_1_43	0.517	0.023	424	27	0.0662	0.0017	415	10	4	1020
DZ_1_44	0.79	0.042	450	130	0.0951	0.0028	576	21	6	157
DZ_1_45	2.11	0.12	1270	180	0.1988	0.0048	1194	37	7	44
DZ_1_46	0.861	0.036	621	52	0.1031	0.0023	634	14	3	726
DZ_1_47	0.811	0.038	592	74	0.0985	0.0022	605	15	4	304
DZ_1_48	0.826	0.045	560	100	0.1004	0.0021	612	15	6	189
DZ_1_49	0.833	0.046	620	90	0.101	0.0024	618	16	5	159
DZ_1_50	0.744	0.039	500	120	0.0909	0.0019	555	14	5	183
DZ_1_51	0.835	0.04	612	43	0.0994	0.0026	612	15	3	947
DZ_1_52	2.75	0.12	1345	56	0.2058	0.0058	1206	31	9	304
DZ_1_53	0.749	0.034	544	39	0.0926	0.0024	568	14	3	627
DZ_1_54	0.439	0.021	331	76	0.0588	0.0016	367	11	4	312
DZ_1_55	0.807	0.036	587	82	0.0971	0.0023	598	15	5	287
DZ_1_56	0.508	0.022	416	32	0.0675	0.0014	420.6	8.9	4	1190
DZ_1_57	0.818	0.04	622	80	0.0999	0.0026	613	14	5	207

Grain number	$^{207}Pb/^{235}U$ ratio	±(2σ, %)	$^{207}Pb/^{235}U$ age (Ma)	±Ma (2σ)	$^{206}Pb/^{238}U$ ratio	±(2σ, %)	$^{206}Pb/^{238}U$ age (Ma)	±Ma (2σ)	discordance (%)	U conc (ppm)
DZ_1_58	4.46	0.25	1717	50	0.31	0.015	1739	71	4	580
DZ_1_59	1.875	0.084	1065	66	0.1716	0.0044	1017	23	6	241
DZ_1_61	0.813	0.036	550	110	0.099	0.002	598	13	4	300
DZ_1_62	0.519	0.025	404	69	0.0683	0.0014	419.4	9.6	5	270
DZ_1_63	0.942	0.04	664	33	0.1096	0.0023	670	14	3	605
DZ_1_64	4.14	0.18	1661	67	0.2958	0.0057	1669	29	4	128
DZ_1_65	5.16	0.21	1852	47	0.3345	0.0087	1861	42	4	307
DZ_1_66	6.16	0.26	2001	80	0.352	0.011	1945	55	6	136
DZ_1_67	0.518	0.026	377	98	0.0672	0.0017	419.5	9.2	4	278
DZ_1_68	0.837	0.04	598	84	0.0998	0.0022	613	13	4	236
DZ_1_69	1.1	0.062	700	140	0.1235	0.0027	745	22	6	72
DZ_1_70	0.766	0.034	557	59	0.094	0.002	577	12	4	307
DZ_1_71	0.85	0.048	612	94	0.0977	0.0025	599	15	6	182
DZ_1_72	2.57	0.11	1281	40	0.2215	0.0046	1288	25	3	293
DZ_1_73	0.844	0.038	636	46	0.0995	0.0019	611	12	4	377
DZ_1_74	2.32	0.12	1250	110	0.2133	0.0048	1252	27	4	72
DZ_1_75	0.973	0.062	570	160	0.1115	0.0024	675	22	7	118
DZ_1_76	0.516	0.025	402	50	0.0671	0.0022	416	13	3	558
DZ_1_77	1.005	0.057	685	78	0.1182	0.0025	720	15	5	142
DZ_1_78	6.27	0.27	2003	48	0.3701	0.0096	2027	44	4	256
DZ_1_79	6.12	0.3	1977	46	0.356	0.011	1959	53	5	384
DZ_1_80	0.922	0.048	673	84	0.1068	0.0027	661	15	4	173
Brejeira Formation (DZ12)										
DZ_12_1	0.7	0.032	390	200	0.0875	0.0019	500	26	8	50
DZ_12_2	0.436	0.011	345	22	0.0586	0.001	364.6	5.9	3	764
DZ_12_3	7.04	0.11	2108	18	0.3812	0.0067	2082	31	2	236
DZ_12_4	0.731	0.059	730	230	0.0898	0.0023	517	38	10	33
DZ_12_5	0.822	0.034	593	45	0.0976	0.002	598	11	3	335
DZ_12_6	0.856	0.029	553	47	0.1008	0.0017	609	12	4	252
DZ_12_7	0.927	0.043	533	42	0.099	0.0016	593	13	7	327
DZ_12_9	0.808	0.022	565	49	0.0979	0.0014	596.3	9.1	4	287
DZ_12_10	0.872	0.025	657	43	0.1034	0.0017	635	10	4	202
DZ_12_11	0.668	0.021	540	19	0.0823	0.0022	511	13	3	727
DZ_12_12	3.603	0.084	1512	50	0.2723	0.0045	1548	26	4	103
DZ_12_13	7.42	0.15	2149	20	0.3972	0.0082	2153	38	3	425
DZ_12_14	0.962	0.042	620	130	0.1133	0.002	687	18	6	80
DZ_12_15	0.838	0.042	420	170	0.0996	0.0018	588	23	8	64
DZ_12_17	6.14	0.16	1993	55	0.3621	0.0063	1989	36	4	64
DZ_12_19	0.835	0.023	559	48	0.0993	0.0016	605	10	3	302
DZ_12_20	0.852	0.016	609	25	0.1013	0.002	620	12	3	663
DZ_12_22	0.838	0.024	608	43	0.0998	0.0018	613	13	3	428
DZ_12_23	0.818	0.022	568	40	0.097	0.0015	593	10	4	279
DZ_12_24	7.5	0.11	2172	16	0.3963	0.0075	2149	34	4	386
DZ_12_25	0.836	0.066	450	260	0.0998	0.0024	597	34	10	78
DZ_12_26	1.127	0.033	708	64	0.1247	0.0022	753	17	4	191
DZ_12_27	0.852	0.018	585	51	0.1009	0.0016	619	11	4	309
DZ_12_28	0.924	0.03	580	130	0.1058	0.0021	643	19	5	140
DZ_12_30	9.63	0.15	2395	18	0.449	0.008	2387	35	3	209
DZ_12_31	5.342	0.054	1865	13	0.3212	0.0046	1794	22	5	425
DZ_12_32	0.51	0.023	290	120	0.0671	0.0015	415	12	7	174
DZ_12_33	3.512	0.05	1519	17	0.2702	0.004	1540	20	3	545
DZ_12_34	4.736	0.08	1775	24	0.3168	0.0052	1775	28	3	207
DZ_12_36	1.8	0.02	1042.7	7.6	0.1746	0.0024	1037	13	1	1648
DZ_12_37	0.73	0.05	590	140	0.0878	0.0023	534	20	9	60
DZ_12_38	1.046	0.019	731	31	0.1188	0.0019	726	13	3	412
DZ_12_39	0.719	0.03	470	110	0.0881	0.0015	546	14	7	103
DZ_12_40	0.922	0.032	500	120	0.107	0.0021	641	15	6	114
DZ_12_41	9.38	0.17	2357	26	0.4377	0.0081	2336	38	4	263
DZ_12_42	0.434	0.024	20	220	0.0595	0.0014	350	16	9	94
DZ_12_43	0.511	0.018	423	47	0.0664	0.0012	415.1	8.8	5	282
DZ_12_45	0.684	0.024	432	87	0.0819	0.002	498	15	5	155
DZ_12_46	0.442	0.013	342	27	0.0598	0.001	371.6	7.2	4	563
DZ_12_47	1.109	0.032	722	51	0.1221	0.0023	740	16	3	210
DZ_12_48	9.91	0.21	2423	38	0.4524	0.0096	2407	40	4	70
DZ_12_49	0.77	0.048	410	130	0.0889	0.0024	540	14	6	160
DZ_12_51	12.88	0.24	2664	24	0.5095	0.0099	2649	39	4	111
DZ_12_52	0.859	0.028	518	75	0.1022	0.0016	619	13	4	150
DZ_12_53	0.696	0.041	320	190	0.0873	0.0021	520	20	9	73
DZ_12_54	0.674	0.03	330	180	0.0859	0.0017	523	16	6	108
DZ_12_55	0.864	0.017	599	40	0.1042	0.0018	639	12	3	304
Mértola Formation (FM1)										
DZ_12_56	6.344	0.073	2017	20	0.3632	0.0078	1995	32	3	408
DZ_12_57	6.491	0.075	2037	14	0.3741	0.007	2045	33	3	611
DZ_12_58	0.868	0.045	530	140	0.1021	0.0023	618	19	7	77
DZ_12_59	0.869	0.036	574	81	0.1026	0.0022	625	13	5	161

Grain number	$^{207}Pb/^{235}U$ ratio	±(2σ, %)	$^{207}Pb/^{235}U$ age (Ma)	±Ma (2σ)	$^{206}Pb/^{238}U$ ratio	±(2σ, %)	$^{206}Pb/^{238}U$ age (Ma)	±Ma (2σ)	discordance (%)	U conc (ppm)
DZ_12_61	0.508	0.018	383	35	0.0681	0.0012	421.3	8.7	5	353
DZ_12_62	0.679	0.025	492	68	0.0857	0.0014	528	10	5	168
DZ_12_63	7.12	0.11	2129	35	0.383	0.0067	2088	30	3	75
DZ_12_64	0.775	0.055	480	150	0.0929	0.002	561	20	10	83
DZ_12_65	4.395	0.074	1706	26	0.2902	0.0047	1636	23	5	194
DZ_12_66	0.464	0.013	362	29	0.05846	0.00088	365.4	6.8	4	423
DZ_12_67	6.346	0.095	2016	17	0.3584	0.0058	1972	27	3	318
DZ_12_68	0.86	0.029	607	38	0.1044	0.0024	635	15	3	421
DZ_12_69	13.88	0.2	2718	16	0.524	0.0083	2708	35	3	138
DZ_12_70	0.763	0.021	564	34	0.0931	0.0018	575	12	4	360
DZ_12_71	0.844	0.022	612	44	0.1024	0.0017	624.1	9.7	4	257
DZ_12_72	1.448	0.017	904	13	0.1483	0.002	890	12	2	878
DZ_12_73	5.9	0.14	1950	27	0.3227	0.0069	1799	35	9	300
DZ_12_74	0.904	0.033	570	100	0.1052	0.0023	626	19	6	103
Upper Triassic Silves Sandstones (TL1)										
TL1_2	20.22	0.66	3122	30	0.619	0.015	2950	320	4	298
TL1_3	6.15	0.32	2102	29	0.3717	0.0084	1590	350	6	252
TL1_5	0.17	0.22	616	11	0.096	0.004	270	250	8	180
TL1_6	0.06	0.21	606	13	0.0931	0.0037	280	190	8	196
TL1_7	0	0.26	580	11	0.0872	0.0044	160	230	10	142
TL1_9	5.44	0.74	2020	43	0.344	0.013	1480	390	6	66
TL1_10	0.631	0.061	566	11	0.0908	0.0022	470	100	4	1094
TL1_11	0.01	0.12	328	7.4	0.0513	0.0019	90	150	9	276
TL1_14	0.722	0.086	603	13	0.1001	0.0023	160	360	4	521
TL1_15	0.05	0.26	507.2	9.7	0.0768	0.0041	100	140	10	101
TL1_17	0.49	0.17	593	12	0.095	0.0031	340	210	8	167
TL1_19	0.6	0.14	593	13	0.0954	0.0028	510	130	7	225
TL1_20	0.38	0.15	515	14	0.0796	0.0028	262	98	8	147
TL1_21	0.45	0.18	593	13	0.0942	0.0033	330	220	8	152
TL1_22	0.87	0.17	760	13	0.122	0.0038	230	120	6	170
TL1_27	0.41	0.16	507	13	0.0823	0.0026	420	99	9	285
TL1_28	0.47	0.15	546	14	0.0847	0.003	273	86	8	196
TL1_29	0.03	0.1	315.8	6.3	0.049	0.002	90	150	8	289
TL1_30	0.45	0.12	569	11	0.0894	0.0029	400	110	5	436
TL1_31	0.18	0.11	318.9	5.7	0.0513	0.0022	180	140	8	271
TL1_32	0.5	0.071	459	12	0.0737	0.0018	364	90	6	665
TL1_33	1.72	0.14	966	23	0.1614	0.0039	570	120	7	360
TL1_35	1.6	0.13	927	18	0.1544	0.004	500	140	6	192
TL1_36	0.33	0.15	452	13	0.0688	0.0025	35	22	9	151
TL1_40	0.28	0.26	587	12	0.0934	0.0041	380	260	10	116
TL1_42	0.3	0.28	571	10	0.0906	0.005	-310	500	10	101
TL1_43	0.55	0.1	534	18	0.0829	0.0026	435	86	6	573
TL1_44	0.54	0.17	601	12	0.097	0.0033	290	280	6	240
TL1_45	0.6	0.26	598	15	0.0987	0.0039	540	180	9	129
TL1_46	1.21	0.29	1039	23	0.171	0.0057	840	230	6	147
TL1_48	0.79	0.15	666	14	0.1096	0.0031	630	120	7	204
TL1_50	6.36	0.47	2082	34	0.3778	0.0095	1790	370	5	138
TL1_52	0.67	0.12	633	12	0.1019	0.003	550	140	7	255
TL1_53	0.54	0.28	579	15	0.0936	0.004	410	250	10	120
TL1_55	0.4	0.25	681	14	0.1105	0.0041	390	250	9	126
TL1_56	16.87	0.65	2956	29	0.577	0.013	2710	380	5	96
TL1_57	0.66	0.12	557	10	0.0911	0.0027	510	150	7	248
TL1_58	0.478	0.078	434.2	8.8	0.0689	0.0019	204	51	7	245
TL1_59	0.78	0.16	625	17	0.1033	0.0032	590	110	6	268
TL1_60	0.696	0.088	589	11	0.0968	0.0026	470	180	5	415
TL1_61	0.4	0.12	397.5	8.4	0.0645	0.0022	320	130	8	226
TL1_63	0.65	0.17	592	12	0.0958	0.0034	350	300	8	154
TL1_64	0.46	0.17	573	12	0.094	0.0034	450	170	8	164
TL1_67	0.515	0.069	466	11	0.0736	0.002	30	15	7	361
TL1_68	0.225	0.061	302.5	6.1	0.0493	0.0014	264	52	7	455
TL1_69	0.74	0.11	622	12	0.1027	0.0027	560	140	6	261
TL1_70	0.584	0.086	579	11	0.0939	0.0029	480	120	5	466
TL1_74	1.26	0.27	967	19	0.1608	0.0053	780	280	6	146
TL1_75	0.46	0.16	597	13	0.097	0.003	350	210	6	282
TL1_76	0.33	0.15	433	10	0.0674	0.0025	220	120	7	247
TL1_77	0.97	0.13	765	14	0.1252	0.0033	630	170	6	309
TL1_78	0.6	0.17	665	14	0.1067	0.0034	530	160	6	279
TL1_79	0.256	0.08	306.6	6.8	0.0504	0.0017	245	92	7	422
TL1_80	0.62	0.21	561	12	0.0922	0.0038	510	170	10	138
TL1_81	2.29	0.13	1221	19	0.2085	0.0049	1140	210	3	407
TL1_82	0.646	0.067	572	13	0.0924	0.0022	515	57	5	461
TL1_84	0.56	0.19	688	11	0.1094	0.0035	350	230	6	164
TL1_85	-0.23	0.74	686	18	0.1036	0.0098	40	450	10	42
TL1_86	0.5	0.12	584	10	0.0935	0.0029	180	250	7	211
TL1_88	0.51	0.28	636	13	0.1011	0.0048	440	250	8	92

ANNEX III Detrital zircon U-Pb Data

Grain number	$^{207}Pb/^{235}U$ ratio	±(2σ, %)	$^{207}Pb/^{235}U$ age (Ma)	±Ma (2σ)	$^{206}Pb/^{238}U$ ratio	±(2σ, %)	$^{206}Pb/^{238}U$ age (Ma)	±Ma (2σ)	discordance (%)	U conc (ppm)
Upper Triassic Silves Sandstones (CM2)										
CM2_7	2.81	0.53	1330	150	0.2826	0.0092	1604	46	3	214
CM2_8	0.431	0.074	362	51	0.0721	0.0025	448	15	8	1327
CM2_9	1.01	0.44	700	210	0.1795	0.0066	1064	36	7	188
CM2_11	0.87	0.38	670	190	0.1544	0.0064	925	36	4	257
CM2_13	0.25	0.24	300	170	0.0868	0.004	536	24	6	246
CM2_14	0.106	0.092	76	97	0.0427	0.0015	269.7	9.2	5	671
CM2_16	0.03	0.2	20	190	0.0463	0.0029	291	18	5	380
CM2_17	2.66	0.54	1270	160	0.2451	0.0083	1412	43	4	195
CM2_22	0.12	0.48	600	200	0.099	0.0076	611	45	6	144
CM2_24	0.02	0.27	110	220	0.0469	0.0041	295	25	7	252
CM2_25	0.46	0.21	350	160	0.0953	0.0033	588	20	4	358
CM2_27	0.25	0.2	220	150	0.0702	0.0035	437	21	4	508
CM2_28	2.8	0.67	1320	200	0.2701	0.0098	1542	50	4	140
CM2_30	2.44	0.99	1330	230	0.294	0.012	1660	59	5	111
CM2_31	8.6	1.8	2280	210	0.469	0.02	2479	90	4	58
CM2_32	0.49	0.54	620	240	0.1743	0.0075	1036	41	5	154
CM2_40	2.65	0.9	1460	180	0.297	0.012	1673	62	7	70
CM2_41	0.27	0.2	180	170	0.0937	0.0033	577	20	4	343
CM2_43	4.72	0.26	1773	47	0.2971	0.0078	1677	39	9	517
CM2_45	4.08	0.57	1620	120	0.3049	0.0088	1715	44	8	134
CM2_47	2.8	1.5	1550	300	0.338	0.019	1881	91	10	64
CM2_49	0.77	0.29	580	170	0.1542	0.0052	924	29	4	356
CM2_53	0.61	0.44	580	230	0.1589	0.0073	950	41	5	179
CM2_54	4.31	0.61	1700	120	0.332	0.01	1843	50	5	140
CM2_56	0.141	0.086	121	83	0.054	0.0021	339	13	4	766
CM2_62	0.54	0.26	370	190	0.1028	0.004	631	23	4	315
CM2_63	19.2	1.4	3053	69	0.615	0.019	3096	76	4	109
CM2_64	4.8	1.7	1850	250	0.394	0.019	2141	88	6	51
CM2_67	2.97	0.37	1386	96	0.2644	0.0075	1513	37	3	288
CM2_68	4.21	0.63	1660	130	0.3048	0.0086	1715	42	6	232
CM2_70	3.8	1.9	1810	310	0.361	0.019	1985	89	7	43
CM2_71	1.34	0.94	1040	250	0.18	0.014	1062	76	7	95
CM2_74	0.24	0.3	300	230	0.1003	0.0052	616	30	5	206
CM2_77	5.6	0.58	1906	93	0.3575	0.0099	1969	47	4	188
CM2_78	6.18	0.37	2002	51	0.3705	0.0096	2031	45	2	342
CM2_80	0.33	0.22	310	170	0.0953	0.0043	587	26	5	253
CM2_81	0.56	0.2	400	140	0.091	0.0035	562	21	4	412
CM2_82	9.4	1.3	2340	140	0.453	0.018	2405	78	4	73
CM2_83	0.17	0.32	300	210	0.0869	0.005	537	30	7	141
CM2_85	0.67	0.62	990	200	0.1533	0.0085	921	48	7	79
CM2_86	0.13	0.32	290	220	0.0809	0.0051	501	31	6	207
CM2_87	3.52	0.79	1520	180	0.296	0.01	1670	52	4	140
CM2_88	6.33	0.9	2080	110	0.414	0.016	2229	74	6	50

ANNEX IV

Apatite U-Pb data

ANNEX IV Apatite U-Pb Data

Grain number	$^{207}Pb/^{235}U$ ratio	±(2σ, %)	$^{206}Pb/^{238}U$ ratio	±(2σ, %)	$^{206}Pb/^{207}Pb$ ratio	±(2σ, %)	^{207}Pb age (Ma)	±Ma (2σ)
Ossa Morena								
PIAS1_1	5.07	0.19	0.0921	0.0019	0.396	0.015	331.96	12.84
PIAS1_2	4.75	0.23	0.0886	0.0018	0.392	0.017	322.26	13.48
PIAS1_3	3.11	0.14	0.0749	0.0019	0.309	0.014	321.02	11.48
PIAS1_4	10.72	0.38	0.1376	0.0032	0.557	0.019	323.12	22.16
PIAS1_5	6.06	0.28	0.0999	0.0025	0.447	0.022	320.47	18.93
PIAS1_6	5.94	0.33	0.0964	0.0026	0.453	0.026	304.96	21.17
PIAS1_7	4.06	0.17	0.0849	0.0017	0.343	0.015	340.99	12.03
PIAS1_8	6.74	0.28	0.1058	0.0024	0.466	0.021	323.65	18.89
PIAS1_9	3.17	0.14	0.0779	0.0014	0.301	0.013	338.45	9.94
PIAS1_10	7.25	0.3	0.1125	0.0025	0.469	0.023	341.21	21.56
PIAS1_11	5.14	0.24	0.0952	0.0016	0.39	0.019	347.33	15.24
PIAS1_12	6.34	0.21	0.1033	0.0021	0.445	0.016	332.79	14.71
PIAS1_13	9.39	0.46	0.1301	0.0027	0.534	0.025	328.79	26.38
PIAS1_14	3.81	0.16	0.0832	0.0014	0.327	0.015	344.49	11.30
PIAS1_15	4.25	0.16	0.0868	0.0017	0.36	0.016	337.17	12.68
PIAS1_16	6.12	0.25	0.1036	0.0021	0.426	0.016	348.85	14.83
PIAS1_17	4.78	0.2	0.0916	0.0016	0.372	0.016	347.06	12.95
PIAS1_18	4.66	0.19	0.0899	0.0017	0.378	0.017	336.59	13.52
PIAS1_19	4.31	0.2	0.0872	0.0014	0.362	0.018	337.36	13.36
PIAS1_20	3.81	0.15	0.0815	0.0018	0.334	0.013	333.19	11.05
PIAS1_21	11.5	0.41	0.1425	0.0029	0.588	0.021	300.46	24.64
PIAS1_22	3.08	0.13	0.0777	0.0015	0.29	0.012	344.16	9.81
PIAS1_23	3.92	0.14	0.0825	0.0017	0.348	0.016	328.34	12.30
PIAS1_24	3.98	0.15	0.0835	0.0015	0.344	0.015	334.82	11.47
LP1_1	3.39	0.41	0.0848	0.007	0.307	0.032	364.50	36.15
LP1_2	6.66	0.67	0.1084	0.0054	0.468	0.053	329.80	47.16
LP1_3	3.62	0.35	0.0846	0.0037	0.325	0.033	351.82	26.25
LP1_4	6.2	0.55	0.1018	0.0037	0.459	0.04	316.71	33.52
LP1_5	6.69	0.53	0.1066	0.0052	0.454	0.037	336.05	34.48
LP1_6	5	0.42	0.0971	0.0035	0.38	0.03	362.27	25.82
LP1_7	6.6	0.46	0.1101	0.0048	0.433	0.03	365.43	29.88
LP1_8	4.69	0.41	0.0931	0.0038	0.364	0.032	358.92	27.05
LP1_9	7.73	0.72	0.1196	0.0048	0.483	0.037	350.23	36.83
LP1_10	3.96	0.61	0.0882	0.0044	0.331	0.048	362.66	36.96
LP1_11	3.83	0.42	0.085	0.0038	0.338	0.038	344.89	29.09
LP1_12	3.77	0.4	0.0808	0.0043	0.344	0.039	324.07	29.66
LP1_13	1.14	0.16	0.0601	0.0032	0.138	0.02	337.62	19.95
LP1_14	5.36	0.47	0.0923	0.0046	0.411	0.037	321.85	30.78
LP1_15	7.7	0.68	0.1105	0.0057	0.513	0.047	296.71	43.09
LP1_16	3.8	0.44	0.08	0.004	0.341	0.039	322.73	28.85
LP1_17	2.41	0.22	0.0691	0.0037	0.25	0.023	327.88	21.19
LP1_18	4.23	0.4	0.0868	0.0039	0.358	0.034	338.65	27.23
LP1_19	2.26	0.19	0.0691	0.0032	0.241	0.02	332.70	18.54
Mértola Formation								
FM1_1	15.12	0.77	0.1738	0.0074	0.644	0.033	287.59	46.80
FM1_2	13.73	0.73	0.1656	0.0065	0.612	0.026	317.01	36.16
FM1_3	27	1.7	0.2798	0.013	0.704	0.039	336.34	86.45
FM1_4	6.86	0.35	0.1066	0.0038	0.461	0.021	330.15	21.04
FM1_5	23.9	1.4	0.2576	0.011	0.682	0.038	355.65	77.48
FM1_6	24.5	1.3	0.2735	0.012	0.663	0.032	424.41	69.90
FM1_7	12.26	0.59	0.1555	0.0062	0.568	0.024	352.51	32.39
FM1_8	13.42	0.68	0.1677	0.0062	0.587	0.024	355.49	34.17
FM1_9	29.2	1.4	0.3031	0.012	0.714	0.03	341.29	72.85
FM1_10	10.4	0.78	0.1262	0.0066	0.621	0.048	229.48	49.23
FM1_11	19.4	1.4	0.211	0.012	0.649	0.029	344.75	51.73
FM1_12	4.32	0.25	0.0881	0.0035	0.361	0.02	341.67	19.12
FM1_13	20.64	1.1	0.2208	0.0095	0.675	0.035	313.61	62.06
FM1_14	26	1.5	0.2678	0.011	0.701	0.037	327.26	78.61
FM1_15	6.6	0.35	0.1058	0.004	0.457	0.022	330.99	21.99
FM1_16	14.2	1.2	0.1707	0.01	0.581	0.035	370.46	50.85
FM1_18	28.1	1.7	0.2796	0.013	0.731	0.044	269.56	97.63

ANNEX IV Apatite U-Pb Data

Grain number	$^{207}Pb/^{235}U$ ratio	±(2σ, %)	$^{206}Pb/^{238}U$ ratio	±(2σ, %)	$^{206}Pb/^{207}Pb$ ratio	±(2σ, %)	^{207}Pb age (Ma)	±Ma (2σ)
FM1_19	13.45	0.68	0.1663	0.0063	0.594	0.027	342.91	37.44
CST1-4_1	13.3	0.73	0.1574	0.0067	0.615	0.032	296.71	41.52
CST1-4_2	9.12	0.46	0.1279	0.0047	0.516	0.024	341.46	27.01
CST1-4_3	13.21	0.66	0.1608	0.0062	0.603	0.025	319.24	34.02
CST1-4_4	16.7	0.84	0.1893	0.0075	0.651	0.029	303.82	44.99
CST1-4_5	15.17	0.86	0.1761	0.0072	0.624	0.031	320.78	44.72
CST1-4_6	14.45	0.76	0.1734	0.0068	0.613	0.029	331.29	41.46
CST1-4_7	15.2	0.77	0.1768	0.0071	0.62	0.031	327.96	44.84
CST1-4_8	15.03	0.87	0.1873	0.0071	0.586	0.029	400.67	44.56
CST1-4_9	10.48	0.57	0.136	0.0052	0.558	0.028	317.82	32.17
CST1-4_10	16.61	0.84	0.1883	0.0073	0.641	0.031	317.80	47.44
CST1-4_11	14.41	0.75	0.1737	0.0069	0.6	0.029	350.40	41.65
CST1-4_12	26.3	1.4	0.2788	0.012	0.686	0.034	378.55	75.33
CST1-4_13	11.57	0.64	0.1448	0.0058	0.587	0.029	305.07	35.16
CST1-4_14	16.16	0.89	0.1837	0.0076	0.635	0.029	318.71	43.91
CST1-4_15	16.09	0.82	0.1865	0.0078	0.623	0.03	342.37	45.98
CST1-4_16	14.74	0.91	0.1762	0.0078	0.609	0.03	342.71	43.92
CST1-4_17	19.4	0.97	0.2078	0.0087	0.695	0.031	258.36	52.45
CST1-4_18	14.4	0.83	0.1745	0.0074	0.606	0.031	343.52	44.57
CST1-4_19	15.28	0.9	0.1782	0.0075	0.616	0.028	336.56	41.57
CST1-4_20	18.66	1.1	0.2134	0.0086	0.648	0.03	350.74	51.98
OL1_1	25.9	2.1	0.265	0.016	0.746	0.068	218.43	142.72
OL1_2	13.06	0.56	0.1549	0.0038	0.619	0.029	286.68	36.20
OL1_3	14.58	0.58	0.1753	0.004	0.617	0.026	329.35	36.70
OL1_4	13.95	0.63	0.167	0.0044	0.612	0.03	319.83	40.19
OL1_5	2.62	0.15	0.0747	0.0018	0.265	0.015	345.59	11.93
OL1_6	14.94	0.61	0.1802	0.0044	0.609	0.027	350.91	39.05
OL1_7	6.42	0.32	0.1118	0.0031	0.405	0.022	395.63	21.79
OL1_8	14.25	0.6	0.1648	0.004	0.62	0.028	304.57	37.16
Mira Formation								
AO1_1	16.1	0.95	0.1843	0.0088	0.64	0.028	312.17	43.32
AO1_2	13.88	0.78	0.1634	0.0075	0.617	0.025	305.89	35.25
AO1_3	17.3	1.1	0.1957	0.0092	0.638	0.032	335.99	51.38
AO1_4	2.16	0.17	0.072	0.0032	0.219	0.015	358.78	17.74
AO1_5	14.36	0.8	0.1685	0.0077	0.625	0.028	304.82	39.72
AO1_6	11.46	0.62	0.1426	0.0064	0.574	0.023	315.31	29.49
AO1_7	14.9	1.4	0.168	0.01	0.647	0.055	273.26	73.97
AO1_8	18.27	1.1	0.199	0.0094	0.658	0.034	308.80	55.03
AO1_9	13.55	0.77	0.154	0.0072	0.629	0.03	272.25	38.71
AO1_10	11.61	0.65	0.1509	0.0072	0.558	0.025	353.88	33.87
AO1_11	13.64	0.84	0.1564	0.0074	0.627	0.033	279.29	42.74
AO1_12	17.83	1.1	0.1903	0.01	0.683	0.032	254.34	50.24
AO1_13	6.28	0.43	0.1069	0.0051	0.43	0.025	357.22	26.63
AO1_14	9.86	0.61	0.1356	0.0067	0.53	0.026	347.37	32.28
AO1_15	17.58	1.1	0.1932	0.0093	0.665	0.035	287.84	54.98
AO1_16	15.36	0.87	0.1879	0.0088	0.595	0.028	388.26	44.58
AO1_17	11.18	0.6	0.1452	0.0064	0.563	0.019	334.19	26.37
AO1_18	12.48	0.79	0.1552	0.0077	0.577	0.029	340.49	38.88
AO1_19	16.62	0.95	0.1927	0.0089	0.619	0.027	360.80	43.91
AO1_20	12.7	0.7	0.1532	0.0073	0.6	0.027	307.25	35.69
AO1_21	11.56	0.6	0.1515	0.0065	0.562	0.023	350.45	31.14
AO1_22	16.27	0.91	0.1878	0.0084	0.626	0.028	340.25	43.91
AO1_23	7.61	0.43	0.1141	0.0049	0.492	0.021	325.68	23.36
AO1_24	12.87	0.74	0.1566	0.0073	0.594	0.028	322.04	37.48
AO1_25	12.91	0.69	0.1601	0.007	0.584	0.023	342.59	32.59
AO1_26	12.67	0.69	0.1539	0.0068	0.604	0.026	303.68	34.32
AO1_27	16.35	0.98	0.1857	0.0084	0.65	0.033	299.22	50.03
Brejeira Formation								
AR1_2	13.5	3.4	0.143	0.017	0.8	0.19	44.66	220.24
AR1_3	6.18	0.36	0.1471	0.0044	0.312	0.02	625.64	28.30
AR1_4	7.6	1.4	0.1126	0.0091	0.58	0.12	241.63	107.36
AR1_5	26.4	1.4	0.301	0.012	0.629	0.041	558.29	94.63

ANNEX IV Apatite U-Pb Data

Grain number	$^{207}Pb/^{235}U$ ratio	±(2σ, %)	$^{206}Pb/^{238}U$ ratio	±(2σ, %)	$^{206}Pb/^{207}Pb$ ratio	±(2σ, %)	^{207}Pb age (Ma)	±Ma (2σ)
AR1_6	1.88	0.12	0.1071	0.0022	0.1265	0.009	604.98	14.02
AR1_7	11.6	3.4	0.15	0.02	0.54	0.26	373.39	301.41
AR1_8	8.5	2.5	0.147	0.02	0.62	0.29	270.20	333.17
AR1_9	3.36	0.57	0.1205	0.0049	0.198	0.028	615.70	34.69
AR1_10	4.49	0.9	0.0998	0.0089	0.47	0.11	301.70	88.90
AR1_11	1.83	0.2	0.0664	0.0024	0.202	0.021	339.84	16.16
AR1_12	8.93	0.74	0.1756	0.0062	0.364	0.033	678.74	48.12
Upper Triassic Silves Sandstones								
SC1_1	9.26	0.43	0.1258	0.0026	0.538	0.026	313.55	26.48
SC1_2	6.16	0.31	0.1002	0.0024	0.452	0.026	317.23	21.66
SC1_3	5.03	0.27	0.0888	0.0025	0.419	0.024	303.97	18.68
SC1_4	8.91	0.35	0.1235	0.0028	0.527	0.026	318.57	26.17
SC1_5	2.44	0.1	0.0664	0.0012	0.264	0.014	307.92	9.10
SC1_6	9.79	0.48	0.1284	0.0033	0.552	0.032	305.75	33.06
SC1_7	8.42	0.47	0.1199	0.0027	0.52	0.034	315.79	32.50
SC1_8	6.03	0.31	0.1071	0.0032	0.397	0.027	385.57	24.92
QR1_1	2.96	0.46	0.0731	0.0046	0.316	0.047	309.21	32.74
QR1_2	23.5	1.3	0.2389	0.0081	0.729	0.044	230.26	83.70
QR1_3	27.1	1.7	0.2683	0.01	0.749	0.043	214.29	92.21
QR1_4	19.11	0.97	0.2172	0.0072	0.627	0.033	395.42	56.84
QR1_5	19.85	0.97	0.2131	0.0085	0.695	0.036	265.52	61.60
QR1_6	5.9	2	0.136	0.014	0.37	0.13	518.68	141.41
TL1_1	3.48	0.21	0.0785	0.0023	0.313	0.023	333.83	16.96
TL1_2	4.34	0.25	0.1127	0.0027	0.281	0.019	506.23	19.97
TL1_3	7.99	0.36	0.1291	0.0037	0.463	0.024	398.95	26.40
TL1_4	8.85	0.52	0.1653	0.0043	0.393	0.028	602.37	37.43
TL1_5	6.12	0.41	0.1147	0.0032	0.39	0.033	419.35	30.99
TL1_6	6.47	0.43	0.1002	0.0038	0.484	0.041	291.77	33.79
TL1_7	6.16	0.36	0.1334	0.0039	0.33	0.023	549.36	27.72
TL1_8	3.93	0.52	0.0937	0.0042	0.303	0.046	405.51	37.27
TL1_9	19.2	1.7	0.232	0.016	0.623	0.049	432.08	91.23
TL1_10	11.11	0.57	0.149	0.0054	0.558	0.029	349.26	35.88
TL1_11	4.29	0.8	0.1258	0.0078	0.258	0.05	586.36	58.25
TL1_12	6.25	0.42	0.1398	0.0039	0.319	0.02	587.30	26.17
TL1_13	32.6	3.7	0.416	0.023	0.598	0.075	910.34	223.38
TL1_14	17.59	0.87	0.2347	0.0082	0.546	0.032	584.12	59.35
TL1_15	39.4	3.7	0.395	0.029	0.747	0.051	343.56	157.99
TL1_16	38	1.3	0.4156	0.0093	0.654	0.021	713.85	67.38
TL1_17	8.63	0.58	0.1604	0.004	0.383	0.024	596.53	31.99
TL1_18	18.07	0.82	0.2026	0.0059	0.647	0.029	333.44	47.16
TL1_19	18.92	0.68	0.2031	0.0047	0.68	0.023	277.95	38.26
TL1_20	15.53	0.54	0.1772	0.0036	0.631	0.027	312.65	38.34
TL1_21	7.45	0.7	0.1254	0.0063	0.431	0.047	418.80	49.27
TL1_22	10.71	0.79	0.1414	0.0052	0.568	0.041	319.44	46.49
TL1_23	8.8	1.5	0.136	0.014	0.426	0.043	459.96	63.97
TL1_24	10.16	0.53	0.1714	0.0036	0.439	0.026	564.54	35.21
TL1_25	7.3	0.45	0.126	0.0036	0.423	0.031	428.69	32.06
TL1_26	4.51	0.7	0.1281	0.0067	0.274	0.05	581.66	55.69
Monchique Alkaline Complex								
MM3_1	2.84	0.29	0.0332	0.0017	0.594	0.051	66.06	14.15
MM3_2	2.54	0.27	0.0339	0.0017	0.54	0.051	82.37	14.57
MM3_3	2.24	0.18	0.0296	0.0015	0.55	0.056	69.45	13.87
MM4_1	2.64	0.19	0.0324	0.0014	0.598	0.051	63.39	13.69
MM4_2	1.29	0.11	0.02148	0.00083	0.434	0.039	70.56	7.31
MM4_3	3.46	0.32	0.0432	0.0028	0.584	0.066	89.70	23.69
MM5_1	2.16	0.19	0.0285	0.0019	0.541	0.058	68.95	14.14
MMP1_g2_1	29.4	1.9	0.27	0.014	0.776	0.039	140.82	86.11
MMP1_g2_2	5.56	0.25	0.0603	0.002	0.671	0.035	82.68	17.49
MMP1_g2_3	6.07	0.47	0.0668	0.0038	0.678	0.051	87.79	28.06
MMP1_g2_4	4.31	0.45	0.06	0.0041	0.588	0.078	122.23	38.49
MMP1_g2_5	3.63	0.28	0.0448	0.0022	0.599	0.057	87.45	21.07

ANNEX V

Apatite REE data

ANNEX V-Apatite REE chondrite normalized data (ppm)

	La	Ce	Pr	Nd	Sm	Eu	Gd	Tb	Dy	Ho	Er	Tm	Yb	Lu
Pias1-g1	943.0	1239.1	1268.3	1265.9	1728.9	159.6	1492.1	1602.5	1518.9	1090.5	998.9	927.5	999.3	753.5
Pias1-g2	892.1	1237.5	1325.0	1358.1	2400.1	65.2	2239.4	2391.5	2009.9	1407.2	1150.7	1156.3	1018.3	830.4
Pias1-g3	964.4	1301.7	1370.5	1341.3	2053.9	94.0	1981.5	2134.9	1891.4	1439.1	1248.8	1259.7	1106.6	870.5
Pias1-g4	986.9	1369.3	1449.9	1406.1	2353.6	106.0	2287.5	2555.1	2149.5	1616.8	1450.1	1453.5	1355.1	1088.8
Pias1-g5	1104.8	1353.6	1319.0	1215.6	1749.4	101.6	1658.8	1861.6	1716.3	1365.1	1254.0	1342.1	1294.7	1059.0
Pias1-g6	902.7	1034.8	1017.0	895.2	1129.6	186.9	1035.0	1159.9	1100.8	940.0	894.0	914.9	814.1	662.5
Pias1-g7	810.7	1158.9	1282.8	1339.6	2230.4	81.2	2152.3	2250.2	1918.2	1385.0	1170.5	1100.2	981.6	728.3
Pias1-g8	1223.7	1467.6	1400.4	1249.4	1551.3	117.5	1363.8	1557.6	1597.4	1238.7	1225.1	1197.5	1347.3	1059.5
Pias1-g9	1011.5	1400.2	1502.3	1612.2	2240.4	117.9	2048.5	2022.6	1835.3	1303.9	1090.5	861.0	866.4	653.8
Pias1-g10	1011.9	1286.5	1305.0	1191.0	1826.4	98.3	1751.4	2018.7	1797.5	1405.6	1259.5	1354.1	1281.0	1047.6
Pias1-g11	882.7	1296.5	1448.4	1557.6	2450.1	102.3	2323.0	2308.2	2110.6	1512.3	1298.6	1052.4	1013.8	731.2
Pias1-g12	1102.6	1397.6	1345.6	1244.1	1753.4	106.8	1632.5	1862.6	1907.9	1411.7	1352.0	1299.8	1425.6	1089.2
Pias1-g13	977.5	1337.5	1396.1	1388.3	2305.2	75.2	2145.9	2296.4	2091.1	1416.7	1242.3	1167.8	1275.7	926.9
Pias1-g14	960.3	1313.5	1333.1	1315.1	1986.3	107.2	1789.1	2033.6	1918.7	1335.6	1234.6	1137.3	1261.4	952.4
Pias1-g15	1096.2	1421.5	1391.5	1365.4	2035.1	103.4	1888.2	2079.4	2025.1	1460.4	1348.5	1242.5	1401.4	1071.3
Pias1-g16	1047.1	1368.5	1360.5	1324.7	2044.7	94.6	1827.0	2067.4	1976.3	1386.8	1287.3	1188.4	1294.9	976.6
Pias1-g17	931.3	1278.1	1387.9	1346.9	2309.9	68.3	2117.3	2388.3	2051.0	1451.4	1253.0	1265.4	1187.4	900.3
Pias1-g18	924.3	1246.7	1375.8	1326.9	2278.9	67.3	2170.1	2384.8	2018.4	1430.3	1205.7	1250.0	1164.5	901.8
Pias1-g19	1122.3	1517.3	1566.9	1598.2	2303.7	143.8	2066.1	2217.6	2082.4	1493.8	1370.5	1266.0	1339.1	1010.3
Pias1-g20	935.8	1322.6	1449.1	1493.5	2566.2	62.1	2328.6	2495.3	2170.7	1419.5	1213.8	1106.9	1177.5	869.3
Pias1-g21	1081.5	1386.4	1401.9	1350.2	2099.0	101.0	1875.8	2147.8	2023.2	1420.1	1322.6	1247.4	1368.0	1021.9
Pias1-g22	1210.2	1456.0	1323.3	1244.9	1543.9	126.0	1355.3	1564.2	1627.4	1301.3	1303.7	1231.1	1404.5	1103.2
Pias1-g23	1069.8	1436.9	1442.6	1422.6	2136.0	109.4	1919.1	2173.7	2079.0	1446.3	1358.0	1255.2	1424.8	1071.1
Pias1-g24	965.0	1316.6	1360.8	1343.6	2161.2	96.0	1969.6	2164.5	2017.7	1362.8	1242.9	1115.1	1212.1	916.9
LP1-g1	4768.5	5534.4	5586.6	5652.9	4668.9	341.6	3424.4	2733.9	2283.6	1846.6	1542.5	1150.5	976.1	803.0
LP1-g2	4111.9	4786.6	5005.5	5094.6	4775.8	326.1	3776.7	3048.2	2558.8	2159.9	1814.4	1415.4	1221.9	1036.5
LP1-g3	3918.3	4724.2	4826.4	5214.5	4812.1	350.8	3880.4	3094.8	2622.1	2145.6	1824.2	1399.8	1186.9	995.4
LP1-g4	6401.3	7433.5	7314.0	7329.0	5775.2	455.6	4164.9	3320.0	2811.8	2195.1	1810.7	1350.5	1170.2	934.5
LP1-g5	3800.3	4512.0	4661.7	4897.6	4461.2	324.7	3524.6	2773.9	2361.1	1915.8	1622.3	1230.6	1068.6	888.8
LP1-g6	4805.7	5715.2	5517.6	5467.1	4729.5	315.3	3545.9	2832.8	2375.5	1914.6	1597.0	1175.2	965.6	789.9
LP1-g7	1828.2	2582.9	2906.1	3313.9	3310.6	303.8	2824.4	2263.6	1962.1	1630.1	1373.8	1049.9	895.4	785.5
LP1-g8	3987.6	4764.7	4884.0	5198.3	4574.6	343.9	3525.6	2858.9	2441.4	1986.6	1647.5	1264.0	1064.6	882.1
LP1-g9	3192.0	3902.6	3985.9	4292.9	4131.8	357.1	3427.6	2807.6	2401.6	1991.2	1657.3	1289.4	1132.8	923.2
LP1-g10	4570.1	5254.5	5309.4	5451.1	4591.9	328.3	3429.3	2755.2	2322.3	1834.6	1537.5	1156.2	976.1	822.7
LP1-g11	4916.9	5768.3	5882.3	5907.5	4900.4	349.6	3573.2	2818.7	2365.9	1873.1	1563.9	1115.5	913.0	758.3
LP1-g12	5859.4	7111.9	7197.7	7372.1	6547.4	417.8	5010.2	4092.3	3499.3	2811.9	2362.3	1733.4	1481.4	1200.0
LP1-g13	3817.0	4635.9	4757.4	4909.2	4512.2	296.0	3510.8	2823.9	2349.3	1934.4	1627.7	1240.3	1082.2	896.5
LP1-g14	4523.7	5300.6	5563.5	5782.0	5174.3	385.0	3935.1	3124.9	2641.0	2137.0	1769.9	1327.5	1126.7	942.9
LP1-g15	3994.4	4844.5	5274.2	5537.2	5228.7	360.0	4062.4	3205.6	2660.3	2192.9	1801.1	1361.3	1165.8	979.2
LP1-g16	4669.6	5498.0	5812.6	5992.3	5189.7	365.1	4027.8	3149.5	2630.0	2117.4	1727.5	1277.4	1096.7	900.4
LP1-g17	4260.5	5072.9	5178.7	5326.2	4285.5	312.5	3041.5	2385.4	2030.2	1627.6	1349.1	1012.5	864.4	716.0
LP1-g18	4425.5	5077.0	5474.3	5541.5	4880.8	330.6	3768.0	3006.8	2508.5	2014.5	1721.0	1250.7	1106.8	936.4
LP1-g19	5291.5	6165.7	6397.6	6344.2	5697.3	374.0	4406.8	3530.9	2985.8	2432.6	2040.1	1536.8	1302.7	1090.2
FM1-g1	7037.9	7341.6	7194.3	6856.0	5138.3	491.4	3504.2	2505.6	2037.7	1595.5	1293.1	958.2	764.8	633.1
FM1-g2	2987.4	3472.6	3390.6	3351.6	2418.2	609.5	1422.4	896.8	656.1	466.1	348.9	232.0	165.4	126.2
FM1-g3	10645.4	8122.5	6357.7	4866.3	2105.5	641.2	998.0	560.3	383.6	291.3	220.5	151.8	125.5	96.7
FM1-g4	3916.5	4487.2	4517.6	4487.8	3199.5	779.5	1792.2	1127.9	804.3	584.2	431.2	287.9	214.0	159.7
FM1-g5	10427.7	7712.7	5719.9	4380.1	1838.3	561.2	877.4	502.4	350.9	258.1	201.4	141.3	118.6	100.1
FM1-g6	3257.4	3861.2	3840.2	3840.8	2849.4	692.4	1680.1	1088.2	786.7	565.0	412.2	278.7	211.0	153.8
FM1-g7	1888.0	2074.8	1993.5	1888.9	1830.1	682.2	1587.9	1728.7	1815.7	1608.6	1474.5	1250.5	1100.4	907.2
FM1-g8	10736.6	6082.3	3529.0	2277.7	766.7	327.7	364.7	193.8	145.3	116.7	107.6	83.1	90.7	94.1
FM1-g9	3630.8	4235.2	4157.7	4030.5	2931.8	727.8	1659.3	1065.9	764.2	550.0	401.3	272.4	198.9	143.0
FM1-g10	2598.6	2952.3	2841.7	2708.8	2252.7	748.5	1439.2	1060.4	821.6	586.3	463.1	332.1	257.9	200.2
FM1-g11	6035.7	5019.3	3776.1	2731.6	983.9	553.0	464.2	238.8	170.7	136.1	115.7	95.4	89.4	109.9
FM1-g12	10393.8	8731.4	6669.8	5027.2	2146.6	572.6	1064.0	676.3	513.7	407.3	356.0	291.5	251.8	207.4
FM1-g13	1631.3	1572.9	1317.6	1087.2	562.8	267.4	311.7	192.0	146.7	122.4	110.6	92.1	79.1	77.0
FM1-g14	4091.2	3901.7	3158.0	2335.1	1131.1	262.1	622.3	419.2	360.8	335.8	357.8	337.2	358.6	385.0
FM1-g15	7163.8	4186.5	2401.3	1592.4	548.2	269.1	261.7	139.3	102.8	84.6	75.3	61.9	57.3	62.7
FM1-g16	4018.2	4316.2	4361.5	4202.7	2847.7	722.6	1547.3	957.2	698.6	482.0	369.2	242.0	188.2	137.9
FM1-g17	5123.0	5605.0	5288.1	4631.5	2786.8	618.0	1510.2	1074.2	874.3	713.7	689.1	649.7	718.6	696.9
FM1-g18	3441.0	3876.2	3899.1	3895.4	2850.8	727.3	1617.0	1015.7	743.0	514.7	392.3	270.1	193.0	146.5

ANNEX V-Apatite REE chondrite normalized data (ppm)

	La	Ce	Pr	Nd	Sm	Eu	Gd	Tb	Dy	Ho	Er	Tm	Yb	Lu
CST1-4-g1	2773.8	2354.3	1697.3	1330.1	607.8	248.5	310.7	183.7	140.1	108.6	92.2	76.6	64.1	61.0
CST1-4-g2	8624.8	6086.7	3949.7	2617.4	893.7	402.3	414.3	229.4	168.9	139.8	129.5	107.2	101.6	97.2
CST1-4-g3	3489.4	3476.0	2955.7	2653.5	1696.4	487.1	985.7	610.7	460.3	347.3	284.9	211.2	167.6	135.6
CST1-4-g4	3593.1	3265.1	2456.0	1964.6	970.9	359.8	491.9	288.1	223.5	164.2	142.7	113.2	97.1	87.8
CST1-4-g5	3256.8	3031.8	2403.2	2045.3	1129.4	373.9	609.1	357.4	263.9	198.6	161.1	116.2	105.2	91.4
CST1-4-g6	3487.9	3207.9	2513.4	2041.8	1037.7	364.7	526.4	308.5	230.9	180.6	150.4	114.6	102.4	90.1
CST1-4-g7	3328.2	3374.5	2961.3	2729.4	1743.4	485.2	964.3	589.0	425.6	304.6	238.6	177.9	132.8	109.8
CST1-4-g8	3634.0	3303.3	2466.5	2006.1	949.3	358.1	486.5	294.0	216.9	171.1	150.0	116.6	98.8	90.6
CST1-4-g9	9292.9	5587.6	3334.6	2197.5	792.5	348.1	370.1	193.8	145.6	117.1	102.8	85.5	80.9	85.0
CST1-4-g10	3631.2	3346.0	2520.5	1914.9	893.2	350.0	422.7	243.8	190.2	147.0	131.2	112.7	98.8	89.5
CST1-4-g11	3247.6	3246.8	2809.3	2526.3	1537.5	470.0	867.2	530.8	402.3	296.7	237.5	185.5	135.9	111.1
CST1-4-g12	2954.0	2810.5	2323.2	2109.1	1245.3	346.8	708.1	431.4	309.5	229.1	176.4	128.3	96.8	79.3
CST1-4-g13	4859.6	4387.0	3492.5	2861.6	1583.7	507.6	908.0	532.4	405.6	301.9	258.4	188.4	157.7	141.8
CST1-4-g14	3047.0	3143.1	2851.0	2668.9	1754.4	510.2	988.9	595.7	444.8	324.4	254.9	184.1	145.7	117.1
CST1-4-g15	3054.5	2845.6	2301.9	1925.5	1064.4	356.5	573.8	345.3	250.6	189.0	158.7	121.8	94.9	87.0
CST1-4-g16	3949.9	3557.5	2865.8	2392.6	1216.8	395.4	662.5	382.4	297.8	221.6	178.6	138.1	111.9	93.9
CST1-4-g17	2587.4	2780.9	2611.8	2502.7	1735.1	439.0	999.6	619.0	450.7	324.1	242.3	165.5	124.9	97.9
CST1-4-g18	3527.3	3310.2	2658.8	2298.2	1301.4	427.0	735.2	438.2	319.2	235.8	193.6	139.6	111.8	99.4
CST1-4-g19	2856.5	3113.3	2854.6	2723.1	1946.3	475.4	1162.7	732.1	523.4	391.3	297.3	208.1	143.3	115.5
CST1-4-g20	3711.2	3484.3	2860.8	2469.9	1345.1	383.0	733.3	426.2	297.7	222.0	174.5	126.7	96.9	86.7
CT1-13-g1	1708.1	1476.5	1144.7	935.0	537.4	61.5	390.9	265.2	223.9	211.1	193.4	164.7	136.0	129.3
CT1-13-g2	2400.2	3303.0	3587.4	3822.3	3858.9	279.0	3186.3	2579.7	2162.5	1828.2	1520.7	1246.8	972.3	866.9
CT1-13-g3	1741.2	2263.9	2309.7	2202.8	1472.7	479.7	872.4	687.5	589.2	509.1	487.5	507.6	492.2	474.7
CT1-13-g4	361.6	492.3	621.8	851.7	1605.4	306.0	1915.2	1788.4	1597.5	1440.6	1272.9	1093.7	861.7	722.9
CT1-13-g5	8893.0	7549.8	6198.9	4782.3	2175.2	727.6	1013.5	593.8	417.5	335.1	271.5	226.6	168.9	147.7
CT1-13-g6	2185.4	2342.4	2233.1	2129.9	1594.4	408.5	1184.8	842.3	683.2	591.1	486.0	383.4	270.5	224.4
CT1-13-g7	7136.9	6273.1	5525.1	4535.0	2318.2	710.2	1182.9	691.0	481.1	370.0	297.8	223.9	164.0	134.8
OL1-g1	5569.6	4986.8	4298.8	3570.4	1444.5	832.8	610.1	305.9	183.8	122.8	75.8	52.6	37.7	28.4
OL1-g2	11187.8	7075.3	4437.1	2978.0	1040.8	428.9	435.9	237.4	169.5	127.7	112.1	86.1	77.4	74.2
OL1-g3	9398.3	5978.5	3791.8	2620.3	954.3	387.8	409.9	223.3	161.7	121.0	104.7	76.9	72.7	64.7
OL1-g4	5208.3	4327.1	3151.0	2510.5	1177.9	453.3	597.9	351.2	261.3	204.5	169.7	119.6	107.7	95.0
OL1-g5	11872.5	7185.3	4157.2	2744.4	903.9	347.8	407.0	214.2	152.4	120.9	104.4	85.1	73.9	77.5
OL1-g6	227.8	433.4	684.2	1012.6	1179.6	508.3	1025.2	827.4	772.5	731.7	728.8	673.2	701.9	724.3
OL1-g7	8973.5	5956.4	4042.0	2956.0	1140.7	433.6	491.8	270.1	194.4	139.5	115.2	89.9	72.0	62.8
OL1-g8	1126.3	1647.0	2004.5	2402.3	2771.5	499.6	2428.8	2095.0	1765.5	1502.5	1470.3	1407.3	1074.8	849.0
SC1-g1	9021.8	4759.5	2817.8	2039.5	851.4	219.5	447.5	261.2	191.4	156.8	138.4	104.9	96.8	88.2
SC1-g2	6974.6	4213.0	2366.8	1624.1	625.4	315.0	331.1	189.2	146.3	112.2	100.8	87.0	77.0	81.4
SC1-g3	2428.5	2528.4	2311.2	2193.8	1384.4	494.7	797.5	495.0	364.1	266.5	215.8	151.8	127.8	105.7
SC1-g4	6635.3	5007.5	3308.4	2277.5	871.3	332.7	415.3	239.3	176.2	134.4	116.3	97.5	81.2	76.9
SC1-g5	5651.7	4893.3	3557.5	2682.8	1164.6	482.1	521.4	277.2	206.7	152.5	130.4	110.7	91.4	85.4
SC1-g6	7004.0	3395.1	1874.7	1397.5	619.2	182.9	345.8	199.9	150.8	117.4	102.9	83.6	70.8	70.3
SC1-g7	6959.8	4668.2	3022.4	2228.2	998.1	369.1	480.5	288.6	216.5	171.0	141.6	108.1	93.2	93.7
SC1-g8	298.1	423.4	514.9	707.7	1002.2	352.7	1104.6	1000.9	890.4	709.3	582.8	434.3	360.4	277.8
AO1-g1	9696.8	6445.5	3948.3	2737.5	1031.6	378.4	452.5	247.6	175.7	134.1	116.8	87.5	77.0	74.3
AO1-g2	1284.6	1213.2	923.3	750.2	383.5	209.7	199.2	121.9	96.4	81.9	74.4	65.7	57.4	63.1
AO1-g3	71.3	56.0	43.3	36.0	23.3	10.6	13.1	14.4	7.7	10.0	10.4	7.6	9.2	9.0
AO1-g4	9699.0	7361.1	5066.8	3606.0	1360.5	470.5	564.0	324.6	237.4	187.9	157.8	125.3	110.3	98.3
AO1-g5	2591.1	2301.7	1638.8	1318.2	632.1	290.7	323.1	200.2	158.3	128.2	113.8	90.9	83.6	83.2
AO1-g6	6618.1	5122.2	3484.0	2373.3	912.3	240.6	433.1	248.6	185.6	158.3	143.5	120.1	116.1	107.7
AO1-g7	4330.9	2716.3	1532.6	1048.6	398.4	190.1	216.2	121.8	90.1	78.0	72.1	61.6	62.3	65.2
AO1-g8	76.5	56.3	40.6	26.6	27.4	15.2	12.9	12.0	11.4	8.8	8.1	9.5	5.7	7.7
AO1-g9	5790.3	4058.7	2551.4	1883.2	795.8	332.1	413.8	230.0	173.8	137.1	125.6	101.1	91.6	89.8
AO1-g10	8851.6	5367.5	3112.6	2021.7	696.7	289.0	286.8	155.6	112.8	88.1	75.5	61.2	55.7	47.5
AO1-g11	2188.2	1840.5	1320.8	1011.4	472.1	209.5	241.6	154.5	115.7	93.0	80.5	62.0	53.4	60.2
AO1-g12	2928.0	2659.4	1967.2	1550.6	764.6	386.1	404.1	248.0	181.8	145.4	127.1	102.6	89.8	91.0
AO1-g13	11089.9	7096.8	4164.6	2783.5	915.1	379.5	400.1	217.5	141.1	109.6	106.4	84.1	80.8	68.4
AO1-g14	7746.0	5994.4	4040.2	2820.8	994.1	335.0	434.6	242.1	178.2	148.7	134.4	112.5	103.0	86.8
AO1-g15	1688.0	1575.9	1155.5	930.4	449.4	234.1	257.7	152.2	116.2	100.4	90.5	71.5	70.9	69.2
AO1-g16	2111.9	1917.6	1448.1	1228.0	633.9	276.4	344.9	194.1	153.2	117.6	103.4	78.0	74.3	76.5
AO1-g17	6910.7	5760.1	4142.6	3082.2	1325.1	354.3	619.5	339.4	250.1	192.7	163.8	134.9	118.2	101.3
AO1-g18	2414.5	2326.2	1798.2	1531.3	767.5	323.5	411.9	246.6	185.1	142.8	124.7	97.4	85.2	79.2
AO1-g19	2234.0	1904.7	1336.0	1102.5	536.6	251.0	285.6	165.4	125.9	103.1	96.2	76.1	70.7	72.3
AO1-g20	285.9	640.9	1029.6	1586.1	1829.6	560.4	1369.4	1113.2	971.6	846.1	779.3	679.4	641.0	590.5

ANNEX V-Apatite REE chondrite normalized data (ppm)

	La	Ce	Pr	Nd	Sm	Eu	Gd	Tb	Dy	Ho	Er	Tm	Yb	Lu
AO1-g21	3212.4	3381.5	2945.6	2937.2	2040.7	409.8	1391.2	1022.5	875.3	732.4	603.4	441.0	350.9	286.5
AO1-g22	77.3	57.4	39.9	40.6	25.4	5.8	12.3	13.7	10.4	5.5	11.5	10.8	5.3	11.7
AO1-g23	5777.0	4967.4	3918.3	3413.1	1717.2	394.6	960.4	580.5	462.2	370.6	330.1	255.5	208.7	179.1
AO1-g24	9771.0	7446.8	5070.5	3466.1	1277.7	447.6	540.2	304.5	222.0	182.9	159.5	130.9	119.9	108.9
AR1-g1	791.6	1299.1	1594.5	1977.4	2650.0	775.1	2510.3	2384.7	2258.8	1932.6	1771.6	1460.0	1233.3	1038.1
AR1-g2	48.6	130.6	194.7	248.5	230.3	170.7	185.2	132.8	117.4	98.8	93.5	72.3	68.6	67.1
AR1-g3	20641.3	13433.3	8468.5	5692.7	2192.6	1265.9	1104.6	627.5	455.6	329.6	277.3	199.9	171.2	153.8
AR1-g4	820.3	1157.1	1155.3	1157.3	722.6	348.3	394.5	218.8	146.9	111.8	90.7	74.4	64.6	59.2
AR1-g5	164.0	269.1	342.2	478.4	592.8	135.4	643.6	615.4	632.3	628.2	642.1	570.4	524.4	557.6
AR1-g6	1549.0	1307.3	943.2	760.2	394.1	214.4	239.6	155.8	123.4	112.5	115.5	94.3	104.8	112.9
AR1-g7	2554.4	2315.3	1665.7	1279.1	542.5	250.9	287.5	158.7	126.1	109.7	104.8	93.7	94.7	104.9
AR1-g8	291.5	478.9	639.8	850.7	999.8	330.8	965.0	843.2	774.3	675.6	582.8	411.9	325.7	280.6
AR1-g9	5062.8	2789.3	1351.2	883.5	281.8	278.1	174.8	93.4	72.1	70.6	72.2	62.6	67.4	91.8
AR1-g10	9.0	12.4	19.2	28.5	55.2	62.2	100.0	108.3	124.0	131.2	144.5	130.9	127.0	139.7
QR1-g1	6825.4	4295.9	2507.4	1744.0	620.4	263.8	276.8	148.4	103.8	86.0	76.5	66.3	53.0	55.1
QR1-g2	2853.9	3341.4	3238.5	3213.4	2501.0	617.1	1574.5	1064.7	827.1	610.3	494.2	349.2	264.8	192.1
QR1-g3	1231.3	1290.1	1223.5	1284.0	889.4	558.3	626.0	410.2	321.8	251.1	197.8	138.9	111.0	91.1
QR1-g4	41.5	108.3	199.5	356.9	2044.8	5544.7	10254.3	8942.9	5610.7	3167.1	1896.9	963.9	525.3	291.2
QR1-g5	3121.0	2822.9	2376.7	2189.6	1360.9	483.2	873.1	589.0	474.5	380.6	325.8	248.4	201.3	163.2
QR1-g6	1210.0	1152.2	900.7	766.7	350.7	233.6	164.4	88.5	67.7	54.0	48.2	40.3	34.4	31.8
TL1-g1	178.3	230.1	259.6	308.9	399.8	382.3	492.5	432.3	442.0	384.3	334.4	213.7	154.5	123.3
TL1-g2	48.6	130.6	194.7	248.5	230.3	170.7	185.2	132.8	117.4	98.8	93.5	72.3	68.6	67.1
TL1-g3	419.5	628.2	687.2	784.3	1089.8	559.8	1252.3	1345.1	1241.5	955.0	742.2	455.3	289.4	206.7
TL1-g4	4315.4	4262.0	3331.3	2661.8	1210.9	520.2	572.3	305.4	211.7	158.5	148.2	112.3	96.2	81.3
TL1-g5	1585.0	1123.0	641.0	444.2	194.7	121.1	120.0	69.9	62.0	56.9	57.1	56.3	56.4	72.1
TL1-g6	5062.8	2789.3	1351.2	883.5	281.8	278.1	174.8	93.4	72.1	70.6	72.2	62.6	67.4	91.8
TL1-g7	1284.8	1316.7	1132.7	1089.7	691.8	388.5	455.4	308.7	253.0	206.6	188.2	139.2	114.8	100.8
TL1-g8	9.0	12.4	19.2	28.5	55.2	62.2	100.0	108.3	124.0	131.2	144.5	130.9	127.0	139.7
TL1-g9	1549.0	1307.3	943.2	760.2	394.1	214.4	239.6	155.8	123.4	112.5	115.5	94.3	104.8	112.9
TL1-g10	20641.3	13433.3	8468.5	5692.7	2192.6	1265.9	1104.6	627.5	455.6	329.6	277.3	199.9	171.2	153.8
TL1-g11	1522.9	2499.5	2960.4	3296.9	3994.6	88.3	3495.3	3248.8	3076.9	2486.6	2255.8	1922.5	1796.4	1476.9
TL1-g12	164.0	269.1	342.2	478.4	592.8	135.4	643.6	615.4	632.3	628.2	642.1	570.4	524.4	557.6
TL1-g13	1478.9	1575.9	1387.7	1306.1	770.0	479.2	440.5	274.8	217.8	166.2	139.5	118.2	110.6	100.3
TL1-g14	820.3	1157.1	1155.3	1157.3	722.6	348.3	394.5	218.8	146.9	111.8	90.7	74.4	64.6	59.2
TL1-g15	5589.0	4877.3	3410.3	2515.5	1086.8	481.1	511.3	268.6	189.2	136.7	124.8	91.7	83.9	78.2
TL1-g16	791.6	1299.1	1594.5	1977.4	2650.0	775.1	2510.3	2384.7	2258.8	1932.6	1771.6	1460.0	1233.3	1038.1
TL1-g17	291.5	478.9	639.8	850.7	999.8	330.8	965.0	843.2	774.3	675.6	582.8	411.9	325.7	280.6
TL1-g18	6306.4	5513.6	3990.0	2982.3	1304.3	564.1	632.7	330.2	225.8	178.1	152.4	113.0	105.6	93.0
TL1-g19	41.7	38.9	40.3	55.7	95.5	184.9	157.5	152.1	162.8	167.1	183.7	171.9	167.5	177.5
TL1-g20	320.3	443.4	565.1	757.5	668.5	384.7	537.6	457.1	493.2	487.9	549.0	555.1	548.6	530.2
TL1-g21	422.0	711.1	844.6	1067.3	952.2	962.0	738.4	506.6	416.5	332.3	292.5	221.5	185.6	173.3
TL1-g22	187.2	334.1	508.2	699.7	758.8	528.4	532.1	401.8	333.0	273.7	252.1	205.3	196.0	178.4
TL1-g23	1909.3	2276.8	2254.9	2399.2	1940.3	555.2	1533.9	1158.9	1024.5	857.0	776.5	589.2	481.5	391.3
TL1-g24	2554.4	2315.3	1665.7	1279.1	542.5	250.9	287.5	158.7	126.1	109.7	104.8	93.7	94.7	104.9
TL1-g25	1443.6	1362.0	931.5	748.6	352.9	183.4	190.2	106.6	85.7	73.4	71.4	57.9	56.9	65.8
TL1-g26	301.6	421.7	497.6	616.7	707.0	520.2	667.1	459.4	364.9	300.2	274.8	228.2	223.9	251.9
CM2-g1	1617.1	1678.1	1633.7	1858.3	1533.3	310.9	1301.0	918.5	821.3	669.5	606.9	451.4	361.4	306.2
CM2-g2	1717.8	1694.0	1604.5	1710.1	1065.7	572.7	589.1	324.5	232.6	168.2	130.3	87.9	68.0	52.4
CM2-g3	7611.0	4946.5	3282.3	2600.6	1057.0	539.8	513.6	239.7	165.3	123.2	105.4	73.9	71.9	74.9
CM2-g4	1598.8	1578.9	1516.9	1630.9	1134.7	717.4	824.7	508.9	412.2	315.4	262.1	183.1	148.7	120.9
CM2-g5	5013.6	4441.8	3572.1	3078.7	1472.1	539.6	714.1	365.6	283.2	207.2	171.3	126.8	117.8	99.6
CM2-g6	7236.8	6712.2	6212.0	6049.2	3981.9	914.8	2624.0	1632.5	1376.4	1076.7	934.4	699.9	550.6	454.7
MM1-g1	6635.3	5007.5	3308.4	2277.5	871.3	332.7	415.3	239.3	176.2	134.4	116.3	97.5	81.2	76.9
MM1-g2	7004.0	3395.1	1874.7	1397.5	619.2	182.9	345.8	199.9	150.8	117.4	102.9	83.6	70.8	70.3
MM1-g3	9021.8	4759.5	2817.8	2039.5	851.4	219.5	447.5	261.2	191.4	156.8	138.4	104.9	96.8	88.2
MM1-g4	6959.8	4668.2	3022.4	2228.2	998.1	369.1	480.5	288.6	216.5	171.0	141.6	108.1	93.2	93.7
MM1-g5	2428.5	2528.4	2311.2	2193.8	1384.4	494.7	797.5	495.0	364.1	266.5	215.8	151.8	127.8	105.7
MM1-g6	6974.6	4213.0	2366.8	1624.1	625.4	315.0	331.1	189.2	146.3	112.2	100.8	87.0	77.0	81.4
MM1-g7	5651.7	4893.3	3557.5	2682.8	1164.6	482.1	521.4	277.2	206.7	152.5	130.4	110.7	91.4	85.4
MMP1-g1	7118.9	5044.1	3629.6	2790.3	1242.1	794.5	636.5	359.2	269.8	196.2	155.4	114.0	95.6	78.0
MMP1-g2	23807.0	11837.7	5990.6	3515.7	1236.5	730.2	681.9	420.2	342.8	300.2	282.9	241.6	213.6	183.7
MMP1-g3	35647.9	14108.4	5790.5	2863.0	839.9	525.0	500.7	332.4	293.8	273.8	278.2	251.5	227.3	187.2
MMP1-g4	21670.1	11266.4	5912.7	3714.0	1374.7	774.5	737.8	437.9	352.1	298.1	263.4	225.7	194.5	166.2
MMP1-g5	23996.4	13389.1	7415.8	4786.2	1819.0	1050.8	951.9	564.6	447.1	368.1	322.2	252.8	222.1	178.6